NUCLEATION AND CRYSTAL GROWTH IN THE LITHIA-BARIA-SILICA SYSTEM

A Thesis presented by

EDWARD GORDON ROWLANDS

For the degree of

Doctor of Philosophy

of

The University of Sheffield

Department of Ceramics, Glasses and Polymers,
The University of Sheffield

July, 1976

ACKNOWLEDGEMENTS

I wish to thank my supervisor, Dr P.F. James, for the constant encouragement and many discussions which have enabled this thesis to be undertaken and completed.

Thanks are also due to Professor R.W. Douglas and many of the lecturing and technical staff for their interest and practical assistance, and to my wife for her infinite patience.

The author is also grateful to the Science Research Council for financial support.

CONTENTS

SUMMARY

Internal crystallisation occurs for a wide range of compositions in the lithia-baria-silica system without the deliberate addition of nucleating agents. The eutectic subsystem $Li_2Si_2O_5$-$BaSi_2O_5$ has been studied in detail using optical microscopy, differential thermal analysis and X-ray diffraction. Internal nucleation of either $Li_2Si_2O_5$ or $BaSi_2O_5$ was observed, the overall nucleation rates decreasing with liquidus temperature. Crystal growth rates at a given temperature increased with $BaSi_2O_5$ content, there being a large increase close to stoichiometric $BaSi_2O_5$. Either primary phase dendritic growth or two phase eutectic growth was observed.

The thermodynamic data required for an analysis of nucleation kinetics in the system $Li_2Si_2O_5$-$BaSi_2O_5$ could be calculated from liquidus data. Three methods of analysing nucleation kinetics were identified, which all gave values of the pre-exponential factor far greater than predicted by homogeneous nucleation theory. It was found that theory could not be fitted to data below the temperature of maximum nucleation. Below that temperature the experimental rates were too low according to the nucleation parameters calculated from the experimental rates at higher temperatures. These parameters were all found to be dependent on composition. A temperature dependent interfacial energy could account for the large values of the pre-exponential factor. The shape of the critical nucleus was shown to be important in determining the average interfacial energy calculated from nucleation kinetics. Estimations of the critical nucleus size were found to be reasonable and the interfacial energies obtained from nucleation kinetics agreed approximately with calculations based on a simple theoretical model.

Crystal growth kinetics in the $Li_2Si_2O_5$-$BaSi_2O_5$ system were adequately described by Arrhenius plots. Small additions of $Li_2Si_2O_5$ to $BaSi_2O_5$ caused a large decrease in the growth parameters. For larger additions of $Li_2Si_2O_5$ the growth parameters remained almost constant, similar to those obtained for stoichiometric $Li_2Si_2O_5$. Analogous behaviour was observed in the $Na_2Si_2O_5$-$BaSi_2O_5$ system.

SYMBOLS

Operator signs

d	Ordinary differential
$\frac{\partial}{\partial}$	Partial differential coefficient
Δ	Excess of final over initial value
$\sum$	Summation
$\int$	Integral
$\ln$	Natural logarithm
$\log_{10}$	Logarithm to base 10

Capital English Characters

A	Area, and pre-exponential factor in homogeneous nucleation rate equation
A'	Pre-exponential factor in normal growth rate equation
A''	Pre-exponential factor in surface nucleation growth rate equation
A_D	See equation (4.5)
A'_D	See equation (4.29)
A_E	Pre-exponential factor in eutectic growth rate equation
A_m	Molar area of a phase, see equation (5.23)
A_η	See equation (4.23)
A'_η	See equation (4.31(a))
A_s	Pre-exponential factor in heterogeneous nucleation rate equation
D	Diffusion coefficient in nucleation rate equation

D_o	Pre-exponential factor in nucleation rate diffusion coefficient
D'	Diffusion coefficient in growth rate equation
D'_o	Pre-exponential factor in growth rate diffusion coefficient
G	Gibbs free energy per mole
G_i^{ℓ}	Partial molar free energy of component 'i' in solution
$G_i^{o\ell}$, G_i^{os}	Molar free energies of pure solid and pure liquid component 'i' respectively
ΔG	Thermodynamic driving force for nucleation and crystal growth (defined as the change in Gibbs free energy per mole of solid phase when a solid phase is formed in a liquid, neglecting any interfacial free energy contributions)
$\Delta G'$	Total change in Gibbs free energy on crystallisation (neglecting interfacial free energy contribution)
ΔG_D	Diffusion activation free energy per mole or 'molecule' for nucleation
$\Delta G'_D$	Diffusion activation free energy per mole or 'molecule' for crystal growth
ΔG_η	Activation free energy per mole for viscous flow
ΔG_v	Thermodynamic driving force for nucleation and crystal growth per unit volume of solid phase
$\Delta_m G$	Change in Gibbs free energy on mixing
H	Enthalpy
ΔH_D	Activation enthalpy, see equation (4.4)
$\Delta H'_D$	Activation enthalpy, see equation (4.28)
ΔH_f	Heat of fusion per mole
ΔH_x	Effective heat of fusion, see equation (1.6)
ΔH_η	Activation enthalpy, see equation (4.25)
$\Delta_m H$	Enthalpy of mixing

I	Homogeneous nucleation rate
I_c	Nucleation rate at the critical nucleation temperature (usually taken as 1 cm^{-3} sec^{-1})
I_{max}	Maximum homogeneous nucleation rate
I_o	Steady state homogeneous nucleation rate
I_s	Heterogeneous nucleation rate per unit area of substrate
^vI_s	Heterogeneous nucleation rate per unit volume of liquid
M	Magnification
N_A	Number of spherulites intersected by a plane of unit area, and Avogadro's number
N_i	Number of moles of composition or phase 'i', and number of spherulite sections in size class 'i'
N_s	Number of 'atoms' of a liquid in contact with a substrate surface
^vN_s	Number of surface substrate atoms per unit volume of liquid
N_v	Number of molecules, spherulites etc. per unit volume
O_s	Total surface area of a substrate
R	Gas constant and general symbol for alkali metal
S	Entropy, or interfacial area
ΔS_D	Activation entropy, see euqation (4.4)
$\Delta S'_D$	Activation entropy, see equation (4.28)
ΔS_f	Entropy of fusion
ΔS_ℓ	Entropy change, see equation (5.20)
ΔS_η	Activation entropy, see equation (4.25)
ΔS_s	Entropy change, see equation (5.18)

ΔS_x	Effective entropy of fusion, see equation (1.6)
T	Temperature
T'	See equation (4.16)
T_c	Critical nucleation temperature (nucleation rate usually taken as 1 cm^{-3} sec^{-1}).
T_E	Eutectic temperature
T_g	Glass transformation temperature (referred to as 'D.T.A. T_g' when determined by D.T.A.)
T_L	Liquidus temperature
T_m	Melting point
T_{max}	Temperature corresponding to maximum nucleation or crystal growth rate
T_r	Reduced maximum nucleation temperature equals T_{max}/T_m
T_u	Temperature at which the crystal growth rate is 0.1 μm sec^{-1}
T_x	Effective melting point, see equation (1.6), and temperature for which D.T.A. crystallisation exotherm is at its maximum
$T'_x - T''_x$	Temperature range of D.T.A. crystallisation exotherm
ΔT	Supercooling below melting point, liquidus temperature, or eutectic temperature, and temperature change observed in D.T.A.
ΔT_c	Supercooling at the critical nucleation temperature
ΔT_{max}	Temperature difference between temperature of maximum nucleation and temperature of interest
U	Bonding energy
V	Volume
V_c	Volume of a cluster
V_m	Molar volume

W	Free energy change for the formation of a cluster
W^*	Free energy change for the formation of a critical nucleus
W'^*	Free energy change for the formation of a two dimensional critical nucleus in surface nucleation growth
W_E	Free energy change for the formation of a unit volume of a two phase eutectic
W^*_{het}	Value of W* for heterogeneous nucleation
W^*_{hom}	Value of W* for homogeneous nucleation
W^*_{max}	Value of W* at the temperature of maximum nucleation
X	Characteristic dimension e.g. diameter, and volume fraction
X_i	Characteristic dimensinn of size class 'i'
$\bar{z}$	Average value of the reciprocals of a characteristic dimension for all size classes, see equation (2.8)

Small English characters

a,b,c	Dimensions of an orthorhombic cluster
a	Constant, see equation (2.1), and see equation (2.13)
a_i^{ℓ}	Activity of component 'i' in solution relative to pure liquid component 'i'
b	Cooling rate and average interfacial entropy, see equation (4.3)
c	Constant, see equation (4.17)
c_p	Specific heat at constant pressure
d	Diameter of a section through a spherical spherulite
d_{max}	Maximum diameter of a section observed when a plane intersects a system containing spherical spherulites
f	Site factor for crystal growth

h	Planck's constant, and high temperature modification
i	Number of atoms
k	Boltzmann's constant
k, k', k''	Constants, see equations (3.3), (3.4) and (3.5)
k'	Shape factor, see equation (1.51)
k_1, k_6	Shape factors, see equation (2.7)
k_2, k_3, k_4, k_5	Shape factors, see equations (5.3), (5.4), (5.7) and (5.8)
k_A	Constant, see equation (4.15)
ℓ	Length, and low-temperature modification
$^m/_o$	Molecular percentage
n	Number of atoms or molecules
$p( )$	Probability function
r	Radius
s	Number of atoms facing a crystal across a liquid-crystal interface
t	Time
t_i	Impingement time, see equation (3.21)
u	Growth rate
u_{max}	Maximum growth rate
u_R	Reduced growth rate, see equation (1.55)
v	Volume occupied by one atom or molecule
$^w/_o$	Weight percentage
x_i	Mole fraction of component 'i'
y_{AB}	Interlamellar spacing in a two phase eutectic, A-B
y'_{AB}, y''_{AB}	Minimum and maximum values of y_{AB}

Greek characters

α	Constant for regular solution model, and extent of dissociation
γ_i	Activity coefficient of component 'i', equals a_i/x_i
η	Viscosity
η_o	Pre-exponential factor in viscosity equation, see equation (4.25)
θ	Contact angle in heterogeneous nucleation, and X-ray diffraction angle equals 2θ
$f(\theta)$	Function of the contact angle, see equation (1.37)
λ	Growth incurred by the transfer from a liquid to a crystal of one atom across the liquid-crystal interface, approximately equal to one inter-atomic spacing
ν_o	Vibrational frequency
ρ	Density
σ	Interfacial or surface energy
$\bar{\sigma}$	Average interfacial or surface energy
σ_E	Edge surface energy
σ_i	Interfacial energy of the 'i'th facet of a non-spherical cluster
σ_{ij}	Interfacial energy of an interface between phases 'i' and 'j'
$\bar{\sigma}_o$	Average interfacial enthalpy, see equation (4.3)
τ	Induction time for nucleation
τ_o	Pre-exponential factor in equation for τ, see equation (1.31)
$\phi(T)$	Function of temperature, see equation (1.59)
$\phi'(T)$	Function of temperature, see equation (4.19)

Subscripts and superscripts

c	Refers to crystal phase
cs	Refers to crystal-substrate e.g. σ_{cs}

i	Refers to component 'i' and to facet 'i' of a non-spherical cluster
ℓ	Refers to liquid phase
ℓc	Refers to liquid-crystal e.g. $\sigma_{\ell c}$
s	Refers to solid phase, and substrate
t	Indicates after time 't'
*	Indicates a property of the critical nucleus
o	Quantity related to standard state, generally a pure phase
-	Mean quantity

CHAPTER 1

INTRODUCTION

Chapter 1 - Introduction

INTRODUCTION

The glass industry has traditionally developed glass compositions which are resistant to crystallisation. Compositions are chosen which undergo the required shaping processes without exhibiting any devitrification, a term used to describe the uncontrolled crystallisation of glass. This refers to crystallisation either from the surface of the glass or from foreign bodies within its bulk.

However, with the advent of the glass-ceramic process, whereby ceramic articles can be prepared by the controlled crystallisation of glass, attention has also been focused on how to regulate crystallisation rather than prevent it. Glass-ceramic formation is generally considered to require the presence of a nucleation catalyst which, by causing nucleation to occur preferentially at a large number of certain sites, enables the formation of a fine-grained material. Theoretically, however, crystallisation may occur without the aid of any such heterogeneous mechanism. In these cases crystallisation is referred to as being homogeneous. According to experiment there are indeed several glasses which form glass-ceramics without any intentional addition of a catalyst. Thus in the absence of any obvious heterogeneous mechanism, it is assumed that these glasses undergo homogeneous crystallisation.

In general there are two main stages in the heat treatment schedule for producing a fine-grained glass-ceramic. The first stage involves the nucleation of a large number of crystals at a temperature where the growth rate is low. This ensures that the first nuclei formed do not transform the rest of the glass into a coarse-grained material. The second stage is a heat treatment at a higher temperature

where the growth rate is relatively large and the article is converted into a ceramic of almost 100% crystallinity.

From a technological viewpoint a study of crystal nucleation and growth is therefore very important. However, these processes are also important with respect to fundamental studies of the crystallisation of supercooled liquids. Glass is a very convenient medium for this, since the diffusion processes and atomic rearrangements which control crystallisation occur relatively slowly. Hence it is possible to arrest the crystallisation process by rapid cooling and examine the 'frozen-in' structure using convenient methods of examination.

In this thesis crystal nucleation and growth in the system Li_2O-BaO-SiO_2 are investigated. It has been previously found that in the two binary systems Li_2O-SiO_2 and BaO-SiO_2 crystal nucleation occurs without the addition of a nucleating agent and is apparently homogeneous. Thus this system was expected to provide a wide range of crystallisation behaviour and one in which direct measurements of nucleation and growth rates could be obtained with little experimental difficulty.

The aim of this research was to examine the kinetics of crystal nucleation and crystal growth in terms of existing crystallisation theory. In order to discuss the results, a theoretical discussion has been made of the thermodynamics and kinetics of phase transformation. The thermodynamics of crystallisation are developed from first principles since the author is aware of no reference that gives a discussion in sufficient detail for the present purposes. The theories of nucleation and growth have been summarised from several textbooks[1-4].

1.1 The thermodynamics of crystallisation

The rate at which a supercooled liquid crystallises is governed by two processes. First, the rate at which crystal nuclei form within the liquid, and secondly, the rate at which such nuclei subsequently grow. Both processes involve the transformation of supercooled liquid into the crystalline state. This transformation is favoured by the lowering in volume Gibbs' free energy of the supercooled system which thereby occurs. The change in volume Gibbs' free energy (which neglects any surface energy contributions such as those involved in the formation of nuclei) is referred to as the thermodynamic driving force, ΔG, the value of which enters directly into the theories of nucleation and growth. It is generally expressed as the free energy change per mole of solid phase, neglecting surface effects, when the solid phase is formed within the parent liquid. It should be mentioned that the Gibbs' free energy change has been specified since this refers to a system at constant pressure. However, the alternative Helmholtz free energy change, which is specified for a system at constant volume, is little different in value since any pressure-volume work is negligible for the crystallisation of a small amount of solid phase in a liquid.

The value of ΔG depends not only on the temperature of the supercooled liquid, but also on its composition if more than one component is present. Consider first a one component system. ΔG can be expressed as

$$\Delta G = \Delta H - T\Delta S \qquad (1.1)$$

where ΔH and ΔS refer to the enthalpy difference and entropy difference

respectively between the solid and liquid phases per mole of solid phase at temperature T. Thus

$$\begin{aligned} \Delta H &= H^s - H^\ell \\ \Delta S &= S^s - S^\ell \end{aligned} \tag{1.2}$$

But at the melting point, T_m

$$\begin{aligned} \Delta H &= -\Delta H_f = -(H^\ell - H^s) \\ \Delta S &= -\Delta S_f = -(S^\ell - S^s) \end{aligned} \tag{1.3}$$

where ΔH_f and ΔS_f are the enthalpy of fusion and entropy of fusion respectively. Thus below T_m, ΔG is given by

$$\Delta G = -\Delta H_f + T\Delta S_f - \int_T^{T_m} \Delta c_p dT + T\int_T^{T_m} \frac{\Delta c_p}{T} dT \tag{1.4}$$

where Δc_p is the difference in specific heats between the crystalline and liquid phases at constant pressure. In general Δc_p can be expressed in terms of an interpolation formula

$$\Delta c_p = A + BT + CT^2 \tag{1.5}$$

However, it is often found that ΔG v.T is linear over temperature ranges as large as 200°C. This occurs when Δc_p is small. Thus over a specified temperature range ΔG is given by

$$\Delta G = -\Delta H_x + T\Delta S_x \tag{1.6}$$

where ΔH_x and ΔS_x are two numerically derived values. A further approximation can be made if $\Delta c_p \sim 0$. ΔG is then given by the well known expression

$$\Delta G = - \Delta H_f + T\Delta S_f \tag{1.7}$$

Since at T_m, $\Delta G = 0$, $\Delta S_f = \Delta H_{f/T_m}$

$$\therefore \quad \Delta G = \frac{- \Delta H_f (T_m - T)}{T_m} \tag{1.8}$$

Equation (1.8) shows clearly the dependence of ΔG on the supercooling $(T_m - T)$. A similar expression can be obtained from equation (1.6) viz.

$$\Delta G = \frac{- \Delta H_x (T_x - T)}{T_x} \tag{1.9}$$

Hence ΔH_x and T_x can be considered as the effective heat of fusion and melting point respectively for the specified temperature range being considered.

It is of interest to calculate the error in neglecting Δc_p, since for many silicate systems specific heat data is unavailable. However, in JANAF Thermochemical Tables[5], data is given for lithium disilicate, $Li_2Si_2O_5$. Table 1.1 compares the values of ΔG calculated from the tables with those calculated from equation (1.8). At a supercooling of 500°C, the error in ΔG is only about 4%. As discussed later, this is approximately the supercooling at which crystal nucleation occurs in $Li_2Si_2O_5$ glass. It is found that a 4% error in ΔG has only a

Table 1.1 Calculation of ΔG for $Li_2Si_2O_5$

T (°K)	ΔT (°K)	$\Delta G'$ (K cals mole^{-1})	$\Delta G''$ (K cals mole^{-1})
600	707	-6.45	-6.96
700	607	-5.62	-5.97
800	507	-4.79	-4.99

where

$$\Delta G' = \frac{-\Delta H_f (T_m - T)}{T_m}$$

$T_m = 1307^{\circ}K$

$\Delta H_f = 12.86$ K cals mole^{-1}

$\Delta c_p = 0$

and

$$\Delta G'' = \frac{-\Delta H_x (T_x - T)}{T_x}$$

$T_x = 1377^{\circ}K$

$\Delta H_x = 11.43$ K cals mole^{-1}

$\Delta c_p \neq 0$

where T_x and ΔH_x are numerical constants, calculated from JANAF Tables[5].

relatively small effect on a quantitative analysis of the nucleation results.

Whilst the supercooling is important in determining the temperature dependence of ΔG, the magnitude of ΔG depends also on $\Delta S_f = \Delta H_{f/T_m}$. Figure 1.1 shows the normalised thermodynamic driving force $\Delta G/\Delta H_f$, which is equal in magnitude to the reduced supercooling, $\Delta T/T_m$, plotted as a function of T_m. For a given ΔH_f, the supercooling required to achieve a certain driving force increases with melting point. Thus for the compounds $Na_2Si_2O_5$ and $BaSi_2O_5$, which have similar heats of fusion but melting points of 874°C and 1420°C, a supercooling of 350°C in the former case is equivalent to a supercooling of about 520°C in the latter case. However, by experiment it is found that vitreous $BaSi_2O_5$ has a much stronger tendency to crystallise than vitreous $Na_2Si_2O_5$. This may be partly attributed to the much larger supercoolings 'possible' for $BaSi_2O_5$ glass. Thus the supercooling at the transformation temperature for $BaSi_2O_5$ glass is about 300°C greater than for $Na_2Si_2O_5$ glass. Below the transformation temperature, of course, crystallisation only proceeds at an undetectable rate.

Consider now the crystallisation of a pure solid from a two component solution. Figure 1.2 shows the molar volume free energy of this solution A-B as a function of composition at a given temperature. ΔG for the formation of say pure crystalline A may be estimated as follows. Let N_A moles of pure solid A form from a solution originally containing N_x moles of the composition x_A. There will then be $N_{x'}$ moles of the composition x_A', the composition of the remaining liquid. The total change in volume free energy (neglecting any surface free energy) will be given by

FIG.1.1. THE NORMALISED THERMODYNAMIC DRIVING FORCE AS A FUNCTION OF MELTING POINT FOR A ONE COMPONENT SYSTEM AT VARIOUS SUPERCOOLINGS.

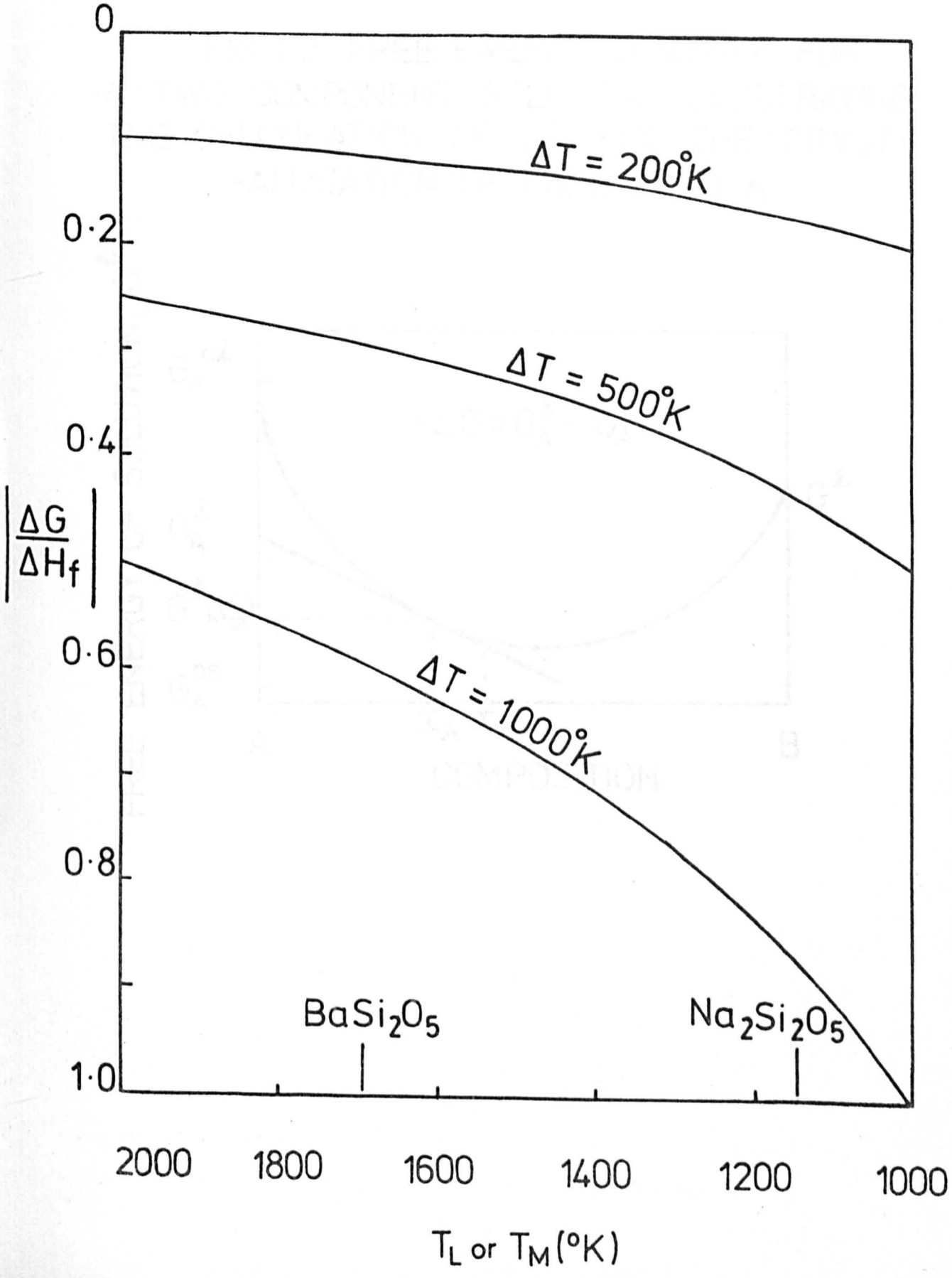

FIG.1.2. FREE ENERGY DIAGRAM FOR A TWO COMPONENT SOLUTION, ILLUSTRATING THE CALCULATION OF ΔG FOR THE CRYST--ALLISATION OF PURE SOLID A.

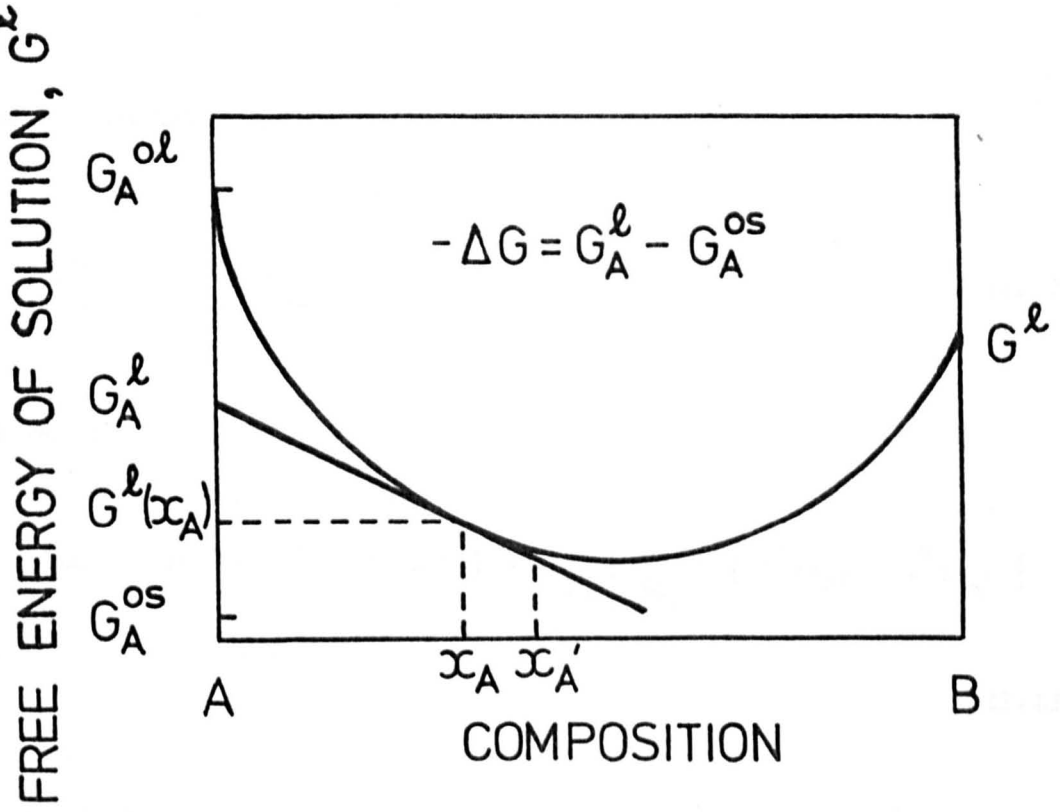

$$\Delta G' = N_{x'} G^{\ell}(x_A') + N_A G_A^{os} - N_x G^{\ell}(x_A) \tag{1.10}$$

where G^{ℓ} is the molar volume free energy of the solution (a function of composition) and G_A^{os} is the molar volume free energy of pure solid A, both at temperature T. Remembering that

$$N_{x'} + N_A = N_x \tag{1.11}$$

and by the Lever Rule

$$\frac{N_{x'}}{N_A} = \frac{1 - x_A}{x_A - x_{A'}} \tag{1.12}$$

we obtain

$$\Delta G' = N_A \left\{ G_A^{os} - G^{\ell}(x_A) \right\} + \left[\frac{1 - x_A}{x_A - x_{A'}} \right] \left\{ G^{\ell}(x_A') - G^{\ell}(x_A) \right\} \tag{1.13}$$

If $N_A << N_{x'}$

$$\Delta G' = N_A \left\{ G_A^{os} - G^{\ell}(x_A) \right\} + (x_A - 1) \frac{dG^{\ell}}{dx_A} \tag{1.14}$$

$$\therefore \Delta G = \frac{\Delta G'}{N_A} = - \left\{ G^{\ell}(x_A) - G_A^{os} \right\} + (1 - x_A) \frac{dG^{\ell}}{dx_A} \tag{1.15}$$

Hence ΔG is equal to $- [G_A^{\ell} - G_A^{os}]$ in Figure 1.2. G_A^{ℓ} is in fact the partial molar free energy of component A in a solution of

composition x_A and can be expressed in terms of the activity of component A, a_A^{ℓ}. Thus

$$G_A^{\ell} = G_A^{o\ell} + RT \ln a_A^{\ell} \tag{1.16}$$

where $G_A^{o\ell}$ is the molar volume free energy of pure liquid A at temperature T. Also, from equation (1.8)

$$G_A^{os} = \Delta G^{\circ} + G_A^{o\ell} = - \frac{\Delta H_f (T_m - T)}{T_m} + G_A^{o\ell} \tag{1.17}$$

Hence ΔG is given by

$$\Delta G = - \frac{\Delta H_f (T_m - T)}{T_m} - RT \ln a_A^{\ell} \tag{1.18}$$

It should be noted that as the transformation proceeds the composition of the residual liquid changes, thus altering the value of x_A. Hence equation (1.18) only applies when small amounts of solid A separate ($N_A << N_x$). Thus ΔG in this case is not the overall free energy change per mole on crystallisation as it was in a one component system. The calculation of ΔG in multicomponent systems is further discussed in Appendix A1.1. In general it can be shown that equation (1.18) applies to the crystallisation of the 'i'th component of any system.

The presence of the activity in equation (1.18) generally prevents the calculation of ΔG. Activity data is not easily determined and it is often unavailable in glass forming systems. However, using the well known method of 'freezing-point depression' it is possible to

calculate activity data at liquidus temperatures. This data can then be extended to lower temperatures if certain approximations are made[6]. Consider again a two component system A-B. The phase diagram of this system and its free energy at the liquidus temperature T_L are shown in Figure 1.3. At the liquidus temperature, solution of composition x_A is in equilibrium with pure solid A. Thus we can write

$$G_A^{\ell} = G_A^{os} \text{ for composition } x_A, T = T_L$$

where G_A^{ℓ} is defined by the intercept on the free energy axis of A of the tangent to the free energy curve at composition x_A. Thus from equations (1.16) and (1.8), at $T = T_L$, we obtain

$$RT_L \ln a_A^{\ell} = - \frac{\Delta H_f (T_m - T_L)}{T_m}$$

$$\therefore \ln a_A^{\ell} = - \frac{\Delta H_f}{R} \left(\frac{1}{T_L} - \frac{1}{T_m} \right) \qquad (1.19)$$

This expression for the activity of A at its liquidus temperature is exact, apart from the neglect of specific heat contributions. In order to calculate a_A^{ℓ} at temperatures below T_L, the system is assumed to be approximately described by a thermodynamic model. In anticipation of the thermodynamic properties of certain compositions in the systems Na_2O-BaO-SiO_2 and Li_2O-BaO-SiO_2, which will be discussed in Chapter 4, only the very simple ideal model is considered here. In Appendix A1.2, the regular type model is discussed in detail, as this is of more general application to silicate systems.

FIG. 1.3. SIMPLE BINARY EUTECTIC SYSTEM AND THE CORRESPONDING FREE ENERGY DIAGRAM AT TEMPERATURE T_L.

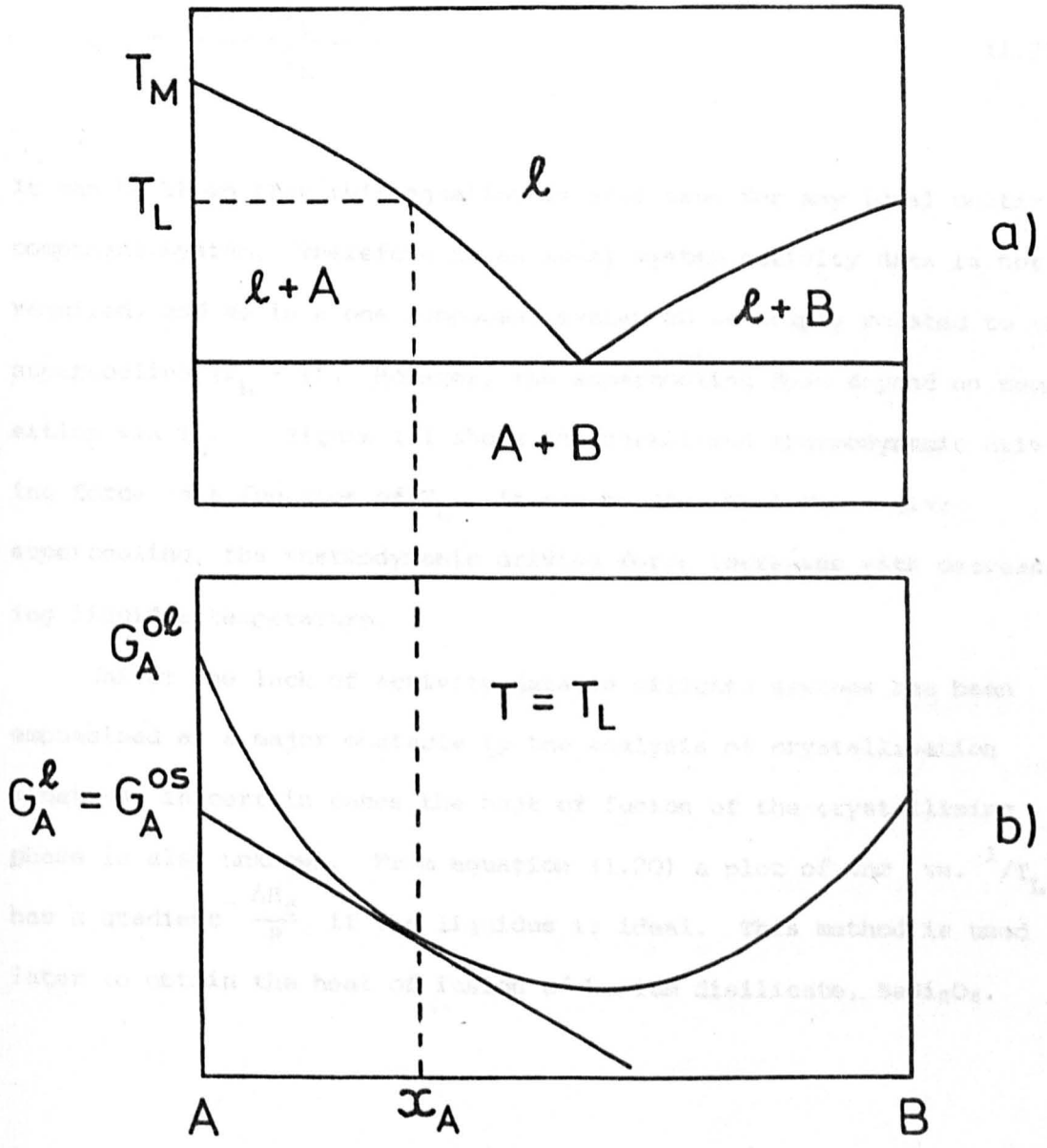

In an ideal system $a_i^{\ell} = x_i$. Thus equation (1.19) becomes

$$\ell n x = -\frac{\Delta H_f}{R}\left(\frac{1}{T_L} - \frac{1}{T_m}\right) \qquad (1.20)$$

Hence substituting into equation (1.18), ΔG in an ideal binary system is given by

$$\Delta G = -\frac{\Delta H_f (T_L - T)}{T_L} \qquad (1.21)$$

It can be shown that this equation is also true for any ideal multicomponent system. Therefore in an ideal system activity data is not required, and as in a one component system ΔG is simply related to the supercooling $(T_L - T)$. However, the supercooling does depend on composition via T_L. Figure 1.1 shows the normalised thermodynamic driving force as a function of T_L. It can be seen that for a given supercooling, the thermodynamic driving force increases with decreasing liquidus temperature.

Whilst the lack of activity data in silicate systems has been emphasised as a major obstacle to the analysis of crystallisation kinetics, in certain cases the heat of fusion of the crystallising phase is also unknown. From equation (1.20) a plot of $\ell n x$ vs. $^1/T_L$ has a gradient $-\frac{\Delta H_f}{R}$, if the liquidus is ideal. This method is used later to obtain the heat of fusion of barium disilicate, $BaSi_2O_5$.

1.2 The rate of crystal nucleation

The preceding discussion has been solely concerned with the decrease in volume free energy which occurs when a molar volume of crystalline phase is formed within a metastable liquid system. This decrease in energy was referred to as a driving force, for without this energy decrease crystallisation would not proceed. However, the mechanisms by which this transformation occurs were not mentioned. Thus no distinction was made as to whether the crystalline phase was forming as discrete crystals or upon crystals already present in the liquid. These two processes are of course nucleation and growth. One essential difference between the two processes is the large increase in interfacial free energy which occurs during nucleation. In comparison, crystal growth will not cause any large change in interfacial free energy, if in simple terms the interface is only advancing. It should be mentioned, however, that the interfacial free energy may be an important factor in more complex growth models. In this section a brief review of nucleation theory is given, growth rate theory being discussed in the next section.

In a given liquid thermal fluctuations may lead to the formation of a cluster of atoms or molecules, the configuration of which is similar to that in the solid. If the liquid is supercooled, such fluctuations should be stable. However, the fact that supercooling can be attained shows that such fluctuations are not necessarily stable. Consider the formation of a spherical cluster in a one component liquid. The work involved, i.e. the free energy change, is given by

$$W = \frac{4}{3}\pi r^3 \frac{\Delta G}{V_m} + 4\pi r^2 \sigma \qquad (1.22)$$

where ΔG is the change in free energy on crystallisation per mole

V_m is the molar volume of the crystallising phase

r is the radius of the cluster

and σ is the interfacial energy between the crystal and the liquid. At small values of r the surface energy term will predominate and W will be positive. However, as r increases the volume term will predominate and W will become negative. The situation is shown qualitatively in Figure 1.4. r* is referred to as the critical radius. If a cluster is smaller than r* it will redissolve, but if it is greater than r* the cluster can lower its free energy and become stable by increasing in size. Clusters smaller than r* are often referred to as embryos, and those greater than r* are called nuclei. Clusters of critical size are called critical nuclei and their free energy of formation is W*. Expressions for r* and W* are obtained by differentiating equation (1.22) with respect to r. Thus for a spherical nucleus

$$r^* = -\frac{2\sigma V_m}{\Delta G}$$

$$W^* = \frac{16\pi\sigma^3 V_m^2}{3\Delta G^2} \qquad (1.23)$$

More generally for non-spherical nuclei it can be shown that

$$X^* = -\frac{k_4 \bar{\sigma} V_m^2}{\Delta G}$$

$$W^* = \frac{k_5 \bar{\sigma}^3 V_m^2}{\Delta G^2} \qquad (1.24)$$

where X is a dimension of the nucleus, $\bar{\sigma}$ is an average interfacial surface energy, and k_4 and k_5 are shape factors. These more general

FIG. 1.4. FREE ENERGY OF FORMATION OF A SPHERICAL CLUSTER AS A FUNCTION OF ITS RADIUS.

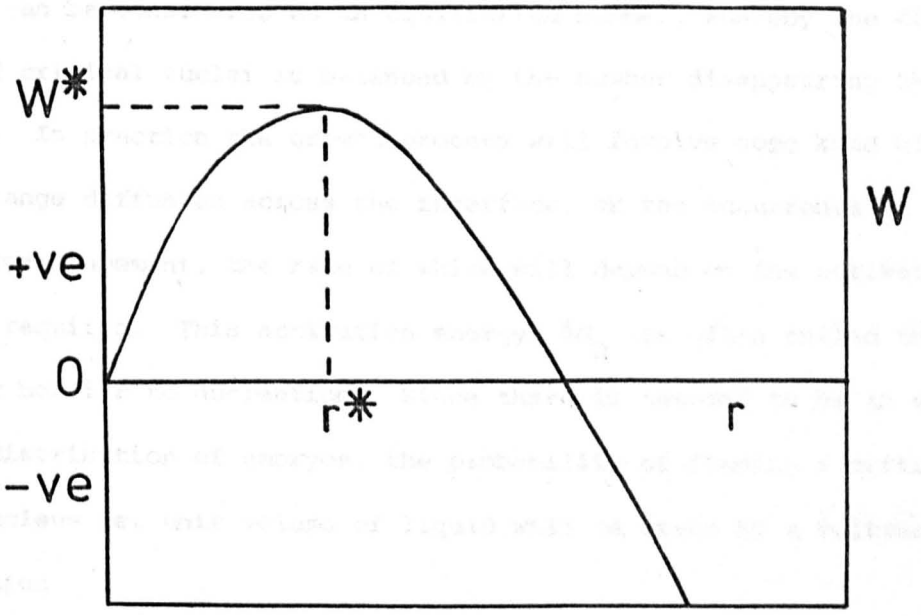

equations are discussed in a later chapter. W*, which is the maximum change in free energy, is referred to as the thermodynamic barrier to nucleation. Once an embryo achieves a free energy of W*, it can become a stable nucleus by growing larger.

The process of nucleation can therefore be considered in terms of the rate at which critical nuclei are able to form and how quickly they subsequently grow. Embryos are assumed to grow by unimolecular steps. If this growth process is not too fast, then a steady state distribution of embryos will be set up. Thus the number of critical nuclei can be considered as an equilibrium number, whereby the formation of critical nuclei is balanced by the number disappearing through growth. In practice the growth process will involve some kind of short range diffusion across the interface, or the occurrence of a local rearrangement, the rate of which will depend on the activation energy required. This activation energy, ΔG_D is often called the kinetic barrier to nucleation. Since there is assumed to be an equilibrium distribution of embryos, the probability of finding a critical size nucleus per unit volume of liquid will be given by a Boltzmann expression

$$p(r^*) = \exp\left(-\frac{W^*}{kT}\right) \tag{1.25}$$

The probability of a unimolecular jump occurring is also given by an exponential expression. Thus the probability of a critical nucleus increasing in size by one molecule is given by

$$p(n^* \rightarrow n^* + 1) = \exp\left(-\frac{\Delta G_D}{kT}\right) \tag{1.26}$$

Hence the rate of nucleation, I, will be given by

$$I \propto p(r^*)\ p(n^* \rightarrow n^* + 1) \tag{1.27}$$

$$= A \exp\left(-\frac{W^*}{kT}\right) \exp\left(-\frac{\Delta G_D}{kT}\right) \tag{1.28}$$

where A is a constant, often referred to as the pre-exponential factor. An approximate value of A is given by

$$A \simeq N_V \frac{kT}{h} \tag{1.29}$$

where N_V is the number of 'molecules' or 'formula units' of the component per unit volume in the liquid. It can be shown that a more rigorous treatment of the nucleation process still gives the same expression as equation (1.28). The constant A, however, does depend on the exact assumptions made and it is in fact a more complex function of temperature.

Equation (1.28) was derived for nucleation in a one component liquid. A similar approach can also be used for nucleation in multicomponent liquids. However, the probability of finding a critical sized nucleus will be reduced in proportion to the mole fraction of the nucleating component. Thus in general equation (1.28) is multiplied by the mole fraction of the crystallising component. As before, W^* is a function of ΔG and σ. ΔG in multicomponent systems has already been discussed. σ, the energy associated with unit area of the interface, now depends not only on the change in molecular order which occurs in the region of the interface, but also on the chemical composition gradient which must be present at the crystal-liquid interface. The kinetic barrier to nucleation, ΔG_D is also more

complex. In addition to the molecular reorientations required to form an ordered crystal, 'unmixing' also has to occur whereby the remaining uncrystallised liquid becomes slightly depleted in the nucleating component. Thus the kinetic barrier is now determined by relatively long range diffusion processes, in which ΔG_D may probably be identified with the activation energy for diffusion of the most slowly moving component.

Consider now the variation of I with temperature. ΔG_D in equation (1.28) is expected to be relatively insensitive to temperature change, but W* (equation (1.23)) decreases with supercooling. In Figure 1.5 normalised nucleation curves (I/A vs. T) are plotted for a one component system in which the heat of fusion is 10 Kcals $mole^{-1}$ and the melting point is 1600°K (1327°C). The curves are plotted for various values of σ and ΔG_D. In each case the nucleation rates increase very rapidly with supercooling up to a maximum at temperature T_{max}, and then decrease again. If the lowest experimentally observable nucleation rate is fixed at 1 cm^{-3} sec^{-1} and the theoretical value of A is taken as 10^{35} cm^{-3} sec^{-1}, then no observable nucleation is expected to occur until the supercooling corresponding to $I/A = 10^{-35}$ is attained. This kind of behaviour is found to occur by experiment, and the temperature at which the nucleation rate suddenly increases is called the critical nucleation temperature, T_C. The value of T_C is sensitive to both changes in σ and ΔG_D. From Figure 1.5 T_C decreases as σ or ΔG_D increase. The position of the maximum nucleation rate, T_{max} also depends on σ and ΔG_D. Increasing σ decreases T_{max} (curves a,b and c,d) whereas increasing ΔG_D increases T_{max} (curves a,c and c,d). This causes curves of the same ΔG_D but different σ to be close at low temperatures but approach T_m apart,

FIG. 1.5. THEORETICAL NUCLEATION CURVES CALCULATED FROM EQUATION 1.28.

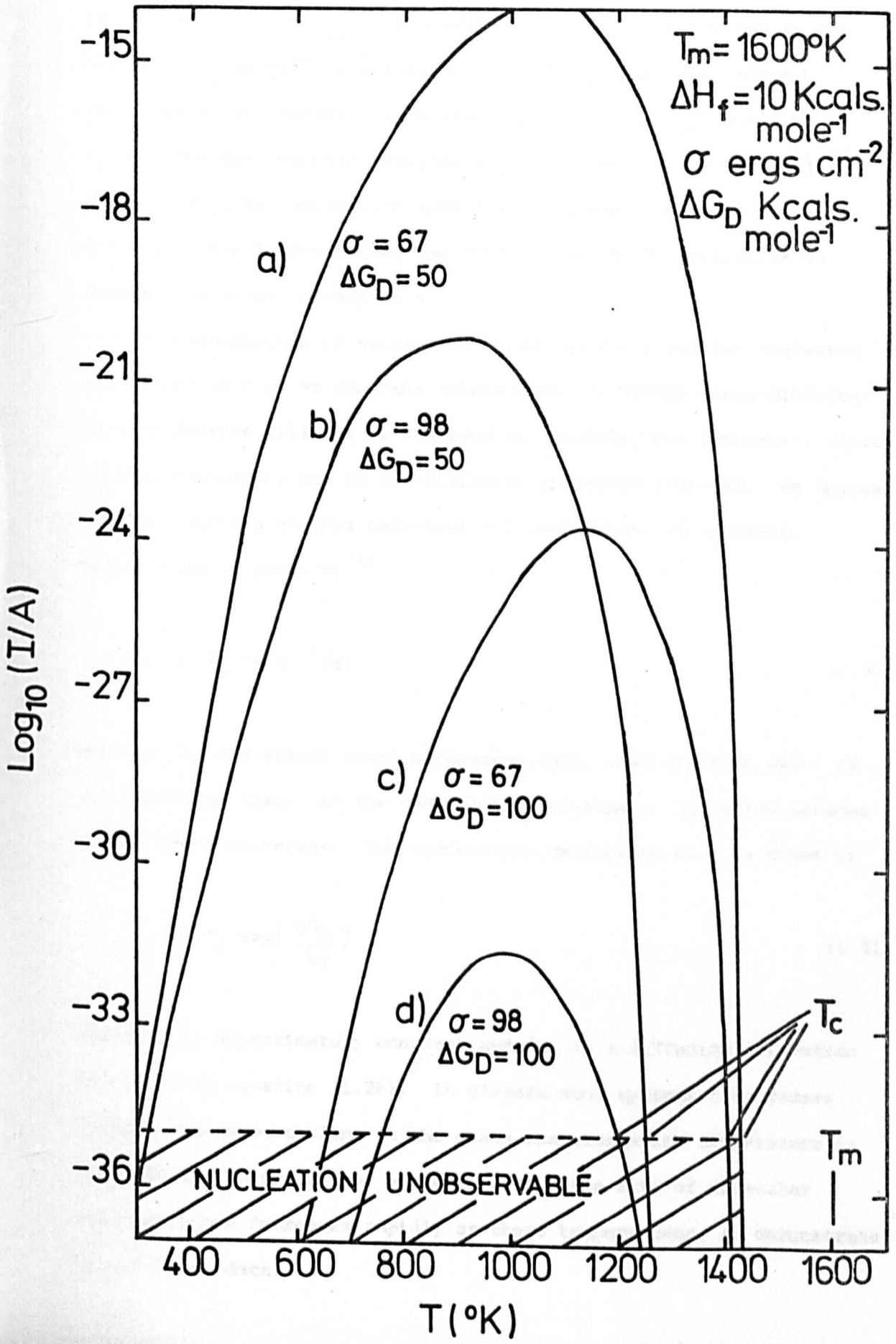

whereas curves of the same σ but different ΔG_D are close near T_m and far apart below T_{max}. It should be noted that a maximum in the nucleation rate would still occur even if ΔG_D were zero, since σ also opposes the nucleation process. In this case T_{max} would be at $T_m/3$. For one component liquids ΔG_D is assumed to have a similar value to ΔG_η, the activation energy for viscous flow. The use of viscosity data in describing the kinetic barrier to nucleation is referred to later in Chapter 4.

The description of nucleation theory so far given has neglected the effect of time at constant temperature. A steady state distribution of embryos will not be achieved immediately, but requires a finite time to establish, due to the diffusion processes involved. An approximate description of this behaviour for small times at constant temperature is given by[4]

$$I = I_o \exp(-\tau/t) \qquad (1.30)$$

where I_o is the steady state nucleation rate, t is the time and τ is the induction time. As the temperature decreases, diffusion becomes slower and τ increases. The temperature dependence of τ is given by

$$\tau = \tau_o \exp\left(\frac{\Delta G_D}{kT}\right) \qquad (1.31)$$

where τ_o is approximately constant and ΔG_D is a diffusion activation energy as in equation (1.26). In glassforming systems τ increases rapidly with supercooling as the glass transformation temperature is approached. This would be expected, since the rate of molecular reorientations decreases rapidly at these temperatures, as demonstrated by viscosity data.

Another factor so far ignored, is concerned with the surface energy term of equation (1.22). This equation was derived for the formation of a spherical cluster in which no other phases were involved, besides the crystallising phase and the supercooled liquid. This is referred to as homogeneous nucleation. However, nuclei may also form on any substrate with which the liquid is in contact. When this occurs, the process is called heterogenecus nucleation. The substrate may be the container wall or it may be a solid dispersed throughout the liquid. Figure 1.6 shows a cluster which has formed on a solid surface, the contact angle being θ. Equation (1.22) for the work involved in forming a cluster now becomes

$$W = \frac{V_c \Delta G}{V_m} + S_{\ell c}\,\sigma_{\ell c} + S_{cs}\,(\sigma_{cs} - \sigma_{\ell s}) \qquad (1.32)$$

where V_c is the volume of the cluster

$S_{\ell c}, S_{cs}$ are the surface areas of the liquid-crystal and the crystal-substrate interfaces respectively

and $\sigma_{\ell c}, \sigma_{cs}$ and $\sigma_{\ell s}$ are the interfacial energies between liquid-crystal, crystal-substrate, and liquid-substrate respectively.

The cluster is a spherical cap of radius r. Assuming a static equilibrium between the three phases and also that the substrate is plane, the following equations can be derived:-

$$\sigma_{\ell s} = \sigma_{cs} + \sigma_{\ell c} \cos\theta \qquad 0 \leqslant \theta \leqslant \pi \qquad (1.33)$$

$$V_c = \frac{4}{3}\pi r^3 \left(\frac{2 - 3\cos\theta + \cos^3\theta}{4} \right) \qquad (1.34)$$

FIG.1.6. FORMATION OF A CRYSTAL CLUSTER ON A SOLID SUBSTRATE.

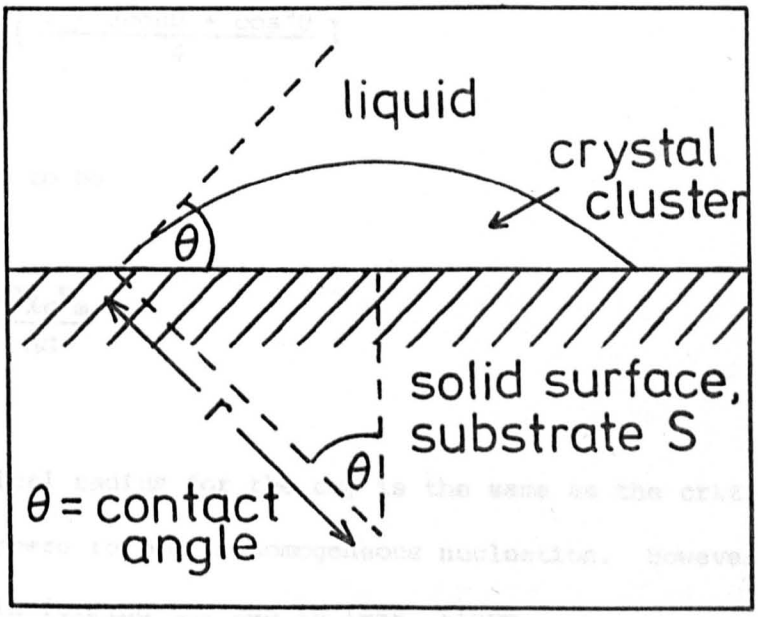

$$S_{\ell c} = 2\pi r^2(1 - \cos\theta) \tag{1.35}$$

$$S_{cs} = \pi r^2 \sin^2\theta \tag{1.36}$$

Substituting these equations into equation (1.32) and differentiating with respect to r, W* is found to be

$$W^*_{het} = \frac{16\pi\sigma^3_{\ell c} V^2_m}{3\Delta G^2} f(\theta) \tag{1.37}$$

where $f(\theta) = \left(\frac{2 - 3\cos\theta + \cos^3\theta}{4} \right)$

and r* is found to be

$$r^* = - \frac{2\sigma_{\ell c} V_m}{\Delta G} \tag{1.38}$$

Hence the critical radius for the cap is the same as the critical radius for a sphere formed in homogeneous nucleation. However, the work involved in forming the cap is less, since

$$W^*_{het} = W^*_{hom} f(\theta) \tag{1.39}$$

and $f(\theta) \leq 1$, $0 \leq \theta \leq \pi$. Thus the presence of the substrate causes a lowering in the thermodynamic barrier to nucleation. A low value of W^*_{het} is obtained if there is high degree of wetting between the crystal phase and the substrate i.e. θ is small. This can be achieved if both crystal phase and substrate have similar crystal structures. There will then be only a slight crystallographic mismatch at the crystal-

substrate interface. Such an idea has been put forward to explain the effect of nucleation agents on crystallisation. In many cases it is found that appreciable internal crystallisation only occurs if such agents are present. Because of this, these agents are referred to as nucleation catalysts.

Whilst W* may be considerably reduced by the presence of a nucleation catalyst, the rate of heterogeneous nucleation also depends on the total area of substrate in contact with the liquid. Equation (1.25) now refers to the probability of finding a critical sized nucleus per unit area of substrate. Using the same reasoning as before, the nucleation rate per unit area of substrate, I_s, is given by

$$I_s = A_s \exp\left(-\frac{W^*_{het}}{kT}\right) \exp\left(-\frac{\Delta G_D}{kT}\right) \tag{1.40}$$

where A_s is a constant. A_s is approximately given by

$$A_s = \frac{N_s}{O_s} \frac{kT}{h} \tag{1.41}$$

where N_s is the number of 'atoms' in the liquid which are in contact with the substrate and O_s is the total surface area of the substrate in the system. (Compare A_s with A in equation (1.29)). The heterogeneous nucleation rate per unit volume is clearly

$$^{v}I_s = {}^{v}N_s \frac{kT}{h} \exp\left(-\frac{W^*_{het}}{kT}\right) \exp\left(-\frac{\Delta G_D}{kT}\right) \tag{1.42}$$

where $^{v}N_s$ is the number of surface substrate 'atoms' per unit volume.

The nucleation theory discussed in this review is often called classical theory, because of several assumptions made during the derivation of the nucleation equation. First, it is assumed that embryos can

be treated as bulk material, the volume free energy per mole being independent of the size of the embryo. Secondly, it is assumed that each embryo has a sharp boundary with a well defined surface energy. In fact there will be a gradient, both in degree of ordering and chemical composition, as one passes from the crystal phase to the liquid. The surface energy will also depend onthe size of the embryo, for very small embryos. Thirdly, the use of the Boltzmann function to describe the distribution of embryos is not strictly correct, although this requires only a slight correction to classical theory. These errors in the classical theory will be further discussed in a later chapter.

1.3 The rate of crystal growth

The rate at which a crystal nucleus grows will depend on the rate at which 'atoms' arrive and remain at the surface of the nucleus. Initially, when the nucleus is microscopic (but greater than r*), the growth rate will also be affected by the curvature of the nucleus-liquid interface, since as the nucleus grows there will be an increase in the interfacial surface energy. However, as the nucleus becomes macroscopic in size, i.e. the nucleus can be considered a crystal, this increase in surface energy can be neglected in comparison with the decrease in volume free energy which occurs. Thus the crystal can be treated as having a planar interface. It should be emphasised, however, that surface energy considerations may still be important in governing the growth of a crystal. This will become apparent in the following discussion.

Normal Growth

Consider first the growth of a crystal where it is assumed that all atoms arriving at the crystal-liquid interface are able to join the crystal to become solid. this occurring equally well at any point on the surface of the crystal. This process, referred to as normal growth, is qualitatively shown in Figure 1.7. In order that atoms may cross the interface between crystal and surrounding liquid, they have to acquire an activation energy $\Delta G_D'$. The number of atoms crossing the interface per unit time will be given by

$$\frac{di}{dt}(\ell \rightarrow c) = s\,\nu_o \exp\left(-\frac{\Delta G_D'}{kT}\right) \qquad (1.43)$$

where s is the number of atoms in the liquid (ℓ) facing the crystal (c) across the interface and ν_o is the frequency at which each atom vibrates due to thermal energy. The exponential term in equation (1.43) represents the probability of finding an atom with sufficient thermal energy to leave the liquid and join the crystal. Once an atom has crossed the interface to the crystal, its energy is reduced, relative to an atom in the liquid by $\frac{v}{V_m}|\Delta G|$, where v is the volume occupied by an atom and V_m is the molar volume of the crystalline phase. Thus for an atom to jump from the solid to the liquid the activation energy required is higher than for the reverse process and equal to $\left(\Delta G_D' + \frac{v|\Delta G|}{V_m}\right)$. The number of such jumps per unit time is given by

$$\frac{di}{dt}(c \rightarrow \ell) = s\,\nu_o \exp\left\{-\left(\Delta G_D' + \frac{v|\Delta G|}{V_m}\right)/kT\right\} \qquad (1.44)$$

FIG. 1.7. FREE ENERGY PER ATOM AS A FUNCTION OF POSITION RELATIVE TO A CRYSTAL-LIQUID INTERFACE.

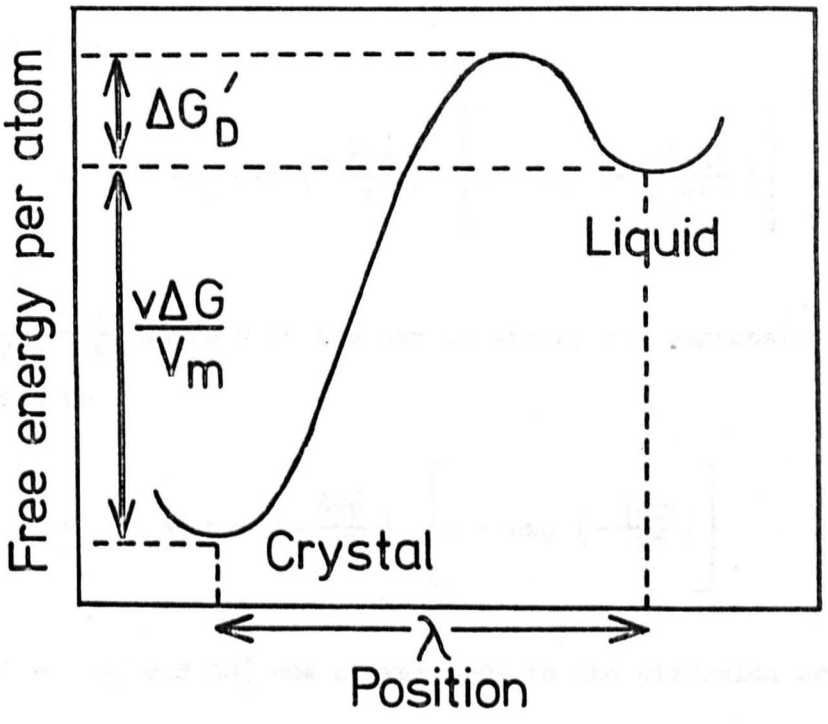

Hence there is a net transfer of atoms from the liquid to the crystal given by

$$\frac{di}{dt}(\ell \rightarrow c) - \frac{di}{dt}(c \rightarrow \ell) = s\,\nu_o \exp\left(-\frac{\Delta G_D'}{kT}\right)\left[1 - \exp\left(-\frac{v|\Delta G|}{V_m kT}\right)\right] \tag{1.45}$$

If s atoms are transferred then the crystal grows by λ, where λ is approximately one interatomic spacing. Thus the growth rate of the crystal is

$$u = \lambda\nu_o \exp\left(-\frac{\Delta G_D'}{kT}\right)\left[1 - \exp\left(-\frac{v|\Delta G|}{V_m kT}\right)\right] \tag{1.46}$$

Since $\frac{v}{V_m k} = \frac{1}{R}$, where R is the gas constant, the expression for u simplifies to

$$u = A' \exp\left(-\frac{\Delta G_D'}{RT}\right)\left[1 - \exp\left(-\frac{|\Delta G|}{RT}\right)\right] \tag{1.47}$$

where $A' = \lambda\nu_o$ and $\Delta G_D'$ now corresponds to the diffusion activation energy per mole.

This equation predicts that a maximum growth rate will be observed, because the thermodynamic term in square brackets increases with supercooling, whilst the kinetic term decreases. Furthermore, the growth rate should be experimentally observable in the vicinity of the melting point or liquidus temperature. These two general predictions are in agreement with experiment. Also, there are two approximations to equation (1.47). First, at small supercoolings

$$1 - \exp\left(-\frac{|\Delta G|}{RT}\right) \simeq \frac{|\Delta G|}{RT}$$

$$\therefore u = \frac{A'|\Delta G|}{RT} \exp\left(-\frac{\Delta G_D'}{RT}\right) \qquad (1.48)$$

Thus u is directly proportional to the thermodynamic driving force. For a one component system $u \propto \Delta T$. Secondly, at large supercoolings

$$\exp\left(-\frac{|\Delta G|}{RT}\right) \ll 1$$

$$\therefore u = A' \exp\left(-\frac{\Delta G_D'}{RT}\right) \qquad (1.49)$$

Hence $\ell n\ u$ is proportional to $^1/T$ and an estimate of $\Delta G_D'$ can be obtained. In Figure 1.8 normalised growth rate curves ($^u/A'$ vs. T) are plotted as a function of $\Delta G_D'$ for a one component system in which ΔH_f = 10 Kcals mole^{-1} and T_m = 1600°K (1327°C). Since $A' \sim 10^6$ cms sec^{-1} and the lowest detectable growth rate is approximately 1 μm per hour, $^u/A' = 10^{-14}$ defines the temperature range over which crystal growth is observable. As in the nucleation process, the temperature corresponding to the maximum rate increases as the diffusion activation energy increases. However, the maximum growth rate occurs at much smaller supercoolings than is the case for the maximum nucleation rate (compare Figures 1.8 and 1.5). Thus in practice we expect the growth rate and nucleation rate curves of a given crystalline phase to be quite far apart. It should be mentioned that the diffusion activation energies for growth and nucleation are not necessarily equal for a given system, since the atomic movements involved may be quite different for the two processes.

FIG. 1.8. THEORETICAL GROWTH RATE CURVES CALCULATED FROM EQUATION 1.47.

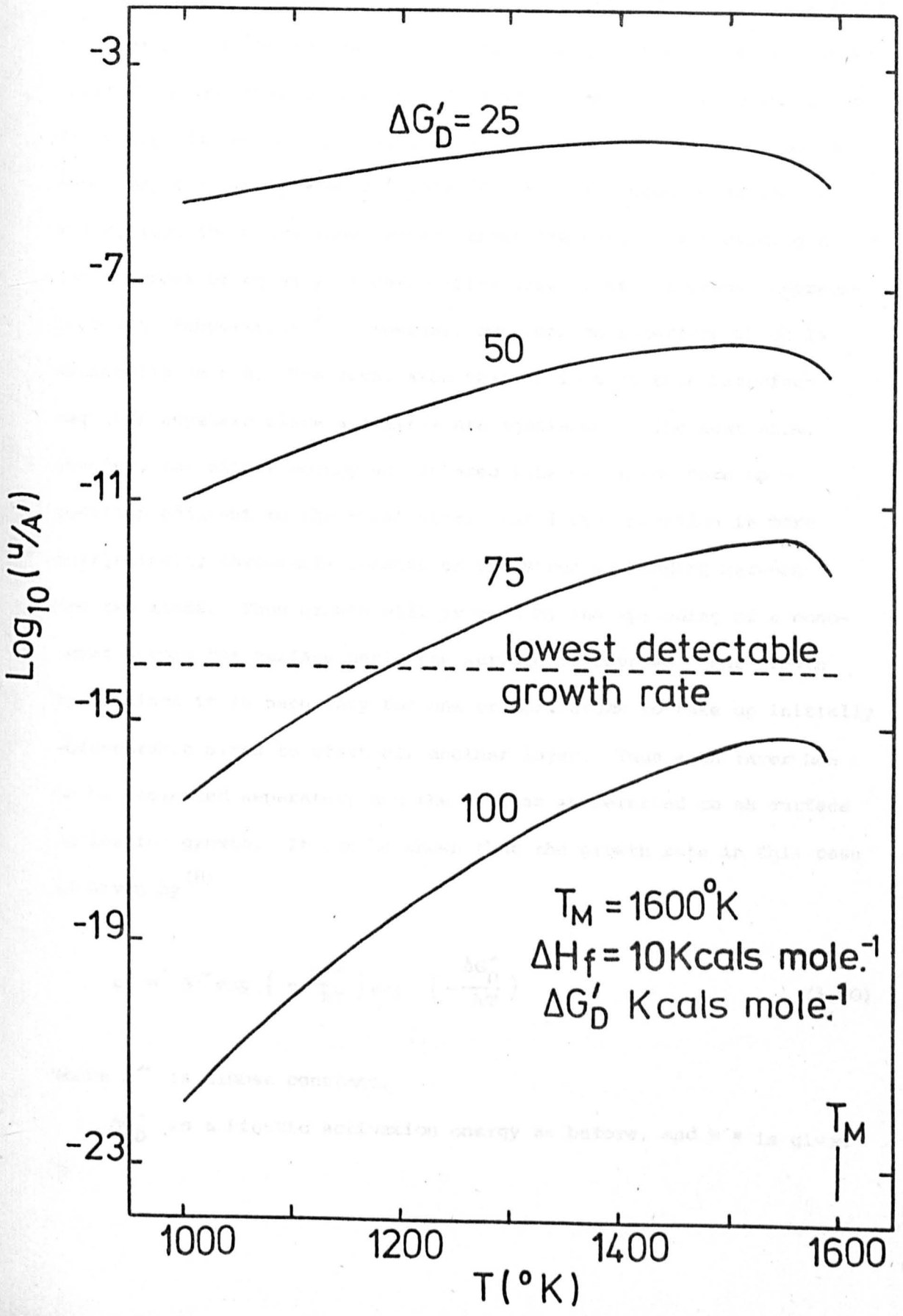

Surface nucleation growth

The growth rate theory so far discussed has assumed that all atoms which arrive at the crystal-liquid interface are able to become incorporated in the growing crystal. Thus atoms can be added to (or leave from) any site on the crystal-liquid interface. In practice such a model may only apply when the interface is very rough on an atomic scale, i.e. there are many imperfections present, thus providing a large number of equally favoured sites which does not change appreciably with temperature[7]. However, consider an interface which is atomically smooth. The first atom that arrives at this interface may join anywhere since all sites are equivalent. The next atom, however, can either occupy an isolated site or it can take up a position adjacent to the first atom. The latter position is more energetically favourable because of the stronger bonding between the two atoms. Thus growth will proceed by the spreading of a monolayer across the surface until the surface is covered. For growth to continue it is necessary for one or more atoms to take up initially unfavourable sites to start off another layer. Thus each layer has to be nucleated separately and the process is referred to as surface nucleation growth. It can be shown that the growth rate in this case is given by[8]

$$u = A'' \exp\left(-\frac{W'^*}{kT}\right) \exp\left(-\frac{\Delta G'_D}{kT}\right) \qquad (1.50)$$

where A'' is almost constant.

$\Delta G'_D$ is a kinetic activation energy as before, and W'^* is given by

$$W'^* = - \frac{k' \sigma_E^2 V_m}{\Delta G} \qquad (1.51)$$

where k' is a shape factor

and σ_E is the specific edge surface energy.

This equation is derived in a similar way to the equations for crystal nucleation (compare equations (1.28) and (1.24) with (1.50) and (1.51)) except the nucleus is now only two dimensional and the thermodynamic barrier W'^* is due to edge surface energy instead of area surface energy. The temperature dependence of surface nucleation growth is more complex than for normal growth. The maximum growth rate does not occur as near to the melting point and for small undercoolings the growth rate is unobservably low (cf. crystal nucleation and the critical nucletion temperature). Also, $\Delta G_D'$ cannot be estimated from a simple log plot of low temperature growth rate data. This type of behaviour is not generally observed for silicate systems.

Screw dislocation growth

Normal growth and surface nucleation growth models are based on the two extreme descriptions of the crystal-liquid interface, viz. atomically rough and atomically smooth. A third model is possible in which the number of interface imperfections (and therefore the number of sites available for growth) is limited. This occurs in screw dislocation growth, whereby growth takes place at step sites provided by screw dislocations intersecting the interface. As shown in Figure 1.9, a ledge is provided which forms a set of sites. As atoms are added to the ledge, it spirals round the dislocation line and continues to provide ledge sites as more atoms arrive at the interface. It can be shown that for a one component liquid the

FIG.1.9. SCREW DISLOCATION IN A CUBIC SOLID SHOWING THE ADDITION OF AN ATOM TAKING PLACE DURING GROWTH.

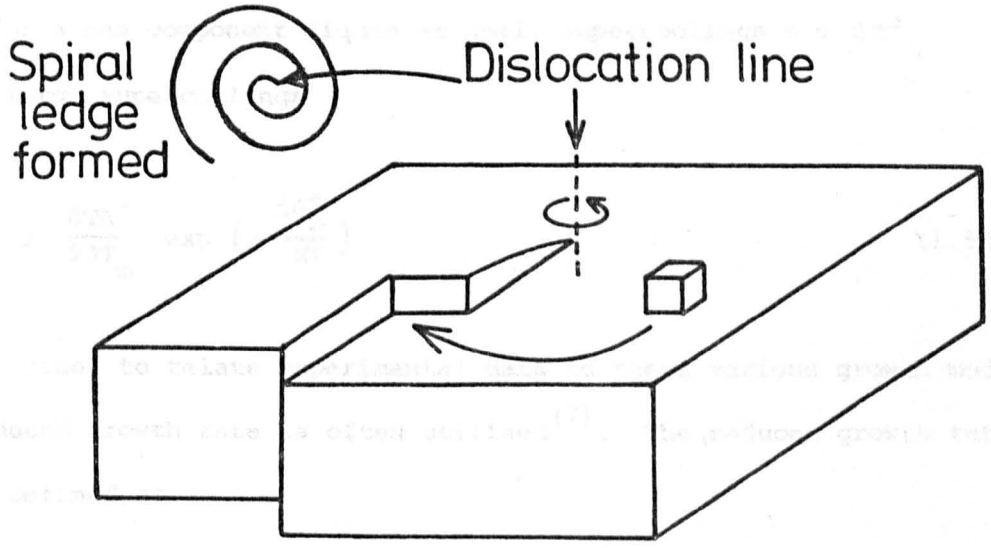

fractional number of such sites, f, on the interface is approximately given by[9]

$$f \approx \frac{\Delta T}{2\pi T_m} \tag{1.52}$$

The resulting growth rate is equal to the normal growth rate multiplied by f, i.e. f is the probability of an atom which arrives at the interface being able to find a growth site. Thus for screw dislocation growth u is given by

$$u \approx \frac{\Delta T A'}{2\pi T_m} \exp\left(-\frac{\Delta G_D'}{RT}\right) \left[1 - \exp\left(-\frac{|\Delta G|}{RT}\right)\right] \tag{1.53}$$

Hence for a one component liquid at small supercoolings $u \alpha \Delta T^2$ and at large supercoolings

$$u \approx \frac{\Delta T A'}{2\pi T_m} \exp\left(-\frac{\Delta G_D'}{RT}\right) \tag{1.54}$$

In order to relate experimental data to these various growth models, the reduced growth rate is often utilised[7]. The reduced growth rate, u_R is defined as

$$u_R = \frac{u\eta}{\left[1 - \exp\left(\frac{|\Delta G|}{RT}\right)\right]} \tag{1.55}$$

where η is the viscosity at temperature T. It is assumed that the diffusion process involved in growth occurs by a similar mechanism to viscous flow. Thus the diffusion coefficient D' can be related to η via the Stokes-Einstein equation given by

$$D' = \frac{kT}{3\pi\lambda\eta} \tag{1.56}$$

where λ is the molecular diameter

and $$D' = D'_o \exp\left(-\frac{\Delta G'_D}{RT}\right) \tag{1.57}$$

The temperature dependence of u_R gives information directly about the temperature dependence of the fraction of preferred growth sites at the interface. In terms of the growth models, the u_R versus ΔT relation for normal growth would be a horizontal line (for all ΔT), for screw dislocation growth a straight line of positive slope passing through the origin (small ΔT), and for surface nucleation growth a curve passing through the origin which exhibits positive curvature (small ΔT).

If the nature of the interface is known it should be possible to predict which model will best describe the experimental growth kinetics. It can be shown that the nature of the interface, i.e. whether it is rough or smooth depends on the entropy of fusion, ΔS_f. A review of the theory is given by Uhlmann[7]. For materials of low ΔS_f (< 2R) the crystal-liquid interface should be quite rough and the growth kinetics are expected to be of the form predicted by the normal growth model. Only a small degree of anisotropy in growth rate as a function of crystallographic orientation is expected. Also, the rate at which a crystal melts above T_m and the rate of growth below T_m should be continuous with the same slope through T_m. For materials of high ΔS_f (> 4-6R) the interface should be smooth and the growth kinetics are expected to be in agreement with the surface nucleation model or the screw dislocation model. A large anisotropy in growth rates is also expected, leading to a faceted interface. In melting, however, the interface will be rough leading to an asymmetry in rates of melting and

growth in the vicinity of T_m.

Finally, in this review of growth rate theory we have not considered the time dependence of the crystal growth rate at a given temperature. A constant growth rate is assumed in one component systems, since the interface is advancing into a region of constant composition. Thus the rate of the process controlling the growth is independent of the interface position and hence the time. However, in multicomponent systems the crystallising phases are often different in composition from the original liquid composition. Hence continual growth of the crystal phase would be expected to involve long range diffusion over distances increasing with time. This would lead to a growth rate proportional to the square root of the time, since the effective diffusion is given by $\sqrt{D't}$, where D' is the diffusion coefficient. It should be remembered, however, that as the remaining uncrystallised liquid becomes richer in the non-crystallising components, the thermodynamic driving force, ΔG will also change, as mentioned in Section 1.1. A further complication is to be expected for multicomponent systems in which surface nucleation is important, since at large supercoolings transient effects will presumably occur, prior to the formation of a steady state distribution of two dimensional embryo on the surface of the growing crystal.

There are, however, certain circumstances in which a crystal is able to grow at a constant rate into a liquid, even though long range diffusion processes are important. First, the growth process may be controlled by the attachment of atoms at the interface rather than by the long range diffusion of atoms through the liquid, i.e. long range diffusion is rapid compared with the attachment rate of atoms. Thus the interface can be regarded as growing into fresh material in which there are virtually no concentration gradients.

Secondly, if the crystal has a long length-to-diameter ratio, rather than being spherical, it is expected to increase in length at a constant rate. This has been predicted theoretically for a needle or thin plate which maintains a constant tip geometry during growth[4]. It should be emphasised that the growth rate is diffusion controlled, but because of the crystal morphology it is possible to obtain steady-state conditions in which the diffusion field does not vary with time.

Finally, linear growth rates can be observed for crystallisation which involves long range diffusion, if the overall composition of the crystallising solid is equal to that of the remaining liquid. The growing crystal will therefore contain several crystal phases, this type of growth being referred to as eutectic growth. Figure 1.10 shows a crystal morphology commonly observed for eutectic growth in a two component system. This is referred to as a lamellar eutectic and consists of regular parallel sheets of one crystal phase, A, interleaved with sheets of the other crystal phase, B. It is thought that one phase nucleates first and then, as this grows, the local enrichment of the component which forms the other phase in the surrounding liquid causes this second phase to nucleate, probably heterogeneously on the solid-liquid interface of the first phase. The lamellar eutectic as a whole advances at a linear growth rate, the interlamellar spacing y_{AB} (i.e. the width of an A + B lamellar pair) remaining constant. At a given temperature there is an optimum value of y_{AB}. In the absence of other considerations there would be a tendency to develop large interlamellar spacings and thereby minimising the interfacial energy associated with the A-B interfaces. However, large spacings are restricted because diffusion of the excess A and B components must occur normal to the

FIG. 1.10. THE GROWTH OF A BINARY LAMELLAR EUTECTIC.

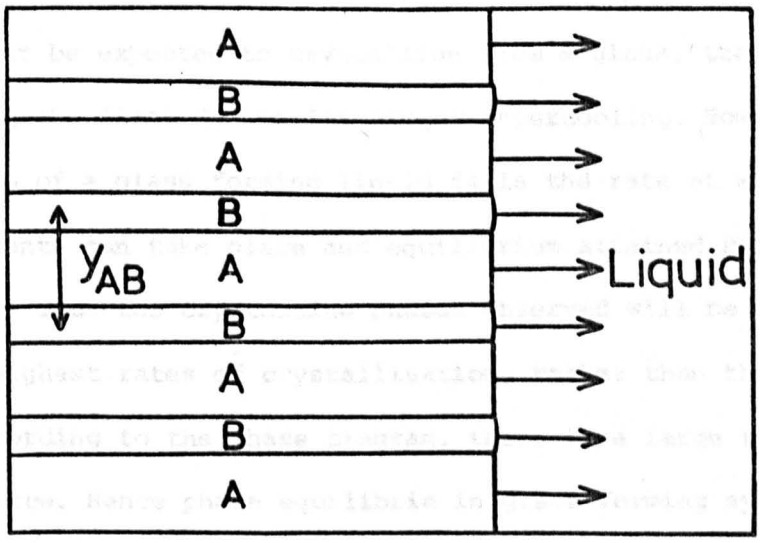

lamellae and parallel to the eutectic-liquid interface. The growth rate is therefore expected to be proportional to D'/y_{AB}. On a semiquantative basis y_{AB} is predicted to be a linear function of $^1/\Delta T$, where ΔT is now the supercooling below the eutectic temperature. Further discussions of eutectic growth can be found in References 1, 2 and 4.

1.4 Phase equilibria in glasses

The equilibrium state of a multicomponent system will generally consist of more than one crystalline phase, when the temperature is below that of the lowest invariant point in the system. Thus several phases might be expected to crystallise from a glass, the primary phase being the first due to its larger supercooling. However, as the temperature of a glass forming liquid falls the rate at which atomic rearrangements can take place and equilibrium attained rapidly decreases. Thus the crystalline phases observed will be those which have the highest rates of crystallisation, rather than those for which, according to the phase diagram, there is a large thermodynamic driving force. Hence phase equilibria in glass forming systems will, in general, be metastable, unless long heat treatments are given.

If the primary phase is first to crystallise, the supercooling can be estimated from phase diagram data. However, if another phase crystallises first, the supercooling is unknown because only equilibrium data can be obtained from a phase diagram. In this case the metastable liquidus is required. As one phase crystallises, the composition of the residual liquid and thus its (metastable) liquidus temperature alters. Figure 1.11 shows a simple binary system A-B in which no immiscibility occurs. In the shaded area both phases A

FIG. 1.11. STABLE AND METASTABLE LIQUIDUS CURVES IN A SIMPLE BINARY EUTECTIC SYSTEM.

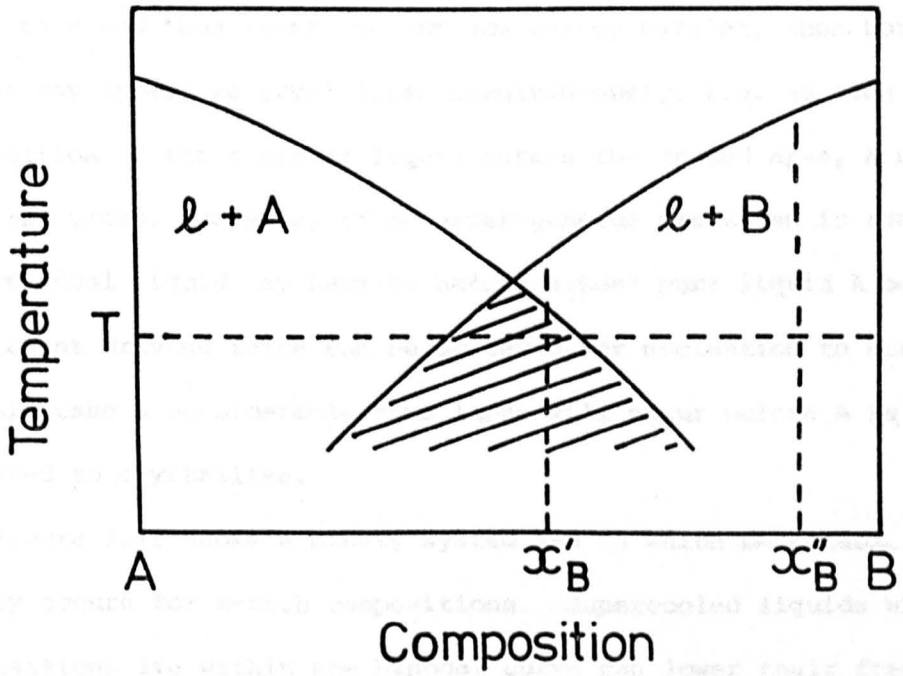

and B can crystallise at temperature T, because ΔG is negative for both phases. Composition x_B' would be expected to nucleate B first since it has the largest supercooling, assuming A and B have the same heat of fusion. However, A may nucleate first if the diffusion activation energy or the interfacial surface energy is lower for that phase. Of course, such factors may prevent both phases from crystallising. Outside the shaded area only one phase can nucleate initially. Thus at temperature T phase B will nucleate first from composition x_B'', if the driving force is large enough. Phase A can only crystallise when the composition of the residual liquid has moved into the shaded area, such that the supercooling is sufficient for nucleation to occur. If A can nucleate heterogeneously on B and thus lower the surface energy barrier, then both phases may appear to crystallise simultaneously, i.e. as soon as the composition of the residual liquid enters the shaded area, A nucleates and grows. However, if no heterogeneous mechanism is available, the residual liquid may have to become almost pure liquid A before sufficient driving force can be achieved for nucleation to occur. In this case a considerable time lapse will occur before A is observed to crystallise.

Figure 1.12 shows a binary system A-B in which metastable immiscibility occurs for B-rich compositions. Supercooled liquids whose compositions lie within the binodal curve can lower their free energy by separating into two liquids. The process of liquid-liquid separation is generally observed to be rapid relative to the process of crystal nucleation, one of the main reasons being the low interfacial surface energy between two liquids as compared with that between a crystal nucleus and a liquid. Thus compositions in the

FIG.1.12. STABLE, METASTABLE, AND UNSTABLE LIQUIDUS CURVES IN A BINARY SYSTEM EXHIBITING METASTABLE IMMISCIBILITY.

SEE TEXT FOR EXPLANATION OF SHADED AREAS a), b) AND c).

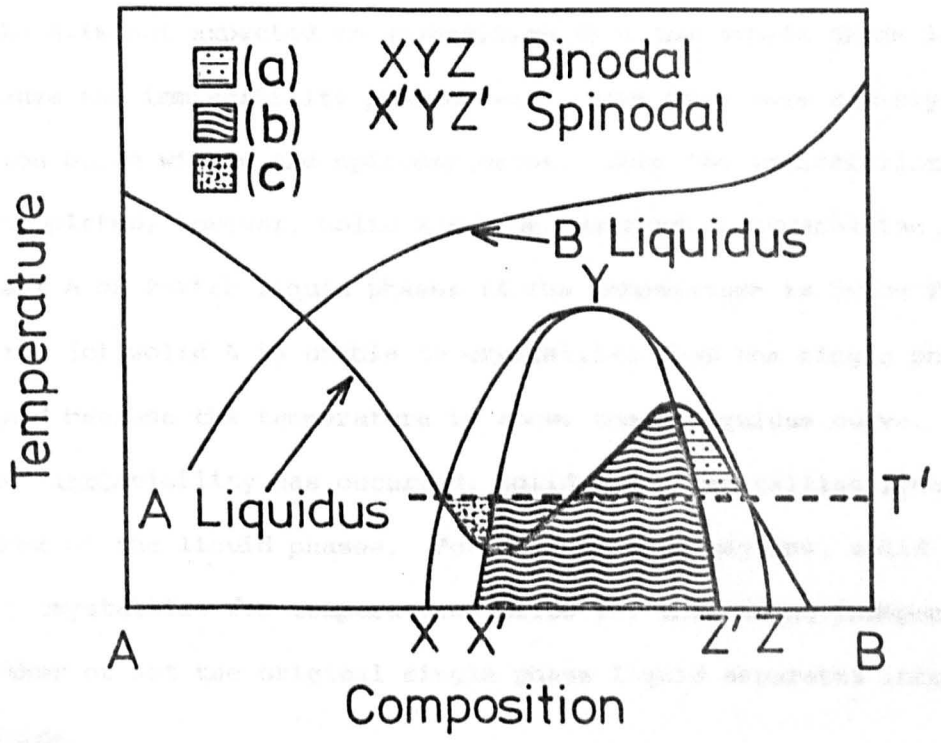

immiscibility region would be expected to separate into two liquids prior to crystallisation occurring. This is particularly the case for those compositions within the spinodal curve, because there is in fact no thermodynamic barrier to liquid-liquid separation in this region, only a kinetic barrier[10]. The liquidus curve for A appears complex, but it can be obtained by considering the free energy curves of solid A relative to those of the supercooled liquid[11,12].

Consider the crystallisation of solid A from compositions within the immiscibility region, assuming that solid B does not crystallise first. In region (a), Figure 1.12, solid A may crystallise from the single phase liquid. However, if the immiscibility process occurs, the solid A will dissolve because the temperature is above the A-liquidus temperature of both A and B-rich liquids. For region (b) solid A is not expected to crystallise from the single phase liquid because the immiscibility process will occur much more rapidly, this region being within the spinodal curve. Once the immiscibility process is completed, however, solid A may be observed to crystallise from either A or B-rich liquid phases if the temperature is below T′. In region (c) solid A is unable to crystallise from the single phase liquid because the temperature is above the A-liquidus curve. Again once immiscibility has occurred, solid A may crystallise from either of the liquid phases. For the unshaded regions, solid A may only crystallise for temperatures below T′, this being independent of whether or not the original single phase liquid separates into two liquids.

Consider now the crystallisation of solid B from compositions within the immiscibility region, assuming that solid A does not crystallise first. Since the B-liquidus temperature (and hence the

supercooling for solid B) is greater for the B-rich liquid phase as compared with the original unseparated liquid, the crystallisation rate of solid B will be increased if immiscibility has already occurred. Within the spinodal curve this will usually be the case. However, for compositions between the spinodal and binodal curves, solid B may crystallise before the immiscibility process occurs. Thus, the composition of the residual liquid may move out of the immiscibility region altogether and immiscibility would not be observed. It is also apparent that the crystallisation of solid B may cause immiscibility to occur in the residual liquid, if the original composition lies to the right of the immiscibility region. This in turn may increase the crystallisation rate of solid A. Similarly, the crystallisation of solid A in an initially homogeneous liquid to the left of the immiscibility region, may cause immiscibility to occur and thereby affect the subsequent crystallisation rate of solid B.

From the foregoing it can be seen that the manner in which a glass forming liquid reaches the equilibrium crystalline state can therefore be complex. Several stages may be involved prior to the equilibrium phases being obtained and in some cases these phases may never occur if the kinetics are too slow.

Review of previous work

1.5 Crystal nucleation in inorganic glass forming systems

The commercial development of glass ceramics was announced by Corning Glass Works in 1957, the work being pioneered by Stookey[13,14] This provoked a great deal of interest in the study of crystal nucleation in glasses. Since the patent compositions generally contained

one or more nucleation catalysts, most research was directed towards understanding the various mechanisms of heterogeneous nucleation and the development of new catalysts. Heterogeneous nucleation is generally brought about by providing sites within the bulk of the glass upon which the desired crystalline phases can nucleate due to the lower interfacial energy between site and crystal as compared with that between crystal and glass. Such sites are provided by precipitating in the glass metallic particles (e.g. Pt, Cu, Ag and Au), fluoride crystals (e.g. NaF, CaF_2), or oxide crystals (e.g. TiO_2, titanates, phosphates, ZrO_2). The last class of catalysts is often associated with liquid-liquid immiscibility since the component added to induce nucleation may also enhance this process as well. Detailed accounts of the work on heterogeneous nucleation are given by McMillan[15] and by Berezhnoi[16].

In certain cases uniform internal crystallisation may be possible without the aid of a catalyst, as discussed by Hillig[17]. He showed that the critical nucleation temperatures of barium disilicate $BaSi_2O_5$ in the system $BaO-SiO_2-TiO_2$ could be interpreted by considering the effect of liquidus temperature and viscosity, without resort to the concept of nucleation catalysis. McDowell[18] also demonstrated the apparently homogeneous nucleation of $BaSi_2O_5$, as well as other barium silicates, in the $BaO-SiO_2$ system. More recently, Burnett and Douglas[19,20] observed that nucleation of $BaSi_2O_5$ appears to be homogeneous in the $Na_2O-BaO-SiO_2$ system. This system is of commercial interest, although the patents specify the use of metal nucleation catalysts[21]. It was found that only compositions near the stoichiometric $BaSi_2O_5$ composition and in the vicinity of the glass forming boundary could be made into glass-ceramics. The critical nucleation

temperature, which was found to be a good description of nucleation behaviour, and the liquidus temperature both decreased as the composition moved away from pure $BaSi_2O_5$. Due to the lack of thermodynamic data no quantitative assessment of homogeneous steady state nucleation theory was possible. However, the non steady state nucleation behaviour was found to be in agreement with simple theory, as discussed in section 1.2.

Lithium disilicate, $Li_2Si_2O_5$, is one of the few other crystalline phases which has been found to nucleate homogeneously in glass forming systems. It is of interest since it commonly occurs in many commercial glass-ceramics. The nucleation of $Li_2Si_2O_5$ from $Li_2Si_2O_5$ glass is assumed to be homogeneous since no intentional catalysts are required and several workers have observed similar nucleation rates.[22-25]. Although $Li_2Si_2O_5$ melts incongruently, the $Li_2Si_2O_5$ composition is completely liquid 1°C above the incongruent melting point. Thus the theoretical congruent melting point must almost be identical with the incongruent melting point. (This can be proved by considering free energy diagrams). Hence $Li_2Si_2O_5$ can be treated as effectively a one component system. Since accurate thermodynamic data is known for $Li_2Si_2O_5$, it has thus been possible to critically assess classical nucleation theory.

Filipovich and Kalinina[22] utilised the position of the maximum nucleation temperature in order to compare their experimental steady state nucleation results with theory. By differentiating equation (1.28) with respect to temperature, it can be shown that for a one component system

$$\frac{\Delta G_D}{\bar{\sigma}^3} = \frac{c}{\Delta T^2_{max}} \left\{ \frac{2T_{max}}{\Delta T_{max}} - 1 \right\} \qquad (1.58)$$

where $c = k_5 \left(\frac{T_m V_m}{H_f} \right)^2$

and ΔT_{max} is the supercooling at the temperature, T_{max} for which the nucleation rate is a maximum, I_{max}. Substituting back into equation (1.28) for $\overline{\sigma}^3$

$$\ln I = \ln A - \frac{\Delta G_D}{kT}\left[1 + \frac{(T_m - T_{max})^3}{(T_m - T)^2\,(3T_{max} - T_m)}\right]$$

$$= \ln A - \frac{\Delta G_D}{k}\,\frac{\phi(T)}{T} \qquad (1.59)$$

$$\therefore \ln \frac{I}{I_{max}} = \frac{\Delta G_D}{k}\left\{\frac{\phi(T_{max})}{T_{max}} - \frac{\phi(T)}{T}\right\} \qquad (1.60)$$

Hence ΔG_D can be estimated from equation (1.59) by plotting ln I vs. $\phi(T)/T$ and a normalised nucleation curve may be obtained via equation (1.60). Filipovich and Kalinina found a good fit for $T > T_{max}$, giving a value of 152 Kcals per mole for ΔG_D. However, for $T < T_{max}$ the experimental steady state nucleation rates fell off much faster than theory would predict. This was explained by comparing ΔG_D with ΔG_η, the activation energy for viscous flow. If simple viscosity theory is to explain the rapid rise in viscosity which occurs as the glass transformation temperature, Tg is approached, then ΔG_η must also rapidly increase. Hence it was concluded that ΔG_D is not constant but rapidly rises in the vicinity of Tg. It should be mentioned that below T_{max} appreciable induction times occur in the case of $Li_2Si_2O_5$ [23]. Hence if nucleation densities were only measured for short heat treatment times, the steady state nucleation rates would be underestimated. Whilst some of the low temperature nucleation rates of Filipovich and Kalinina are in error because of this effect, it will be later shown that the steady state theory still predicts higher rates than those actually observed.

Ito et al[24] also analysed the temperature variation predicted by theory. They assumed that equation (1.28) could be approximated as follows

$$T < T_{max} \qquad I = A \exp\left(-\frac{\Delta G_D}{kT}\right) \tag{1.61}$$

$$T > T_{max} \qquad I = A \exp\left(-\frac{W^*}{kT}\right) \tag{1.62}$$

Using experimental data, ΔG_D was estimated from equation (1.61) and $\bar{\sigma}$ from equation (1.62). It will be shown in Chapter 4 that this method of analysis is not correct since W* and ΔG_D cannot be assumed negligible over any of the temperature range where observable nucleation occurs.

Matusita and Tashiro[25] estimated $\bar{\sigma}$ by substituting viscosity data for the diffusion barrier and obtained

$$\ln \eta I = \text{const} - \frac{k_5 \bar{\sigma}^3 V_m^2}{kT\Delta G^2} \tag{1.63}$$

where η is the viscosity at temperature T. They then plotted $\ln \eta I$ vs. $1/T\Delta G^2$ to estimate $\bar{\sigma}$. The data used was for $T > T_{max}$ and assuming the critical nucleus to be spherical σ was found to be 196 ergs cm^{-2}. Matusita and Tashiro also studied sodium disilicate, $Na_2Si_2O_5$, and potassium disilicate, $K_2Si_2O_5$, glasses and found that the nucleation rates I_{Na} and I_K were unobservably low. From equation (1.63)

$$\ln\left(\frac{\eta_{Li} I_{Li}}{\eta_{Na} I_{Na}}\right) = -\frac{1}{k}\left(W^*_{Li} - W^*_{Na}\right) \tag{1.64}$$

and similarly for potassium disilicate. Since no nucleation was observed in $Na_2Si_2O_5$ and $K_2Si_2O_5$ glasses within a certain time at a

given temperature, upper limits could be put on the values of I_{Na} and I_K, e.g. if no nuclei were observed after say, 10^6 seconds, $I < 10^{-6}$ nuclei cm^{-3} sec^{-1}. Substituting these upper limits into equation (1.64) σ_{Na} was found to be 123 to 144 ergs cm^{-2} and σ_K from 88 to 104 ergs cm^{-2}. These values were obtained for $\frac{I_{Na}}{I_{Li}}$ and and $\frac{I_K}{I_{Li}}$ varying from 10^{-5} to 10^{-30}. Hence, as a first approximation there is little change in the values of σ_{Na} and σ_K even if I_{Na} and I_K are overestimated. Since $\sigma_{Li} > \sigma_{Na} > \sigma_K$, it was concluded that σ was not the factor causing the great difference in nucleation behaviour between $Li_2Si_2O_5$, $Na_2Si_2O_5$, and $K_2Si_2O_5$. Furthermore, it was shown that $\eta_{Li} \sim \eta_{Na}, \eta_K$ over the temperature range of interest. It was concluded therefore that the decreasing order of free energy difference per unit volume

$$\frac{\Delta G_{Li}}{V_{m_{Li}}} > \frac{\Delta G_{Na}}{V_{m_{Na}}} > \frac{\Delta G_K}{V_{m_K}}$$

was the main factor influencing the rate of nucleation in these glasses.

James[23] has made a thorough study of time dependent crystal nucleation in two lithium silicate glasses, one close to the lithium disilicate composition and the other containing 35.5 mole % lithia. It was found that the non steady state theory briefly reviewed in section 1.2 accounted satisfactorily for the time dependence of the estimated nucleation densities and also for the temperature dependence of the induction times. Of more importance with respect to this thesis, it provided accurate data on the steady state nucleation rates over nearly all the temperature range where observable nucleation occurs. These results form an important part of a later discussion

concerned with the analysis of experimental data in terms of classical theory.

Recently, Strnad and Douglas[26] have shown that homogeneous crystal nucleation apparently occurs in the well known Na_2O-CaO-SiO_2 system. As in the Na_2O-BaO-SiO_2 system, internal nucleation was limited to a region near the glass forming boundary and near to stoichiometric compositions. The phases which nucleated were the compounds $Na_2O.2CaO.3SiO_2$ (1:2:3) and $2Na_2O.CaO.3SiO_2$ (2:1:3), for which little thermodynamic data are known. However, an attempt was made to calculate ΔG for the nucleation of 1:2:3 by estimating ΔH_f and the activity of 1:2:3 from phase diagram data, as discussed in section 1.1. For a series of three compositions on the section $(100-2x)SiO_2$ xNa_2O $xCaO$, it was shown for the glass which did not undergo internal nucleation, that the thermodynamic driving force at or above the glass transformation temperature was insufficient for the process to occur. Only at temperatures below Tg was the driving force large enough. Thus nucleation was not observed for that glass.

1.6 Liquid-liquid immiscibility in inorganic glass forming systems

Although a detailed discussion of liquid-liquid immiscibility is beyond the scope of this thesis, it is of interest to consider some studies which have been carried out on the kinetics of the process in relation to classical nucleation theory. This type of phase transformation occurs either by a mechanism of nucleation and growth or spinodal decomposition. In the latter case classical theory is not applicable since there is no nucleation barrier to separation, only a diffusional one. Also, spinodal decomposition, which occurs well within the immiscibility region, results in a connected structure and

isolated droplets are not expected to occur. The following discussion is only concerned with immiscibility which is thought to occur by a process of nucleation and growth, i.e. for compositions near the immiscibility boundary.

Hammel[27] measured the nucleation rates of liquid droplets just within the immiscibility region of a $13^{m}/oNa_2O$-$11^{m}/oCaO$-$76^{m}/oSiO_2$ glass. Since the interfacial energy between two similar liquids is expected to be very low, such a process is almost certainly homogeneous. The parameters ΔG_D and σ were obtained independently from nucleation kinetics. ΔG_D was calculated by measuring the growth rate of the droplets as a function of temperature. σ could be calculated via equation (1.23) in the following manner. Glass specimens containing droplets of a uniform size were placed in a gradient furnace. At higher temperatures where the critical radius was greater than the size of the droplets, the droplets dissolved, but at lower temperatures where the critical size was less than the size of the droplets, the droplets grew. The temperature at which the droplets remained relatively constant in size gave an estimate of the solubility temperature for that droplet size. By varying the initial size of the droplets, r* could be measured as a function of temperature. ΔG was estimated empirically from miscibility gap data using the Lumsden solution model. The method consists of working backwards from immiscibility data to obtain the free energy curve of the liquid as a function of composition and temperature. ΔG can then be obtained, as discussed in section 1.1, by drawing a tangent to the free energy curve at the composition of interest. From a plot of r* vs. $^{1}/\Delta G$, σ was found to be 4.6 ergs cm^{-2}. Knowing ΔG_D, σ, and ΔG, Hammel could calculate theoretical nucleation rates, assuming the theoretical value

for the pre-exponential factor. These calculated rates were found to be in excellent agreement with those obtained by experiment. Hammell also found good agreement between the experimental non-steady state behaviour and that predicted by the simple theory mentioned earlier.

Burnett and Douglas[28] made a thorough examination of liquid-liquid immiscibility in the soda-lime-silica system. The kinetics were studied in detail for two compositions, viz. 10 $^{m}/_{o}$ Na_2O. 10 $^{m}/_{o}$ CaO.80 $^{m}/_{o}$ SiO_2 and 12.5 $^{m}/_{o}$ Na_2O.12.5 $^{m}/_{o}$ CaO.75 $^{m}/_{o}$ SiO_2. The first, which was well within the immiscibility region, separated rapidly into droplets just below the immiscibility temperature and grew by a coarsening process. At lower temperatures, the glass separated into two highly connected phases which also grew by a coarsening mechanism. The rapidity of the mechanism and the connected morphology observed suggested that the separation was not occurring by nucleation and growth. However, the second composition, which was very similar to that studied by Hammel, fell near the limit of the immiscibility region and separated slowly as droplets. Furthermore, a temperature range existed, just below the immiscibility temperature, where phase separation failed to occur unless there had been a previous nucleation treatment at some lower temperature. This is the same kind of behaviour as observed in crystal nucleation, where a critical nucleation temperature exists above which no observable crystal nucleation occurs. Although Burnett and Douglas did not quantitatively analyse the steady state nucleation rates in terms of classical theory, they found that the non-steady state behaviour agreed well with the concept of an induction time.

1.7 Nucleation in organic and metallic systems

A more critical test of classical theory is to independently estimate the parameters ΔG_D and σ by experiments completely removed from nucleation phenomena. Such an estimate of ΔG_D is difficult, because the microscopic process involved in nucleation is not clearly identified. In certain simple cases it may be possible to equate ΔG_D with ΔG_η, the activation energy for viscous flow. However, σ can be accurately measured by macroscopic experiments, since according to classical theory the interface between a microscopic nucleus and a liquid is identical with that between bulk crystalline material and liquid.

Heady and Cahn[29] have recently tested nucleation theory in this way. They studied the immiscibility region in the methylcyclohexane (C_7H_{14}) - perfluoromethylcyclohexane (C_7F_{14}) system. Nucleation measurements were confined to the measurement of the cloud point or critical nucleation temperature as a function of composition. Since the pre-exponential factor is approximately given by

$$A \approx N_v \frac{kT}{h} \qquad (1.29)$$

$$= 10^{22} \times 10^{13} = 10^{35} \text{ cm}^{-3} \text{ sec}^{-1}$$

and ΔG_D is approximately equal to ΔG_η i.e.

$$\exp\left(-\frac{\Delta G_D}{kT}\right) \approx 10^{-2} \quad \text{(for the system } C_7H_{14} - C_7F_{14})$$

we obtain from equation (1.28)

$$\frac{W^*}{kT} \approx 76 - \ln I \qquad (1.65)$$

Heady and Cahn actually assumed a factor of 74. Setting (arbitrarily) ln I = 12 at the cloud point and allowing for possible errors in A, ΔG_D, and ln I they obtained

$$\frac{W^*}{kT_c} = 62 \pm 5 \qquad (1.66)$$

$$\therefore \frac{\Delta G}{V_m} = \left(\frac{\sigma^3/kT_c}{3.69 \pm 0.29} \right)^{\frac{1}{2}} \qquad (1.67)$$

The free energy curve of the system as a function of temperature was determined from total vapour pressure measurements. Thus ΔG could be calculated and an estimate of σ obtained from equation (1.67). σ was then independently determined by measuring the capillary rise of a two phase interface at its point of contact with the container wall. This method gave values of σ lower than those predicted by classical nucleation theory. Expressed as a discrepancy in the supercooling required for the cloud point to occur, it was found that the observed supercoolings were much greater than those predicted from the experimental value of σ. Heady and Cahn concluded therefore that bulk free energy properties could not be applied to nuclei. This might be expected in the C_7H_{14} - C_7F_{14} system, because the low values of σ (< 1 erg cm^{-2}) would imply very small critical nuclei (see equation (1.23)). Hence the critical radius would be comparable to the effective interfacial thickness.

Nucleation in metals has also been analysed in terms of the critical nucleation temperature[30]. However, liquid metals have high fluidities and the growth rates are therefore large. Thus the formation of one nucleus may cause a liquid metal to completely crystallise. Hence the presence of even a few heterogeneous sites will mask any

homogeneous nucleation which would otherwise occur. This problem is overcome by forming the liquid metal into a large number of small droplets, most of which will be free of catalytic impurities. Hence nearly all of the droplets will be observed to crystallise at one supercooling. This is found to occur by experiment and σ has been calculated for several metals using an equation similar to (1.67). The results for different metals are reasonably self consistent. Also, they are of the right magnitude when compared with the few independent values of σ available for metals[31].

1.8 Crystal growth in inorganic glass forming systems

An extensive review of crystal growth in one component glass forming systems is given by Uhlmann in terms of u_R and ΔS_f[7]. This type of analysis requires growth rate data over a wide temperature range, especially in the vicinity of T_m, and also the corresponding viscosity data. Germania, GeO_2 and silica, SiO_2 both have high values of ΔS_f. On crystallising GeO_2 exhibits a non faceted interface and as predicted u_R is independent of supercooling over the full range of supercooling investigated. However, the magnitude of the growth rates predicted by the normal model assuming $\Delta G_D^{'} = \Delta G_\eta$ is less than the experimental growth rates by an order of magnitude. SiO_2, growing as cristobalite, also exhibits non-faceted growth and the reduced growth rate is independent of supercooling. Again, the observed growth rates are an order of magnitude greater than those predicted by the normal model. For both GeO_2 and SiO_2 small departures from stoichiometry and small concentrations of impurities affect the magnitude of the observed growth rates and can cause time dependent growth rates. Sodium disilicate, $Na_2Si_2O_5$ has a high ΔS_f ($\sim$ 4R) and on crystallising it exhibits a faceted

interface morphology down to large supercoolings. The reduced growth rate increases with supercooling but is not of the form predicted by the non-normal models. At large supercoolings there is a linear relation between the reduced growth rate and supercooling which may suggest a screw dislocation mechanism. Assuming this mechanism, the experimental growth rates are two orders of magnitude too large.

Several investigations have been made of the growth rates of tetraborate compounds crystallising from their stoichiometric melts. Sodium tetraborate, $Na_2B_4O_7$, ($\Delta S_f \sim 9R$) exhibits a faceted morphology during growth and the kinetics are well described by the screw dislocation model[32]. A correction was made to allow for the slight rise in temperature (estimated at 5°C) which occurs at the crystal-melt interface due to the high growth rates encountered. Strontium tetraborate, SrB_4O_7 has a very high ΔS_f(~ 13R). Very high growth rates were observed and a temperature rise of 60°C was estimated to occur at the crystal-liquid interface at the maximum growth rate[33]. At small supercoolings the crystals were faceted and the kinetics suggested that the rate of two dimensional nucleation at the interface controlled the growth rate. At large supercoolings spherulitic growth was observed, the kinetics being described by the normal model. However, the magnitude of the observed growth rates were greater by several orders of magnitude than those predicted for normal growth. Other tetraborates which have been studied are lead tetraborate, PbB_4O_7[34] and barium tetraborate, BaB_4O_7[35].

Lithium disilicate, $Li_2Si_2O_5$ also has a high entropy of fusion (~ 5R). Growth rate data has recently been obtained up to T_m[36]. As expected a linear relation was found between u_R and the supercooling, implying a screw dislocation mechanism. No comments were made concerning the crystal morphology.

The above results suggest that the crystal growth models give a reasonable description of the growth kinetics observed for one component glasses. A similar analysis of crystal growth in multicomponent glasses is not available due to lack of viscosity data and the difficulty in estimating ΔG. Several studies have been made of crystal growth in Na_2O-CaO-SiO_2 glasses, as reviewed by Uhlmann[7]. In general a maximum growth rate was observed, the growth rates decreasing with decreasing liquidus temperature and increasing viscosity. The growing crystals had a fibrillar habit and unexpectedly grew at a rate independent of time. Uhlmann suggests that this is because the fibril geometry enables long range diffusion to become a steady state process.

An interesting analysis of growth rate data, not based on the reduced growth rate concept, is given by Marshall in a study of crystal growth in the Li_2O-ZnO-SiO_2 system[37]. The growth rates of the primary phases tridymite and lithium zinc silicate ($Li_2O.ZnO.SiO_2$, 1:1:1) were measured for compositions on the section $xLi_2O.xZnO.(1-2x)\ SiO_2$. For a series of glasses in which the primary 1:1:1 phase crystallised, it was assumed that ΔG would be approximately constant if growth rates for the different compositions were compared at identical supercoolings. Thus independent of the growth model assumed, we can write for small supercoolings

$$\ln u \sim \text{constant} - \frac{\Delta G_D'}{RT} \qquad (1.68)$$

(see equations (1.47) and (1.50)), the supercooling being fixed. Since the same crystalline phase is involved for each composition, $\Delta G_D'$ is expected to be reasonably constant. Thus a plot of ln u vs. $^1/T$

should be a straight line of slope $\Delta G_D'/R$. This was very clearly demonstrated for supercoolings of 50, 75 and 100 degrees, suggesting that the kinetic barrier to growth is adequately described by a constant activation energy. Using this value of $\Delta G_D'$ it should be possible to decide on the appropriate growth model without recourse to viscosity data. Marshall also found that the growth rates of either tridymite or the 1:1:1 phase were constant with time at a fixed temperature for all of the melt compositions studied. He suggested this was because the melt composition ahead of the growing crystal dendrites remained constant, the growth occurring too rapidly for long range diffusion processes to become established in the direction of growth.

A constant activation energy was also found for the growth of $BaSi_2O_5$ in the system $Na_2Si_2O_5$-$BaSi_2O_5$ [20]. For a series of three glasses, the growth rates at large supercoolings (i.e. below T_{max}) were plotted according to the logarithm of equation (1.49). As predicted, linear relationships were obtained, each of the same slope. Thus the surface nucleation model (equation (1.50)) is probably not applicable to this system. However the above plot, often referred to as an Arrhenius plot, does not distinguish between the normal and screw dislocation models, because the temperature variation of the site factor f (equation (1.52)) is masked by the exponential term (equations (1.49) and (1.54)) at large supercoolings.

CHAPTER 2

EXPERIMENTAL TECHNIQUES AND PRELIMINARY SURVEY OF THE Li_2O-BaO-SiO_2 SYSTEM

Chapter 2

Experimental Techniques

Preliminary Survey of the Li_2O-BaO-SiO_2 System

The observation of crystal nucleation and growth in silicate glasses is generally straightforward and, as in this thesis, usually involves light microscopy. However, the accurate determination of nucleation and growth kinetics requires homogeneous glasses, accurate temperature control and a careful analysis of micrographs. In this chapter the experimental techniques used to ensure these conditions are discussed. Also, a general survey of the Li_2O-BaO-SiO_2 system is presented. Specific compositions are discussed in detail in Chapter 3.

2.1 Preparation of glasses

A wide range of lithia-baria-silica glasses were prepared from Belgian sand (99.94 $^{w}/_{o}$ SiO_2) and analar reagent grade lithium and barium carbonates. Batches of 600 g were melted in platinum crucibles in electric furnaces, or gas-fired furnaces if temperatures above 1500°C were required. The melting temperatures were usually 150 to 200°C above the liquidus, the total melting time being 5 hours. During this period the glass was stirred for at least two hours, using a platinum tipped stirrer. The melts were finally cast into rods of about 1 cm diameter and allowed to cool in air. No annealing treatment was given since several of the glasses crystallised rapidly once above their annealing temperatures.

This schedule was generally sufficient to produce homogeneous glass. However, glasses rich in baria often had to be crushed and remelted before homogeneity could be attained. The homogeneity could easily be assessed by heat treating a few specimens and observing whether the resulting crystallisation was uniform or not.

Glasses containing no lithia could not be melted as above. The batch had to be first sintered at just below liquidus temperatures for

24 hours. Sintering in platinum crucibles was not possible since the crucible became pitted, hence alumina crucibles were used. No fluxing of the alumina occurred and the batch came out 'clean', as a plug. This was transferred to a platinum crucible and the usual melting procedure followed.

Several of the glasses were analysed and typical results are shown in Table 2.1. It can be seen that there is good agreement between the target compositions and those actually obtained for the melted glasses. This was achieved by allowing for 0.5 $^{w}/_{o}$ loss of Li_2O and 0.2 $^{w}/_{o}$ loss of BaO, both due to volatilisation. Details of the analytical method are given in Appendix A2.1.

2.2 Heat treatment of glass samples

In order to investigate the crystallisation of these glasses, three electric tube furnaces were employed. First, a Kanthal wound furnace was used for heat treating small specimens in the range 400 to 800°C. The temperature could be maintained to within ± ½°C by means of a Eurotherm temperature controller, type 072, using a Pt/Pt:13% Rh thermocouple. A similar thermocouple, located directly above the specimens, was used to measure the temperature. The furnace was calibrated and found to have a constant zone in which the temperature varied by less than 1°C over 2 cms. Thus a stop was placed in the furnace tube and the specimens, when pushed up to the stop in a small ceramic boat, were in the middle of this constant zone. In general it took about 3 minutes for the temperature to become steady after specimens had been placed in the furnace. The removal of specimens had no effect on the set temperature and hence several specimens could be heat treated together and each one removed from the furnace at the

Table 2.1 Results of analysis of Li_2O-BaO-SiO_2 glasses

m/o Li_2O		m/o BaO		m/o SiO_2	
Nominal	Analysed	Nominal	Analysed	Nominal	By difference
8.33	8.13	25.00	24.85	66.67	67.02
16.67	16.65	16.67	16.98	66.67	66.37
26.67	26.72	6.67	6.65	66.67	66.63

appropriate time. The specimens were generally about 3 mms thick, cut perpendicular to the axes of the glass rods.

Secondly, a platinum wound furnace was used for remelting small quantities of glass. This could be operated up to 1500°C. The tempera- was again maintained by a Eurotherm controller using a Pt/Pt:13% Rh thermocouple. This furnace had no constant zone and so the glass was positioned at the hot spot, where a measuring thermocouple was also located. A small 80% Pt:20% Rh crucible of about 3½ cms^3 was used to contain the glass. Due to the high Rh content of the crucible, the glass could be removed, simply by letting the crucible cool to room temperature, when the sample could be 'knocked out' quite cleanly. The crucible was carried on a small ceramic trolley and could be positioned directly under the measuring thermocouple.

Thirdly, a Kanthal wound furnace similar to the first could be programmed to rise at the same steady rate as the differential thermal analysis (D.T.A.) apparatus. Thus phase changes responsible for D.T.A. peaks could be identified by heat treating powdered samples in this furnace for x-ray powder analysis.

All furnace temperatures were monitored by a 'Cambridge' chart recorder, in addition to being accurately measured by a potentiometer.

For nucleation measurements the as prepared glass was inserted directly into the furnace at the nucleation temperature, for times estimated to give observable nucleation densities. It was generally found that little growth occurred during the process of nucleation. Thus the nucleation stage was followed by a crystal growth stage at a higher temperature, the sample being cooled to room temperature between the two stages. Very little nucleation occurred at this growth stage since the growth temperature was generally above the critical nuclea-

tion temperature and the time of growth was usually quite small (less than 30 minutes). The time and temperature chosen for this second heat treatment were such that the nuclei could be grown, in a controlled manner, as large as possible without coalescence occurring. With a little practice this could be judged by eye, since the specimens become increasingly 'milky' as the internally nucleated crystals grow in size.

An important assumption of the above method is that a negligible number of nuclei redissolve on being heated to the second stage. According to classical theory the size of a critical nucleus increases with rise in temperature (equation (1.23)). Thus a nucleus of critical size at the nucleation temperature will redissolve at the growth temperature. However, during the first stage many of the nuclei that reach critical size will continue to grow and will attain a size larger than the corresponding critical size in the second growth stage. Hence most nuclei will be stable to the increase in temperature required to grow them to observable dimensions. It is assumed therefore that the number of spherulites observed after the growth treatment is a good estimate of the number of nuclei formed at the lower temperature. James[23] gives experimental evidence supporting this assumption.

Internally nucleated crystals could sometimes be found in specimens given only a growth treatment. These crystals formed during the cooling of the glass when first poured and in the subsequent heating up to the growth temperature. Consider the 'ideal' nucleation curve shown in Figure 2.1. The usual hump-shaped curve has been replaced by a triangle. For $T_c \geqslant T \geqslant T_{max}$

FIG. 2.1. IDEAL NUCLEATION CURVE.

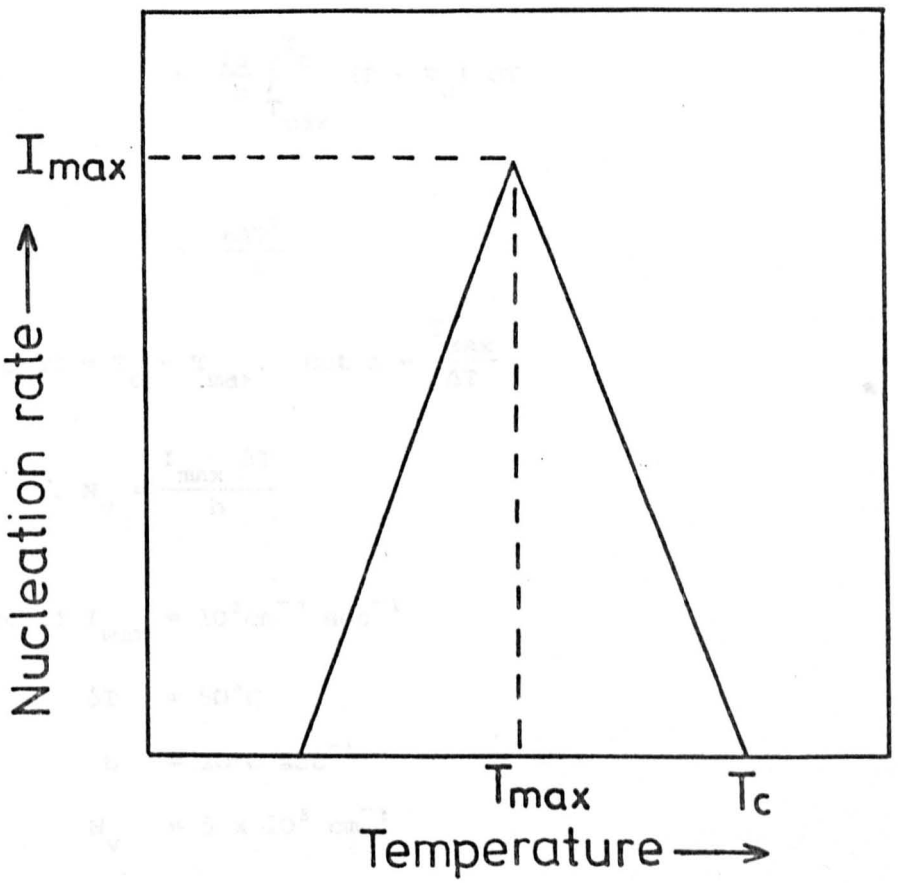

$$I = a(T - T_c) \tag{2.1}$$

where $a = \frac{dI}{dT}$. Hence if a specimen is cooled down from above T_c to room temperature at a rate of $b°C\ sec^{-1}$, the number of nuclei formed in the glass per cm^3 is given by

$$N_v = 2 \int_{T_{max}}^{T_c} I\, dt \tag{2.2}$$

$$= \frac{2a}{b} \int_{T_{max}}^{T_c} (T - T_c)\, dT \tag{2.3}$$

$$= \frac{a\Delta T^2}{b} \tag{2.4}$$

where $\Delta T = T_c - T_{max}$. But $a = \frac{I_{max}}{\Delta T}$

$$\therefore N_v = \frac{I_{max}\, \Delta T}{b} \tag{2.5}$$

Hence if $I_{max} = 10^3 cm^{-3}\ sec^{-1}$

$\Delta T = 50°C$

$b = 10°C\ sec^{-1}$

$N_v = 5 \times 10^3\ cm^{-3}$

The values of N_v calculated from this simple expression are very close to those obtained experimentally for samples only given a growth treatment. This behaviour lends some support to the assumption that nuclei do not readily redissolve once formed. Thus considering the rapid cooling and heating rates involved, any nuclei formed could

have only grown a small amount prior to reaching the growth temperature. While the above estimate of the number of nuclei formed during heating and cooling the glass may seem high, it is generally very small compared with the number formed after a typical heat treatment in the compositions to be discussed. A correction can be made by giving the same growth treatment to both the nucleated specimen and a specimen of the as-poured glass. The difference in N_v can then be attributed to heat treatment at the nucleation temperature. In general, however, nucleation rates were obtained by nucleating several pieces of glass together and removing each one from the furnace at fixed intervals of time. They were then placed together at the growth temperature and removed when sufficient growth had occurred. Thus the number of extraneous nuclei in each specimen, i.e. those not formed during the nucleation treatment, would be the same. In a plot of N_v vs. time, extraneous nuclei were revealed by the presence of a positive intercept on the N_v axis, causing no error in the value of I obtained from the gradient.

Crystal growth measurements were made on samples given a single heat treatment. The samples were similar to those used in the nucleation experiments. Several specimens were inserted in the furnace together, each being removed as required. As a rule of thumb, it was found that in the temperature range studied the time required for observable growth approximately doubled for every 25°C decrease in temperature. In the absence of internal nucleation, the highest temperature for growth rate measurements was determined by specimen size. In this case the surface crystalline layer could grow until the centre of the specimen was reached. However, the presence of even a small number of internal crystal nuclei at elevated tempera-

tures was sufficient to cause rapid crystallisation of the bulk glass and halt the growth of the surface layer. Thus the highest growth temperature was generally limited to that used in the second stage of the nucleation experiments.

2.3 Optical microscopy

The heat treated glass samples were examined in a Leitz reflection microscope at magnifications up to 500 times. The specimens were prepared by mounting on glass microscope slides with pitch, pregrinding with various grades of carborundum and finally polishing with cerirouge (CeO_2). The polished surfaces were then etched in a 10HF:4HCl solution, the strength of which mainly depended on glass composition. Thus for lithia rich compositions 1%HF:0.4%HCl solution was required, whereas for baria rich compositions a 0.25%HF:0.1%HCl solution was sufficient. The etching time was generally 30 seconds, this being the lightest possible etch sufficient to produce contrast. However, James[23] has shown that even somewhat heavier etching treatments produce little error in the measured nucleation densities.

Quantitative information concerning nucleation was sometimes obtained directly by using a calibrated eyepiece graticule. In general, however, nucleation densities were measured indirectly via the optical micrographs obtained. Growth rates were nearly always obtained from direct measurements on heat treated samples, using the eyepiece graticule.

2.4 Method of determining nucleation densities

The number of crystal nuclei per unit volume of heat treated glass was estimated using the technique of De Hoff and Rhines[38] for random plane sections. This involves the measurement of particle intersections made by a random plane section taken through a volume containing the particles. A polished and etched surface is such a section and can therefore be used to measure the number of nuclei present per unit volume. In the Li_2O-BaO-SiO_2 system crystal nuclei generally grew as spherulites which had either a spherical or ellipsoidal shape. It was assumed that for a given heat treatment all spherulites had the same shape, although their sizes might vary.

For spherical spherulites all sections are circular. It can be shown that in this case N_v is given by

$$N_v = \frac{2}{\pi} N_A \bar{Z} \qquad (2.6)$$

where N_A is the number of spherulite intersections per unit area and $\bar{Z}$ is the average value of the reciprocals of the measured diameters of the circular intersections.

Ellipsoidal spherulites have sections which are either elliptical or circular. N_v may be calculated from

$$N_v = \frac{1}{k_1 k_6} N_A \bar{Z} \qquad (2.7)$$

where k_1 and k_6 are shape factors. For prolate ellipsoids (formed when an ellipse is rotated around its major axis) $k_6 = \pi/2$, but k_1 is a function of the ratio of the minor to major axis. For oblate

ellipsoids (formed when an ellipse is rotated around its minor axis) both k_1 and k_6 are functions of the axial ratio. Prolate and oblate ellipsoids can easily be distinguished by searching out the largest circular and elliptical sections. If the largest circular diameter corresponds to the minor axis of the largest ellipse, the ellipsoid is prolate. Alternatively, the ellipsoid is oblate if the largest circular diameter corresponds to the major axis of the ellipse. In this study only prolate ellipsoids were observed. Having determined the type of ellipsoid, the minor to major axis ratio can be estimated by measuring the largest elliptical section as found above. The shape factors for use in equation(2.7) can then be calculated using the equations and graphs supplied by De Hoff and Rhines[39]. $\bar{Z}$ now corresponds to the average value of the reciprocals of the measured minor axes if the ellipsoid is prolate, or to the major axes if the ellipsoid is oblate.

In order to obtain an accurate estimate of N_V at least 200 particles were measured for each heat treatment. For low nucleation densities it was possible to estimate N_V directly by measuring the size of each intersection using a calibrated eyepiece graticule. Knowing the total area of the polished section, or if only part of the section was analysed the area of each field of view, N_A and $\bar{Z}$ could be determined. For high nucleation densities, calculations were made indirectly via micrographs, thus enabling individual intersections to be accurately measured. Large spherulites (> 6 mms on the print) could be measured sufficiently accurately using a ruler, but for small spherulites a calibrated graticule was employed. The graticule was made by photographically reducing a large scale drawing of circles of increasing size. On the final transparency. the circles increased at intervals of 0.25 mms.

The calculations of N_v were considerably speeded up by the use of a programmable Monroe desk calculator. $\bar{Z}$ was calculated from

$$\bar{Z} = \frac{\sum_i N_i \left(\frac{1}{X_1}\right)}{\sum_i N_i} \tag{2.8}$$

where X_i is the size of a diameter, minor axis, or major axis, belonging to the 'i'th class, and N_i the number of such sections. N_v is then given by

$$N_v = \bar{Z} \frac{N}{A} \frac{M^3}{k_1 k_6} \tag{2.9}$$

where M is the magnification at which X_i and the area of the section A were measured, and $N = \sum_i N_i$ is the total number of particle intersections observed.

Occasionally the spherulites formed in a given heat treatment were found to be nearly all the same size. This occurred when the growth rate was very low at the nucleation stage and the nucleation rate very low at the subsequent growth stage. Thus all nuclei are formed together and all achieve the same amount of growth. The expressions for N_v are considerably simplified. Thus for spheres

$$N_v = \frac{N}{A\, d_{max}} M^3 \tag{2.10}$$

where d_{max} is the diameter of the largest section observed, and for prolate ellipsoids

$$N_v = \frac{N}{A\, b_{max}} \frac{M^3}{k_6} \qquad (2.11)$$

where b_{max} is the minor axis of the largest elliptical section observed.

Typical calculations of N_v for both spherical and ellipsoidal spherulites are given in Appendix A2.2.

2.5 Method of determining growth rates

Crystal growth rates were determined above the temperature range where nucleation occurred and, when possible, at temperatures within this range. The main method was to measure the thickness of the crystalline layer which grew from the external surface, as a function of time. If no internal nucleation occurred, it was possible to measure growth rates up to quite high temperatures. For some compositions the dimensions of the internal nuclei were also measured as a function of time. These two methods were found to be in close agreement.

2.6 Other techniques

Identification of crystalline phases was carried out by powder x-ray diffraction using a Philips diffractometer. CuKα radiation was used, the intensity of the diffracted beam being recorded for 2θ values of 10-70°. In general there was good agreement between experimental and published 'd' spacings.

Differential thermal analysis (DTA) was used to further characterize the glasses studied. Samples were finely ground and examined in a

Standata 6-25 instrument using powdered alumina as reference and a heating rate of 10°C min^{-1}. The sample weight could not be kept constant for each run, due to the wide range of densities encountered in the Li_2O-BaO-SiO_2 system. Thus a constant volume of sample was employed, with the same volume of Al_2O_3 as reference. In order to ensure accurate temperature determination, the DTA apparatus was calibrated using compounds of known melting point or those which exhibited a well defined polymorphic transition. DTA provided information concerning the crystallisation of each glass, this being revealed as an exothermic peak on the trace. It was also possible to obtain an estimate of the glass transformation temperature, Tg, from the endothermic dip which occurs prior to the crystallisation peak. This endothermic dip is due to the increase in specific heat which occurs as the glassy network acquires configurational motion. The value of Tg obtained by DTA is dependent on the heating rate used for the analysis. It should be noted that Tg may also be defined in terms of the volumetric and mechanical properties of the glass as a function of temperature. Thus Tg is often defined as the temperature corresponding to a viscosity of 10^{13} poise. In general, different techniques do not give the same value of Tg for a given glass. This is not important for comparing different glasses, if the same technique has been used in each case. However, in order to emphasise the dependence of Tg on the technique used for its evaluation, values of Tg obtained in this study will be referred to as 'DTA Tg'.

General properties of the Li_2O-BaO-SiO_2 system

2.7 Glass formation

Glasses in this system were cast as 1 cm rods and allowed to cool in air. The average cooling rate was about 400°C min^{-1} from the liquidus to the glass transition temperature. The practical limit of glass formation was defined by the failure of these air quenched rods to completely crystallise. Such crystallisation always occurred from the surface to produce columnar type crystals. The resulting rods could be easily fractured. Figure 2.2 shows the limit of the glass forming region defined in this way.

Inside this practical limit of glass formation it was possible to observe a gradual decrease in the tendency to crystallise as one moved away from the glass forming boundary (Figure 2.2). Glasses which underwent extensive surface crystallisation, again exhibited columnar type crystals, but in these cases small lengths of uncrystallised glass still remained. Further inside the glass forming region only slight surface crystallisation was observed. In these cases the crystallisation was confined to a thin surface layer and growth had not proceeded into the bulk of the glass. It was often possible to distinguish individual spherulites on the surface. Finally, completely transparent glasses could be obtained in which no trace of crystallisation was visible. However, the region of completely transparent glasses was limited by the occurrence of liquid-liquid immiscibility for compositions containing more than 70 $^{m}/_{o}$ SiO_2. Such glasses became milky on cooling, unless they were rapidly quenched. Figure 2.2 shows the estimated boundary of the immiscibility region at 600°C as calculated by Charles[40].

FIG. 2.2. GLASS FORMATION IN THE SYSTEM Li_2O-BaO-SiO_2.

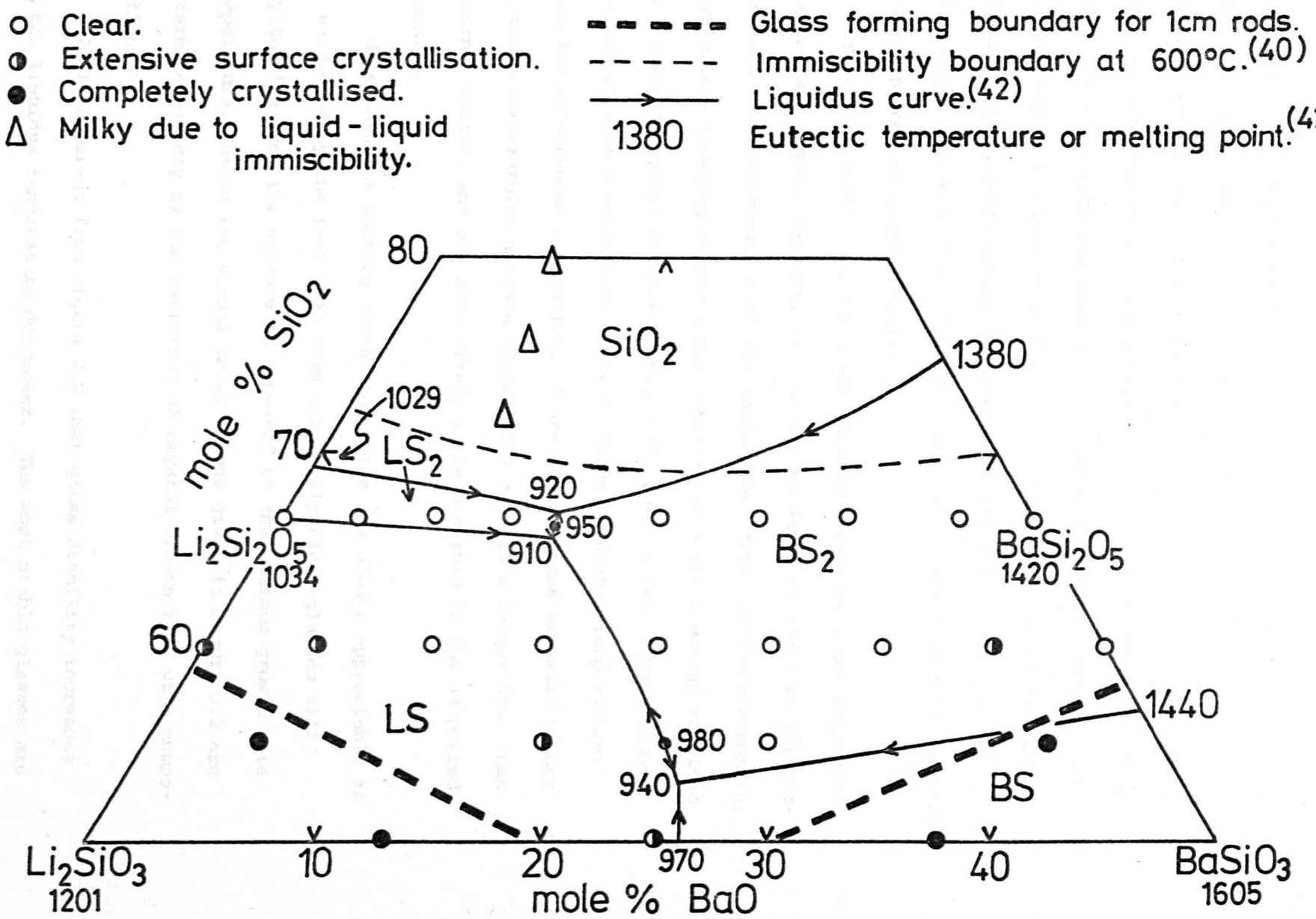

Internal (volume) crystallisation was not observed in the as poured glasses, except for the barium disilicate, $BaSi_2O_5$ composition where in a particular instance one crystal was obtained which had grown to several millimetres diameter. This is because crystal growth rates are in general only appreciable at temperatures which are above those for which internal homogeneous crystal nucleation occurs. Thus if internal nuclei form as a glass cools down, there is little chance of them growing sufficiently to be seen by the eye or the optical microscope. Hence a clear glass may be obtained which in fact contains a large number of crystal nuclei.

Crystal nucleation at the glass surface occurs by a heterogeneous mechanism. Several factors, such as the presence of flaws in the surface and the contamination of the surface by 'dirt' in the atmosphere, may cause a lowering of the total interfacial surface energy involved in forming a crystal nucleus. This lower surface free energy causes the heterogeneous nucleation curve to occur at higher temperatures than for homogeneous nucleation. Since growth rates are also higher at these temperatures surface nuclei will grow to a larger size than internal nuclei, and are more likely to be observed in the as poured glass.

Heterogeneous surface nucleation rates are always appreciable as is evidenced by the fact that even completely clear glasses will crystallise from the surface if reheated to the maximum growth rate temperature. Hence the visual observations given in Figure 2.2 are determined mainly by the variation of crystal growth rate with composition.

It is apparent from Figure 2.2 that glass stability increases as the liquidus temperature decreases. The most stable glasses are

those which are in the vicinity of a eutectic composition. Thus it is possible to obtain some clear glass for the composition 25 $^{m}/_{o}$ Li_2O 25 $^{m}/_{o}$ BaO 50$^{m}/_{o}$ SiO_2, whereas the compositions 50 $^{m}/_{o}$ Li_2O 50 $^{m}/_{o}$ SiO_2 and 50 $^{m}/_{o}$ BaO 50 $^{m}/_{o}$ SiO_2 both crystallise very rapidly. An approximate explanation for this behaviour can be obtained by considering the variation of the maximum growth rate, u_{max}, with liquidus temperature, assuming the normal growth model is applicable. The thermodynamic driving force ΔG is assumed to be ideal, i.e.

$$\Delta G = \frac{-\Delta H_f (T_L - T)}{T_L} \tag{1.8}$$

By differentiating equation (1.47) and setting this equal to zero, T_{max} the maximum growth rate temperature is found to be (see Appendix A2.3)

$$T_{max} = \frac{T_L}{1 + a} \tag{2.12}$$

where

$$a = \frac{R\,T_L}{\Delta H_f} \ln\left(1 + \frac{\Delta H_f}{\Delta G_D'}\right) \approx \frac{R\,T_L}{\Delta G_D'} \tag{2.13}$$

since $\Delta H_f/\Delta G_D'$ is small and less than unity. Substituting back into equation (1.47) for T_{max} we obtain for u_{max}

$$u_{max} = \frac{A'\Delta H_f}{\Delta G_D'} \exp\left\{-\left(1 + \frac{\Delta G_D}{R\,T_L}\right)\right\} \tag{2.14}$$

$\Delta G_D'$ has been assumed constant independent of temperature. If we further assume that $\Delta G_D'$ is also independent of composition for the

growth of a given crystalline phase, then equation (2.14) predicts a decrease in u_{max} as T_L decreases. Hence the amount of surface crystallisation observed will decrease as T_L decreases, in agreement with experiment.

2.8 Differential Thermal Analysis (DTA)

A typical DTA trace obtained from a powdered glass sample is shown qualitatively in Figure 2.3. The position of the endothermic dip at low temperatures corresponds to the glass transition temperature, referred to in this study as 'DTA Tg'. The exothermic peak which occurs at T_x is due to crystallisation of the glass powder. The position of this peak is determined mainly by the growth rate-temperature relationship, unless the internal crystal nucleation rate is high. This is because the glass powder is finely ground and heterogeneous crystallisation can readily occur.

Figures 2.4 and 2.5 show the glass transition and crystallisation temperatures as a function of composition for two constant SiO_2 series, containing $66\frac{2}{3}$ $^m/_o$ SiO_2 and 60 $^m/_o$ SiO_2 respectively. Two interesting features can be observed. First, there is a large increase in the 'DTA Tg' for BaO rich compositions. Secondly, the crystallisation exotherm occurs at progressively higher temperatures as BaO replaces Li_2O. The crystallisation temperature does not vary in the same way as the liquidus temperature, which shows a minimum at the eutectic compositions, but rather it increases with the 'DTA Tg'.

In practice it was found that the 'DTA Tg' and the crystallisation temperature defined the approximate temperature range over which crystal nucleation and growth kinetics could be conveniently measured. Below the 'DTA Tg' crystallisation became increasingly difficult to observe,

FIG. 2.3. D.T.A. TRACE OBTAINED FOR A POWDERED GLASS SAMPLE.

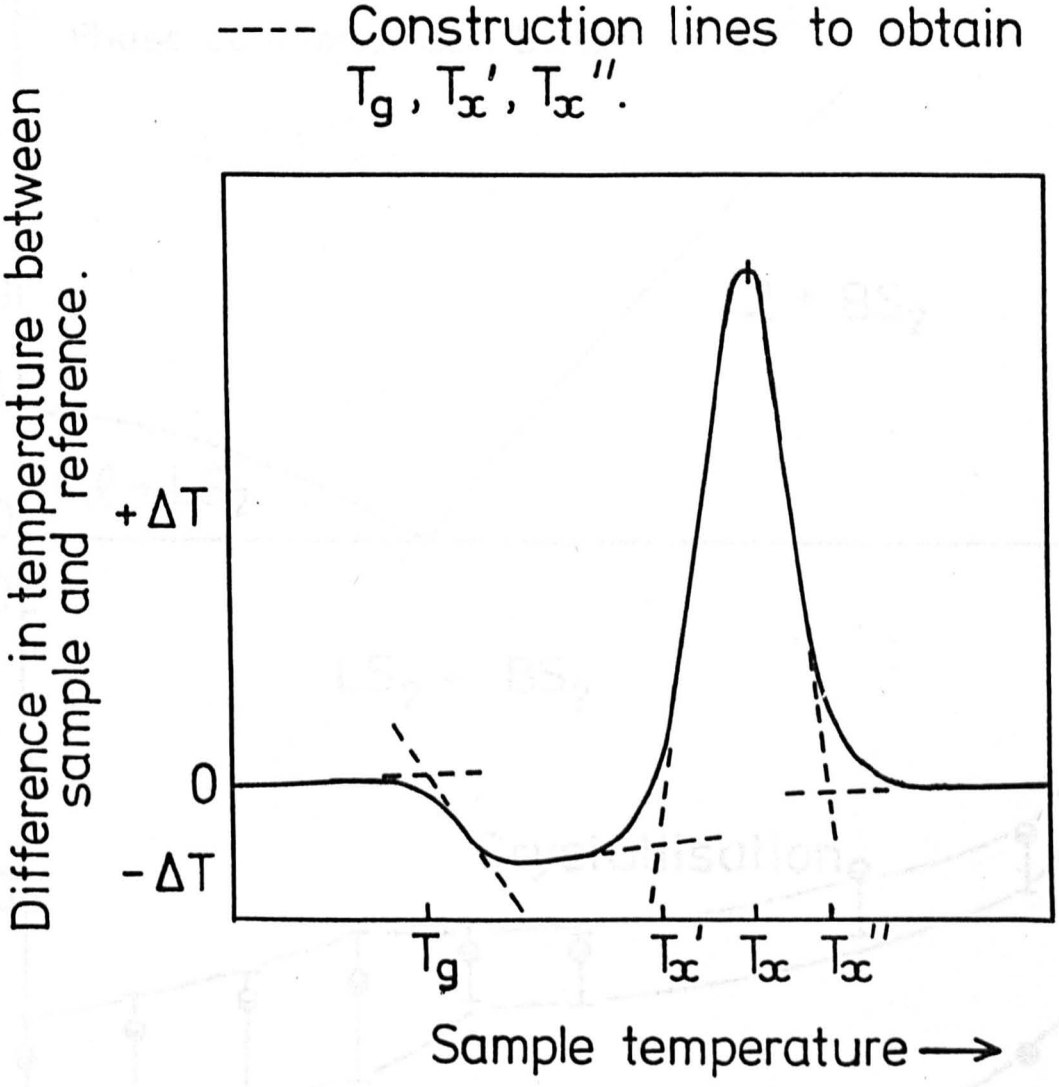

FIG. 2.4. D.T.A. RESULTS FOR THE SYSTEM $Li_2Si_2O_5$ - $BaSi_2O_5$

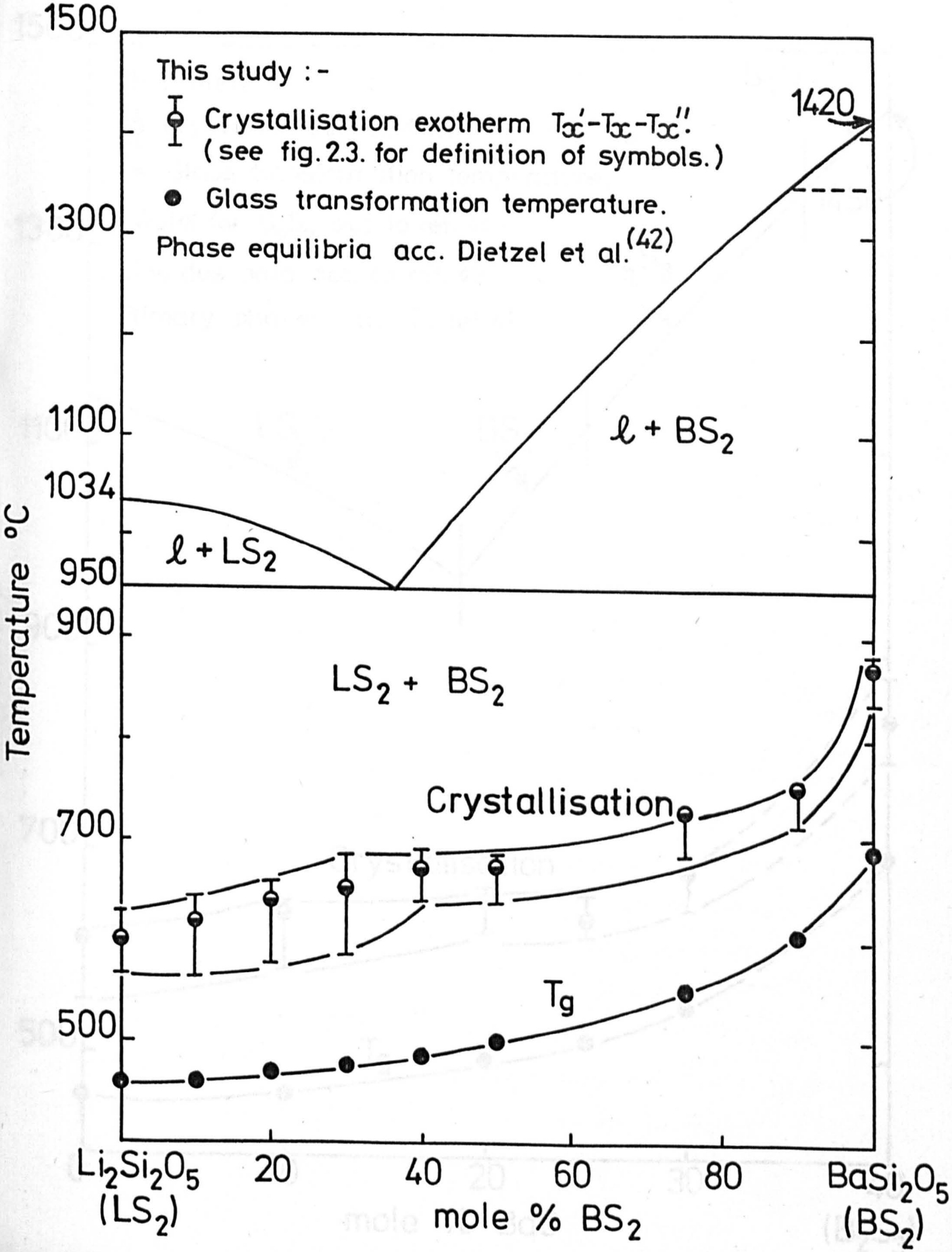

FIG. 2.5. D.T.A. RESULTS FOR THE SECTION $x Li_2O.(40-x)BaO.60\ SiO_2$.

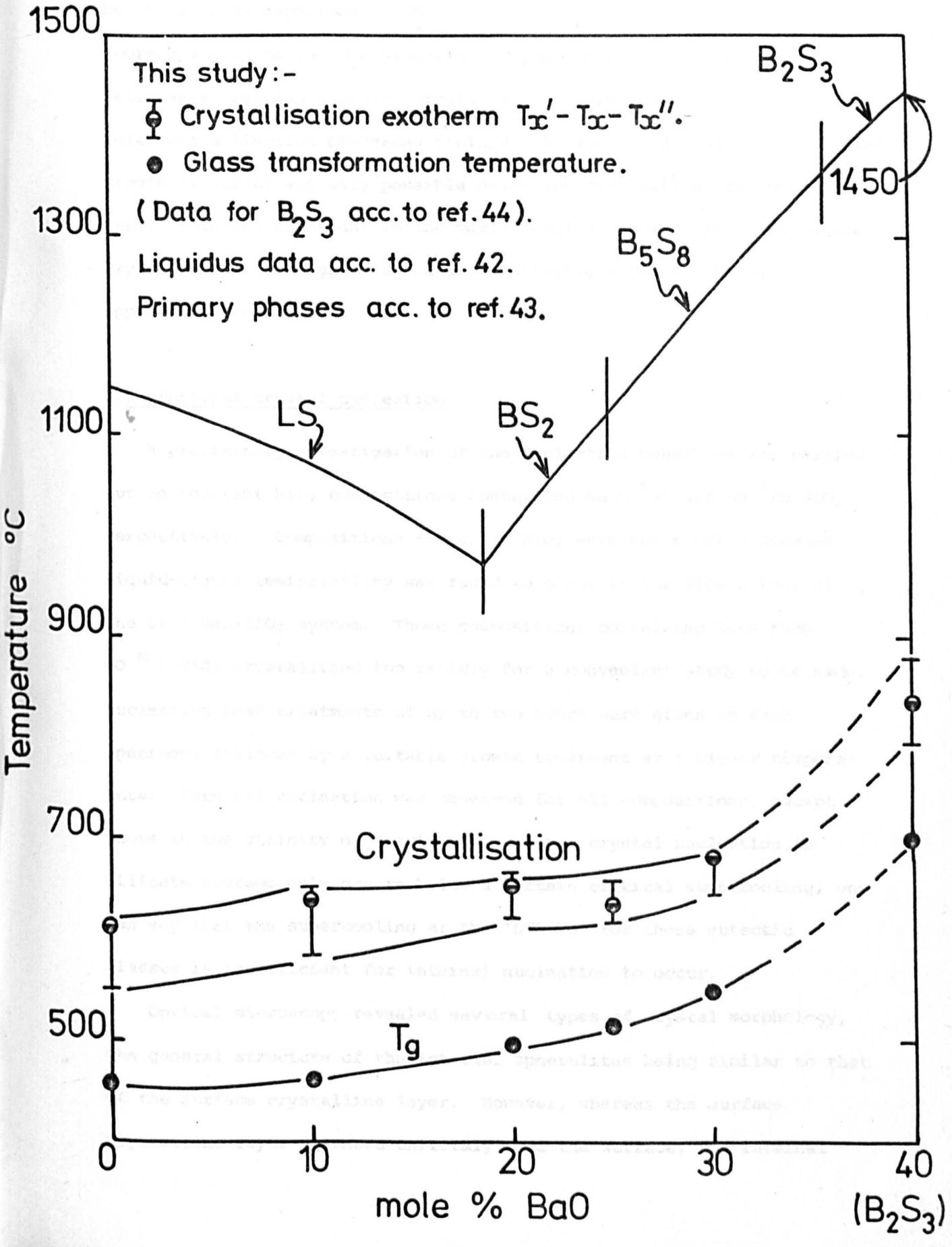

since 'molecular' rearrangements occur on a time scale too large to be observed by experiment. Above the crystallisation temperature (corresponding to the DTA exotherm) crystal growth rates became relatively high and whenever crystal nuclei were present in a glass, bulk crystallisation proceeded rapidly. It was found that the controlled growth of nuclei was only possible below the crystallisation temperature. This was important in the measurement of nucleation rates, where crystal nuclei were grown as large as possible without causing appreciable coalescence.

2.9 Internal crystal nucleation

A preliminary investigation of the nucleation behaviour was carried out on constant SiO_2 compositions containing $66\frac{2}{3}$ $^{m}/_{o}$ and 60 $^{m}/_{o}$ SiO_2 respectively. Compositions richer in SiO_2 were not studied because liquid-liquid immiscibility was found to occur in the SiO_2 corner of the Li_2O-BaO-SiO_2 system. Those compositions containing less than 60 $^{m}/_{o}$ SiO_2 crystallised too rapidly for a convenient study to be made. Nucleation heat treatments of up to two hours were given to each specimen, followed by a suitable growth treatment at a higher temperature. Internal nucleation was observed for all compositions, except those in the vicinity of a eutectic. Since crystal nucleation in silicate systems only occurs below a certain critical supercooling, one can say that the supercooling at the 'DTA Tg' for these eutectic glasses is insufficient for internal nucleation to occur.

Optical microscopy revealed several types of crystal morphology, the general structure of the internal spherulites being similar to that of the surface crystalline layer. However, whereas the surface crystalline layer advanced uniformly from the surface, the internal

spherulites were nct always spherical. The wide range of crystallisation morphologies observed is shown in Figures 2.6 and 2.7.

X-ray diffraction was used to identify the crystallising phases. Specimens given only a nucleation treatment generally exhibited no detectable crystallinity, due to the small size of the nucleated crystals. Two stage heat treatments, however, usually resulted in two or more crystal phases. Since optical microscopy showed only one type of spherulite for any given specimen, it would appear that only one phase nucleates initially, followed by secondary crystallisation of the residual glass in the vicinity of the initial crystal as it grows.

On the $66\frac{2}{3}$ $^{m}/o$ SiO_2 section only two phases could be detected viz. lithium disilicate, $Li_2Si_2O_5$ and barium disilicate, $BaSi_2O_5$. $BaSi_2O_5$ was found to occur as a high or low temperature modification, depending on thermal history and glass composition. In general it was not possible to distinguish between the two forms because the diffraction patterns were often broad or incomplete with respect to the published x-ray data. The presence of both $Li_2Si_2O_5$ and $BaSi_2O_5$ was expected since the $66\frac{2}{3}$ $^{m}/o$ SiO_2 section can be considered as a binary eutectic system of these two components, the eutectic composition being approximately 64 $^{m}/o$ $Li_2Si_2O_5$ 36 $^{m}/o$ $BaSi_2O_5$ (see Figure 2.4). The internal spherulites in $BaSi_2O_5$ rich compositions were found to be radically different in appearance from those present in $Li_2Si_2O_5$ rich compositions, the change occurring in the vicinity of the eutectic composition (see Figure 2.6). Comparison with spherulites in the stoichiometric glass compositions $Li_2Si_2O_5$ and $BaSi_2O_5$ suggested that either $Li_2Si_2O_5$ or $BaSi_2O_5$ nucleated in this system, according to which component was the primary phase. This behaviour is in agreement with the fact that the supercooling is always greatest for the primary phase.

Fig. 2.6 Optical micrographs showing typical internal crystallisation morphologies observed for compositions on the $66\frac{2}{3}$ $^{m}/_{o}$ SiO_2 section of the Li_2O-BaO-SiO_2 system.

Starting from the top:

Composition ($^{m}/_{o}$)		Magnification
Li_2O	BaO	
$33\frac{1}{3}$	0	x200
30	$3\frac{1}{3}$	x50
$26\frac{2}{3}$	$6\frac{2}{3}$	x100
$8\frac{1}{3}$	25	x200
0	$33\frac{1}{3}$	x50

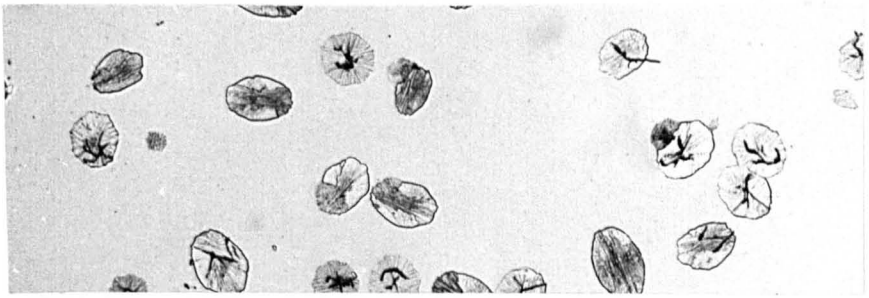

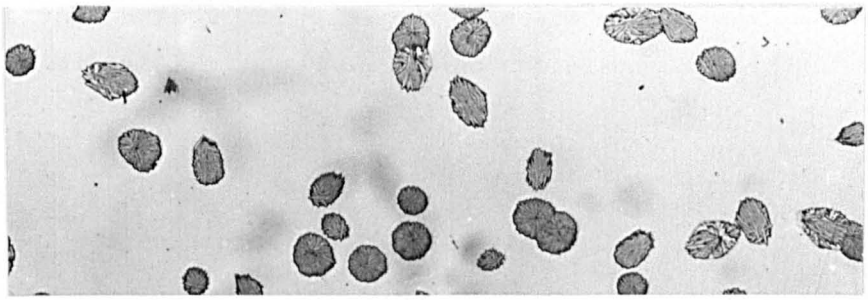

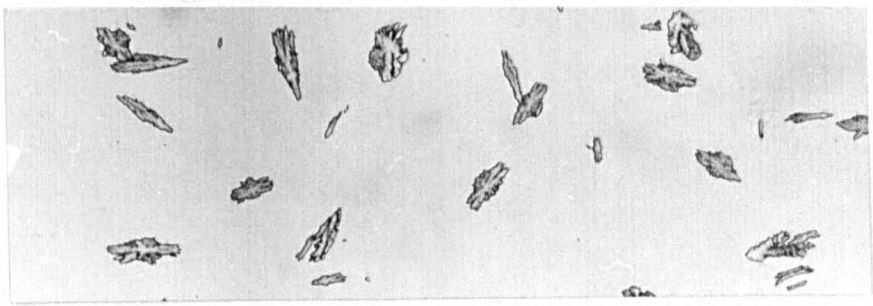

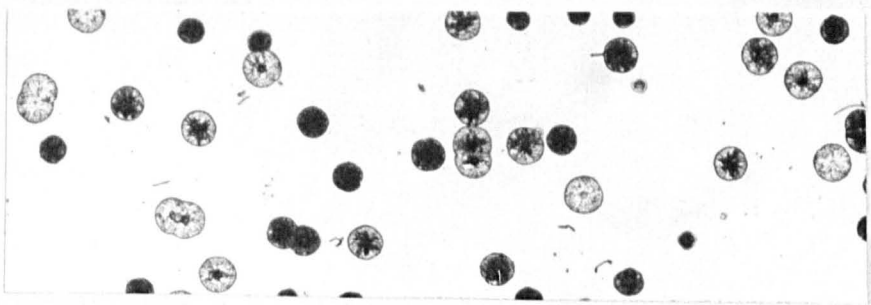

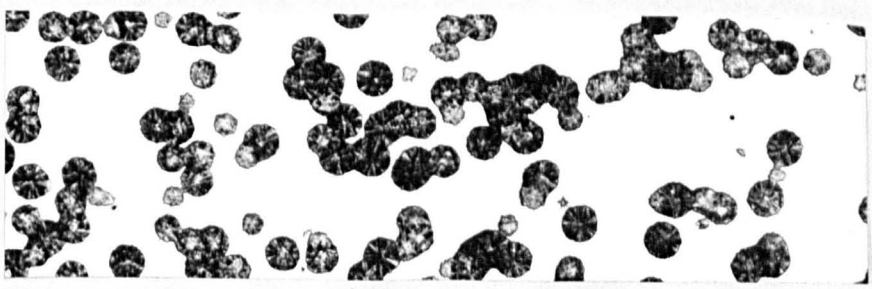

Fig. 2.7 Optical micrographs showing typical internal crystallisation morphologies observed for compositions on the 60 $^{m}/_{o}$ SiO_2 section of the Li_2O-BaO-SiO_2 system.

Starting from the top:

Composition ($^{m}/_{o}$)		Magnification
Li_2O	BaO	
40	0	x500
30	10	x32
15	25	x50
10	30	x100

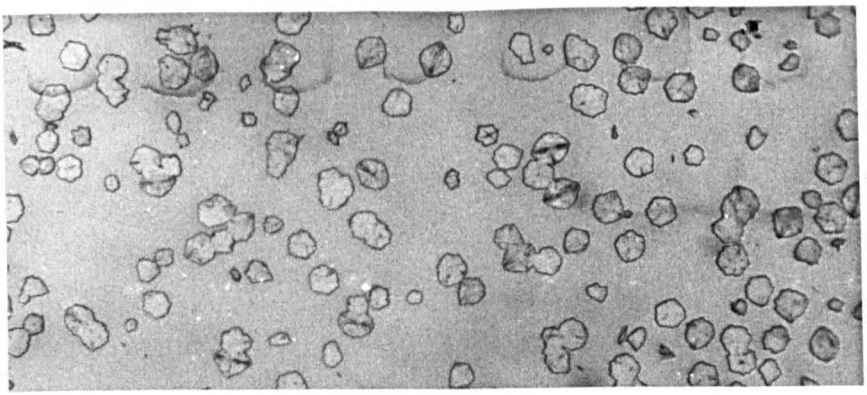

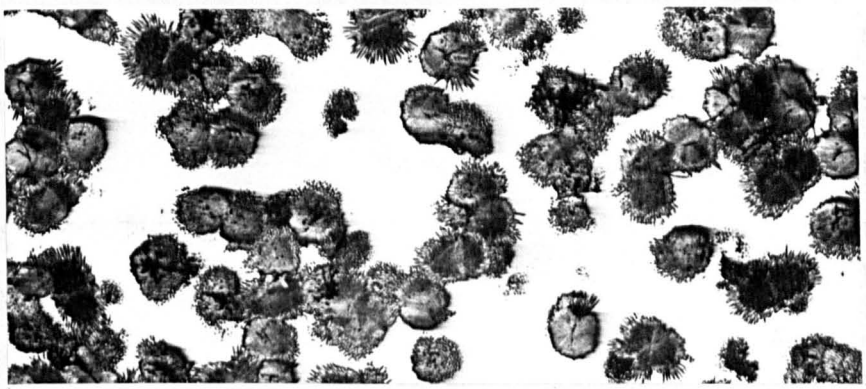

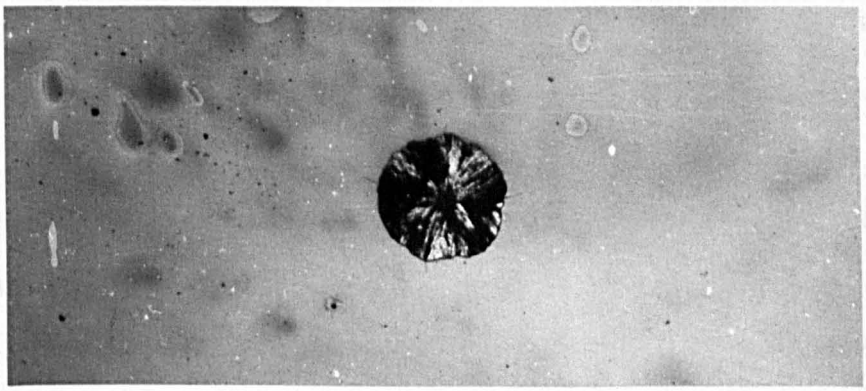

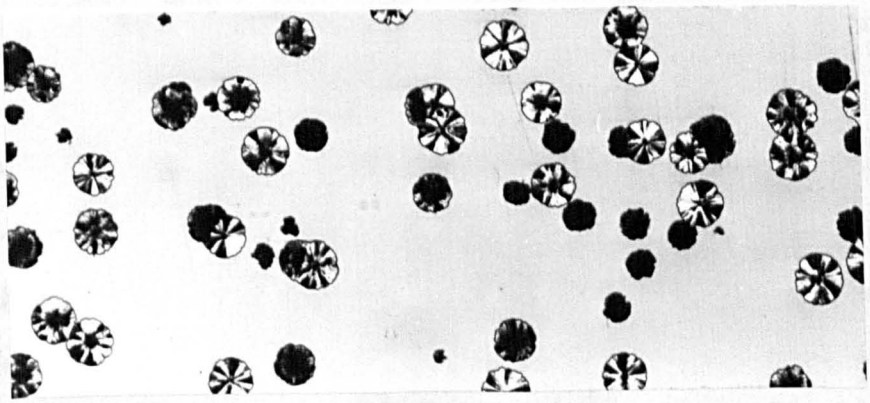

The 60 ^{m}/o SiO_2 section exhibited a more complex crystallisation behaviour. This section is not a simple system, there being several primary phases involved (see Figure (2.5)). X-ray analysis revealed the presence of three crystal phases for some compositions, although in every case optical microscopy revealed only one type of spherulite for a given composition. The 60 ^{m}/o SiO_2 40 ^{m}/o Li_2O glass crystallised to $Li_2Si_2O_5$ plus Li_2SiO_3 (lithium metasilicate) in approximately equal proportions. A comparison of the spherulites with those formed in the stoichiometric $Li_2Si_2O_5$ glass suggested that $Li_2Si_2O_5$ nucleated first, followed by crystallisation of the residual glass to give Li_2SiO_3. However, it should be mentioned that $Li_2Si_2O_5$ and Li_2SiO_3 can form solid solutions containing excess Li_2O and SiO_2 respectively[41]. Thus $Li_2Si_2O_5$ and Li_2SiO_3 may also form by the decomposition of Li_2SiO_3 and $Li_2Si_2O_5$ solid solutions respectively.

The replacement of Li_2O on the 60 ^{m}/o SiO_2 section by increasing amounts of BaO up to 20 ^{m}/o, led to the additional crystallisation of $BaSi_2O_5$, the amount of $Li_2Si_2O_5$ decreasing rapidly relative to that of Li_2SiO_3. This was accompanied by a change in spherulite morphology (see Figure (2.7)). Considering the small amount of $Li_2Si_2O_5$ present, it would appear that the initial nucleating phase has altered to either Li_2SiO_3 or $BaSi_2O_5$. Li_2SiO_3 is considered to be the more likely since $BaSi_2O_5$ was found to nucleate and grow as spherical spherulites on the 66 ^{m}/o SiO_2 section. The composition 60 ^{m}/o SiO_2 20 ^{m}/o Li_2O 20 ^{m}/o BaO has nearly the lowest liquidus temperature on the 60 ^{m}/o SiO_2 section (~ 1000°C) and did not undergo internal nucleation.

Further replacement of Li_2O by BaO up to the composition containing 30 ^{m}/o BaO causes the reappearance of internal nucleation, the spherulites being markedly different from those obtained for the Li_2O

rich compositions described above (see Figure (2.7)). X-ray analysis revealed only the presence of a barium silicate $Ba_5Si_8O_{21}$ (B_5S_8) as a major phase. Thus the spherulites were assumed to be B_5S_8. Unfortunately the composition 60 $^m/_o$ SiO_2 40 $^m/_o$ BaO was not studied in any detail. However, McDowell[18] found that this composition also nucleates internally, the crystalline phase being another barium silicate $Ba_2Si_3O_8$ (B_2S_3), having the same composition as the glass.

Having completed this general survey of crystallisation in the Li_2O-BaO-SiO_2 system, a more detailed study was made of several compositions. The main aim was to quantify the observed crystallisation behaviour in terms of the crystal nucleation and growth theories discussed in Chapter 1. Attention was focused on the $66\frac{2}{3}$ $^m/_o$ SiO_2 section for two reasons. First, the phase equilibria are relatively simple on this section, secondly, a similar section had already been studied in the Na_2O-BaO-SiO_2 system[20]. A detailed study of the 60 $^m/_o$ SiO_2 section was not made because of the more complicated crystallisation behaviour of these compositions. Also, the phase equiibria as determined by Dietzel et al[42] were unclear for this section. Thus, according to Dietzel et al, $BaSi_2O_5$ and $Ba_2Si_3O_8$ form a solid solution which extends into the ternary Li_2O-BaO-SiO_2 system. However, Gunawardane and Glasser[43] have recently shown that the primary phase fields of four barium silicates $Ba_5Si_8O_{21}$, $BaSi_2O_5$, $Ba_3Si_5O_{13}$ and $Ba_2Si_3O_8$ occupy and replace the field of solid solutions shown in the study of Dietzel et al. This modification has little effect on the liquidus temperatures for the 60 $^m/_o$ SiO_2 section. However, beyond the eutectic for BaO rich compositions (see Figure 2.5) three primary phases are present, not a solid solution as was originally

suggested. In light of this recent alteration to the phase equilibria, it has been possible to qualitatively explain the nucleation behaviour of BaO rich compositions on the 60 $^{m}/_{o}$ SiO_2 section. A limited study is presented in Appendix A2.4.

CHAPTER 3

DETAILED PRESENTATION OF EXPERIMENTAL RESULTS FOR THE SYSTEM $Li_2Si_2O_5$ - $BaSi_2O_5$

Chapter 3

3.1 Compositions for which $BaSi_2O_5$ is the primary phase

Whilst $BaSi_2O_5$ is one of the few simple glass forming systems in which internal nucleation apparently occurs without the aid of a nucleation catalyst, its nucleation and growth kinetics had not been measured prior to this study. Thus the determination of the crystallisation kinetics of $BaSi_2O_5$ form an important part of the present work.

The addition of $Li_2Si_2O_5$ to $BaSi_2O_5$, which is equivalent to partly replacing BaO by Li_2O, causes a rapid drop in both liquidus temperature and glass transformation temperature. The former parameter enters directly into classical nucleation theory and therefore it was of interest to measure the change in nucleation kinetics of $BaSi_2O_5$ as the $Li_2Si_2O_5$ content was systematically increased. The glass transformation temperature, T_g, is generally considered to correspond to a constant viscosity value, as discussed in Chapter 2. Thus if the Stokes-Einstein relation is valid for crystal growth, the growth rates at large supercoolings, which are diffusion controlled, might be expected to depend on the value of T_g. This has been studied by measuring crystal growth rates at large supercoolings for a wide range of compositions.

In this section a systematic study of those compositions for which $BaSi_2O_5$ is the primary phase is presented. This includes compositions ranging from 100 ^{m}/o $BaSi_2O_5$ to the eutectic composition 64 ^{m}/o $Li_2Si_2O_5$ 36 ^{m}/o $BaSi_2O_5$. The experimental data is analysed from a theoretical viewpoint in Chapter 4.

3.1.1 Barium disilicate, $BaSi_2O_5$ (T_m = 1420°C)

Preliminary experiments on $BaSi_2O_5$ glass showed that rapid crystallisation occurred at temperatures above 800°C. Thus at 850°C after

20 mins, or 870°C after 10 mins, a large number of spherulites were present throughout the original specimen, very little glass remaining. X-ray analysis revealed only one crystalline phase viz. $BaSi_2O_5$. There are two modifications of $BaSi_2O_5$, a high temperature form (h) stable above 1350°C and a low temperature form (ℓ), these being difficult to distinguish except for the presence of a peak at 2θ equals 25.18 for h-$BaSi_2O_5$ and a peak at 2θ equals 26.00 for ℓ-$BaSi_2O_5$ [45]. For long heat treatment times, especially at high temperatures (≥ 900°C) the observed diffraction patterns were in good agreement with the data for ℓ-$BaSi_2O_5$. Such heat treatments also gave nearly 100% crystallinity. At low temperatures or for short heat treatment times the diffraction patterns exhibited broad peaks which could not be positively identified with $BaSi_2O_5$.

D.T.A. revealed a crystallisation exotherm in the temperature range 835-883°C, as expected from the preliminary experiments. However, a further exothermic peak was observed in the temperature 970-1037°C. In order to determine the cause of this peak, two powdered samples were heat treated at 10°C min^{-1} up to 910°C and 1050°C respectively, and then removed from the furnace for x-ray analysis. The diffraction patterns are shown in Figure 3.1. The specimen heated to 1050°C (curve A) exhibits the main $BaSi_2O_5$ peaks except for the one at 2θ equals 26.65, although it is not possible to distinguish which modification is present. The specimen heated to 910°C (curve B) only exhibits broad peaks, which are in general agreement with the data for $BaSi_2O_5$. Curve B is also typical of specimens heat treated isothermally at low temperatures or for short times. Further information was obtained using optical microscopy. Figure 3.2 shows the microstructures corresponding to curves A and B. It would appear that reorganisation of the spherulites has occurred for the specimen heated to 1050°C. The

FIG. 3.1. X-RAY DIFFRACTION PATTERNS FOR THE COMPOSITION 100 m/o $BaSi_2O_5$.

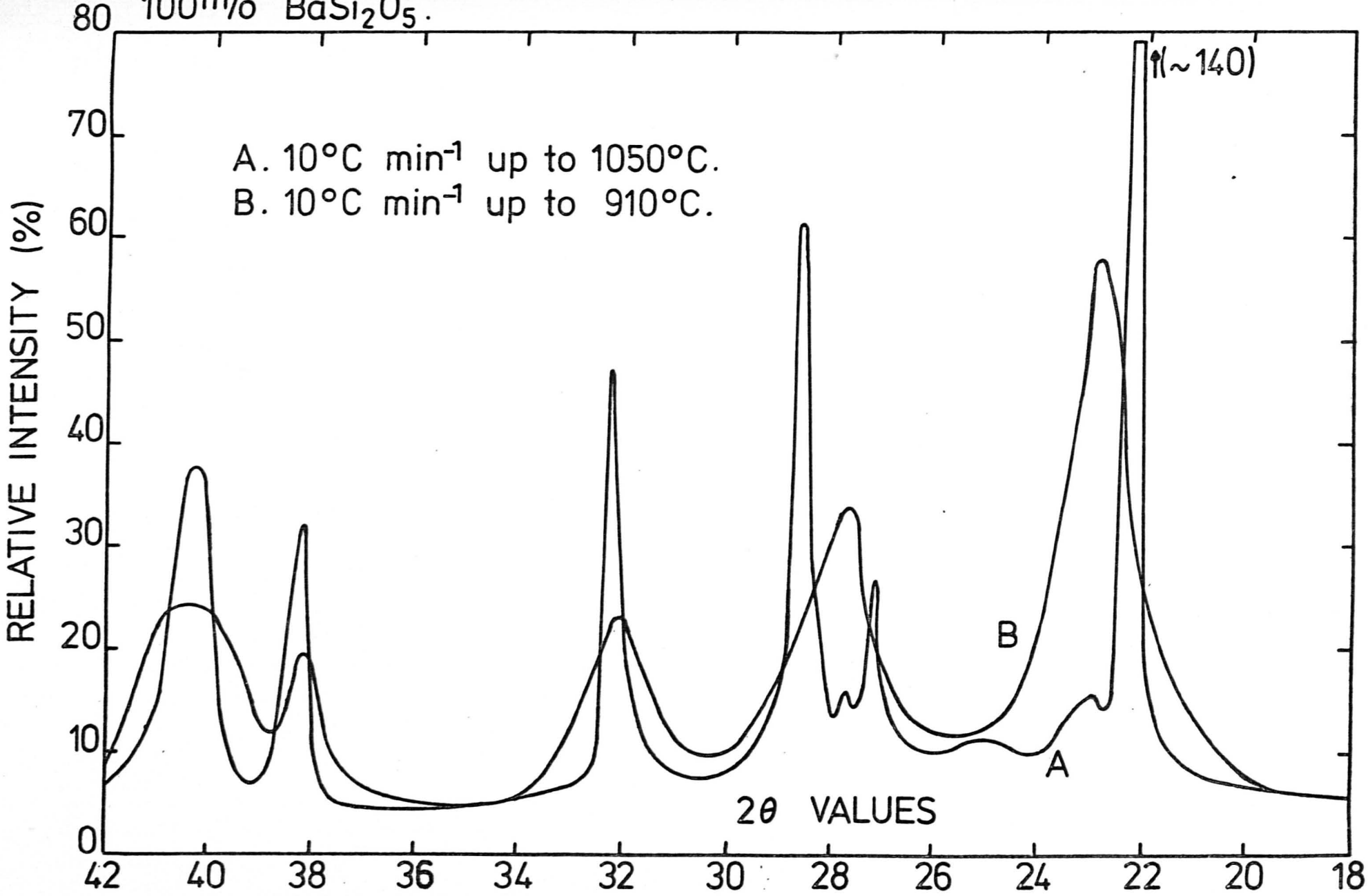

Fig. 3.2 Optical micrographs of the composition 100 $^{m}/_{o}$ $BaSi_2O_5$ heated at 10°C min^{-1} up to

Top: 1050°C

Bottom: 910°C

Magnification: x500

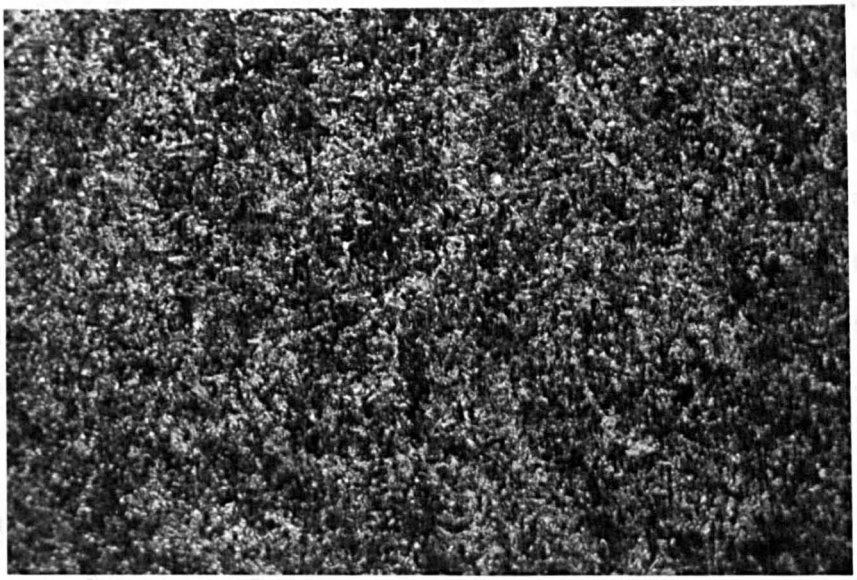

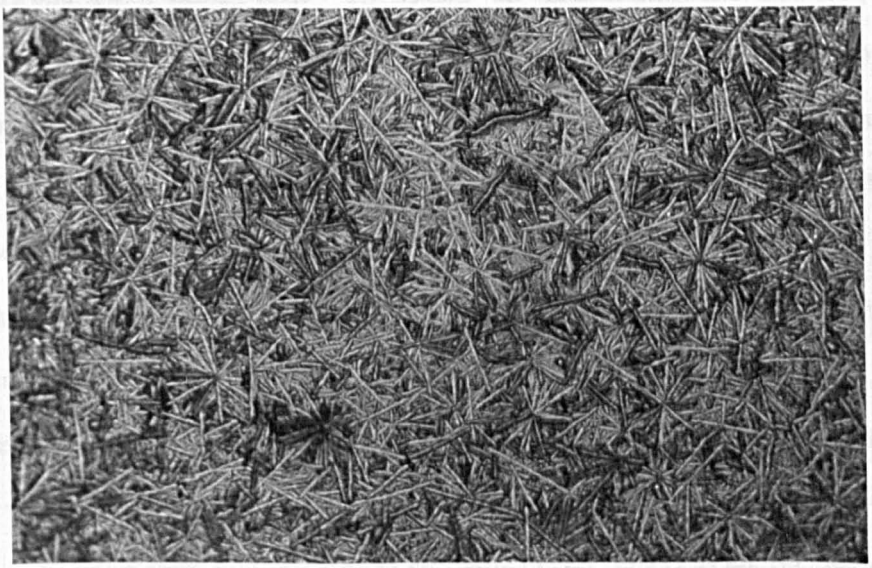

driving force for this process is the large reduction in glass-crystal interfacial area, causing an exotherm on the D.T.A. trace. Line broadening is commonly observed in x-ray diffraction of spherulite bodies, due to the extremely small size of the fibrils which constitute the spherulite. Hence spherulitic reorganisation should result in sharper diffraction peaks, as is indeed observed. This reorganisation of spherulites has also been observed by several other workers[18,20,46,47]. It finally leads to the formation of lath-like crystals.

From the position of the endothermic dip on the D.T.A. trace, 'DTA T_g' was found to be 688°C. Thus heat treatments for kinetic measurements were confined mainly to the temperature range 660-870°C. Below 688°C crystallisation processes occur increasingly slowly and above 870°C crystallisation occurs too rapidly for the kinetics to be accurately measured. For all heat treatments a large number of internal spherulites were observed. In order to determine the nucleation curve it was necessary to determine a suitable growth temperature at which the nucleation rate was relatively low. Examination of heat treatments above 800°C revealed that the spherulites all appeared to be the same size (Figure 3.3). This implies that the nucleation rate is relatively low at these temperatures. To verify this, nucleation densities were measured for several heat treatments above 800°C, the results for which are given in Table 3.1. The numbers are quite high, but there is not a large difference between 828, 848 and 868°C. Table 3.1 also gives the nucleation densities estimated by measuring the size of the largest spherulites only (see equation (2.10)). This method is only accurate if the spherulites are all the same size. Again, the nucleation densities do not vary greatly with time or temperature and are in reasonable agreement with the first calculations.

TABLE 3.1

COMPARISON OF NUCLEATION DENSITIES FOR THE COMPOSITION 100 $^{m}/_{o}$ $BaSi_2O_5$ CALCULATED USING a) A FULL ANALYSIS, EQUATION (2.6) AND b) A SIMPLE ANALYSIS, EQUATION (2.10)

T(°C)	time(mins)	$N_V^{(a)}$ (cm^{-3})	$N_V^{(b)}$ (cm^{-3})
800	47	0.84×10^7	0.94×10^7
	65	1.37	1.23
	80	1.20	1.05
823	16	$\sim 1.36 \times 10^6$	$\sim 1.75 \times 10^6$
	24	1.96	2.13
	32	2.18	2.16
	40	~1.06	~1.55
848	14	1.45×10^6	1.48×10^6
	18	~0.79	~0.90
868	4	6.59×10^5	8.37×10^5
	5	11.63	11.90
	7	7.28	8.84
	10	5.91	7.21

Approximate estimates are given when only a low number of spherulites were measured or when spherulites had begun to impinge on each other.

Fig. 3.3 Optical micrograph of the composition 100 $^{m}/_{o}$ $BaSi_2O_5$ heated at 868°C for 10 minutes.

Magnification: x50

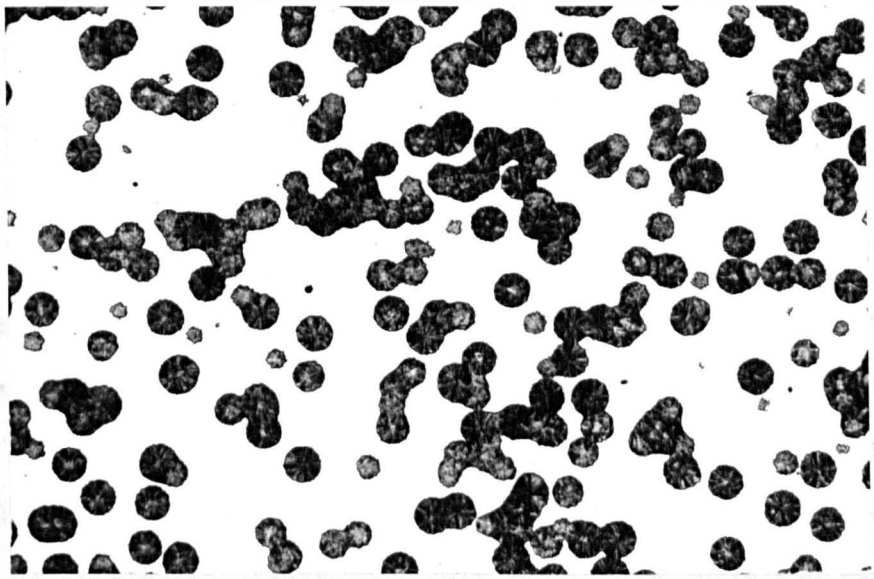

It was assumed, therefore, that the spherulites present in heat treatments above 800°C had nearly all nucleated while the glass was being cooled from the melt and during the subsequent warm up period prior to the heat treatment temperature being attained. From equation (2.5) it was possible to approximately estimate the maximum nucleation rate. Thus

$$I_{max} = \frac{2N_v b}{\Delta T} \simeq \frac{2 \times 10^6 \times 10}{50}$$

$$= 4 \times 10^5 \text{ cm}^{-3} \text{ sec}^{-1}$$

Since optical microscopy is limited to measuring nucleation densities not greater than $\simeq 10^9$ cm^{-3}, an estimate of the longest nucleation period at T_{max} is given by $\frac{10^9}{4 \times 10^5 \times 60} \simeq 42$ mins. In practice nearly all nucleation treatments were limited to about this length of time. Because of such short permissible heat treatments, only two times at each temperature were measured in order to calculate the nucleation rate. Thus to accurately estimate the nucleation curve, it was necessary to obtain nucleation rates at small temperature intervals. A further limitation was imposed by the presence of the extraneous nuclei. These caused rapid bulk crystallisation of the specimen at temperatures above 800°C. As a compromise between avoiding nucleation at the growth stage and growth occurring too rapidly to be controlled, 828°C was chosen as the growth temperature. The length of time for growth was judged visually, sufficient growth having occurred when the specimens became milky but were still nearly transparent. This generally occurred in less than 10 minutes. As a further precaution in calculating the nucleation rate correctly, the two nucleated specimens for each nucleation temperature were given the same growth treatment. Thus the

difference in nucleation densities between the two specimens was due solely to the nucleation treatment.

A summary of the nucleation data obtained is given in Table 3.2., and the nucleation curve is shown in Figure 3.4.. It can be seen that the nucleation rate is negligible above 800°C, as was deduced earlier. It was not possible to accurately measure the size of each spherulite observed. However, growth rate measurements (see Figure 3.9) showed that the growth rate rapidly decreased below 800°C. Thus $u_{828}/u_{749} \approx 72$ compared with $u_{828}/u_{800} \simeq 4$. Hence the spherulites grow mainly at the growth stage and will therefore be all the same size. This was verified by experiment, the maximum spherulite size observed being the same for both treatments at each nucleation temperature, except at 780°C. Nucleation densities were threrfore generally estimated by measuring the size of the largest spherulites (assuming them to be spherical in shape) and counting the number of spherulites present. With careful specimen preparation very small crystals could be clearly distinguished, although their individual sizes would sometimes be difficult to accurately measure. The accuracy of an estimated nucleation density therefore depended on how accurately the largest spherulites were measured. On average about 1,400 spherulites were counted for each heat treatment. Typical micrographs from which measurements were made are shown in Figure 3.5. Very high nucleation rates were observed, the maximum of 1.87×10^6 cm^{-3} sec^{-1} occurring at 700°C. At 700°C and below non-steady state behaviour apparently occurs, since (N_v/t) increases considerably with time. Above 700°C, however, (N_v/t) is approximately constant with time for a given temperature, indicating steady state behaviour. It is probably impossible to accurately measure the induction times using optical microscopy, because of the limitation on the number of spherulites which can be accurately measured by this method.

TABLE 3.2

NUCLEATION DATA AS A FUNCTION OF TIME AND NUCLEATION TEMPERATURE FOR THE COMPOSITION 100 m/o $BaSi_2O_5$

T(°C)	time(mins)	$N_v(cm^{-3})$	$I(cm^{-3}sec^{-1})$
780	20*	4.19	2.70×10^4
	40*	7.43×10^7	
760	40	4.84	1.34×10^5
	80	8.06×10^8	
748	15	3.14	2.80×10^5
	30	5.66×10^8	
740	15	5.48	4.59×10^5
	30	9.62×10^8	
729	15	7.99	7.98×10^5
	30	15.17×10^8	
718	20	1.46	1.45×10^6
	40	3.20×10^9	
700	20	0.81	1.87×10^6
	40	3.05×10^9	
680	90	1.27	2.06×10^5
	135	$\sim 1.83 \times 10^9$	
662	120	1.23	4.21×10^4
	240	4.26×10^8	

* Full analysis used to calculate N_v at 780°C. Using the simple analysis $N_v(20) = 4.28 \times 10^7$ and $N_v(40) = 6.58 \times 10^7$. As expected, $N_v(40)$ is underestimated by the simple analysis, because detectable growth of the nuclei occurs during nucleation as well as at the growth stage.

FIG. 3.4. STEADY STATE NUCLEATION RATE AS A FUNCTION OF TEMPERATURE FOR THE COMPOSITION 100 m/o $BaSi_2O_5$.

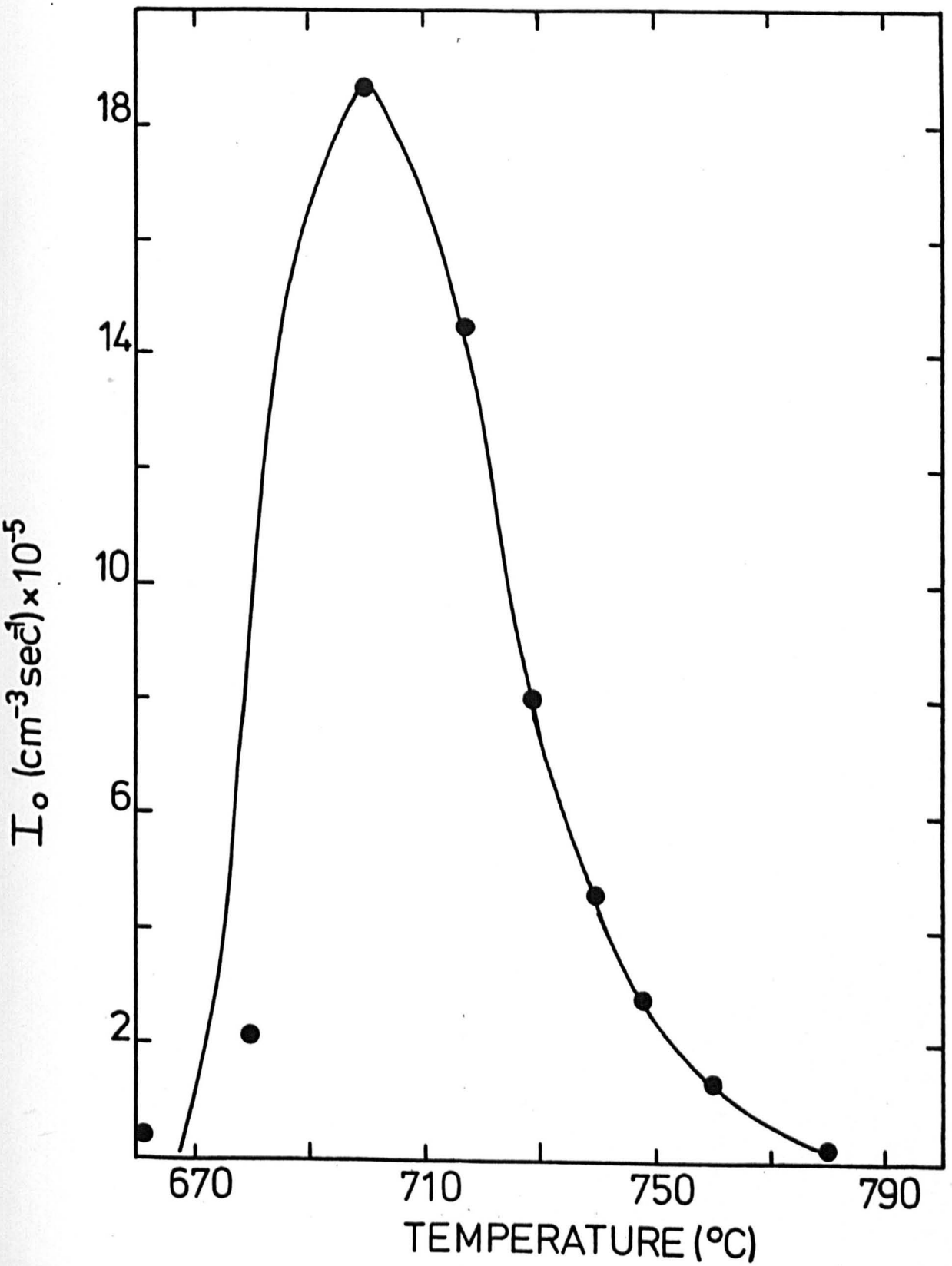

Fig. 3.5 Optical micrographs of the composition 100 m/o $BaSi_2O_5$ heated at

Top: 661°C for 1 and 2 hours, grown at 828°C

Bottom: 700°C for 20 and 40 minutes, grown at 828°C.

Magnification: x200

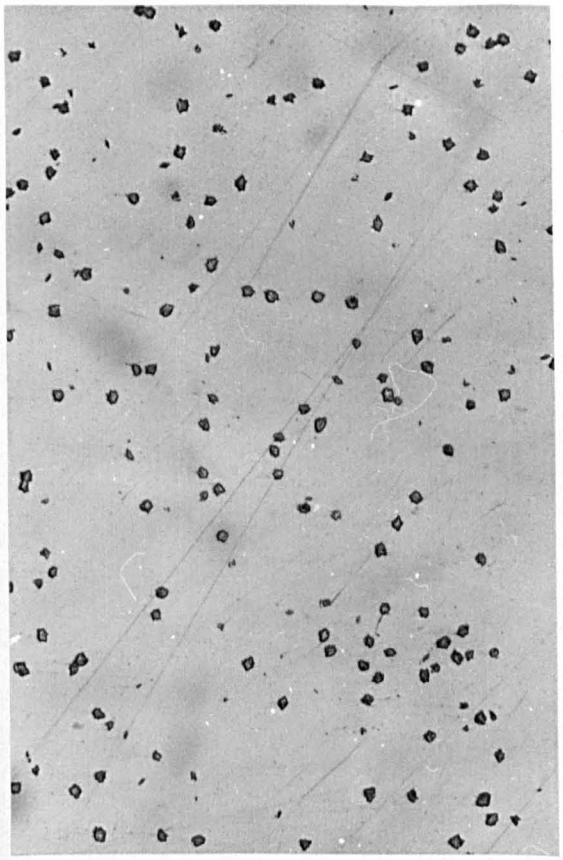

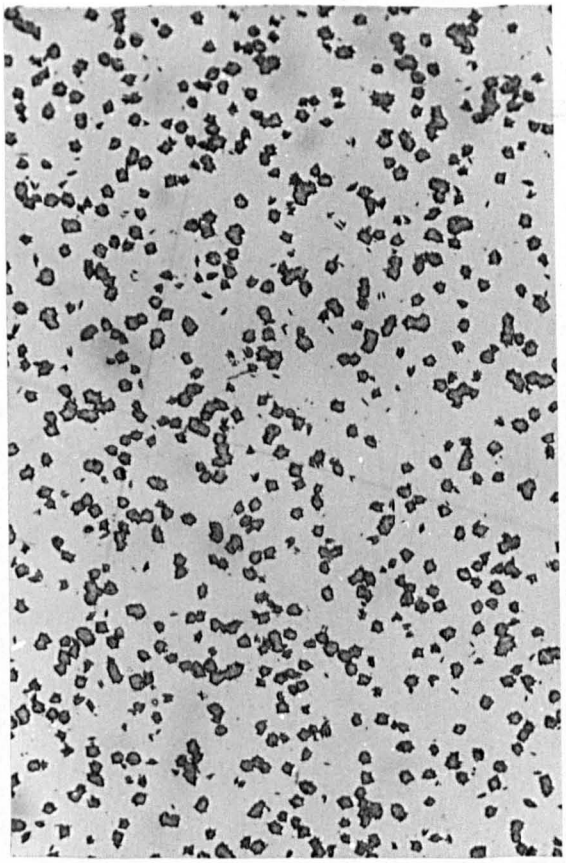

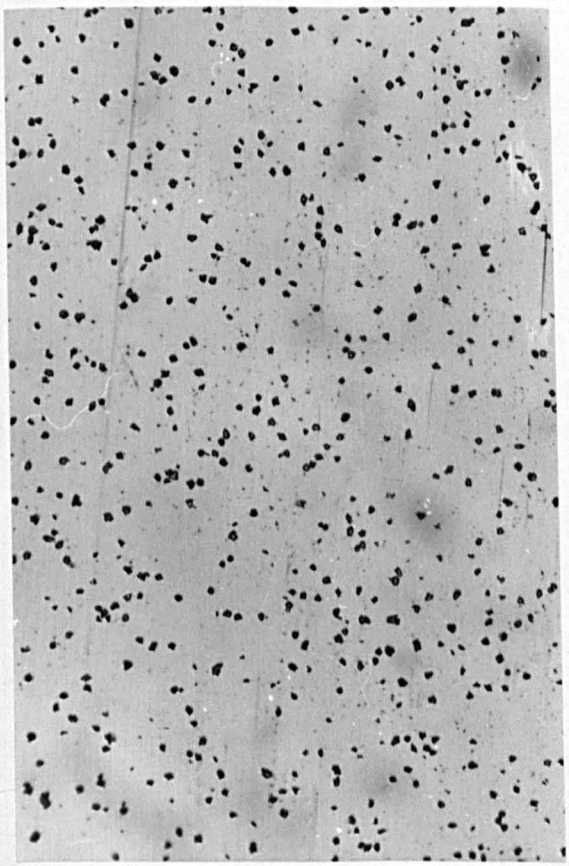

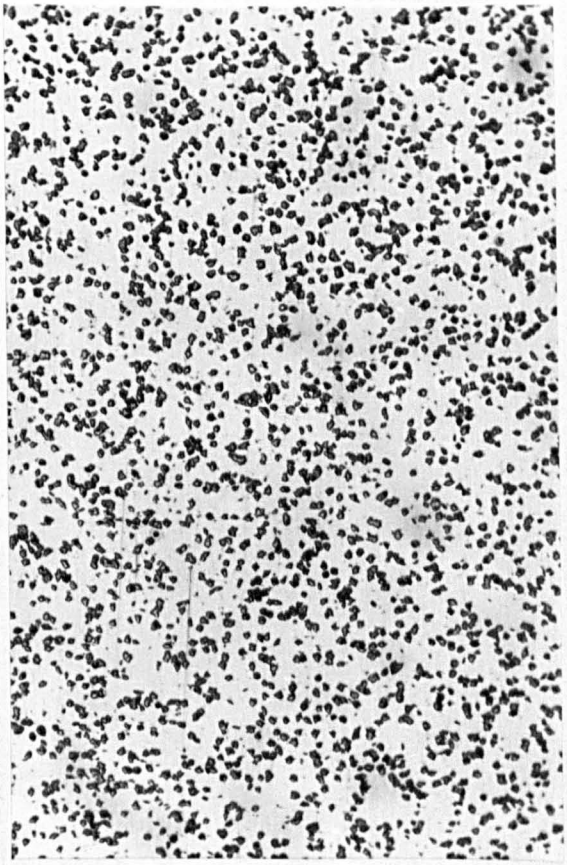

Fig. 3.5 contd/....

Top: 718°C for 20 and 40 minutes, grown at 828°C

Bottom: 760°C for 40 and 80 minutes, grown at 828°C

Magnification: x200

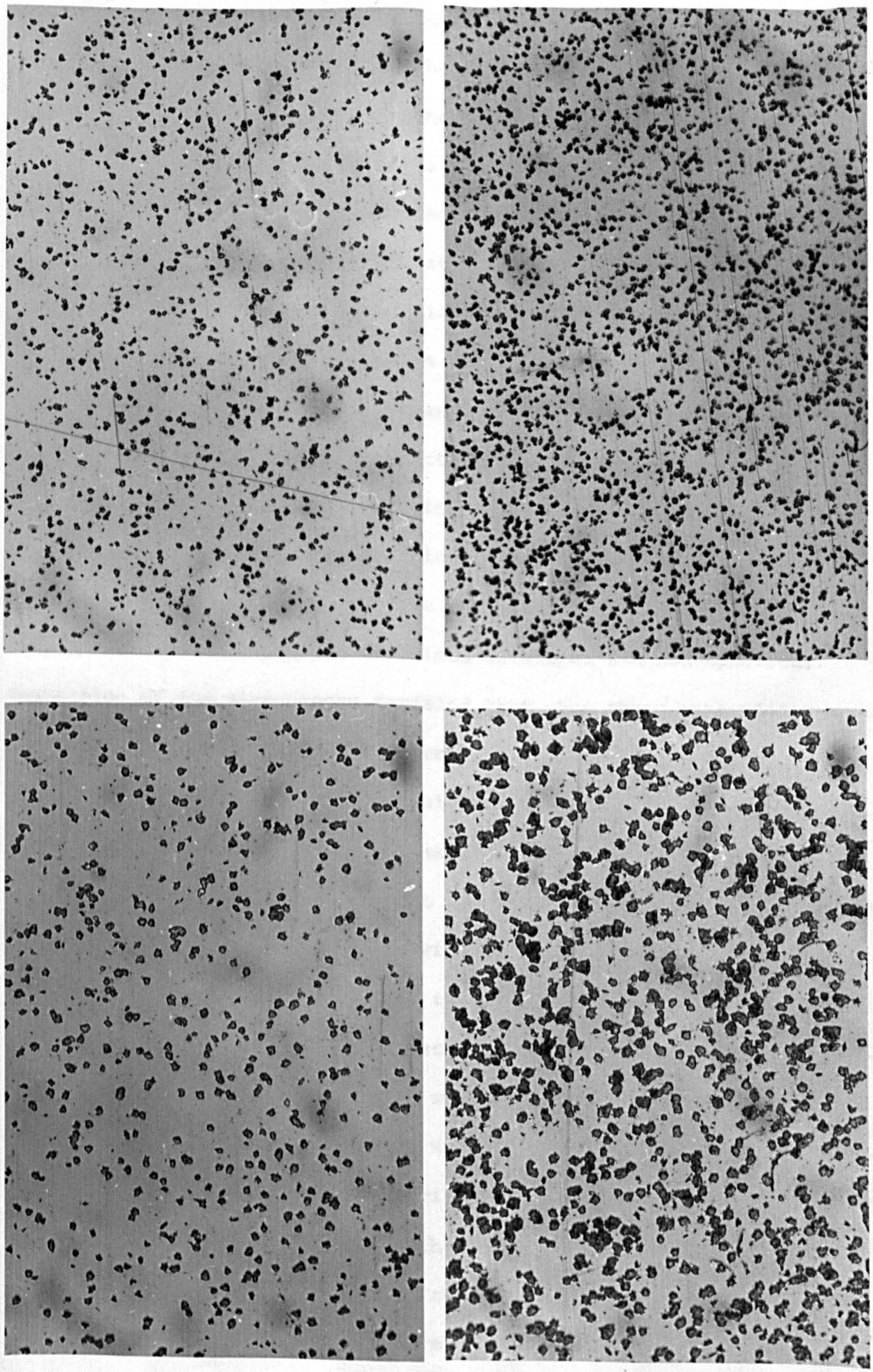

Crystal growth rates were determined in the temperature range 749-868°C. Below 749°C very long heat treatments were required to obtain observable growth. Also, the high nucleation rates at these temperatures caused the spherulites to coalesce at a very early stage of growth. Above 868°C the extraneous spherulites present in the glass caused rapid bulk crystallisation after only short times. In general the growth rates of spherulites were measured, because of the difficulty in measuring the surface crystalline layer at high magnifications. The edges of a polished specimen are generally rounded off and it is difficult to focus correctly on both the specimen edge and the crystal-glass interface. At high growth temperatures the spherulites were found to be almost spherical (see Figures 3.6 (a)) and the diameter was measured as a function of time. However, at lower growth temperatures the spherulites were less developed and non-spherical. Inspection of the micrographs revealed that when these spherulites were sectioned in a certain way, a central fibril could be observed which formed a diameter. This is particularly well illustrated in Figures 3.6 (b) and (c) where the fibril in question is indicated by arrows. These fibrils become more prominent as the growth temperature is lowered and at 725°C only this central fibril is present (Figure 3.7). Thus it appears that the central fibril is closely associated with the original nucleus. This has been recently confirmed by electron microscopy, the results of which will be mentioned later in the section. Growth rates at lower temperatures were therefore determined by measuring the length of this central fibril as a function of time. The growth rates were found to be constant with time at a given temperature (Figure 3.8) and the growth rate curve is shown in Figure 3.9.

Below 800°C there is a positive intercept on the time axis of the length vs. time curves (Figure 3.8), implying a time dependent

Fig. 3.6 Optical micrographs of the composition 100 $^{m}/_{o}$ $BaSi_2O_5$ heated at

(a) Top left: 849^{o}C for 20 minutes

(b) Top right: 774^{o}C for 3 hours

(c) Bottom: 774^{o}C for 4 hours

Magnification: x 500

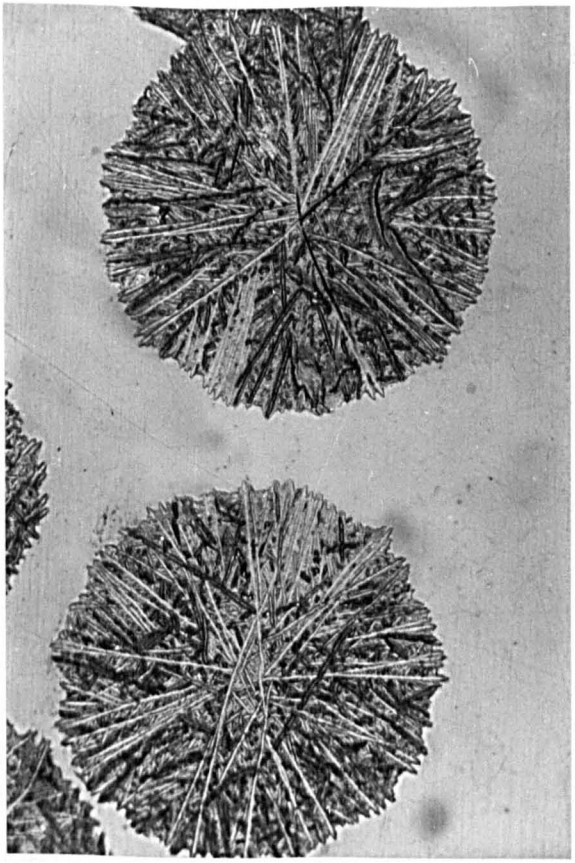

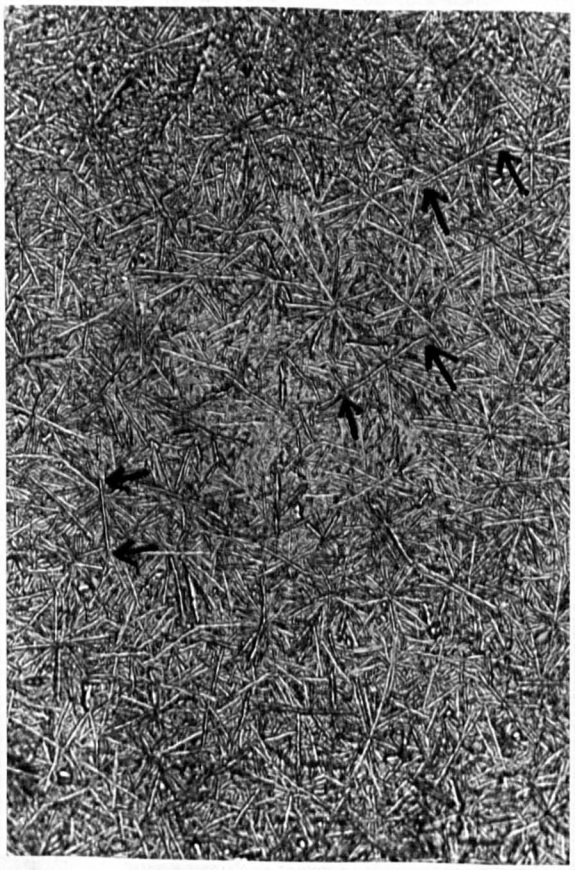

Fig. 3.7 Optical micrographs of the composition 100 $^{m}/_{o}$ $BaSi_2O_5$ heated at 725°C for

Top left: 25 hours

Top right: 30 hours

Bottom: 35 hours

Magnification: x500

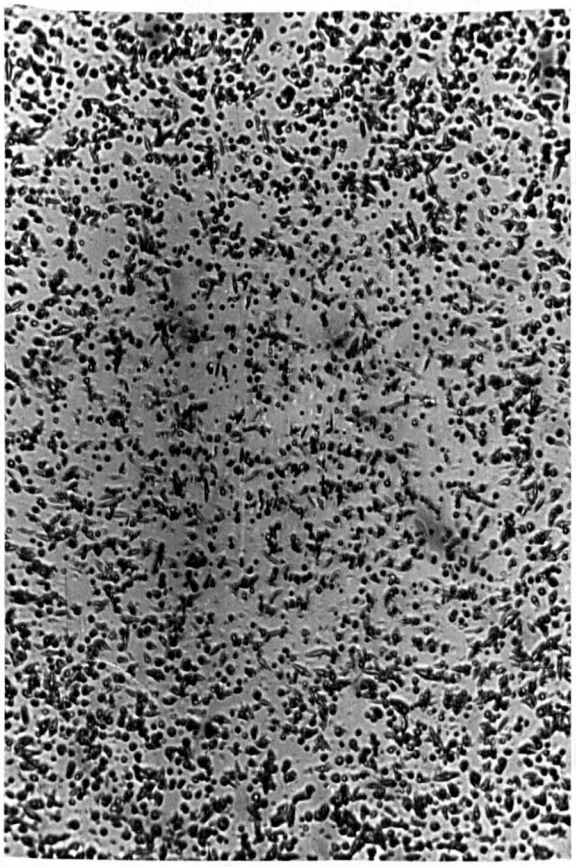

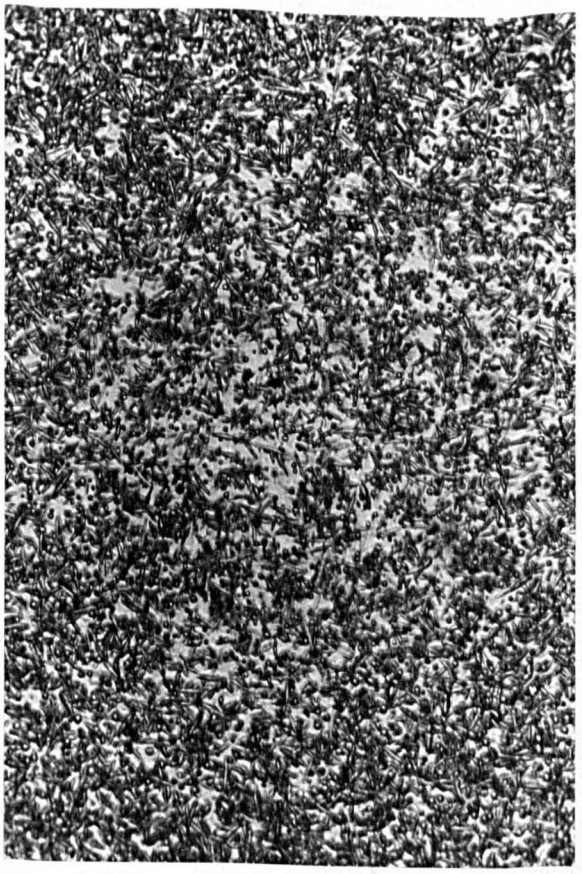

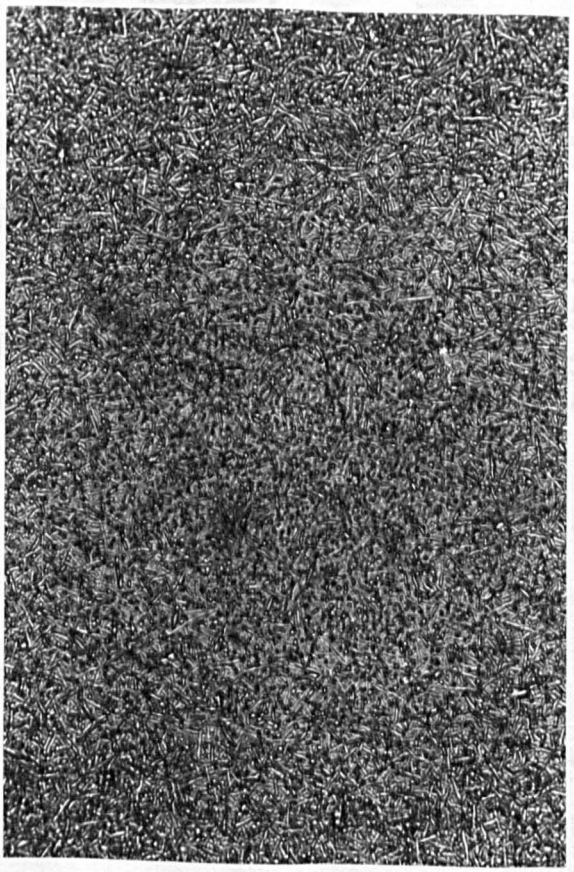

FIG. 3.8. GROWTH RATE MEASUREMENTS FOR THE COMPOSITION 100 m/o $BaSi_2O_5$.

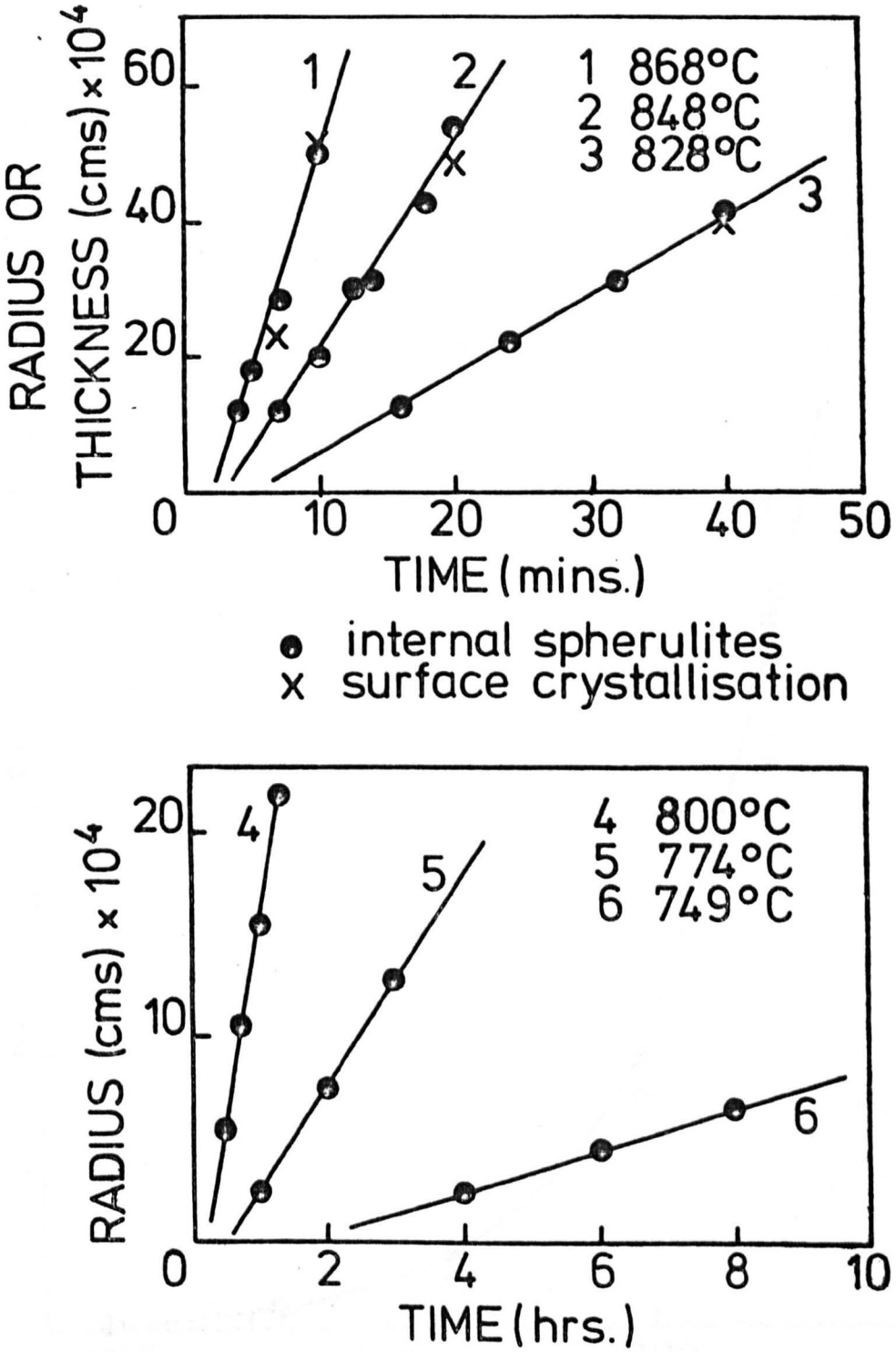

FIG. 3.9. CRYSTAL GROWTH RATE AS A FUNCTION OF TEMPERATURE FOR THE COMPOSITION 100m/o $BaSi_2O_5$.

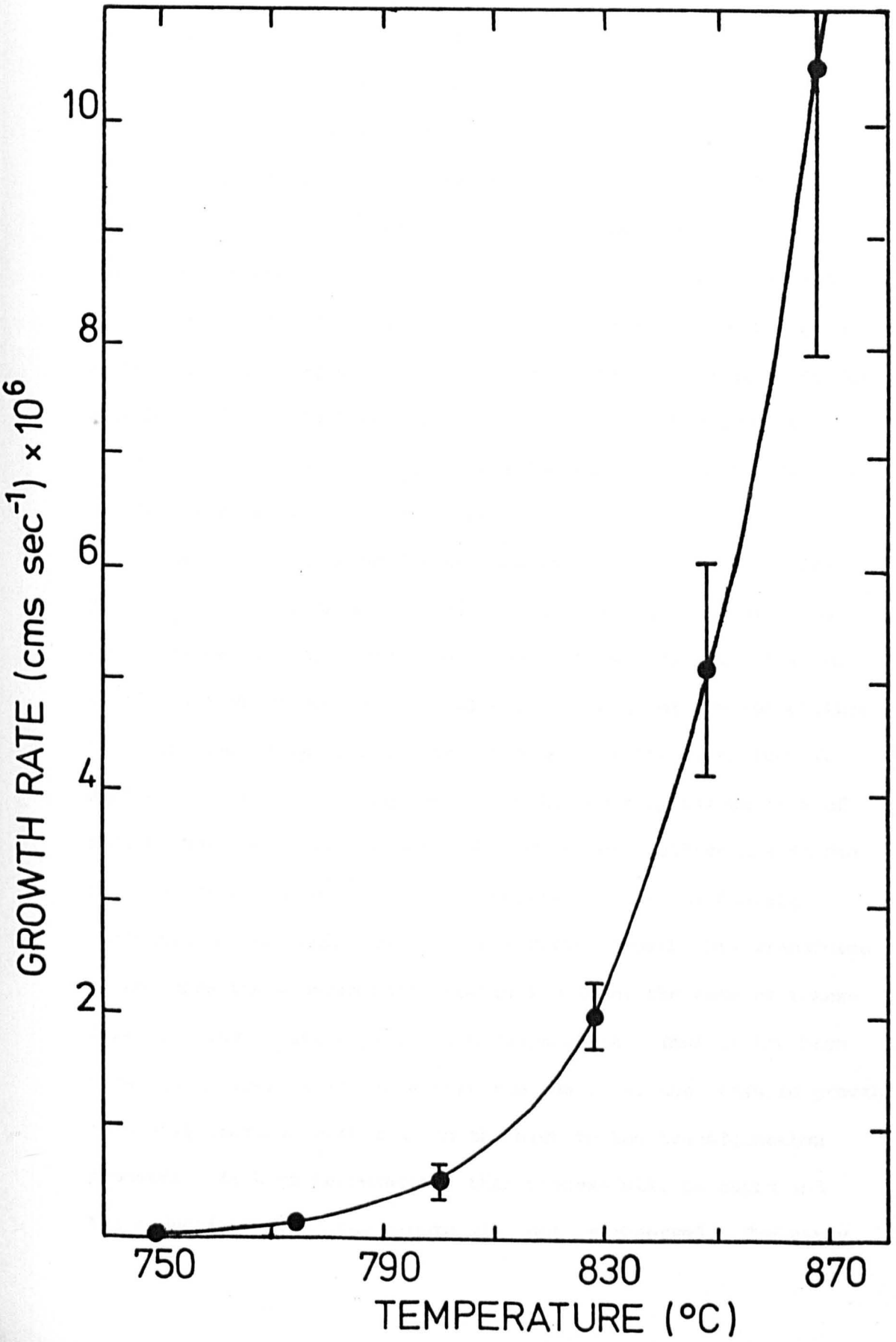

growth rate at the initial stages of growth. As already indicated, induction times for internal nucleation are not expected to be appreciable until about 700°C and below. Thus the induction time for growth is not due to non-steady state internal nucleation behaviour. There are two alternative explanations. First, the crystal growth rate becomes very low below 800°C and at 750°C, for example, it is about 3Å per second. Hence the growing crystal will only become macroscopic in size (say > 1 μm) after about an hour. During this period surface energy considerations may be important, as mentioned in Chapter 1, and the thermodynamic driving force for growth would be effectively reduced. If this is the case, the growth rate will therefore gradually increase with time until the crystal becomes macroscopic in size.

A second explanation for the observed 'induction time' for growth is that the crystal modification of $BaSi_2O_5$ may alter as growth proceeds. As already mentioned, it is generally difficult to identify which modification of $BaSi_2O_5$ (high or low temperature form) is present in crystallised specimens of the glass 100 $^{m}/_{o}$ $BaSi_2O_5$. However, a change from high to low temperature form of $BaSi_2O_5$ has been found to occur during its crystallisation in the Na_2O-BaO-SiO_2 system[20]. It was suggested that the $BaSi_2O_5$ nucleates as the high form, but that during growth this transforms to the more thermodynamically stable low form, the rate of transformation increasing rapidly with temperature. Thus if the high form has a lower growth rate than the low form, the measured growth rate will increase with time as the high to low transformation proceeds. At high temperatures this process will be rapid and the induction period for growth will not be observed. The early

stages of nucleation and growth of $BaSi_2O_5$ in the glass composition 100 $^m/_o$ $BaSi_2O_5$ have been recently studied using electron microscopy[48]. The crystals appear to grow as spheres initially, but at a later stage large spikes or needles are observed to grow from the surface of these spheres (see Figure 3.10). Unfortunately, electron diffraction was unable to identify which modification of $BaSi_2O_5$ is present at each stage. However, these electron microscope observations suggest that the induction period measured by the optical microscope corresponds to the time required for the spheres to develop spike-like growths.

It is of interest to discuss the observations of MacDowell[18] in terms of the kinetic data presented above. He heat treated $BaSi_2O_5$ glass to 700°C at 5°C min^{-1} and then at 1°C min^{-1} to a soak temperature where the specimens were held for one hour. Three soak temperatures were employed viz. 750, 850, and 1000°C. When soaked at 750°C, small spherical particles were observed about 1 μm in size. These were identified as crystalline $BaSi_2O_5$. At 850°C, spherulites about 5 μm had grown with very little glass remaining and at 1000°C the spherulites had changed into lath-like crystals, almost 100% crystallinity being achieved. The present results are in good agreement with these observations. Thus at 750°C a large number of nuclei would be present, but little growth is possible. At 850°C the growth rate is much higher and rapid crystallisation of the whole sample occurs. Assuming all the spherulites to be about 5 μm in size, the number of spherulites present would be approximately 10^{10} cm^{-3}, as expected from the heat treatment schedule. The formation of laths at 1000°C has already been discussed.

It is also interesting to consider the value of the critical nucleation temperature for the $BaSi_2O_5$ glass as predicted from data for $BaSi_2O_5$ nucleating from non-stoichiometric compositions. Data

Fig. 3.10 Electron micrographs of the composition 100 $^{m}/_{o}$ $BaSi_2O_5$ heated at 700°C for

Top left: 70 hours; replica micrograph; magnification x6,220

Top right: 116 hours; replica micrograph; magnification x6,220

Bottom: 116 hours; transmission micrograph; magnification x21,270

(After ref. 48)

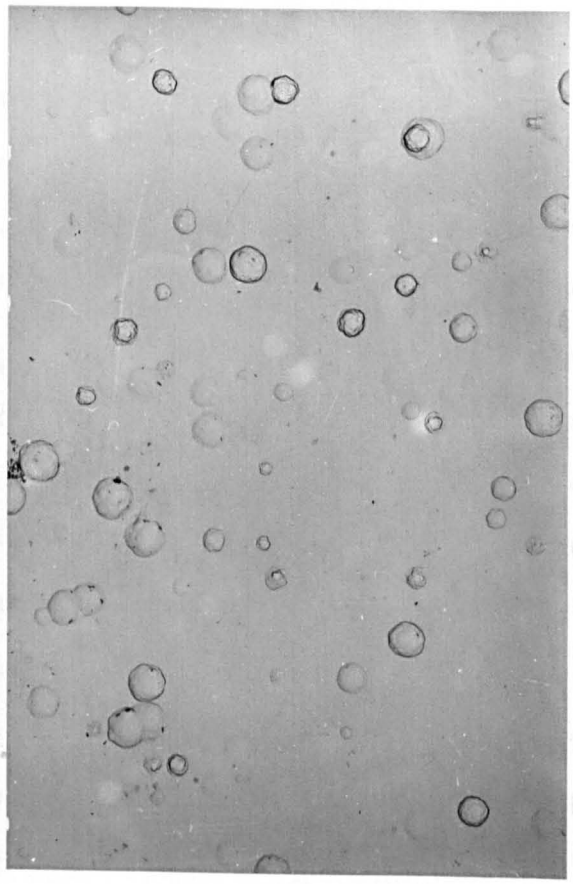

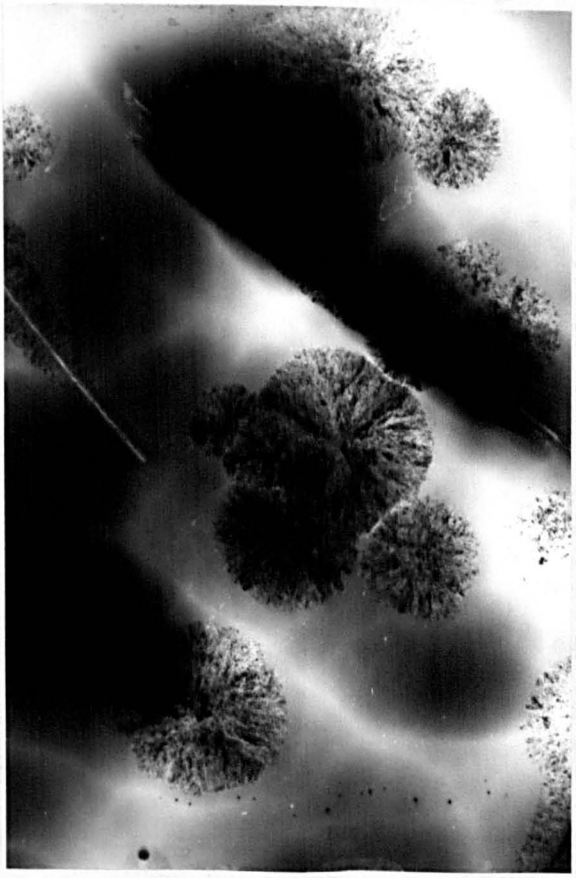

is available for the nucleation of $BaSi_2O_5$ from glasses in the system $Na_2Si_2O_5$-$BaSi_2O_5$ [20]. The critical nucleation temperature, defined as the temperature at which the nucleation rate was 1 nucleus cm^{-3} min^{-1}, was measured as a function of composition. The extrapolated value of T_c for 100 m/o $BaSi_2O_5$ is 1200°C, which is far too high according to the present results. From a logarithmic plot of the nucleation data for $BaSi_2O_5$, T_c is estimated to be about 858°C by extrapolation. It should be mentioned that there appears to be an inconsistency in the data of reference 20. Thus according to their data, T_c is 593°C for 'composition II', which is 50 m/o $Na_2Si_2O_5$-50 m/o $BaSi_2O_5$. However, according to their nucleation curve for this composition, $\log_{10}I$ is not 0 but ≃ 3.7 at this temperature, where I is measured in nuclei cm^{-3} min^{-1}.

3.1.2 10 m/o $Li_2Si_2O_5$-90 m/o $BaSi_2O_5$, Code 10:90 (T_L = 1357°C)

Initial experiments on the 10:90 composition revealed the occurrence of rapid crystallisation above 700°C. Thus after about 20 minutes at 700°C the glass was completely crystallised due to the coalescence of internal spherulites. X-ray analysis revealed only one crystalline phase viz. $BaSi_2O_5$. Thus after 1 hour at 750°C ℓ-$BaSi_2O_5$ was present together with a very small amount of h-$BaSi_2O_5$. No $Li_2Si_2O_5$ was observed. This is not surprising since the glass composition only contains 5.8 weight % $Li_2Si_2O_5$, just within the detectable limit for X-ray analysis, assuming all the $Li_2Si_2O_5$ crystallises. At temperatures higher than 750°C only ℓ-$BaSi_2O_5$ was observed but otherwise the X-ray patterns remained unaltered. However, below 750°C it was not possible to distinguish which modification of $BaSi_2O_5$ was present and also a main $BaSi_2O_5$ peak at 2θ

equals 26.65° was absent. Thus after 2 hours and 75 hours at 765°C respectively, patterns similar to Figure 3.1, curve A, were obtained.

D.T.A. revealed a crystallisation exotherm in the temperature range 713-738°C. This is in agreement with the preliminary experimental results. A smaller exothermic peak was observed having a maximum at about 875°C. In order to determine the cause of this peak, two powdered samples were heat treated at 10°C min^{-1} up to 792 and 907°C respectively and then removed from the furnace for X-ray analysis. Both heat treatments gave sharp patterns. However, at 792°C a small peak was present at 2θ equals 25.18, but no peak at 2θ equals 26.00 implying that h-$BaSi_2O_5$ was present. Also, a main peak at 2θ equals 26.65 was considerably reduced. At 907°C only ℓ-$BaSi_2O_5$ was observed, all the main peaks being present. Observation of bulk specimens given similar heat treatments showed no marked difference in microstructure except that the 907°C specimen is tending to a lath-like morphology (see Figures 3.11 (a) and (b)). Hence from these results it is not possible to attribute the DTA exotherm conclusively to either a modification in crystal structure (high to low) or in crystal morphology. However, 15 minutes isothermal heat treatments showed that above 875°C the crystal structure transformed into laths, the original outline of the spherulites still remaining (see Figures 3.11 (c) and (d)). Thus the exotherm is probably due to a change in morphology and a corresponding lowering of surface energy. As already mentioned, a change from high to low temperature form of $BaSi_2O_5$ has been found to occur during its crystallisation in the Na_2O-BaO-SiO_2 system[19]. Here it was found that during D.T.A. h-$BaSi_2O_5$ crystallised first followed rapidly by its conversion to ℓ-$BaSi_2O_5$. Whilst such a process probably occurs in

Fig. 3.11 Optical micrographs of the composition 10 $^{m}/_{o}$ $Li_2Si_2O_5$-90 $^{m}/_{o}$ $BaSi_2O_5$ heated at

(a) Top left: 10°C min^{-1} up to 792°C

(b) Top right: 10°C min^{-1} up to 907°C

(c) Bottom left: 824°C for 15 minutes

(d) Bottom right: 925°C for 15 minutes

Magnification: x500

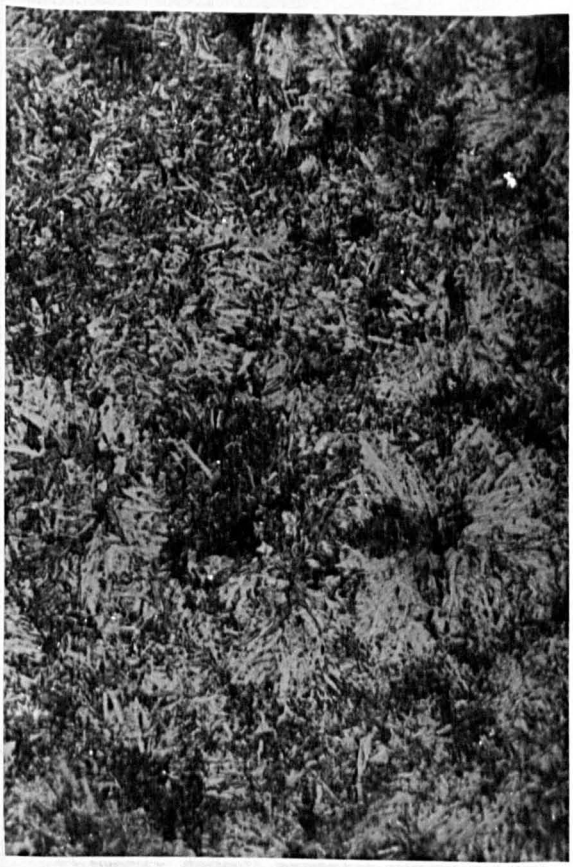

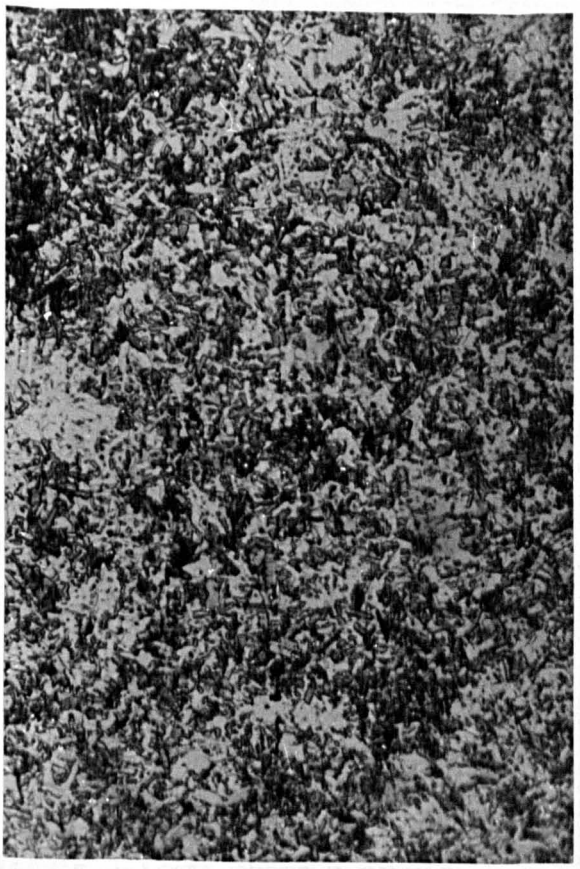

the Li_2O-BaO-SiO_2 system it is not thought that the exothermic peak in question is caused by this, since it did not occur until 140°C after the initial crystallisation. Also, the peak height at 2θ equals 25.18, denoting the presence of h-$BaSi_2O_5$ at 792°C, was only small.

Nucleation densities could only be measured below 700°C because of the rapid crystallisation which otherwise occurred. Since the D.T.A. T_g was found to be 605°C, the lowest temperature considered was 600°C. However, at these temperatures the nucleation rates were found to be very low. Thus at 650°C after 1 hour only five spherulites could be observed on the polished and etched section. No growth treatment was required since at this temperature the growth rate is about 5 μm sec^{-1}. Hence only those nuclei forming in the last few seconds of the heat treatment would remain unobserved. Figure 3.12(a) shows a sample heated at 675°C for 1 hour the number of spherulites present being about 1.1×10^4 cm^{-3}. Assuming all these spherulites grew from nuclei formed during the heat treatment, $I \approx 3$ cm^{-3} sec^{-1}. After 1½ hours at 675°C impingement occurs. At temperatures higher than 675°C impingement is more rapid and prevents the accurate measurement of nucleation densities. However, the size of the spherulites in completely crystallised specimens decreases with increasing temperature (see Figures 3.12(a) to (f)), implying an increase in nucleation rate with temperature above 675°C. An attempt was made to estimate the position of the nucleation curve indirectly by measuring the thickness of the crystalline layer, x, from these micrographs. In general both nucleation and growth are occurring simultaneously. Thus it is possible to apply the Johnson-Mehl equation[1]. Both u and I are assumed to be constant with time, and the volume fraction of crystallised glass is given by

Fig. 3.12 Optical micrographs of the composition 10 ^{m}/o $Li_2Si_2O_5$-90 ^{m}/o $BaSi_2O_5$ heated at

(a) Top left: 675°C for 1 hour

(b) Top right: 675°C for 2 hours

(c) Bottom left: 700°C for 1 hour

(d) Bottom right: 725°C for 1 hour

Magnification: x50

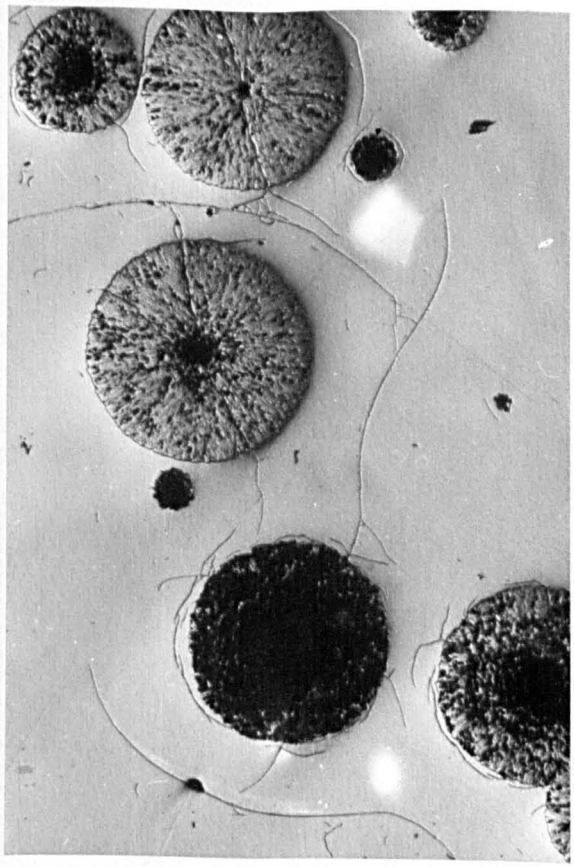

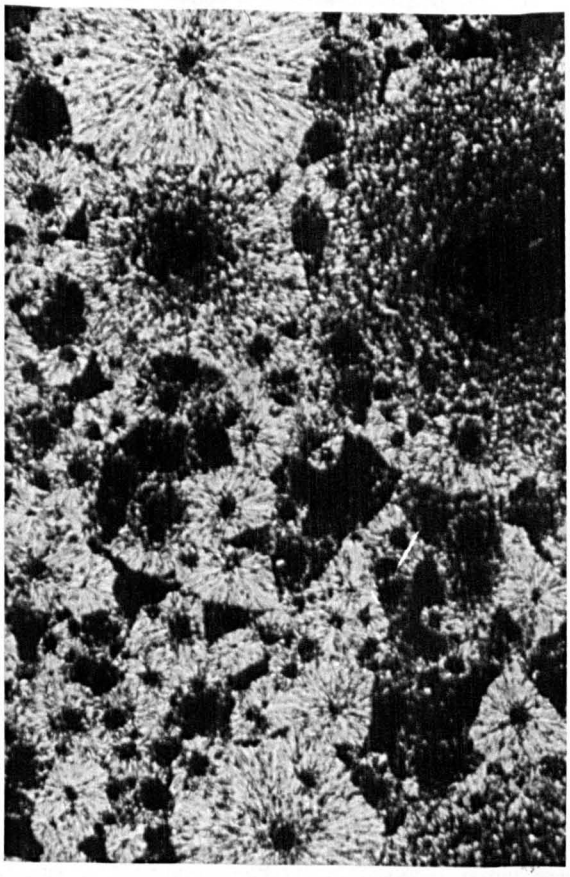

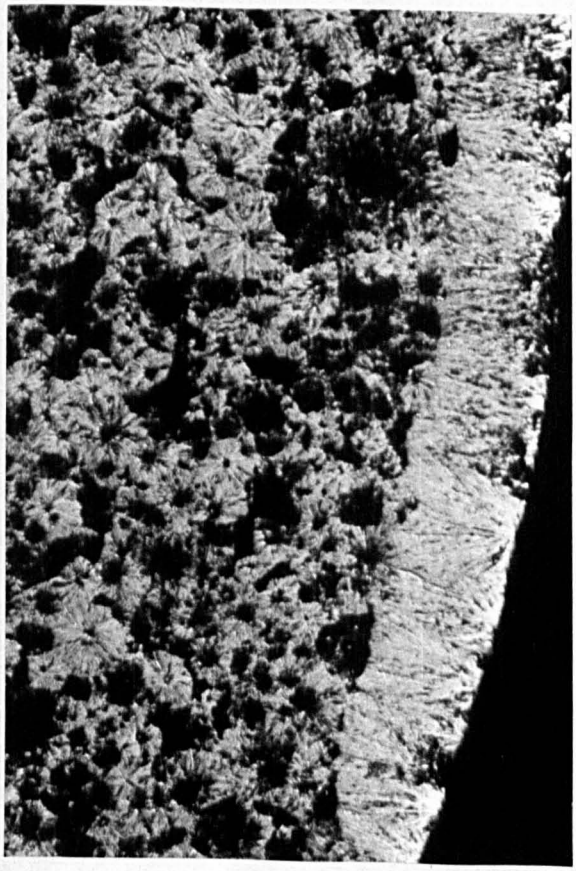

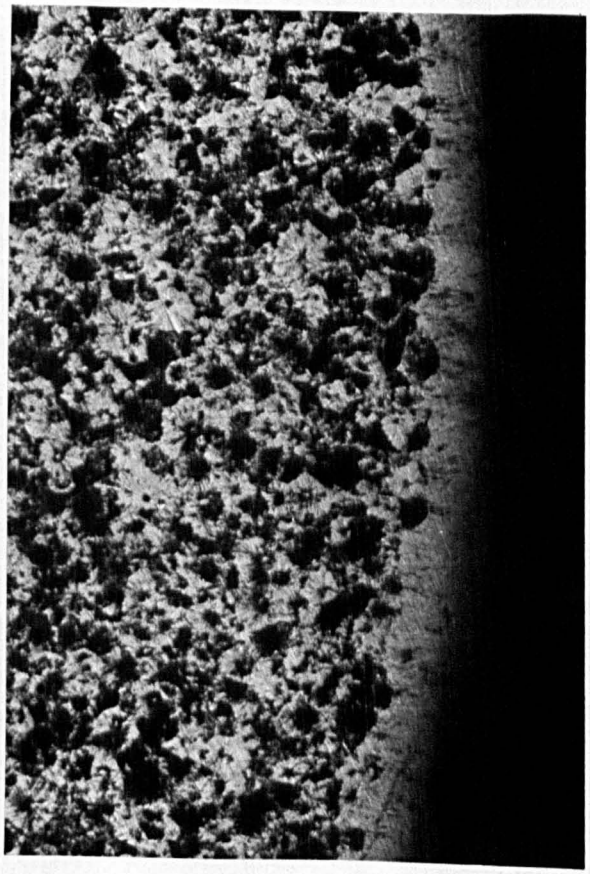

Fig. 3.12 contd/...

(e) Top: 750°C for 1 hour

(f) Bottom: 775°C for 1 hour

Magnification: x50

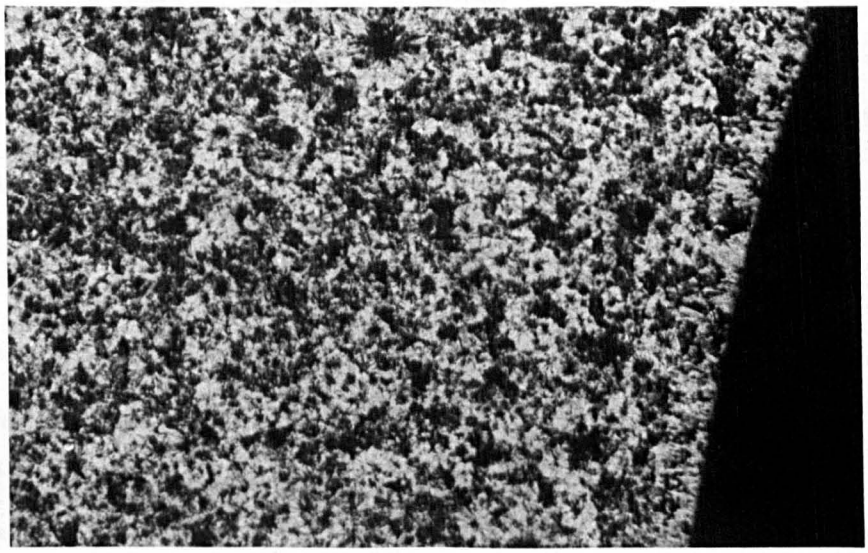

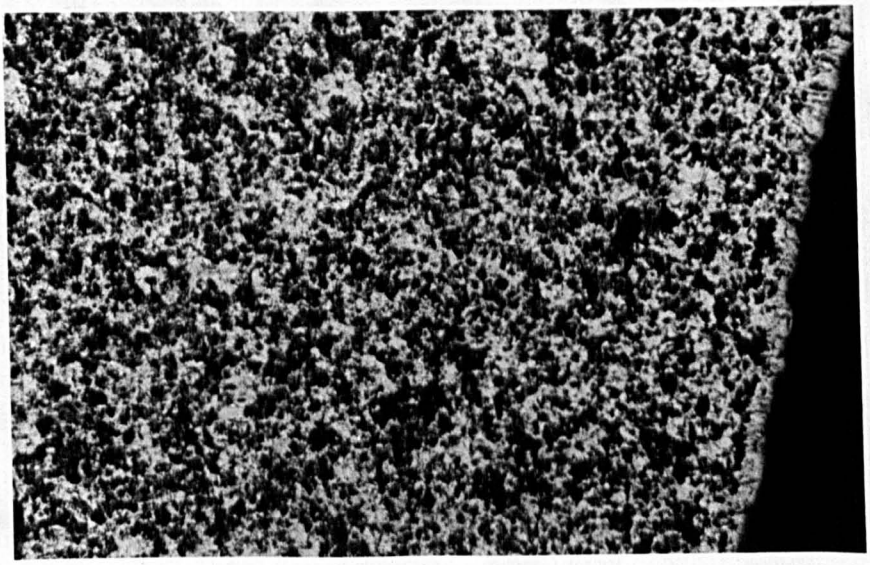

$$X_t = 1 - \exp(-\frac{\pi}{3} u^3 I t^4) \qquad (3.1)$$

where X_t is the volume fraction at time t. An estimate of the time required to completely crystallise the interior glass by internal nucleation is given by

$$t_i = \frac{x(u,I)}{u} \qquad (3.2)$$

where t_i is referred to as the impingement time. For times greater than t_i the surface layer can advance no further because very little glass remains ahead of it. The value of x will also correspond to the radius of the largest spherulite observed, since this spherulite will have been growing from almost the beginning of the heat treatment, that is for the same length of time as the surface layer. Assuming that for $t = t_i$, $X_t \simeq$ constant we obtain

$$\frac{\pi}{3} u^3 I t_i^4 = k, \text{ a constant} \qquad (3.3)$$

$$\therefore \qquad I = k' \frac{u}{x^4} \qquad (3.4)$$

$$\text{or} \qquad x = k'' \sqrt[4]{\frac{u}{I}} \qquad (3.5)$$

Hence for a given growth rate and a low nucleation rate, there will be no hindrance to surface growth and a thick surface layer will result. If however the nucleation rate is high, the surface layer will be arrested quickly and only a thin layer will form.

Values of x were obtained for the 10:90 composition over the temperature range 700-775°C using 1 hour and 2 hours heat treatments.

Since impingement occurred in less than one hour, it was thus possible to obtain two estimates of x. In general identical values of x were obtained for both heat treatments. Figure 3.13(a) shows the values of x and t_i as a function of temperature. The values of t_i were calculated using growth rate data obtained in the temperature range 625-725°C (presented later), this data being extrapolated up to 800°C using a lnu vs. $^1/T$ plot. Since both $^1/x$ and u are increasing over this temperature range, a steady increase in the nucleation rate is predicted (see equation (3.4)). However. the values of t_i at 750 and 775°C are very small and in fact less than the time required for a specimen to reach temperature (estimated to be about 3 minutes). Thus the value of x at these temperatures is not related to the growth rate and nucleation rate at the heat treatment temperature in question. It is determined by how much crystal nucleation and growth occurs during the 'warming-up' period. Of course, the values of t_i will only be approximate, because the growth rate was assumed to be constant, corresponding to its value at the nominal heat treatment temperature. However, it was verified by experiment that impingement times are very short above 725°C. Thus a series of specimens were heat treated at 750°C for 5, 10, 15 and 30 minutes respectively. Another specimen was also given a heat treatment at 750°C for 16 hours, thus ensuring almost 100% crystallinity. A comparison of these various heat treatments using X-ray analysis revealed little difference in the percentage crystallinity, even between the 5 minute and 16 hour heat treatments.

In another series of experiments, specimens were melted above the liquidus temperature and then directly quenched to the temperature of the interest, where they were held for 10 minutes and then further quenched to room temperature. This method ensures that there are no

FIG. 3.13. THICKNESS OF SURFACE CRYSTALLINE LAYER AT IMPINGEMENT AND TIME OF IMPINGEMENT, AS A FUNCTION OF TEMPERATURE FOR THE COMPOSITION $10^{m}/o$ $Li_2Si_2O_5$ - $90^{m}/o$ $BaSi_2O_5$ (CODE 10:90)

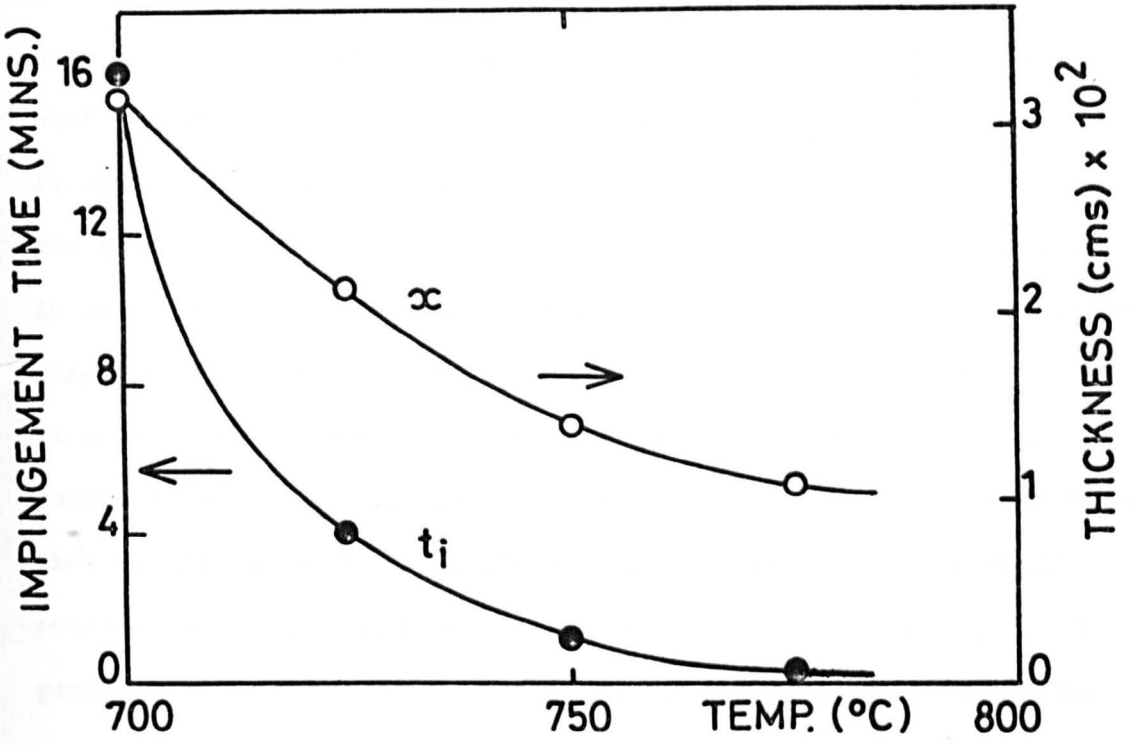

a) As prepared specimen heated directly to temperature of interest.

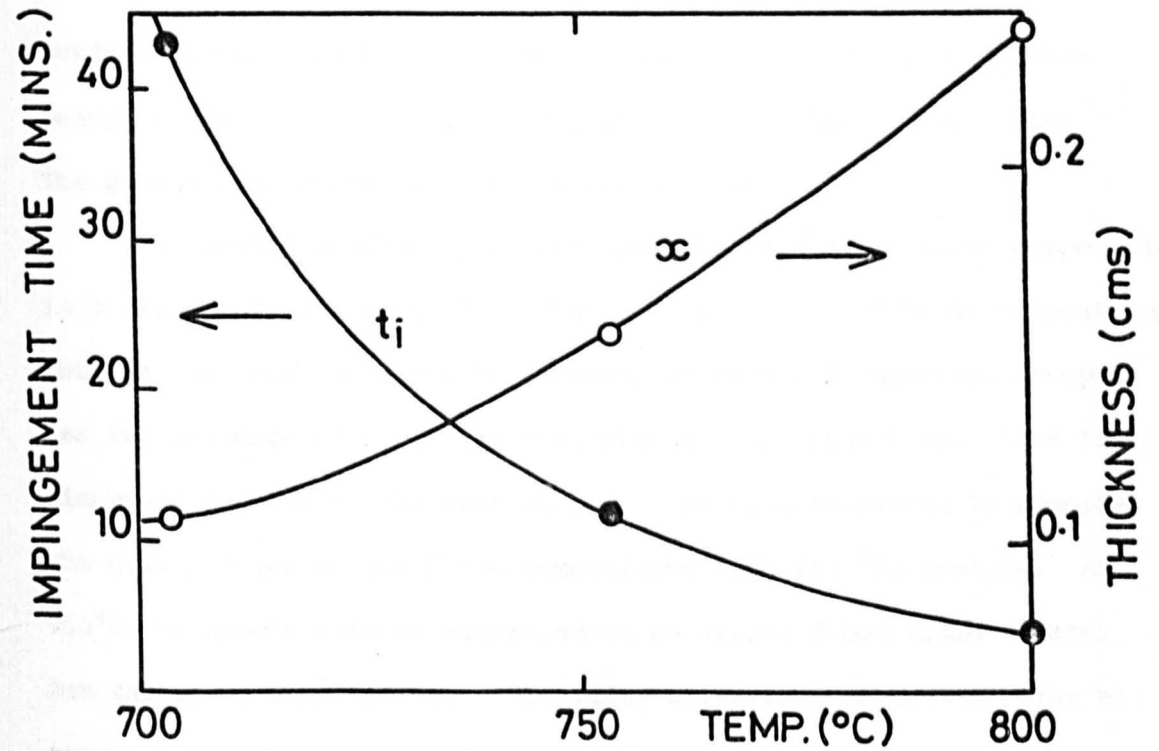

b) Specimen remelted and quenched to the required temperature.

nuclei present in the glass prior to it being placed in the heat treatment furnace. In this case x increases with increasing temperature (see Figure 3.13(b)). The values of t_i, however, decrease as before, but they are obviously overestimates since the specimens were only heat treated 10 minutes. This behaviour is observed because some time is spent at temperatures where the growth rate is higher than that at the temperature of interest. Thus the specimens which are contained in small crucibles would not cool immediately to the furnace temperature. From equation (3.4) a maximum in the nucleation rate is predicted at about 750°C. However, in view of the previous discussion this estimate is probably incorrect. From these experiments it was concluded that whilst the position of the nucleation curve is theoretically obtainable from a measurement of the surface crystalline layer, in practice the occurrence of nucleation and crystal growth before the specimen reaches temperature prevents such a calculation.

Crystal growth rates for the 10:90 composition were determined in the temperature range 625-725°C. The measurements were made on both surface crystallisation and internal spherulites, the growth rates being the same in both cases and constant with time (Figure 3.14). The growth rate curve is shown in Figure 3.15.

The crystal morphology of the spherulites for the 10:90 composition is considerably different from that for the 100 ^{m}/o $BaSi_2O_5$ composition. Thus in this case very little internal structure is apparent except for the presence of a central core within each spherulite. This is discussed further in the next section. It is interesting to compare the growth rates of the 10:90 composition with 100 ^{m}/o $BaSi_2O_5$. At 750°C the growth rate is estimated to be almost 7,000 times greater for the 10:90 composition. This large difference in growth rates at temperatures where the nucleation rate is appreciable, leads to a

FIG. 3.14. GROWTH RATE MEASUREMENTS FOR THE COMPOSITION $10^{m}/o\ Li_2Si_2O_5 - 90^{m}/o\ BaSi_2O_5$ (CODE 10 : 90)

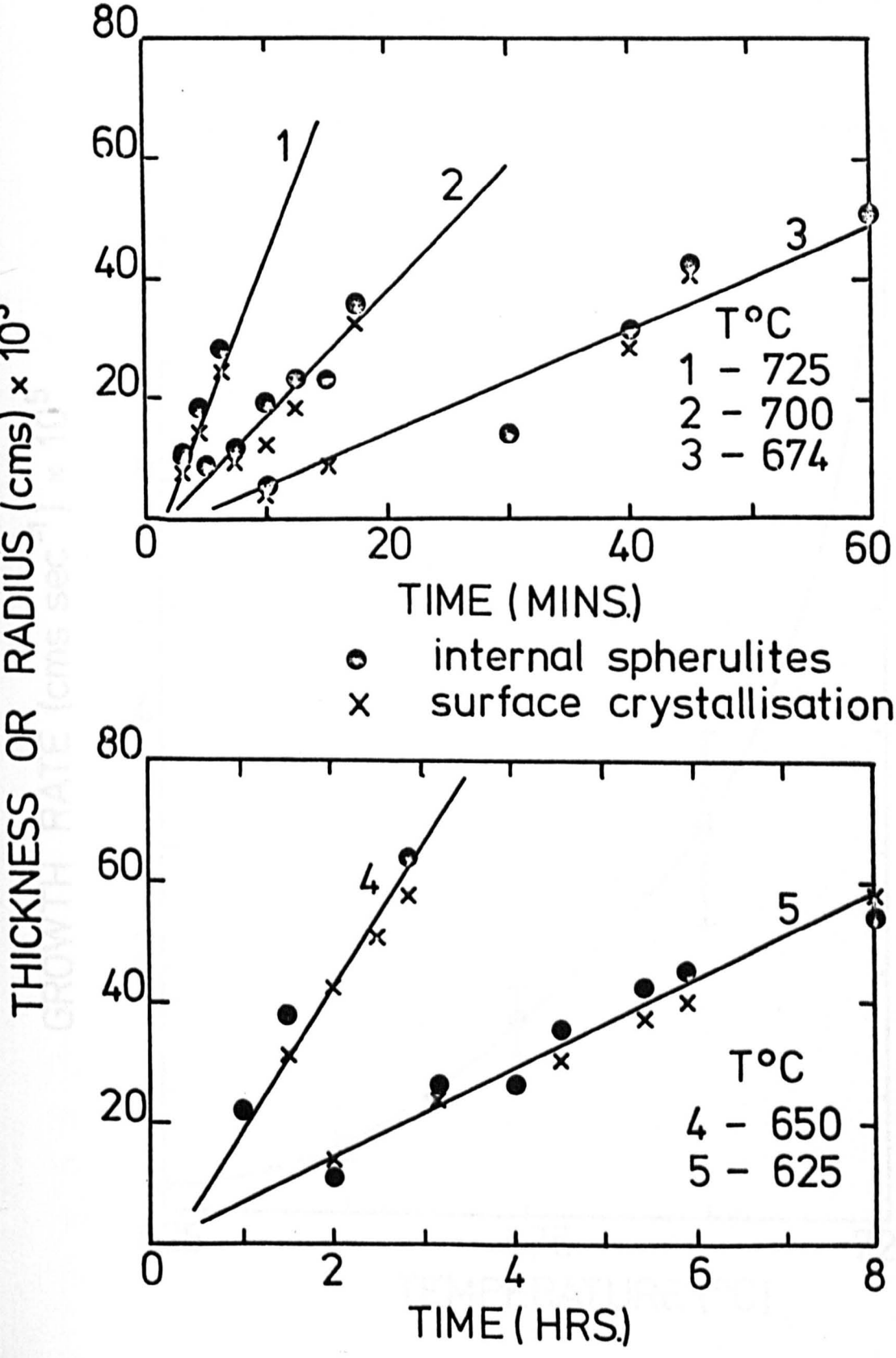

FIG. 3.15. CRYSTAL GROWTH RATE AS A FUNCTION OF TEMPERATURE FOR THE COMPOSITION 10 m/o $Li_2Si_2O_5$ - 90 m/o $BaSi_2O_5$ (CODE 10:90)

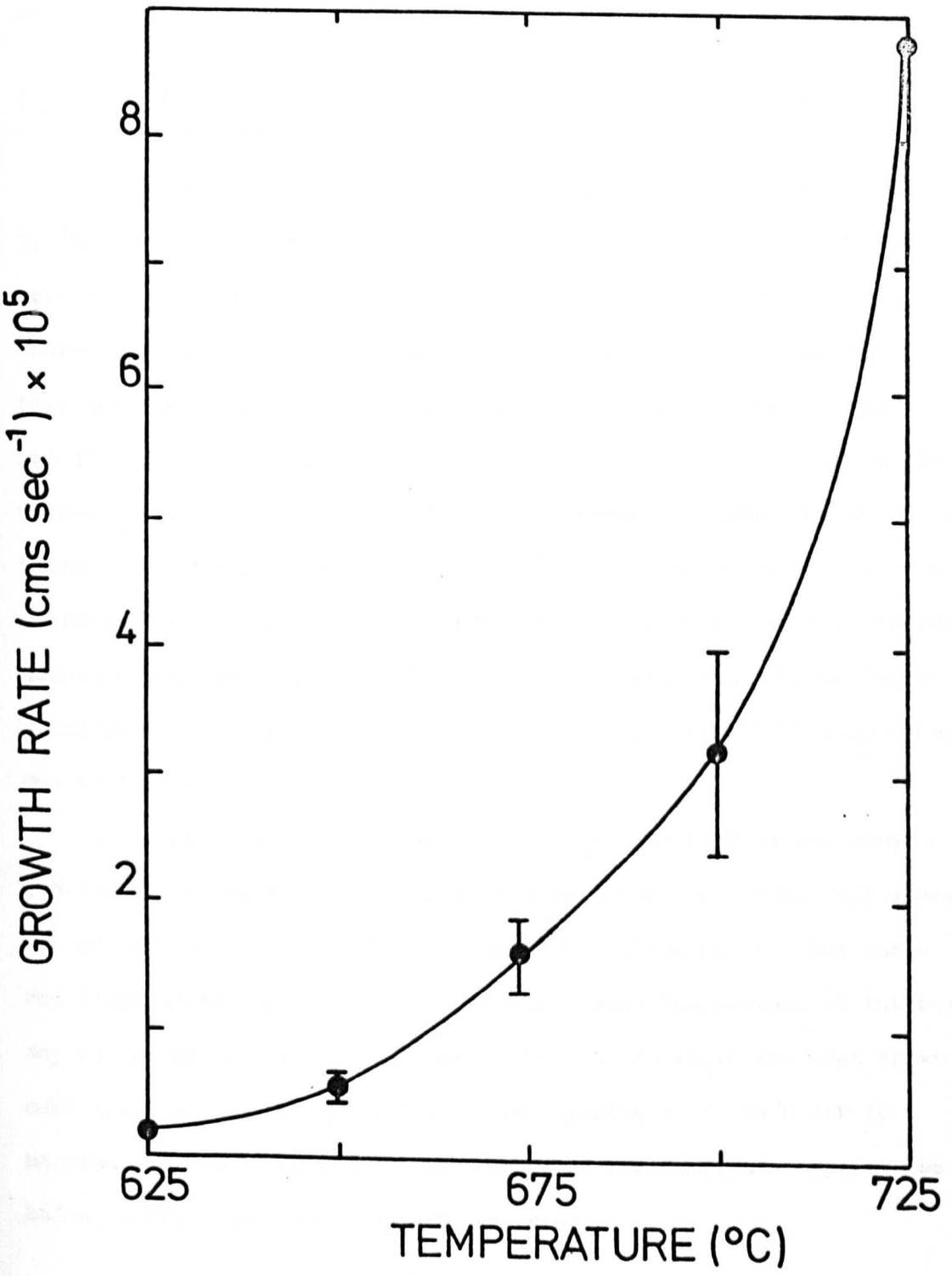

vastly different crystallisation behaviour for the two compositions. Thus whereas the 10:90 composition is virtually crystallised after a few minutes at 750°C, 100 ^{m}/o $BaSi_2O_5$ only begins to show signs of coalescence after 8 hours at that temperature. Further discussion of the difference in crystal growth rates for these two compositions will be given later in this chapter.

3.1.3. 25 ^{m}/o $Li_2Si_2O_5$-75 ^{m}/o $BaSi_2O_5$, Code 25:75 (T_L = 1256°C)

This composition was found to crystallise rapidly above about 720°C. Thus after 10 minutes at 722°C a specimen was almost fully crystalline due to the impingement of internal spherulites. X-ray analysis confirmed the presence of $BaSi_2O_5$ and a small amount of $Li_2Si_2O_5$. Again, it was not possible to positively identify which modification of $BaSi_2O_5$ was present at large supercoolings due to the absence of characteristic peaks. D.T.A. revealed a crystallization exotherm in the temperature range 682-711°C, in agreement with the initial isothermal experiments. A very small exothermic peak was also observed having a maximum at about 880°C. This peak was assumed to be due to a change in crystal morphology, as discussed for the 10:90 composition. The 'D.T.A. T_g' was found to be 550°C.

Nucleation measurements were limited to the temperature range 500-700°C. Above 657°C the nucleation rate was low. Table 3.3 gives the nucleation densities for specimens directly quenched from above the liquidus temperature to the heat treatment temperature of interest. Any nuclei present could only have formed at or above the heat treatment temperature. In general a growth treatment of 675°C for 10 minutes was therefore chosen for specimens nucleated at temperatures below 650°C, where little growth occurred.

TABLE 3.3

NUCLEATION DENSITIES OBSERVED WHEN THE COMPOSITION $25^{m}/o\ Li_2Si_2O_5$-$75^{m}/o\ BaSi_2O_5$ (CODE 25:75) IS QUENCHED FROM ABOVE ITS LIQUIDUS TEMPERATURE DIRECTLY TO A HEAT TREATMENT TEMPERATURE.

Heat treatment	$N_v \times 10^{-4} cm^{-3}$
702-710°C/10 mins	1.73
678-688°C/15 mins	2.84
623-628°C/10 mins	8.87
→ *700°C/15 mins	

* Second heat treatment for growth

In order to locate the nucleation curve, 1 and 2 hour nucleation heat treatments were employed at 25°C intervals, the same growth treatment being used for a given nucleation temperature. The nucleation densities and nucleation rates calculated by difference are given in Table 3.4. Except at 626°C, the spherulites after a given nucleation treatment followed by growth treatment were all nearly the same size (see Figures 3.16). Thus the simple analysis (equation (2.10)) was used to calculate N_v. It can be seen that the spherulites are spherical. The simple analysis and its assumptions have already been discussed for the 100 $^{m}/_{o}$ $BaSi_2O_5$ composition. At 626°C a full analysis (equation (2.6)) was used to calculate the nucleation densities since detectable growth occurred during nucleation, leading to a distribution of spherulite sizes.

In the vicinity of 550°C, i.e. approaching the transformation range, nucleation rates calculated by the above method were expected to be in error due to non-steady state behaviour. Thus more extensive nucleation measurements were made using four times at each temperature. Such measurements were also made at higher temperatures so as to provide an overall check for the nucleation rates based on only two times. These results are shown in Figure 3.17 for both a full analysis, assuming a distribution of spherulite sizes, and a simple analysis, assuming constant sized spherulites. There is good agreement between the two methods of analysis. At 516°C and below it can be seen that nucleation rates calculated from 1 and 2 hour heat treatments will not be steady state. This is shown clearly in Figure 3.18. Curve A is the steady state nucleation curve based on data for long heat treatment times (see Figure 3.17). Curve B is the nucleation curve based on data for 1 and 2 hour heat treatments only (see Table 3.4). At 561°C

TABLE 3.4

NUCLEATION DATA AS A FUNCTION OF TIME AND NUCLEATICN TEMPERATURE FOR THE COMPOSITION $25^{m}/o\ Li_2Si_2O_5$-$75^{m}/o\ BaSi_2O_5$ (CODE 25:75)

T(°C)	time(hrs)	$N_v(cm^{-3})$	$I(cm^{-3}sec^{-1})$
626	1 *	2.65	57.11
	2 *	4.71 x 10^5	
601	1	2.28	596.7
	2	4.43 x 10^6	
576	1	1.01	2.41 x 10^3
	2	1.88 x 10^7	
550	1	3.40	2.36 x 10^3
	2	11.91 x 10^6	
525	1	3.81	6.6
	2	6.20 x 10^4	
500	1	4.01	4.3
	2	5.56 x 10^4	

* Full analysis used to calculate N_v at 626°C. At all other temperatures the simple analysis was used.

Fig. 3.16 Optical micrographs of the composition 25 $^{m}/_{o}$ $Li_2Si_2O_5$-75 $^{m}/_{o}$ $BaSi_2O_5$ nucleated at

Top: 550°C for 1 and 2 hours, grown at 675°C

Bottom: 575°C for 1 and 2 hours, grown at 675°C

Magnification: x200

FIG. 3.17. NUCLEATION DENSITIES VERSUS TIME AS A FUNCTION OF TEMPERATURE FOR THE COMPOSITION 25m/o $Li_2Si_2O_5$ - 75m/o $BaSi_2O_5$ (CODE 25 : 75)

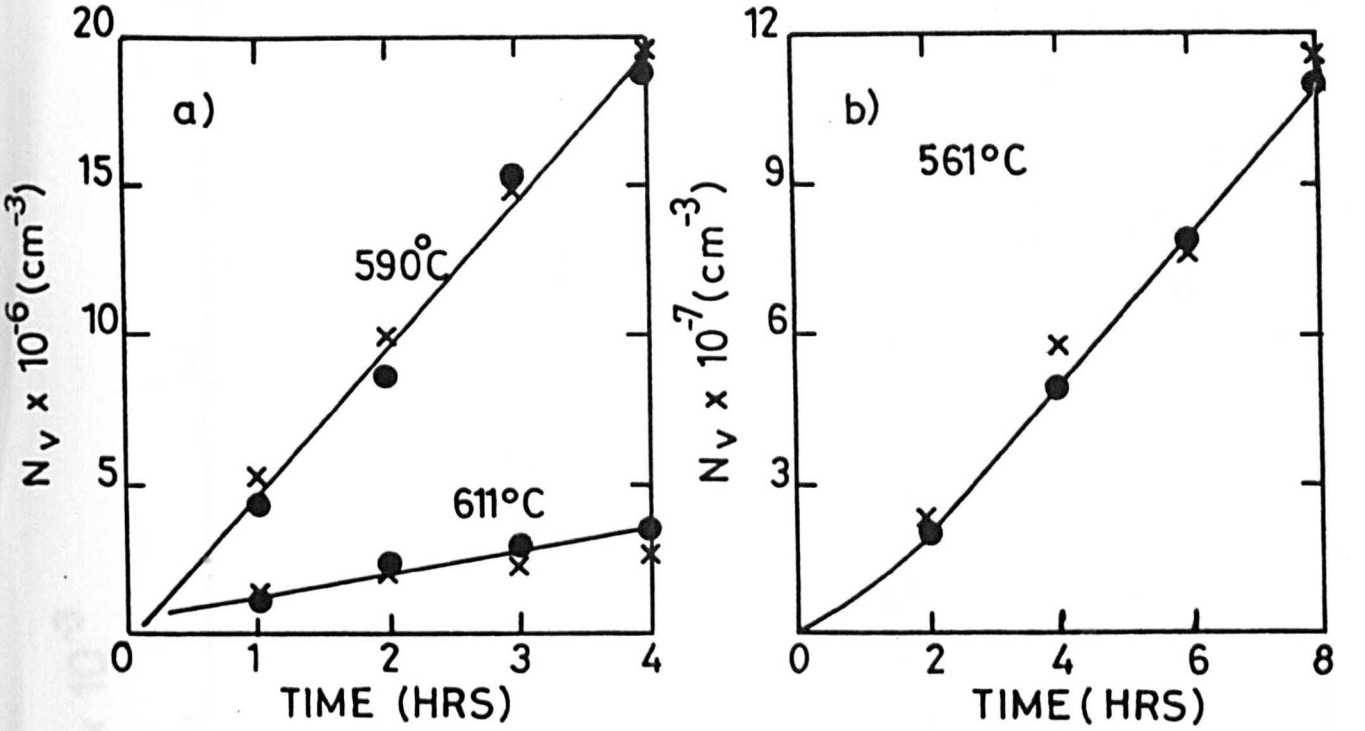

(ALL NUCLEATED SPECIMENS GIVEN GROWTH TREATMENT 675°C / 8–13 MINS.)

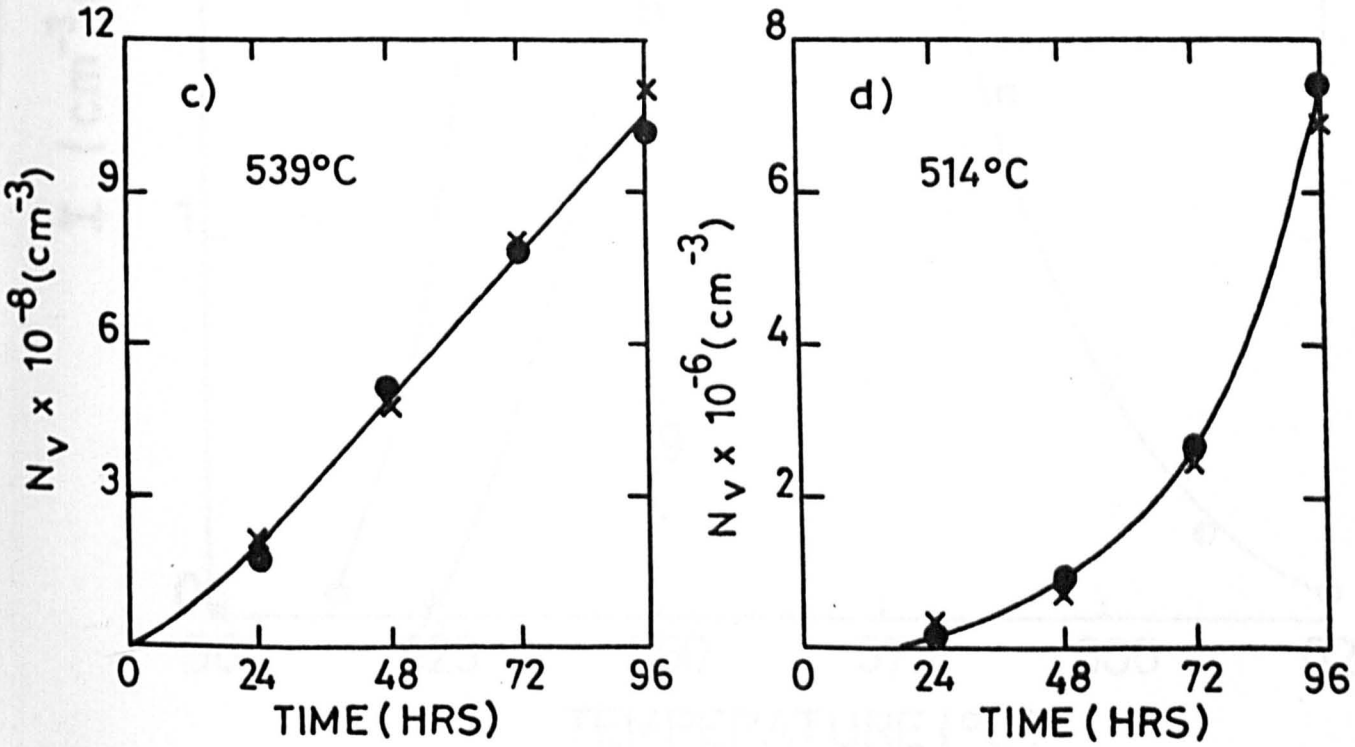

● FULL ANALYSIS

x SIMPLE ANALYSIS

FIG.3.18. NUCLEATION RATE AS A FUNCTION OF TEMPERATURE FOR THE COMPOSITION $25^{m}/_{o}Li_2Si_2O_5 - 75^{m}/_{o}BaSi_2O_5$ (CODE 25:75)

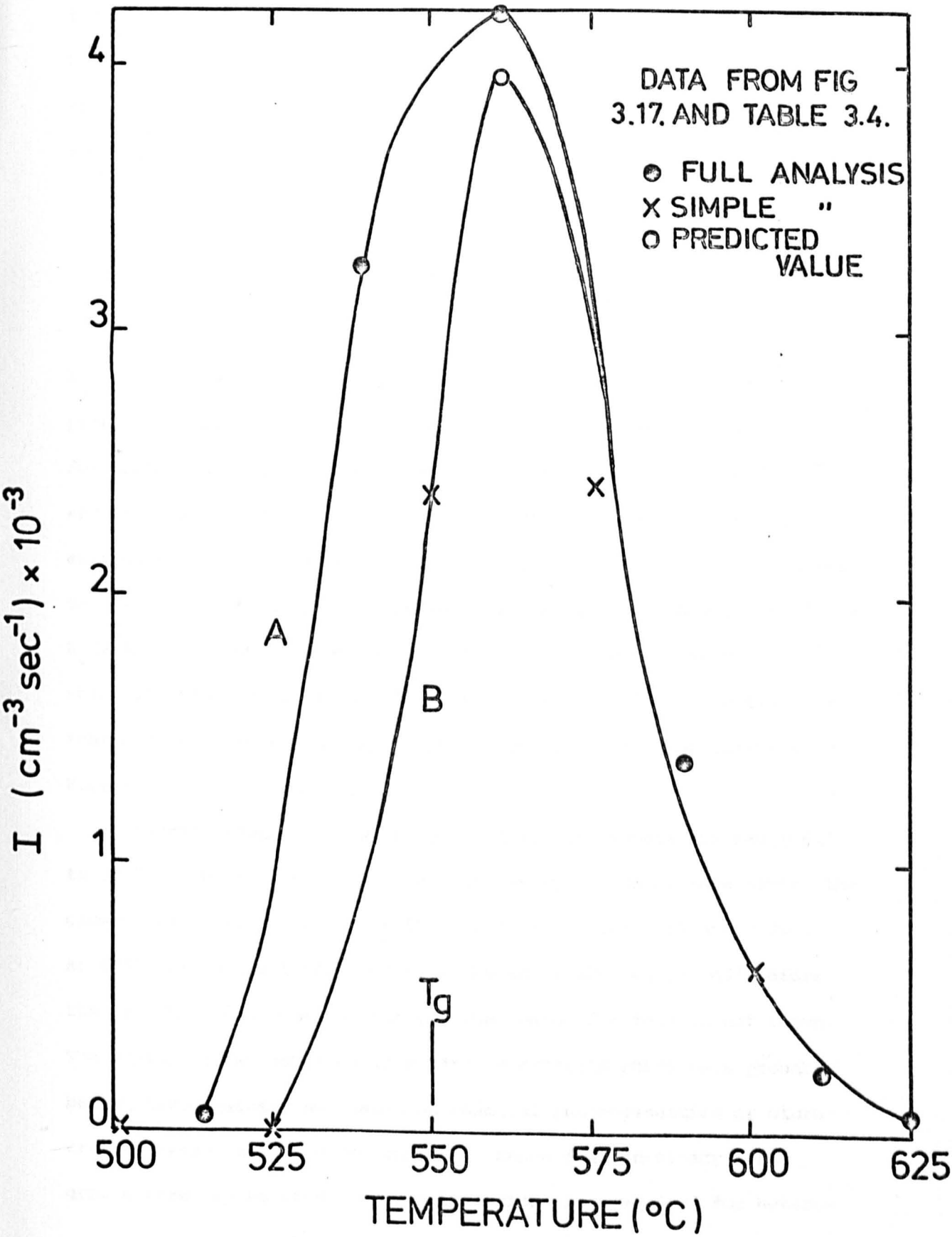

Curve A : Steady state nucleation rates.
Curve B : Nucleation rates based on 1 and 2 hour heat treatments.

and below, curve B predicts nucleation rates considerably lower than the actual steady state values. The difference between curves A and B can be predicted theoretically using non-steady state homogeneous nucleation theory. It can be shown that the nucleation density $N_v(t)$ after time t is given by[23]

$$\frac{N_v(t)}{I_o \tau} = \frac{t}{\tau} - \frac{\pi^2}{6} - 2 \sum_{n=1}^{\infty} \frac{(-1)^n}{n^2} \exp\left(-\frac{n^2 t}{\tau}\right) \qquad (3.6)$$

I_o and τ are simply evaluated by drawing a straight line through the points at longer times in the nucleation density versus time plots. For example at 561°C, I_o and τ are found to be $4{\cdot}19 \times 10^3$ cm^{-1} sec^{-1} and 26 mins respectively (see Figure 3.17(b)). Hence N_v(1 hr) is estimated to be $5{\cdot}42 \times 10^6$ cm^{-3} at 561°C, from equation (3.6). Using this value for N_v(1 hr) and the measured value of $19{\cdot}66 \times 10^6$ cm^{-3} for N_v(2 hr) the apparent nucleation rate is found to be $3{\cdot}96 \times 10^3$ $cm^{-3}sec^{-1}$ which is slightly lower than I_o. Above 561°C the induction times decrease rapidly and are unobservable. Thus the nucleation curves in Figure 3.18 become identical.

Crystal growth rates were obtained in the temperature range 625 to 722°C. The measurements were made mainly on the surface layer, the growth rates being constant with time (see Figures 3.19 and 3.20). At 678°C and below there appears to be an 'induction period' before the growth rate becomes constant. The reason for this is not known. The surface layer develops from surface crystals which have probably been heterogeneously nucleated on chemical inhomogeneities or microcracks present at the glass surface. Hence the non-steady state growth rate may be caused by the induction time required for hetero-

FIG. 3.19. GROWTH RATE MEASUREMENTS FOR THE COMPOSITION 25 m/o $Li_2Si_2O_5$ - 75 m/o $BaSi_2O_5$ (CODE 25:75)

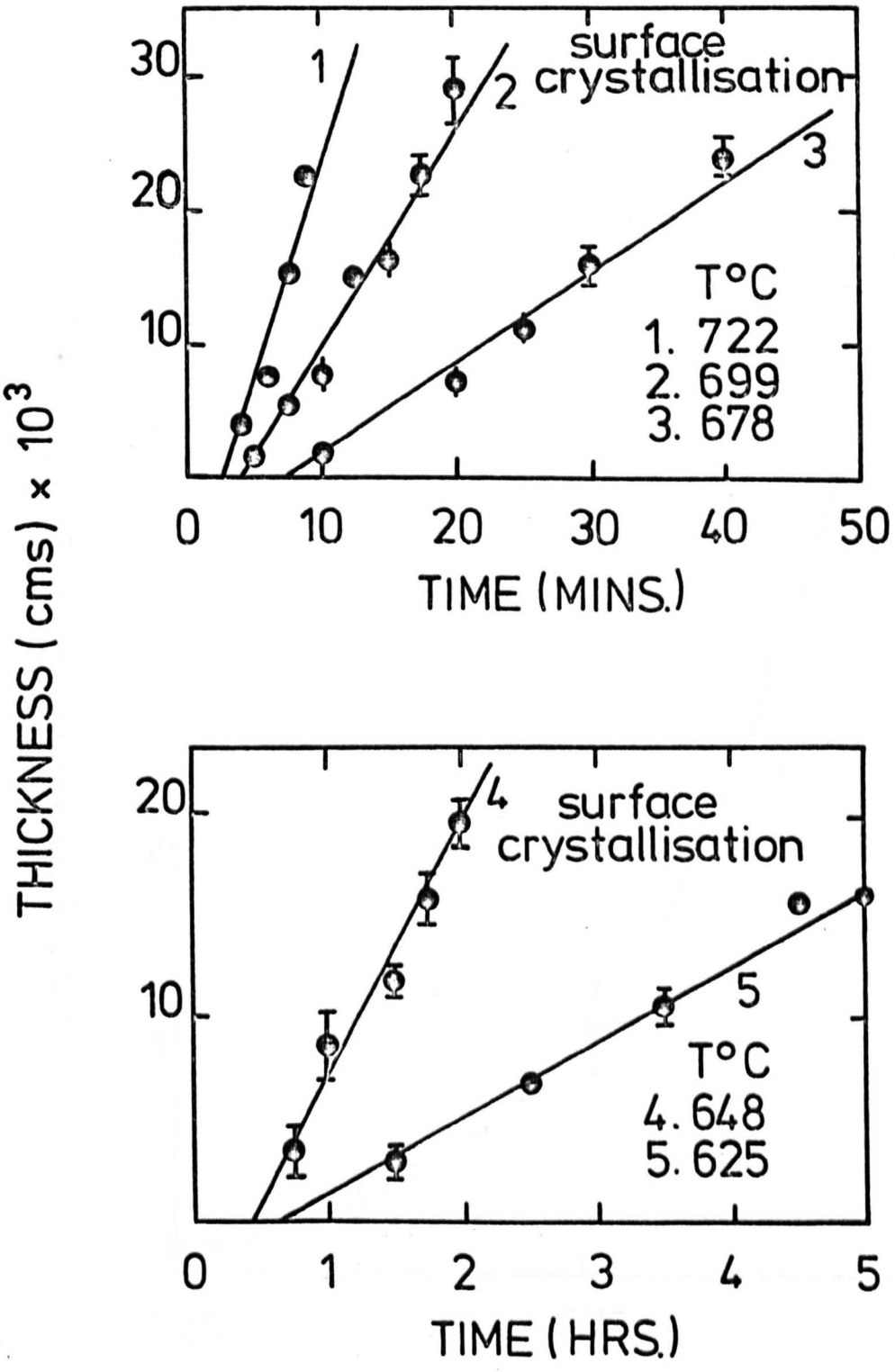

FIG. 3.20. CRYSTAL GROWTH RATE AS A FUNCTION OF TEMPERATURE FOR THE COMPOSITION 25 m/o $Li_2Si_2O_5$ – 75 m/o $BaSi_2O_5$ (CODE 25 : 75)

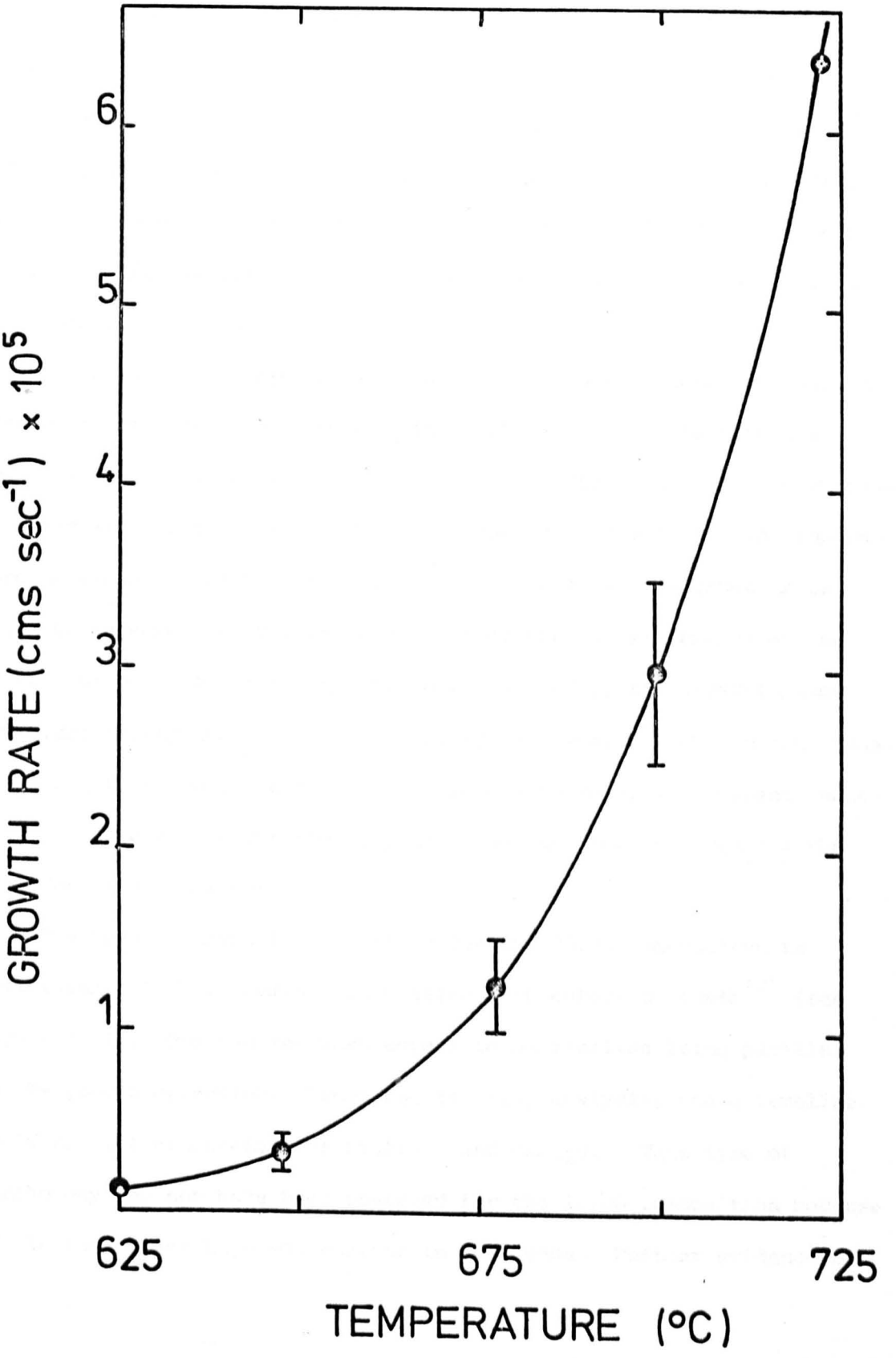

geneous surface nucleation at this temperature. The nucleation data presented earlier showed that the induction time for homogeneous internal nucleation is negligible above about 575°C. From theoretical considerations[23] the induction times for heterogeneous internal nucleation are expected to be even smaller than in the homogeneous case. If we assume that the induction times for surface nucleation and internal nucleation are similar, it seems unlikely that the delay time in surface growth is due to a nucleation induction time. However, we have no measurements of surface nucleation induction times to test this possibility directly.

Two more likely explanations have already been referred to whilst presenting data for the growth of internal $BaSi_2O_5$ crystals in the composition 100 ^{m}/o $BaSi_2O_5$ (section 3.1.1). First, the growing surface crystals will take longer to become macroscopic in size as the temperature decreases. Before attaining macroscopic size, the growth rate might be expected to increase with time as the surface energy of the crystal becomes relatively unimportant. Secondly, the crystal phase may alter during the course of the growth process. If this phase transformation is accompanied by a change in growth rate, an apparent induction period would be observed depending on the time required for the transformation to occur.

The crystal morphology observed for the 25:75 composition is reminiscent of that commonly associated with eutectic growth[2] (see Figure 3.21). One can see what appear to be lamellae lying parallel to the growth direction. According to x-ray analysis, these lamellae would consist alternately of $Li_2Si_2O_5$ and $BaSi_2O_5$. This type of morphology may not have been observed for the 10:90 composition because of the much lower $Li_2Si_2O_5$ content in that case. Further evidence of

Fig. 3.21 Optical micrograph of the composition 25 ^{m}/o $Li_2Si_2O_5$-75 ^{m}/o $BaSi_2O_5$ heated at 722°C for 9 minutes

Top: Internal and surface crystallisation; magnification x100

Bottom: Centre of internal spherulite; magnification x500

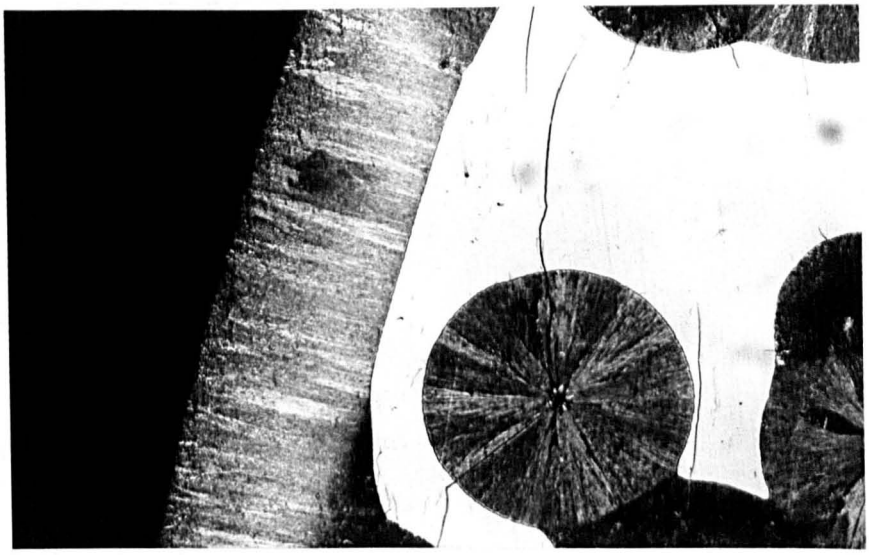

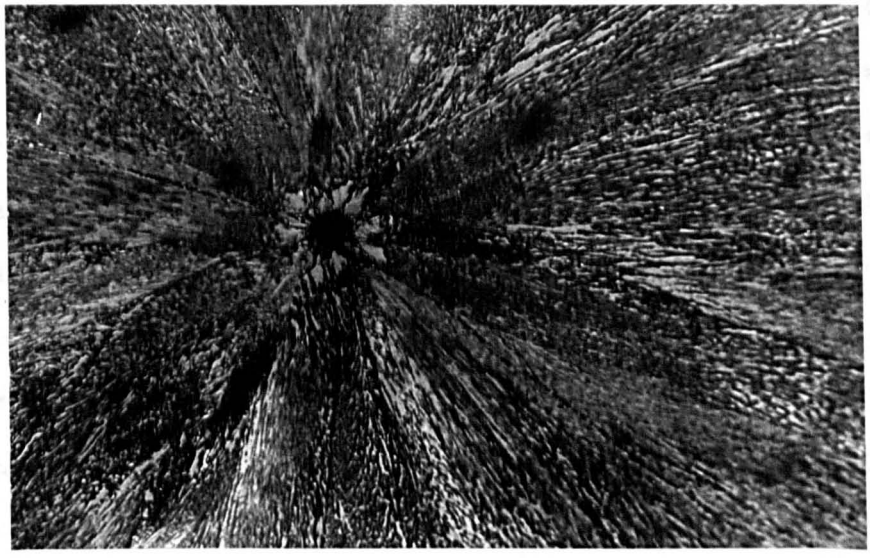

eutectic growth in several glasses will be presented in this chapter. An interesting feature of the internal crystals is the presence of a clearly defined core within each spherulite. A similar morphology was observed for the nucleation of $BaSi_2O_5$ in the Na_2O-BaO-SiO_2 system[20]. Here it was suggested that the core marks the extent of growth of h-$BaSi_2O_5$, this having been precipitated first. Subsequent heating converts this to ℓ-$BaSi_2O_5$, which grows further to produce a spherulitic structure.

3.1.4 50 m/o $Li_2Si_2O_5$-50 m/o $BaSi_2O_5$, Code 50L:50 (T_L = 1065°C)

Preliminary experiments on the 50L:50 composition showed that crystallisation only occurred from the surface and no appreciable internal nucleation was observed. Thus at no temperature did the internal nucleation rate exceed 1 cm^{-3} sec^{-1}. X-ray analysis revealed two crystalline phases viz. $Li_2Si_2O_5$ and a much larger amount of $BaSi_2O_5$. For heat treatments typically used for measuring growth kinetics (650-750°C, 0-2 hrs), it was not possible to determine which modification of $BaSi_2O_5$ was present. Longer heat treatment times gave diffraction patterns which agreed more closely with the standard data. Figure 3.22 compares 1 hr and 26 hr heat treatments at 749°C. After 1 hr none of the characteristic peaks for low or high $BaSi_2O_5$ are present, but after 26 hours there is a strong peak at 2θ equals 26·0° indicating the present of low $BaSi_2O_5$. It is interesting to note that the major $BaSi_2O_5$ peak at 2θ equals 23·3° and also the peaks at 2θ equals 38° to 42° are considerably reduced by the longer heat treatment.

D.T.A. revealed a crystallisation exotherm in the temperature range 637-685°C. Since the internal nucleation rates were very low this peak corresponds to the temperature at which the glass particles

FIG. 3.22. X-RAY DIFFRACTION PATTERNS FOR 50^{m}/o $Li_2Si_2O_5$-50^{m}/o $BaSi_2O_5$.

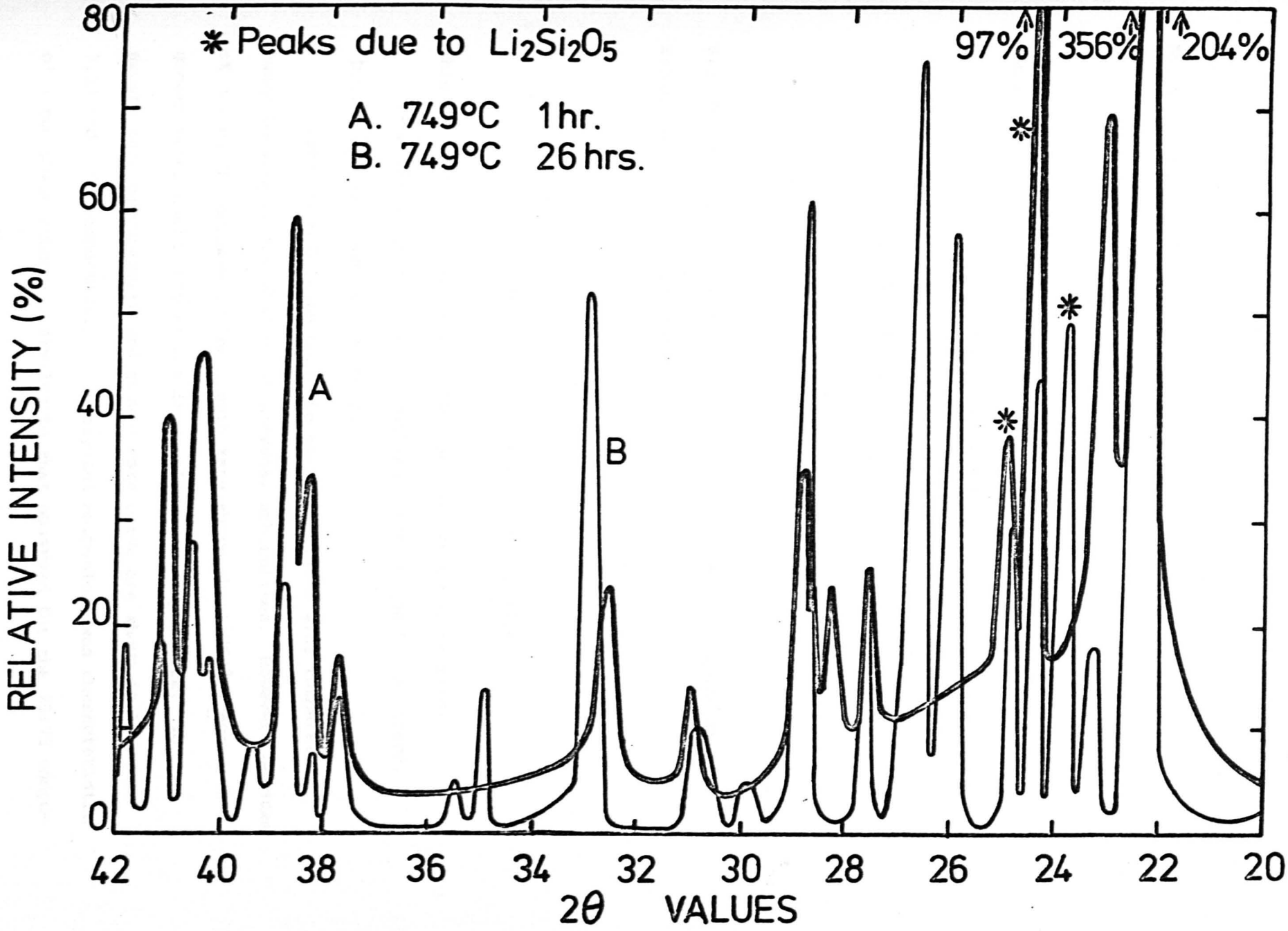

(~ 10 μm in size) completely crystallise from the surface. Thus assuming all the particles to be the same size the amount of growth for a given particle is given by

$$x = \int_{637}^{685} u\,dt$$

assuming that little growth occurs below 637°C.

Since the D.T.A. heating rate is 10°C min^{-1}

$$dT/dt = 1/6°C\ sec^{-1}$$

$$\therefore \quad x = 6\int_{637}^{685} u\,dt$$

From Figure 3.24, $u \sim 4{\cdot}4 \times 10^{-7}(T)$ cms sec^{-1} in the temperature range 637-685°C. Therefore

$$x = 26.4\int_{637}^{685} T\,dT \times 10^{-7}$$

$$\simeq 3\ \mu m \text{ i.e. particles } \sim 6\ \mu m \text{ in size.}$$

This is in good agreement with the approximate particle size.

From the position of the endothermic dip on the D.T.A. trace, 'D.T.A. T_g' was found to be 500°C.

Crystal growth rates could be measured over a wide temperature range because of the absence of internal spherulites. However, because of the rapid increase in the growth rate above about 750°C, accurate growth rates could only be obtained below this temperature. The growth rate measurements and growth rate curve are shown in Figures 3.23 and 3.24 respectively. The crystal morphology was characteristic of a two-phase eutectic, similar to that observed for the 25:75 compo-

FIG. 3.23. GROWTH RATE MEASUREMENTS FOR THE COMPOSITION 50^{m}/o $Li_2Si_2O_5$ - 50^{m}/o $BaSi_2O_5$ (CODE 50L:50)

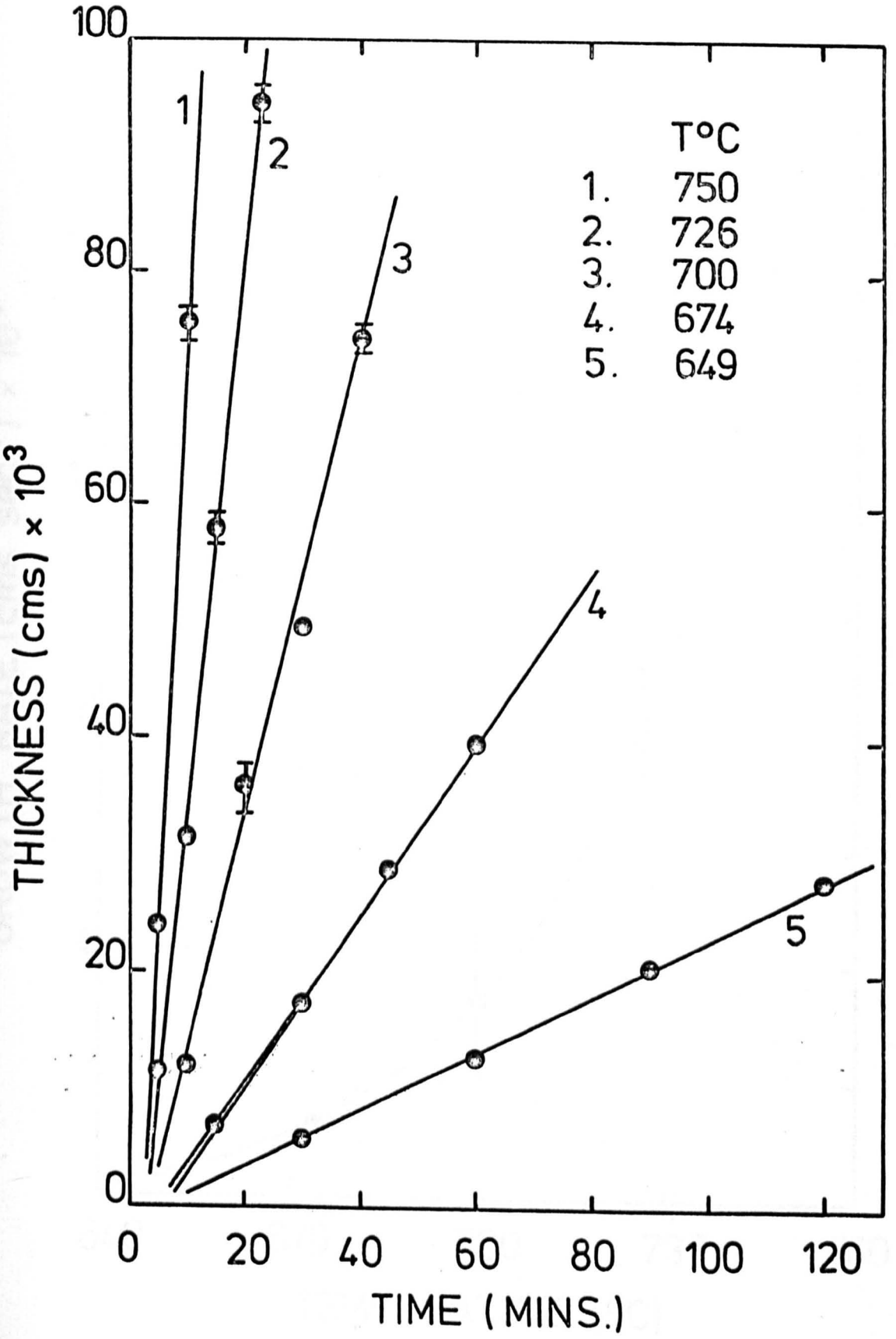

FIG. 3.24. CRYSTAL GROWTH RATE AS A FUNCTION OF TEMPERATURE FOR THE COMPOSITION 50 m/o $Li_2Si_2O_5$ - 50 m/o $BaSi_2O_5$ (CODE 50L:50)

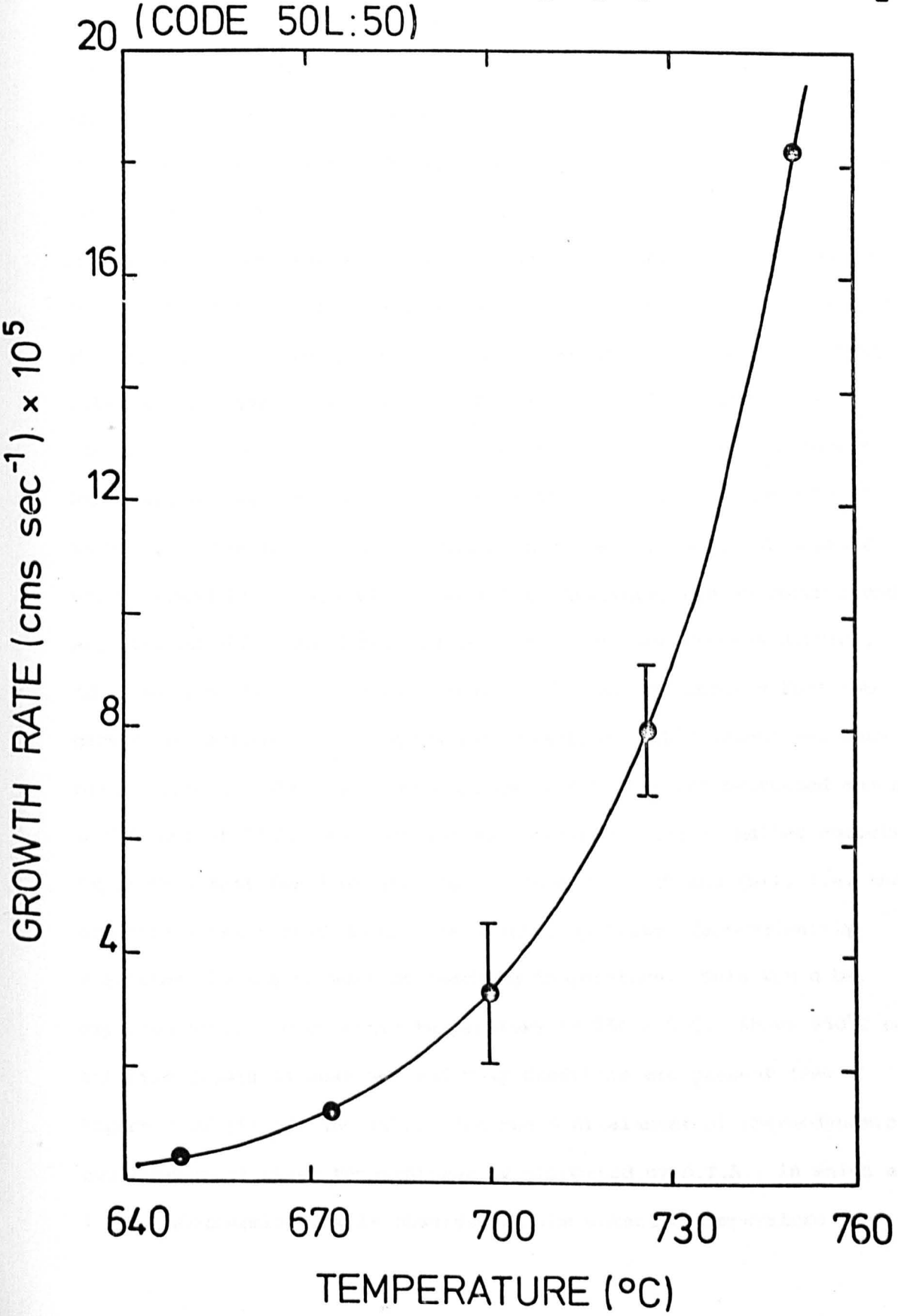

sition (see Figure 3.25). The structure is revealed more clearly by electron microscopy (see Figure 3.26).

If crystal growth does occur by a eutectic mechanism for this composition, then the growth rate of the eutectic layer would be expected to be zero above the eutectic temperature, which is 950°C[42]. Thus further growth rate data was determined above 750°C by heat treating specimens for 3 and 5 minutes at temperatures up to 1000°C. Approximate growth rates were then calculated from the difference in the thickness of the crystalline layer. Up to 873°C the structure of the crystal layer remains a two phase eutectic and the crystal-liquid interface is smooth (see Figure 3.27(a)). At 873°C, however, a 'dendritic' type of structure is also present, with areas of eutectic structure between the dendrites (see Figure 3.27 (b)). Above 873°C it was possible to distinguish two boundaries viz. an inner boundary which marked the extent of the eutectic structure, and an outer boundary, beyond which the dendrites had not grown (see Figures 3.27(c), (d), (e) and (f)). Therefore, above 873°C, it was assumed that two growth mechanisms were in operation, namely eutectic growth and dendritic growth. The growth rate of the eutectic layer decreased above 873°C, and at 948°C the 5 minute heat treatment had a smaller eutectic layer than that for 3 minutes (see Figure 3.27 (g) and (h)), i.e. the eutectic layer formed during the heating up period (approximately 3 minutes) begins to melt on reaching temperature. This would be expected since the eutectic temperature is 950 ± 5°C. Above 950°C no eutectic growth is observed and only dendrites are present (see Figure 3.27 (i) (j) and (k)). The rapid attainment of thermodynamic equilibrium at these temperatures is supported by D.T.A., in which a large endothermic peak is observed at the eutectic temperature when

Fig. 3.25 Optical micrographs of the composition 50 ^{m}/o $Li_2Si_2O_5$-50 ^{m}/o $BaSi_2O_5$ heated at

Top left: 750°C for 5 minutes; magnification x200

Top right: 750°C for 10 minutes; magnification x100

Bottom left: 700°C for 40 minutes; magnification x200

Bottom right: 700°C for 40 minutes; magnification x500

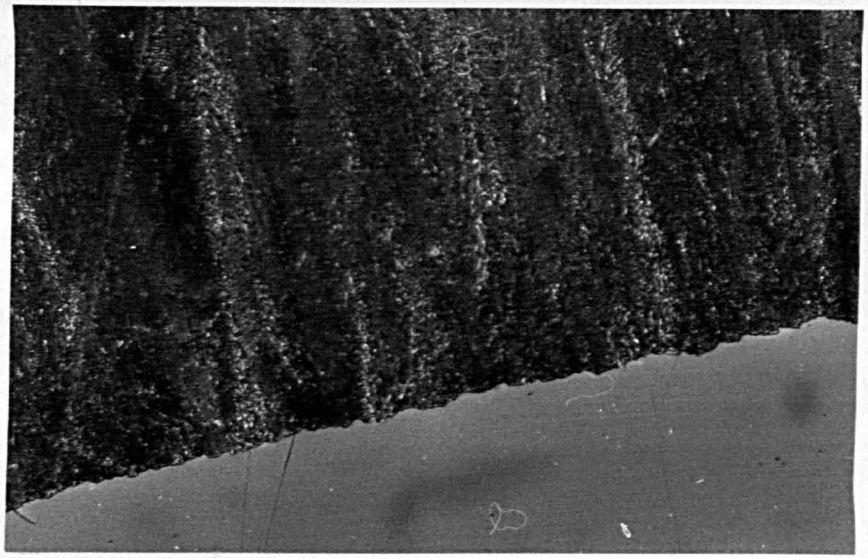

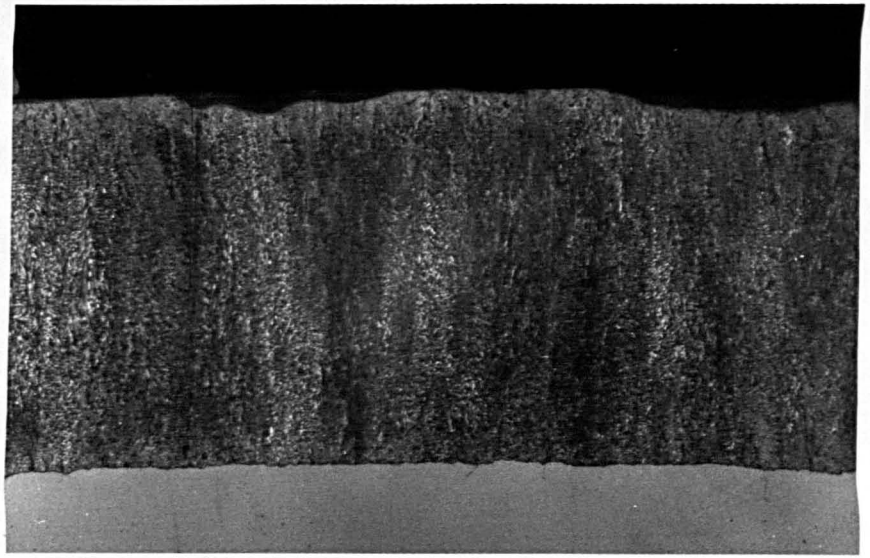

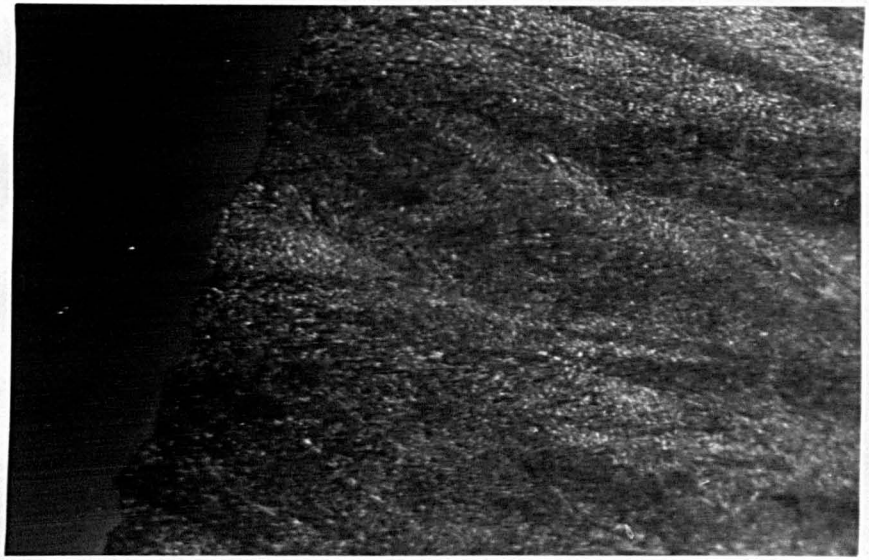

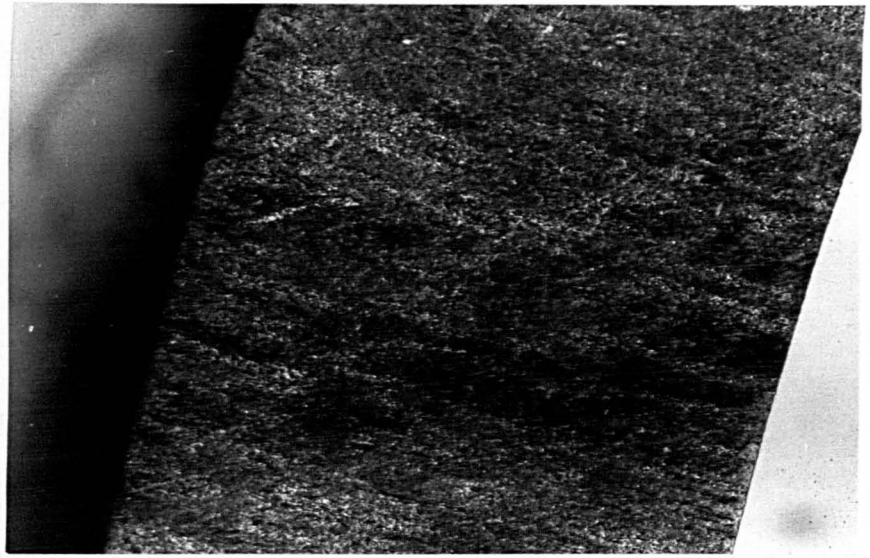

Fig. 3.26 Replica electron micrograph of the composition 50 $^{m}/_{o}$ $Li_2Si_2O_5$-50 $^{m}/_{o}$ $BaSi_2O_5$ crystallised at 700°C.

Magnification x3000

Fig. 3.27 Optical micrographs of the composition 50 ^{m}/o $Li_2Si_2O_5$-50 ^{m}/o $BaSi_2O_5$ heated at

(a) Top left 848°C for 5 minutes; magnification x50

(b) Top right: 873°C for 5 minutes; magnification x100

(c) Bottom left: 898°C for 5 minutes; magnification x100

(d) Bottom right: 898°C for 5 minutes; magnification x32

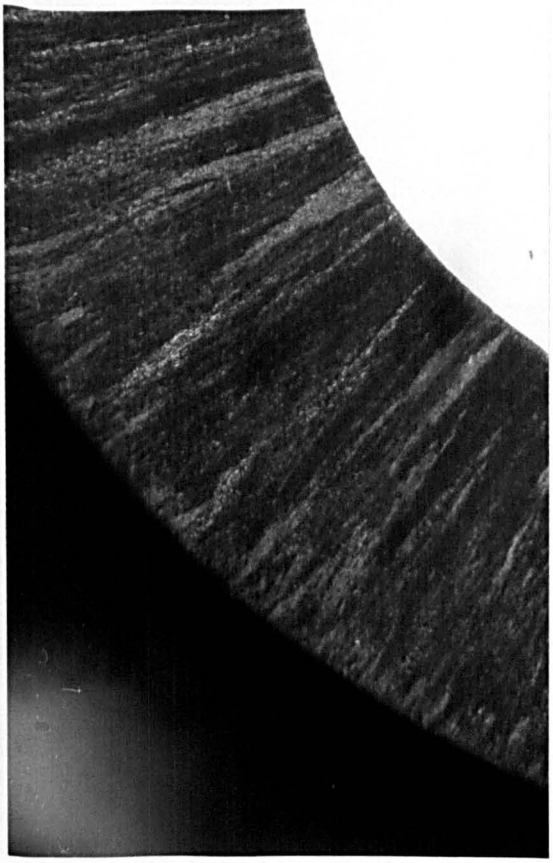

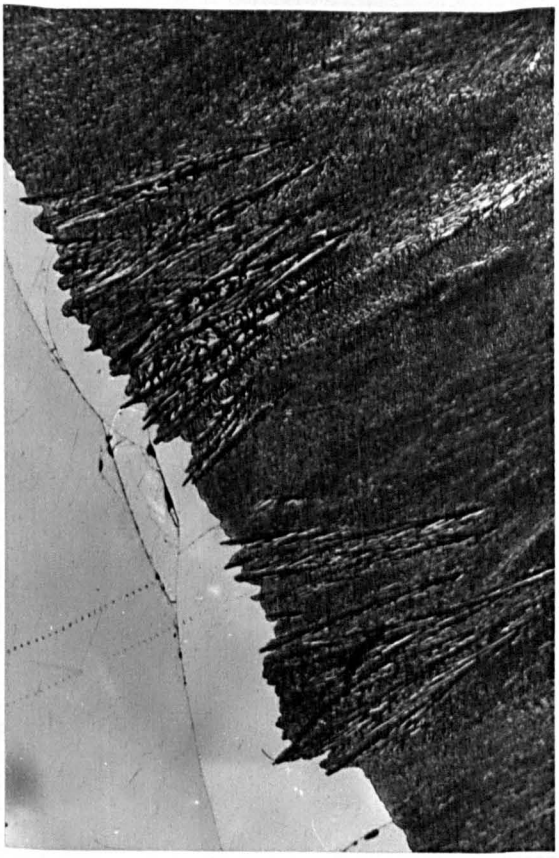

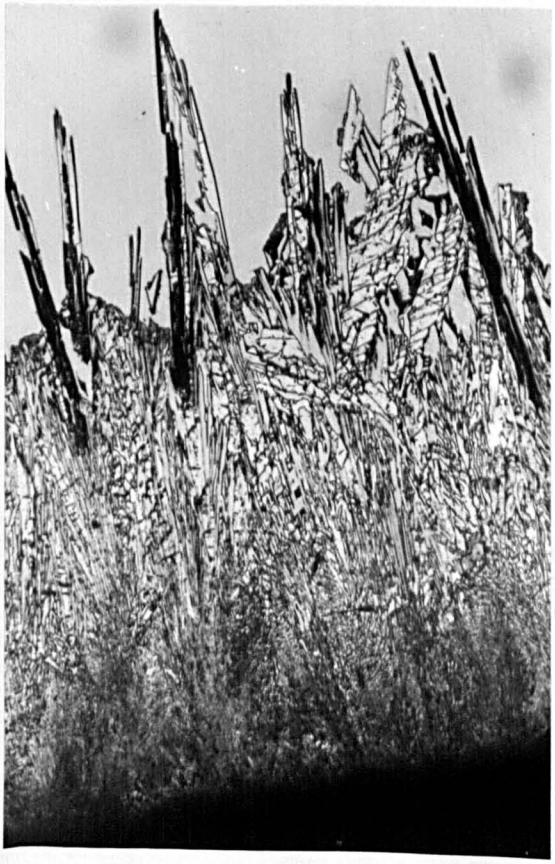

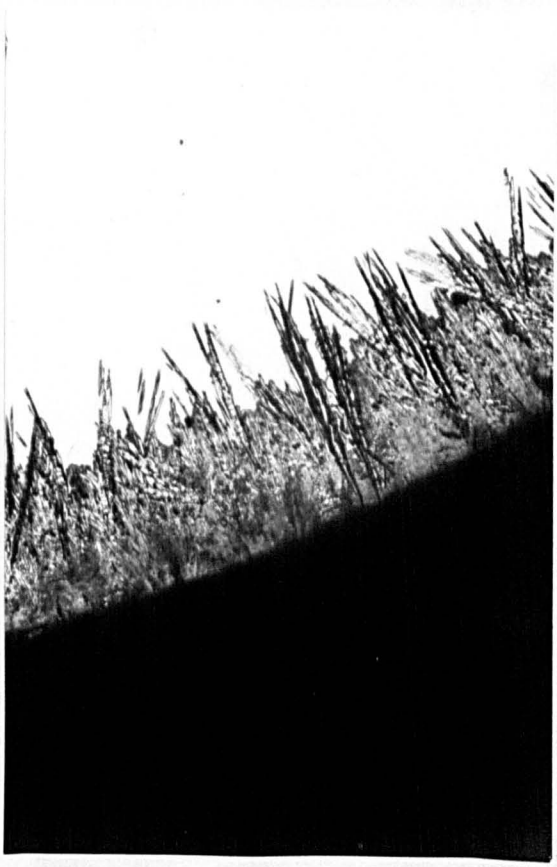

Fig. 3.27 contd/...

(e) Top left: 924°C for 5 minutes; magnification x200

(f) Top right: 924°C for 5 minutes; magnification x32

(g) Bottom left: 948°C for 3 minutes; magnification x100

(h) Bottom right: 948°C for 5 minutes; magnification x100

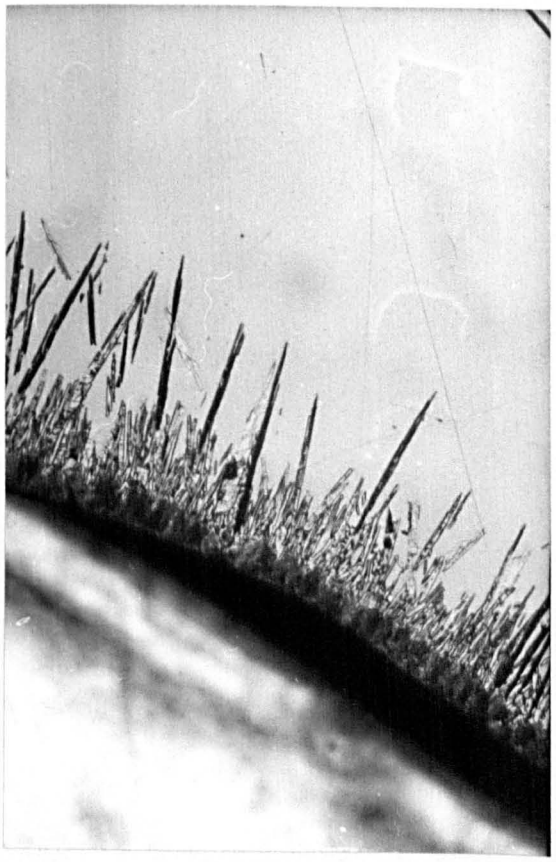

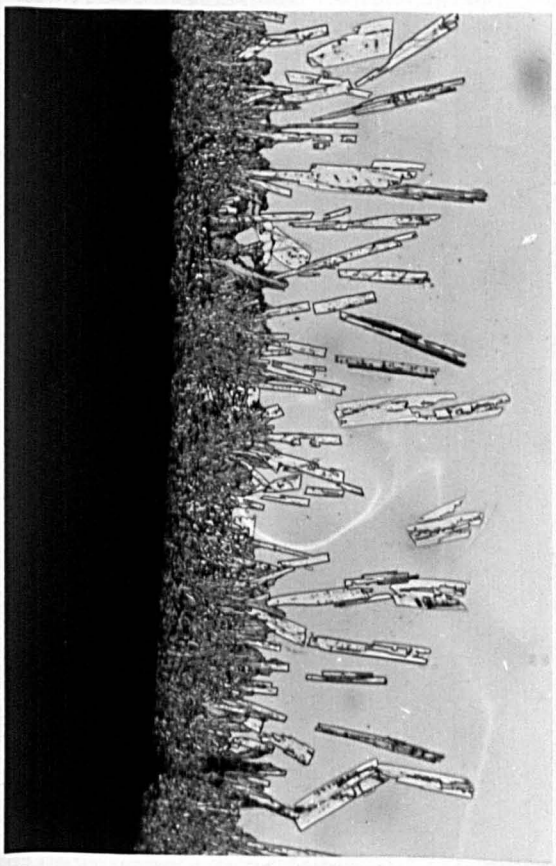

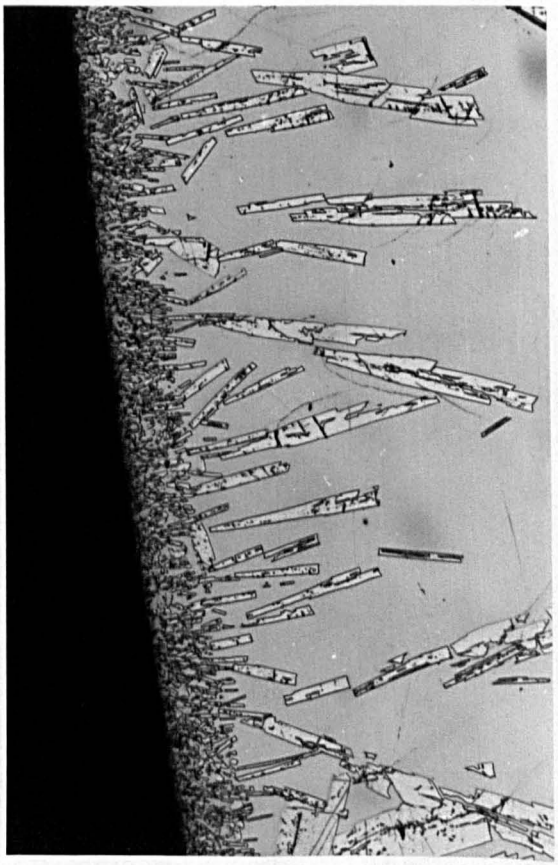

Fig. 3.27 contd/...

(i) Top left: 974°C for 5 minutes; magnification x100

(j) Top right: 974°C for 5 minutes; magnification x32

(k) Bottom: 998°C for 5 minutes; magnification x32

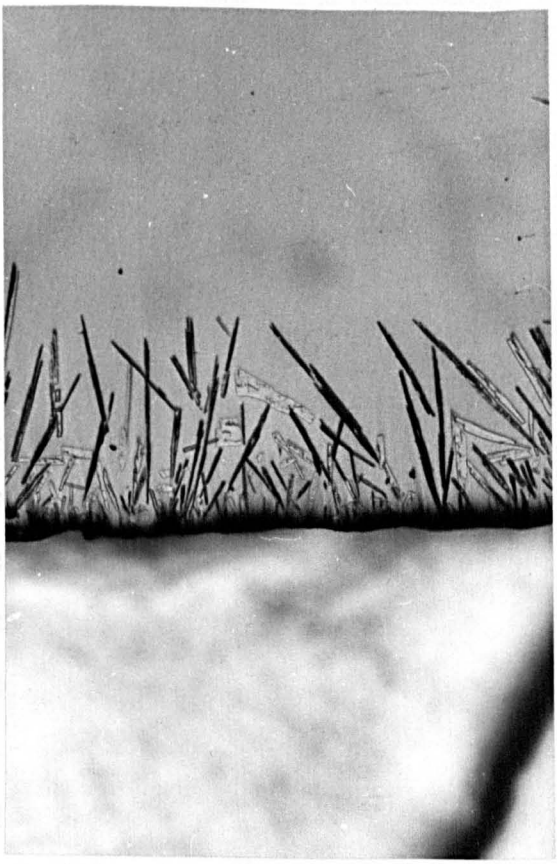

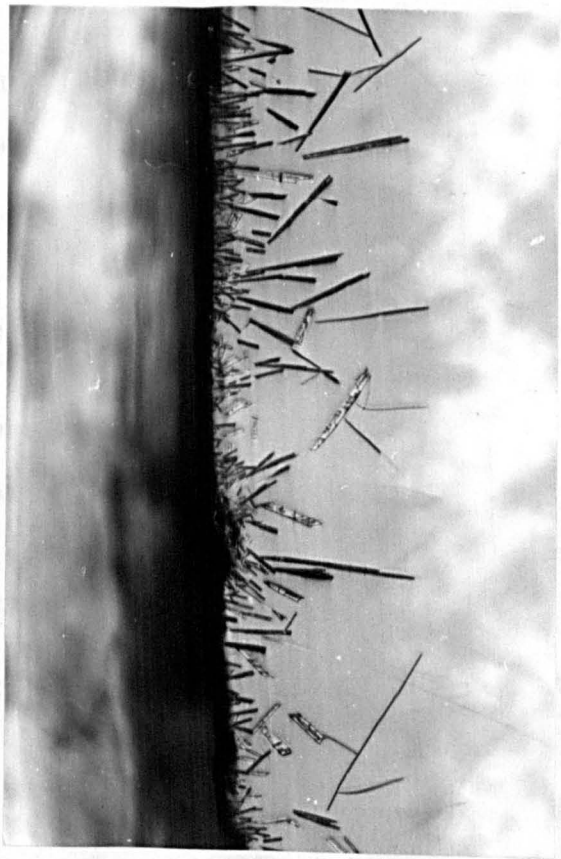

glass powder is heated up from room temperature at 10°C min^{-1}. From the phase diagram, the dendrites are expected to be the primary phase, $BaSi_2O_5$. The dendritic layer has a maximum growth rate at about 898°C. Above this temperature specimens begin to flow and it also becomes difficult to quench the specimens rapidly. Thus the dendritic growth rate curve is only tentative, and it is assumed to be zero at the liquidus temperature, 1065°C. The eutectic and dendritic growth rate curves are both shown in Figure 3.28.

It would appear, therefore, that eutectic growth does occur in the 50L:50 composition, although at temperatures above 873°C $BaSi_2O_5$ dendrites are able to grow more rapidly than the $Li_2Si_2O_5$-$BaSi_2O_5$ eutectic because there is a larger supercooling for the former process ($T_L = T_E + 115°C$). Below 873°C however, the eutectic has an advantage over the primary $BaSi_2O_5$ dendrites, in that diffusion is required over a much smaller distance. For example, at 873°C after 5 minutes, the primary phase $BaSi_2O_5$ dendrites are much wider than the interlamellar spacing of the $Li_2Si_2O_5$-$BaSi_2O_5$ eutectic (see Figure 3.27(b)).

3.1.5 50 m/o $Na_2Si_2O_5$-50 m/o $BaSi_2O_5$, Code 50N:50 (T_L = 1050°C

Whilst the crystallisation behaviour of this composition has already been examined by Burnett and Douglas[20], further measurements have been made in this study in order to facilitate a direct comparison with the 50L:50 composition.

In the Na_2O-BaO-SiO_2 system it was shown that h-$BaSi_2O_5$ nucleates first and this subsequently transforms to the low form on further heat treatment. The nucleation curve for 50N:50 is shown in Figure 3.29. In comparison, 50L:50 has a very low nucleation rate,

FIG. 3.28. CRYSTAL GROWTH RATES AS A FUNCTION OF TEMPERATURE FOR THE COMPOSITION 50 m/o $Li_2Si_2O_5$ - 50 m/o $BaSi_2O_5$. (CODE 50L:50)

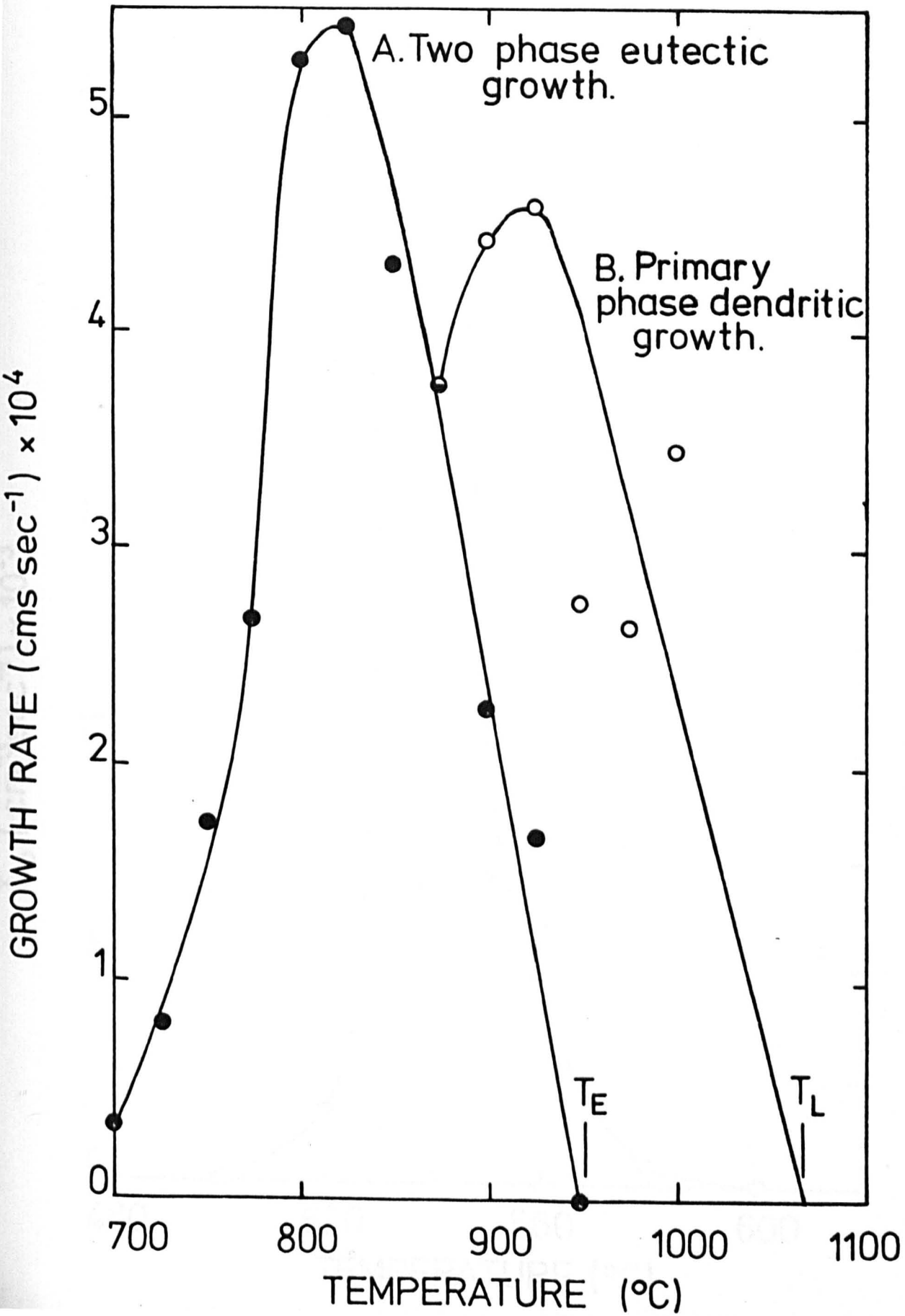

FIG. 3.29. STEADY STATE NUCLEATION RATE AS A FUNCTION OF TEMPERATURE FOR THE COMPOSITION 50 m/o $Na_2Si_2O_5$ - 50 m/o $BaSi_2O_5$ (CODE 50N:50) AFTER REF. 20.

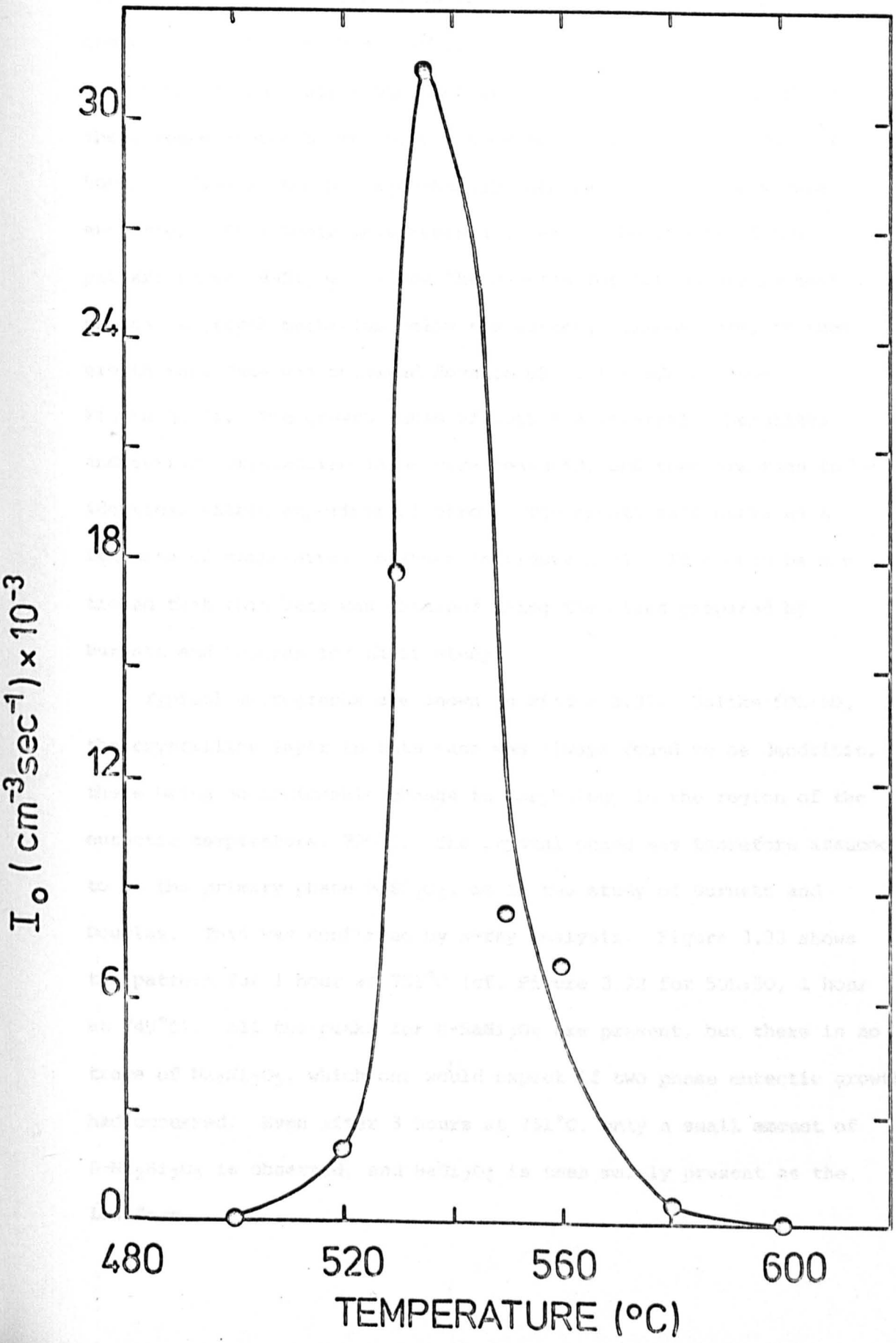

which is surprising because the two compositions have similar liquidus temperatures. It was of interest, therefore, to compare the growth rate data for these two compositions.

Burnett and Douglas measured growth rates at 800°C and above, these temperatures being above the eutectic temperatures, 790°C for 50N:50. (The system $Na_2Si_2O_5$-$BaSi_2O_5$ can be treated as a simple eutectic). Thus their measurements refer to the growth of the primary phase, $BaSi_2O_5$. Since the results for 50L:50 may suggest a change in growth mechanism below the eutectic temperature, further growth rate data was obtained down to 650°C for 50N:50 (see Figure 3.30). The growth rates of both the internal spherulites and surface crystalline layer were measured, and they are seen to be identical within experimental error. The growth rate curve as a function of temperature is shown in Figure 3.31. It should be mentioned that this data was obtained using the glass prepared by Burnett and Douglas for their study.

Typical micrographs are shown in Figure 3.32. Unlike 50L:50, the crystalline layer in this case was always found to be dendritic, there being no noticeable change in morphology in the region of the eutectic temperature, 790°C. The crystal phase was therefore assumed to be the primary phase $BaSi_2O_5$, as in the study of Burnett and Douglas. This was confirmed by x-ray analysis. Figure 3.33 shows the pattern for 1 hour at 751°C (cf. Figure 3.22 for 50L:50, 1 hour at 749°C). All the peaks for h-$BaSi_2O_5$ are present, but there is no trace of $Na_2Si_2O_5$, which one would expect if two phase eutectic growth had occurred. Even after 3 hours at 751°C, only a small amount of β-$Na_2Si_2O_5$ is observed, and $BaSi_2O_5$ is then mainly present as the low form.

FIG. 3.30. GROWTH RATE MEASUREMENTS FOR THE COMPOSITION 50 m/o $Na_2Si_2O_5$ - 50 m/o $BaSi_2O_5$ (CODE 50N : 50)

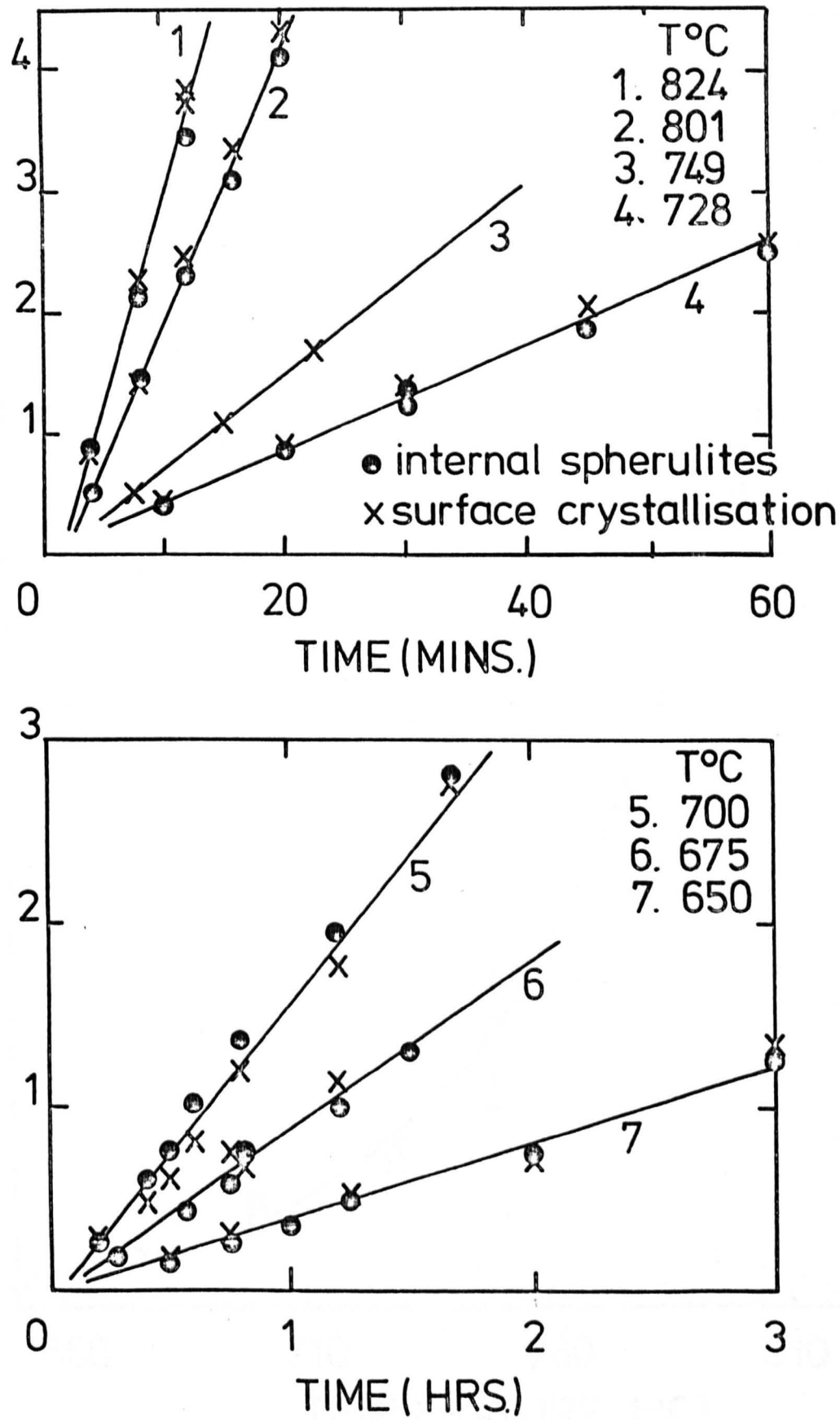

FIG. 3.31. CRYSTAL GROWTH RATE AS A FUNCTION OF TEMPERATURE FOR THE COMPOSITION 50m/o $Na_2Si_2O_5$ - 50m/o $BaSi_2O_5$ (CODE 50N:50)

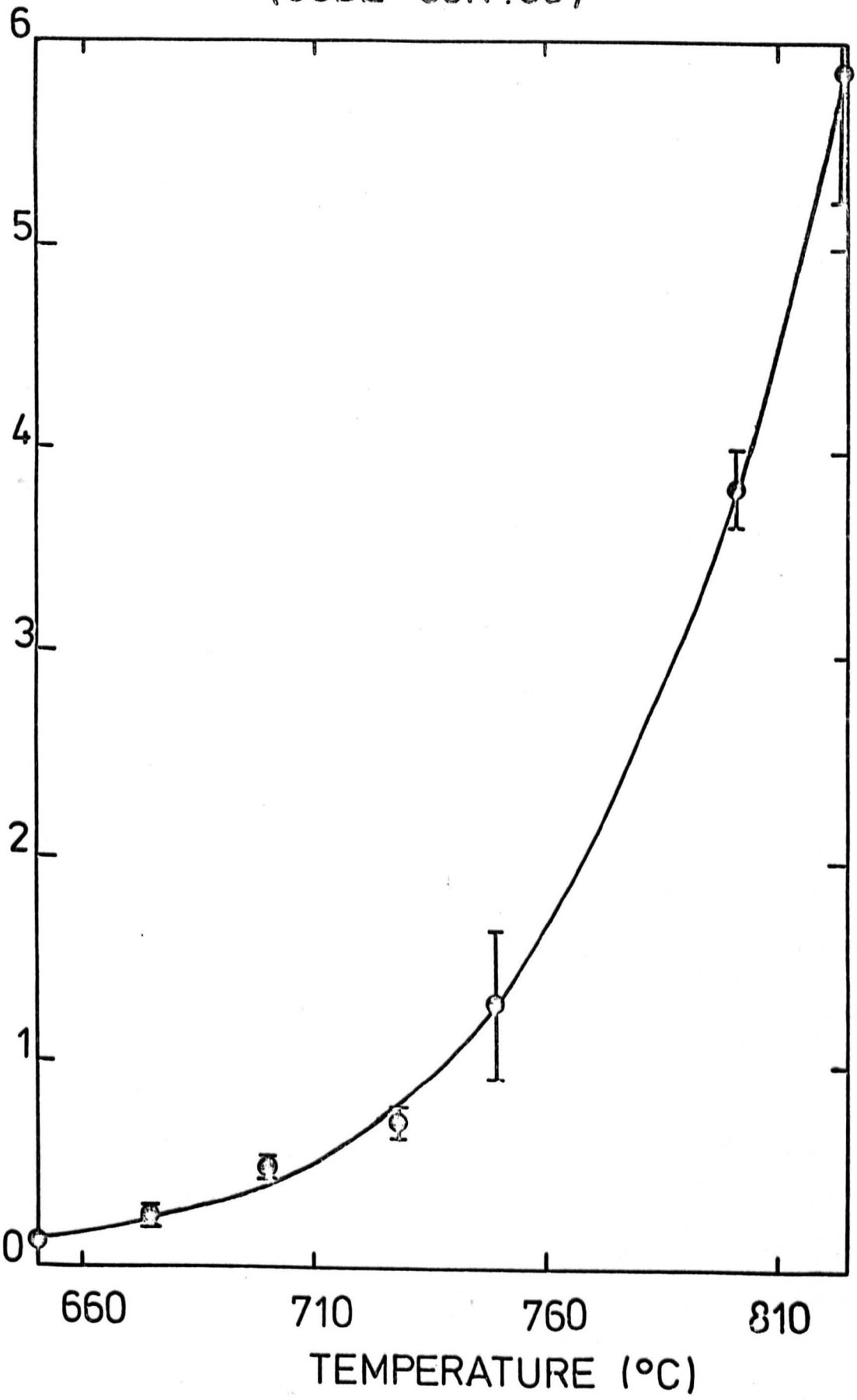

Fig. 3.32 Optical micrographs of the composition 50 ^{m}/o $Na_2Si_2O_5$-50 ^{m}/o $BaSi_2O_5$ heated at

(a) Top: 700°C for 72 minutes; magnification x100, x200

(b) Bottom: 775°C for 27 minutes; surface and internal crystallisation; magnification x200

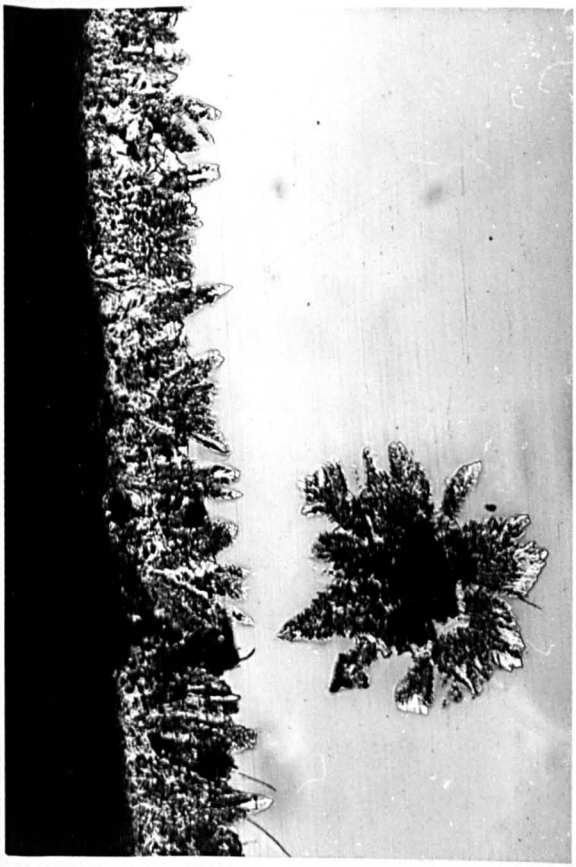

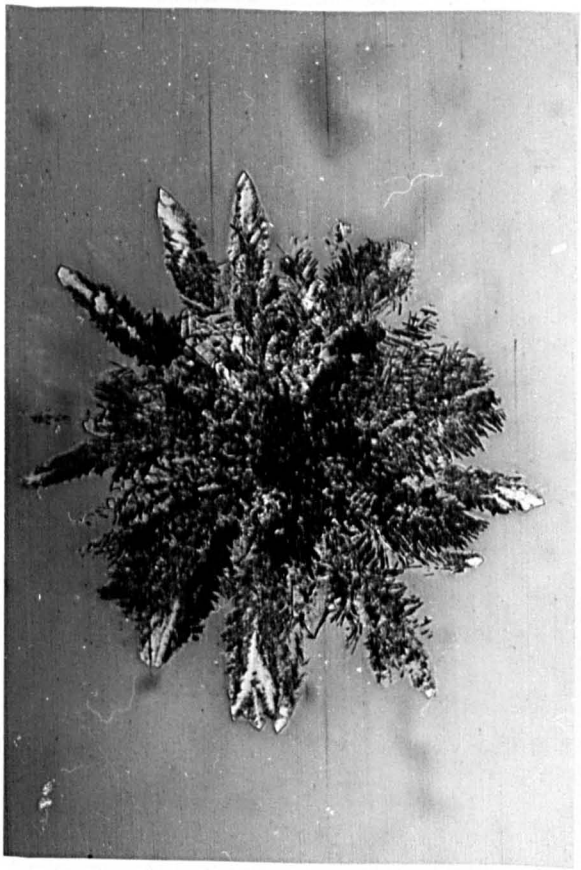

Fig. 3.32 contd/...

(c) Top: 824°C for 12 minutes, internal and surface crystallisation; magnification x100

(d) Bottom: Composition 50 ^{m}/o $Li_2Si_2O_5$-50 ^{m}/o $BaSi_2O_5$ heated at 824°C for 3 minutes; magnification x 100

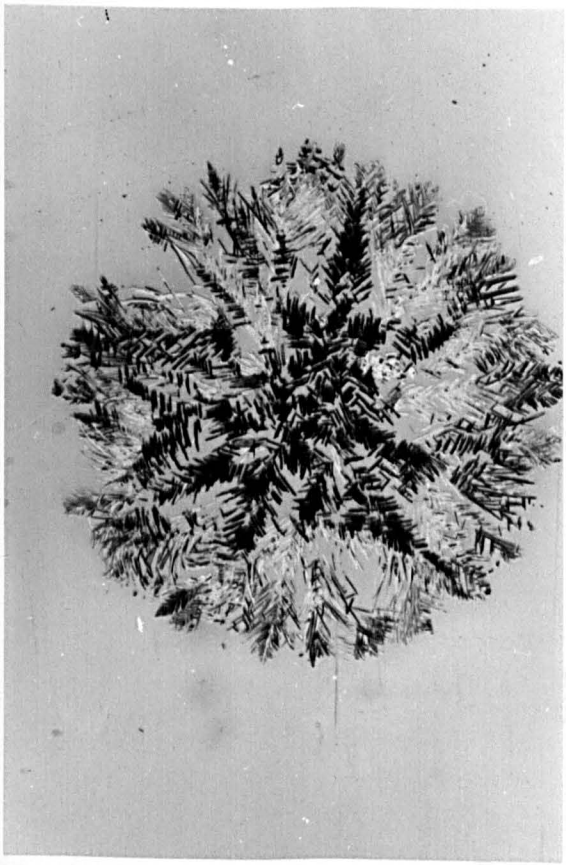

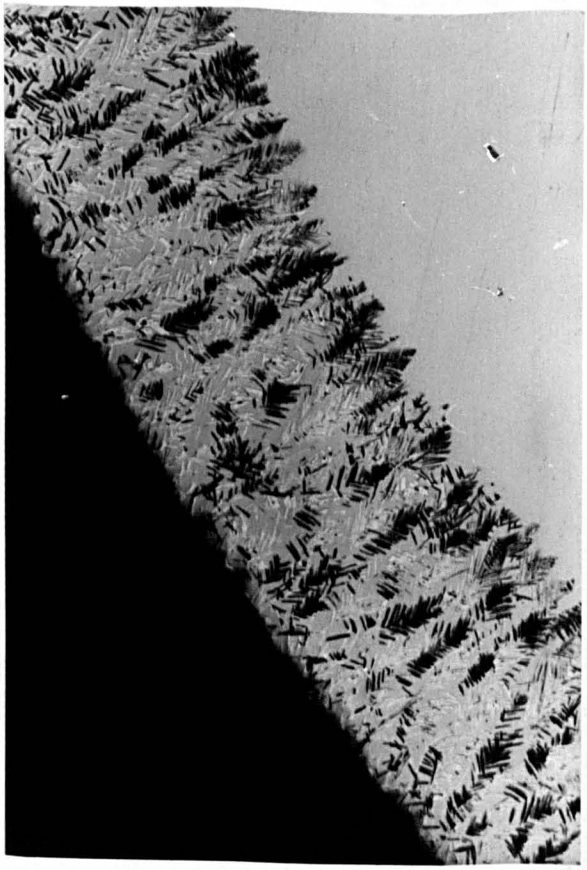

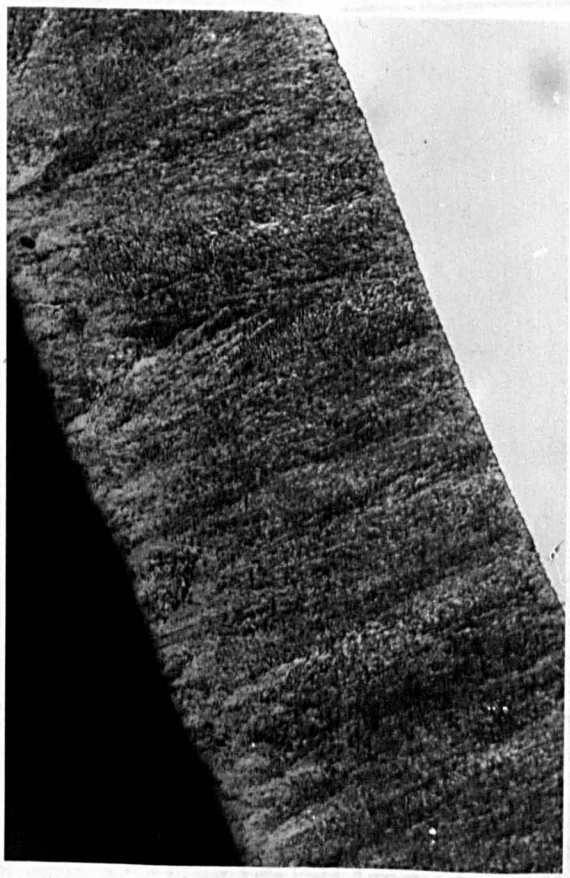

FIG. 3.33. X-RAY DIFFRACTION PATTERN FOR THE COMPOSITION $50^{m}/_{o}Na_2Si_2O_5 - 50^{m}/_{o}BaSi_2O_5$ HEATED AT 751°C FOR 1 HOUR.

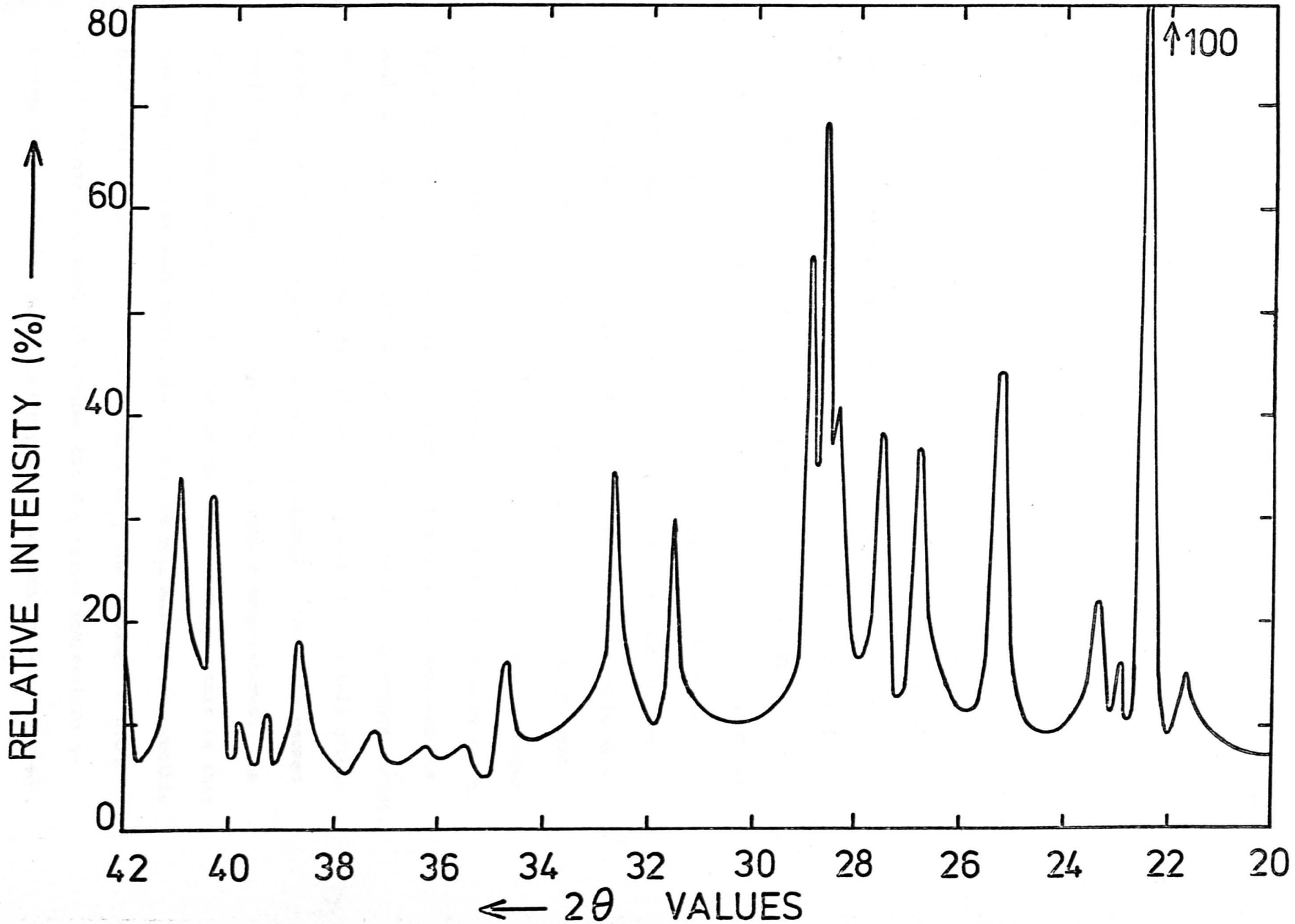

Figures 3.32(c) and (d) very clearly show the difference in crystal growth rate and crystal morphology between the two compositions 50N:50 and 50L:50 at 824°C. Although, 50L:50 does show an dendritic structure above 873°C (see Figure 3.27(f)), it can be seen that for 50N:50 considerable branching has occurred, this appearing to be at a regular angle to the main dendrite stems.

A comparison of growth rate data for 50N:50 and 50L:50 is given in Figure 3.34. It can be seen that the growth rates are considerably lower for 50N:50. Also, the growth rate curve for 50N:50 rises continuously in the region of T_E, in agreement with the crystal morphology observed, although the present results do not lie on the same curve as that estimated by Burnett and Douglas. A possible reason for this is the different heat treatment schedules employed. Thus in the present study the as prepared glass was heated up to the temperature of interest. However, Burnett and Douglas first remelted their samples in a small 60% Pt/40% Rh crucible above the liquidus temperature, thus removing any crystal nuclei present. The samples were then directly quenched to the heat treatment temperature of interest. Since the growth temperatures studied were above T_C, only a few internal nuclei were present and growth measurements could be conveniently made without the specimens rapidly crystallising. In the present study, however, it was only possible to obtain growth rates up to 824°C because nuclei already formed in the glass caused rapid crystallisation of the specimens at higher temperatures. The disadvantage of quenching from above the liquidus temperature is that the quench is not very severe due to the thermal mass of the crucible plus glass. Thus although the crucible only has a volume of about 3 cm^3, it may take about 10 minutes for the sample temperature to become steady, during which time crystal growth has already started to occur.

FIG. 3.34. A COMPARISON OF GROWTH RATE DATA FOR THE COMPOSITIONS 50m/o $Na_2Si_2O_5$ - 50m/o $BaSi_2O_5$ AND 50m/o $Li_2Si_2O_5$ - 50m/o $BaSi_2O_5$.

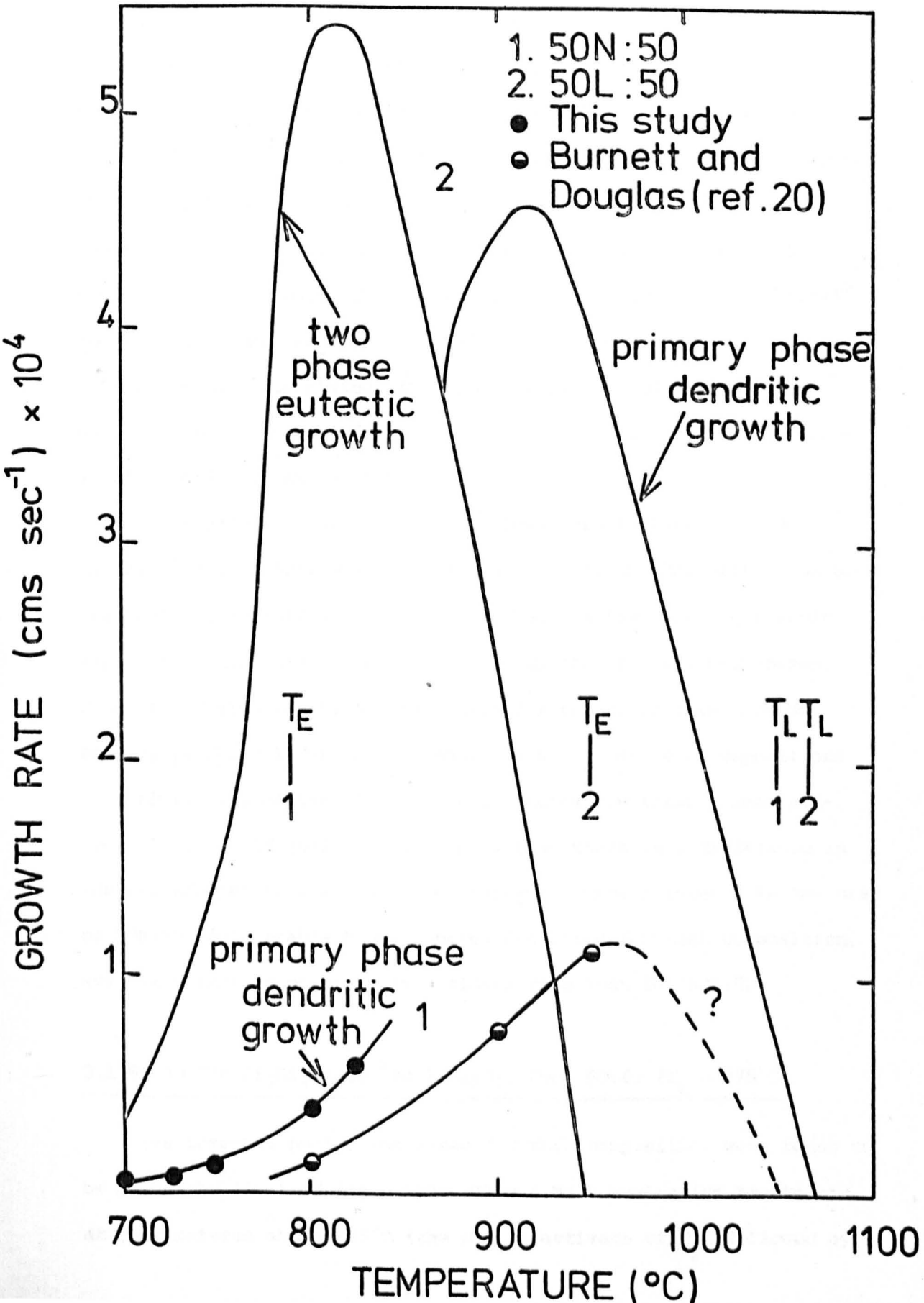

The apparent absence of two phase eutectic growth for 50N:50 is probably due to the low value of the eutectic temperature in the system $Na_2Si_2O_5$-$BaSi_2O_5$. Thus T_E is 160°C lower for 50N:50. The lower dendritic growth rates for 50N:50 are perhaps unexpected, because the crystallising phase is the same for both compositions. Since the liquidus temperatures differ by only 15°C, this would imply that crystal growth involves different diffusion mechanisms in the two cases. As diffusion of Ba^{2+} would be required for dendritic growth in both compositions, it is suggested that the rate controlling diffusion processes involve Na^+ or Li^+ rather than Ba^{2+}. Whilst this may appear surprising, it should be remembered that only one Ba^{2+} ion has to be 'moved' for every two Na^+ or Li^+ ions. This idea is discussed further in Chapter 4.

The higher nucleation rates but lower growth rates for 50N:50 as compared with 50L:50 is unexpected. Whilst the diffusion processes required for nucleation and growth may not be identical, one would expect the same ions to be involved in the controlling mechanisms. Since the thermodynamic driving force for the crystallisation of $BaSi_2O_5$ is shown later to be almost identical for both compositions (the similarity of the liquidus temperatures has already been mentioned), it would qualitatively imply that there is a difference in the interfacial free energies for $BaSi_2O_5$. Thus a lower σ in the case of 50N:50 would enable higher nucleation rates for that composition, even if diffusion occurred at a slower rate than for 50L:50.

3.1.6 60 ^{m}/o $Li_2Si_2O_5$-40 ^{m}/o $BaSi_2O_5$, Code 60:40 (T_L = 975°C)

The internal nucleation rates for this composition were found to be below the limit of detection. Thus 4 hour nucleation treatments at temperatures above 485°C (the D.T.A. estimate of T_g) followed by

a growth treatment at 700°C revealed no internal nuclei. Accurate crystal growth rates were only obtained over a limited temperature range (Figure 3.35). As for the 50L:50 composition, the crystal morphology appeared to be that of a two-phase eutectic (Figure 3.36). In order to determine whether any change in crystal morphology occurred at higher temperatures, 5 minute growth treatments were employed. Up to 850°C the eutectic morphology was observed only, but at 900°C dendrites could also be observed (Figure 3.37(a) and (b)). The thickness of the eutectic and dendritic layers as a function of temperature are shown in Figure 3.38. It can be seen that the two curves are nearly identical, presumably because of the closeness of T_E and T_L (950 and 975°C respectively). The specimen heated at 962°C exhibited only a dendritic layer, which was difficult to measure because of deformation of the specimen (Figure 3.37(c)).

3.2 Compositions for which $Li_2Si_2O_5$ is the primary phase

As mentioned in Chapter 1, the nucleation kinetics of $Li_2Si_2O_5$ crystals from a glass of the same composition have been studied by several workers. However, at the beginning of the present work there was little data concerning the effect of added oxides on the nucleation kinetics of $Li_2Si_2O_5$ from this simple composition. Such information is useful as a basis for understanding the formation of more complex glass ceramics, several of which contain $Li_2Si_2O_5$ as a major crystalline phase.

The addition of $BaSi_2O_5$ to $Li_2Si_2O_5$ (which is equivalent to partly replacing Li_2O by BaO) up to the eutectic composition at 36 $^m/_o$ $BaSi_2O_5$, causes a relatively slow fall in the liquidus temperature and a gradual rise in the glass transformation temperature.

FIG. 3.35. GROWTH RATE MEASUREMENTS AND CRYSTAL GROWTH RATE AS A FUNCTION OF TEMPERATURE FOR THE COMPOSITION $60^{m}/o\ Li_2Si_2O_5$-$40^{m}/oBaSi_2O_5$ (CODE 60:40)

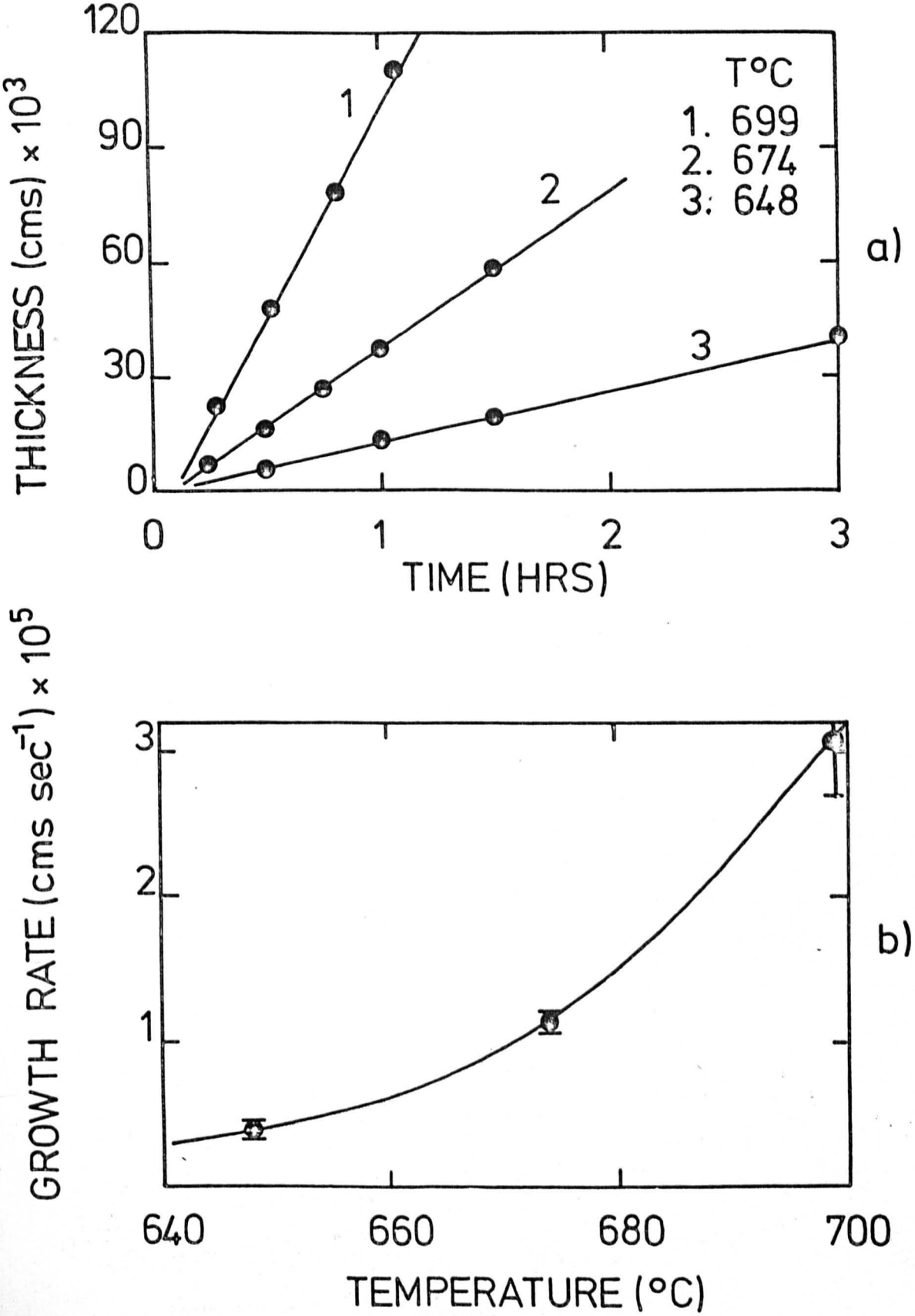

Fig 3.36 Optical micrographs of the composition 60 $^{m}/_{o}$ $Li_2Si_2O_5$-40 $^{m}/_{o}$ $BaSi_2O_5$ heated at 628°C for 3 hours

Top: Magnification x200

Bottom: Magnification x500

Fig. 3.37 Optical micrographs of the composition 60 $^{m}/_{o}$ $Li_2Si_2O_5$-40 $^{m}/_{o}$ $BaSi_2O_5$ heated for 5 minutes at

(a) Top 800°C; magnification x100, x200

(b) Bottom: 900°C; magnification x100, x200

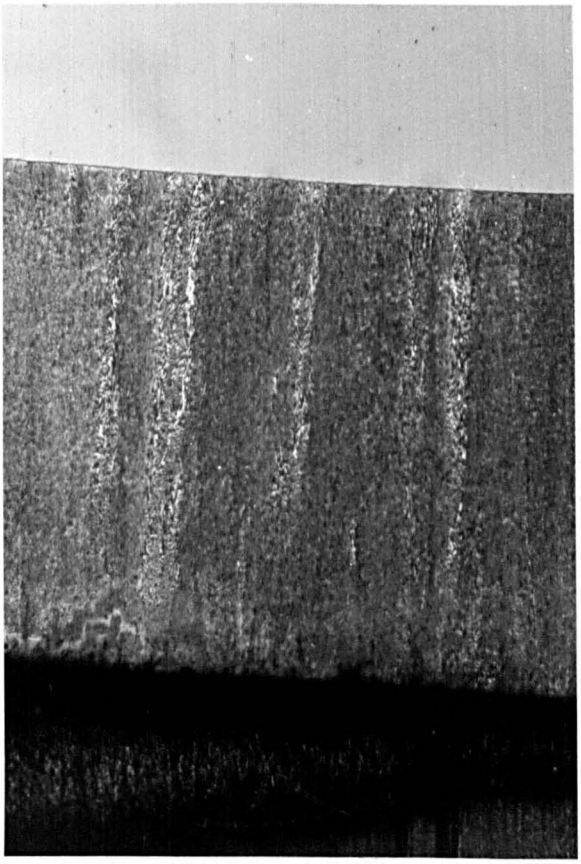

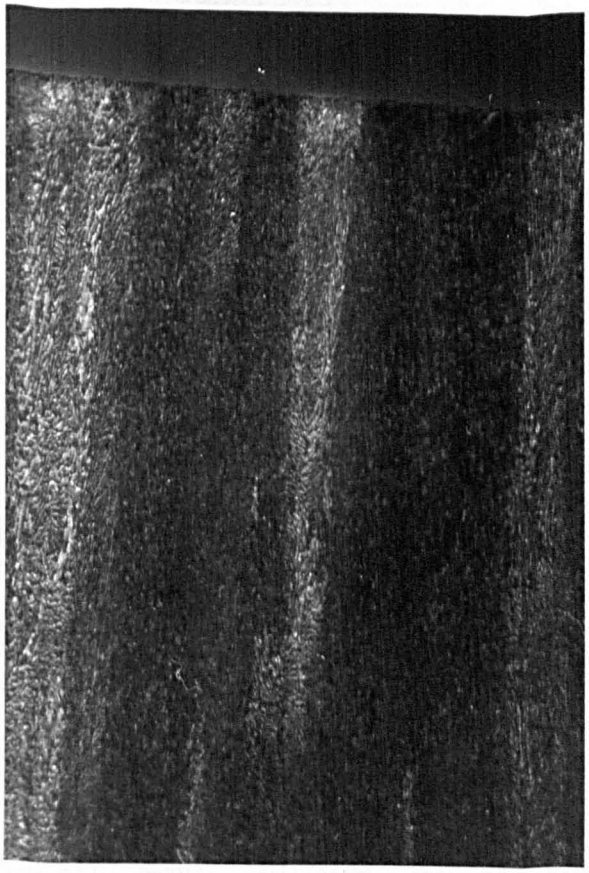

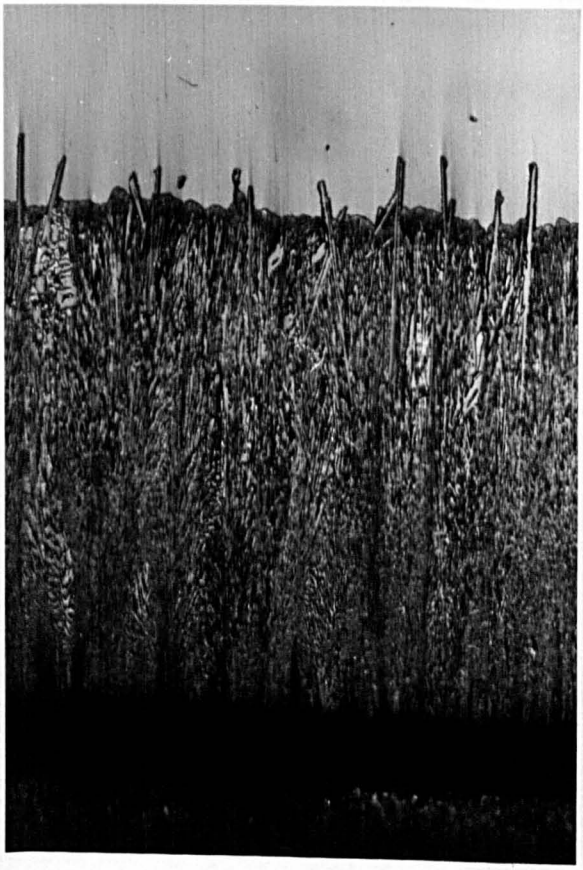

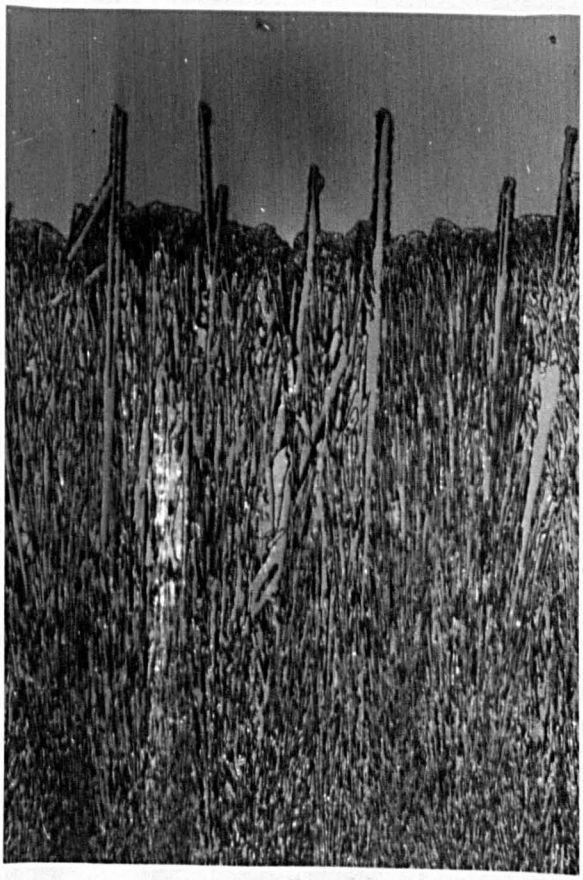

Fig. 3.37 contd/...

(c) 962°C; magnification x200

FIG. 3.38. THICKNESS OF SURFACE CRYSTALLINE LAYER AFTER 5 MINUTES AS A FUNCTION OF TEMPERATURE FOR THE COMPOSITION 60m/o $Li_2Si_2O_5$ - 40m/o $BaSi_2O_5$ (CODE 60:40)

Curve A. Two phase eutectic growth.
Curve B. Primary phase dendritic growth.

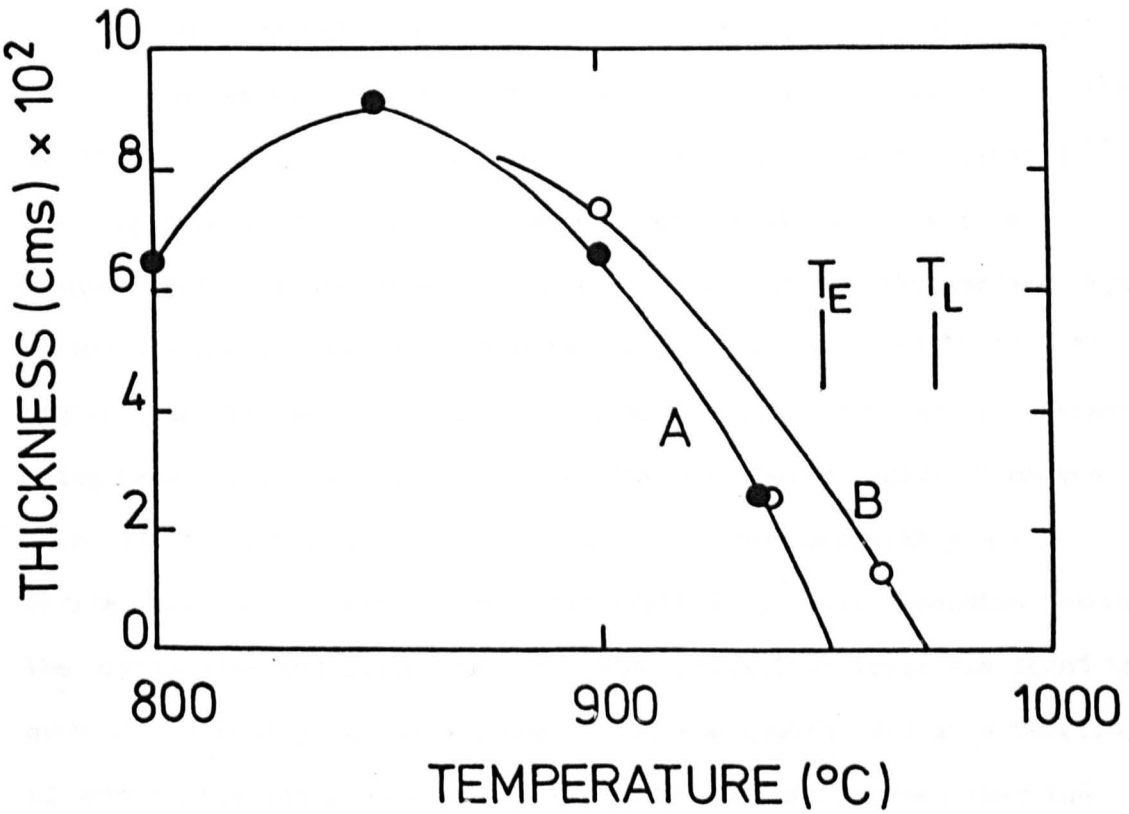

This behaviour is different to that observed when $Li_2Si_2O_5$ is added to $BaSi_2O_5$, which causes a rapid drop in both T_L and 'D.T.A. T_g'. It was of interest, therefore, to measure the nucleation and growth kinetics for $Li_2Si_2O_5$ rich compositions and compare the results with those for compositions rich in $BaSi_2O_5$.

Hence in this section a study of those compositions for which $Li_2Si_2O_5$ is the primary phase is presented. The experimental data is discussed further in Chapter 4.

3.2.1 Lithium disilicate, $Li_2Si_2O_5$ (T_m = 1034°C)

Only the crystal growth kinetics were measured for this composition, since the nucleation kinetics have been well established. Whilst the growth kinetics at large supercoolings have also been measured[24,49], there is some evidence of disagreement between the results (see Figure 3.40). In the present work the growth rate of the surface crystalline layer was measured in the temperature range 550 to 650°C. At higher temperatures internal crystallisation prevented any measurements being made. Also, the specimens fractured on being removed from the furnace, if excessive growth occurred. This was presumably due to thermal stresses, caused by the difference in thermal expansion between the crystalline and glassy phases. The crystalline layer was found to grow at a linear rate (see Figure 3.39), the growth rate as a function of temperature being shown in Figure 3.40. It can be seen that the present data is in reasonable agreement with that of Ogura et al[49], and that the data of Ito et al[24] is apparently too low. Also shown in Figure 3.40 are recent measurements by Amos[50], which again agree with the present study, within experimental error. Typical optical micrographs of the crystalline layer are shown in Figure 3.41. It

FIG. 3.39. GROWTH RATE MEASUREMENTS FOR THE COMPOSITION 100 m/o $Li_2Si_2O_5$.

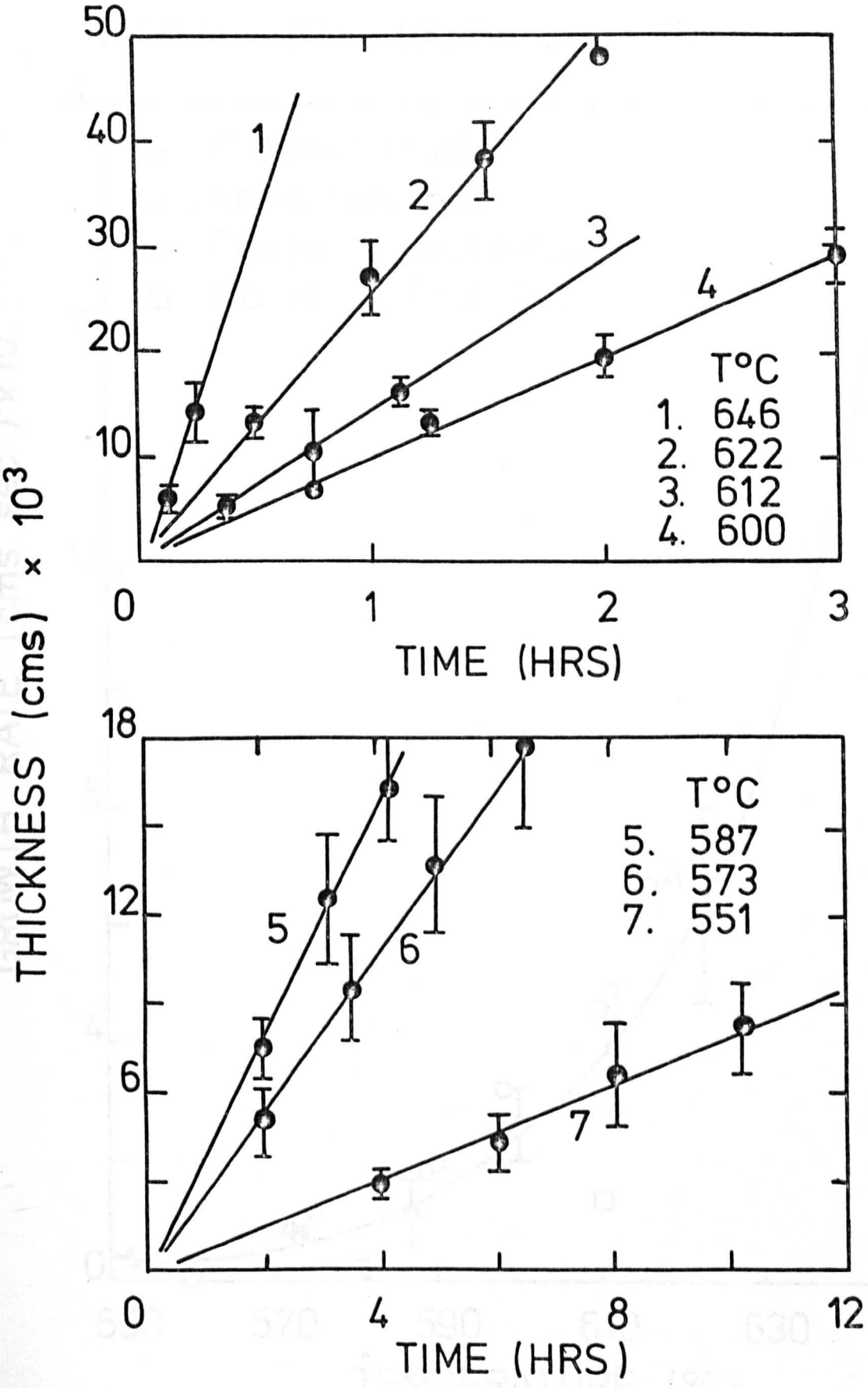

FIG. 3.40. CRYSTAL GROWTH RATE AS A FUNCTION OF TEMPERATURE FOR THE COMPOSITION 100$^{m}/_{o}$ $Li_2Si_2O_5$.

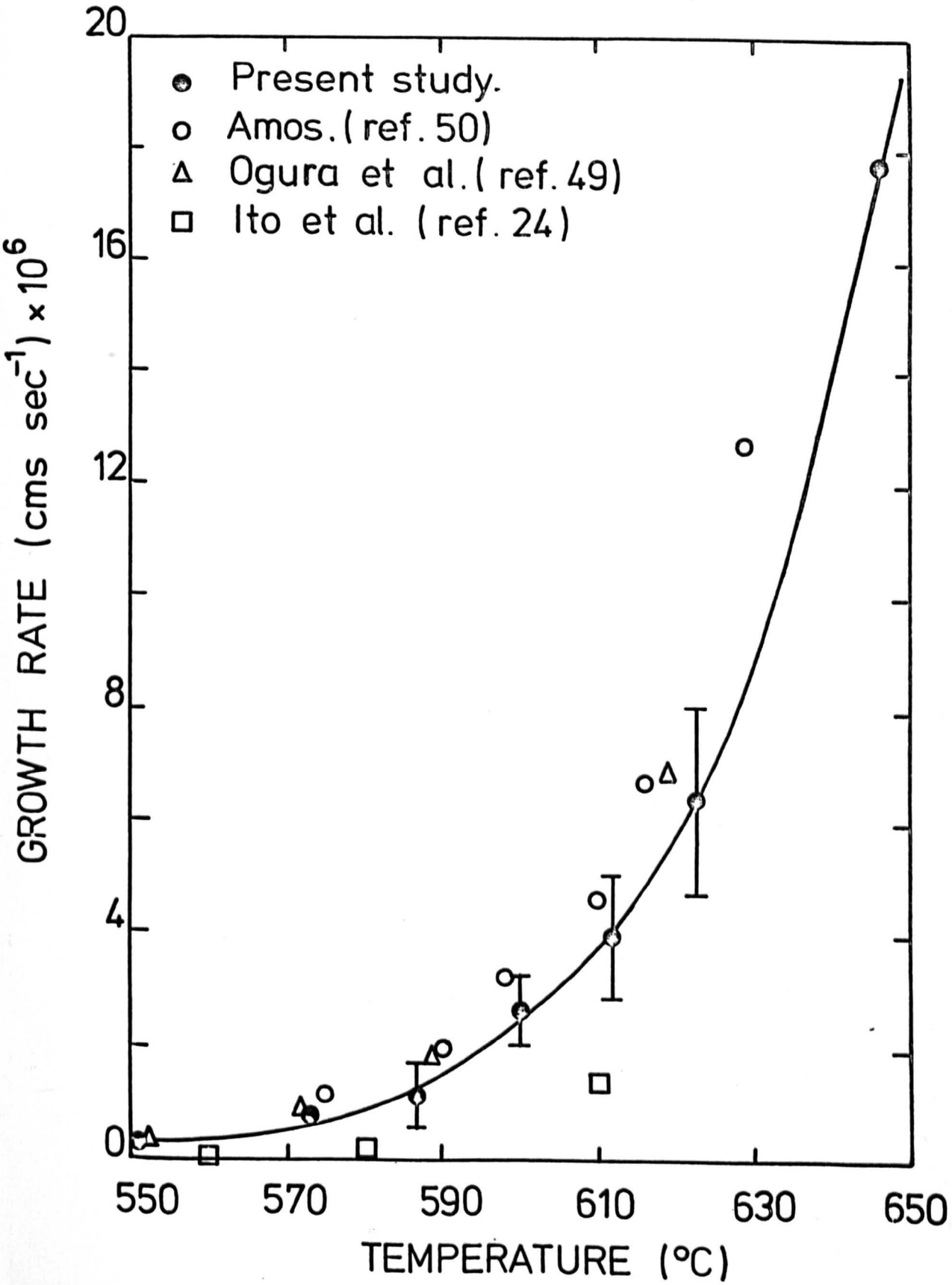

Fig. 3.41 Optical micrographs of the composition 100 $^{m}/_{o}$ $Li_2Si_2O_5$ heated at

(a) Top left: 551°C for 10¼ hours; magnification x200

(b) Top right: 587°C for 3 hours; magnification x200

(c) Bottom left: 578°C for 3 hours; magnification x500

(d) Bottom right: 612°C for 68 minutes; magnification x200

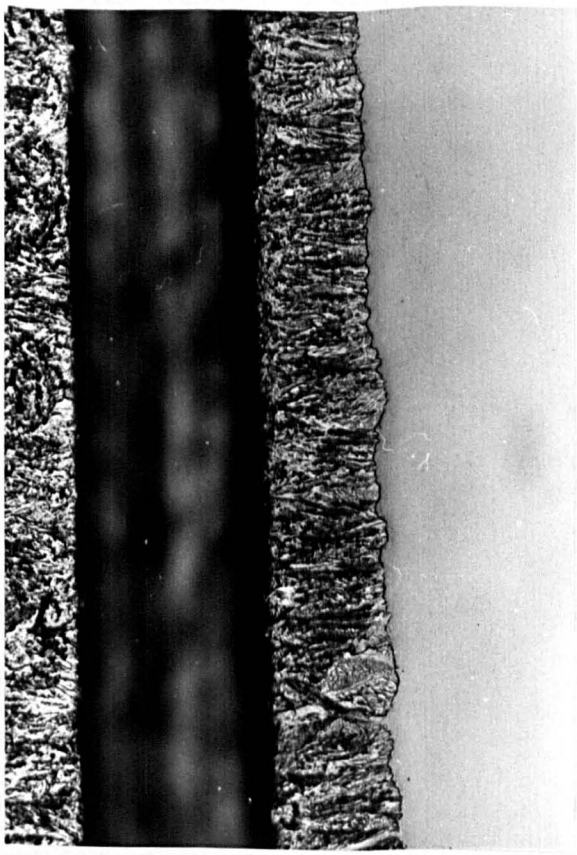

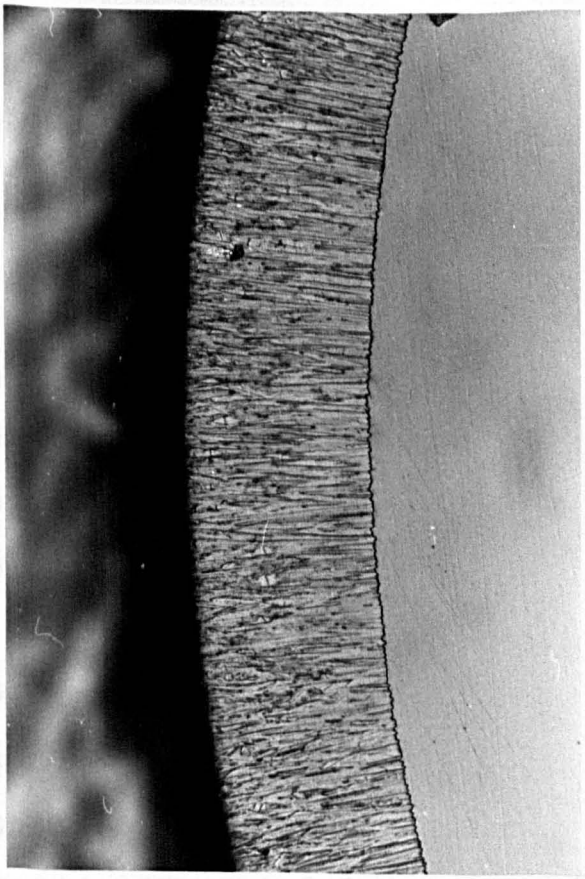

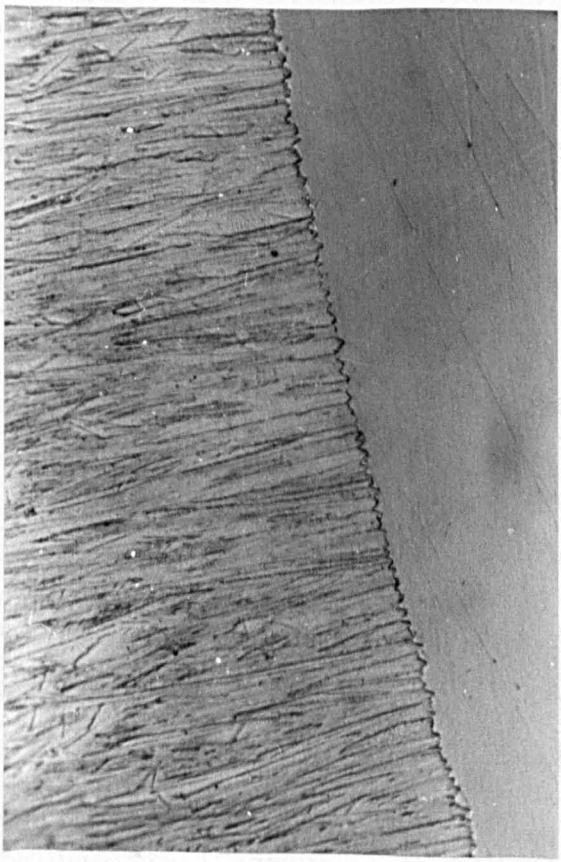

appears to be composed of a large number of crystals which are aligned almost perpendicular to the glass surface and which are faceted at their ends.

Unfortunately, no crystal growth rate measurements were made on the internal spherulites during this study. James[23] found the spherulites to have the shape of a prolate ellipsoid after growth at 560 and 600°C (see Figure 3.42). Although James did not measure the growth rates of the minor or major axes of these ellipsoidal spherulites, his results suggest that the minor to major axial ratio was higher at the higher growth temperature. This would imply that the growth rate as a function of temperature is different for the two axes. A similar conclusion was reached by Ito et al[24]. They measured the growth rates of both the minor and major axes of the internal spherulites as well as the thickness of the surface crystalline layer. From an Arrhenius plot of this data, it was found that the activation energy for crystal growth was identical for the major axis of the internal spherulites and the surface crystallisation, the activation energy for growth of the minor axis being considerably greater.

3.2.2 90 ^{m}/o $Li_2Si_2O_5$-10 ^{m}/o $BaSi_2O_5$, Code 90:10 (T_L = 1030°C)

Preliminary experiments on the 90:10 composition showed that specimens crystallised rapidly above 650°C. Thus at 675°C after 15 minutes, internal spherulites had consumed the bulk of the glass. According to x-ray analysis the major crystalline phase was $Li_2Si_2O_5$, all the main diffraction peaks being observed. There was also a small amount of $BaSi_2O_5$, although it was not possible to determine which modification was present.

Fig. 3.42 Optical micrograph of the composition 100 $^{m}/_{o}$ $Li_2Si_2O_5$, nucleated at 476°C for 1 hour and grown at 600°C for 15 minutes

Magnification x200

(after ref. 23)

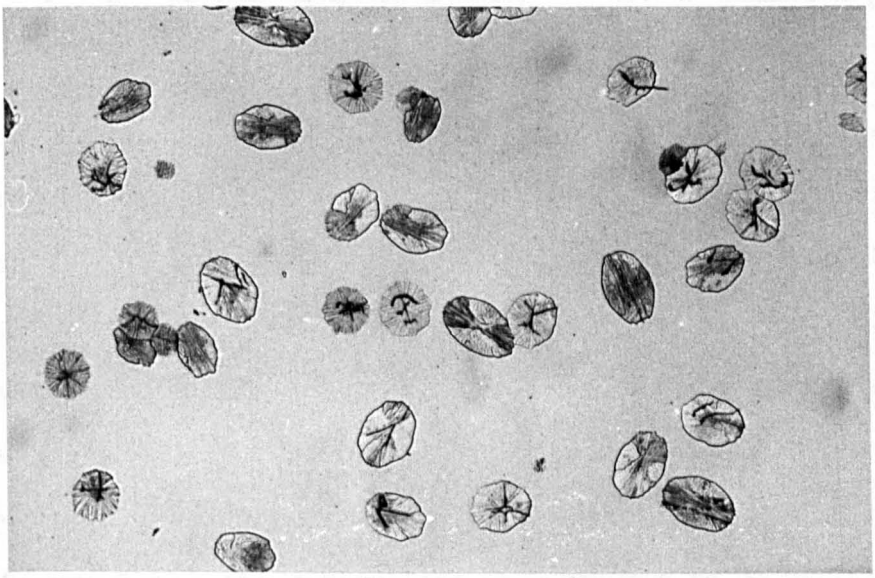

D.T.A. revealed a broad crystallisation exotherm in the temperature range 561°C to 644°C. In addition a point of inflection was observed on the low temperature side of the maximum at 592°C, implying the presence of a second smaller unresolved peak. This was examined further for the 80:20 composition, as discussed in Section 3.2.3. The 'D.T.A. T_g' was found to be 460°C, compared with 461°C which was obtained for the 100 $^m/_o$ $Li_2Si_2O_5$ composition.

The nucleation curve was determined by measuring the difference in nucleation densities between 1 and 2 hour heat treatments in the temperature range 450°C to 600°C. A growth treatment of about 45 minutes at 600°C was required for nucleation temperatures below 575°C. The same growth treatment was given to specimens nucleated at the same temperature, thus eliminating the effect of any nucleation which might have occurred at the growth stage. Typical micrographs are shown in Figure 3.43. The spherulites were assumed to be prolate ellipsoids in shape, since the largest circular sections were equal in length to the minor axes of the largest elliptical sections. The average value of the minor to major axis ratio was 0.64, corresponding to a shape factor of 1.21. Similarly shaped spherulites occur during the crystallisation of the 100 $^m/_o$ $Li_2Si_2O_5$ composition (see Figure 3.42). The nucleation curve is relatively broad, the maximum nucleation rate being only 72 nuclei cm^{-3} sec^{-1} (see Table 3.5 and Figure 3.44). The scatter in the experimental points is mainly due to the low number of spherulites present on several of the micrographs. Compared with the 100 $^m/_o$ $Li_2Si_2O_5$ composition, the maximum nucleation rate has decreased by a factor of about 60 times, the maximum nucleation temperature having risen slightly.

Fig. 3.43 Optical micrographs of the composition 90 ^{m}/o $Li_2Si_2O_5$-10 ^{m}/o $BaSi_2O_5$ nucleated

Top: 1 hour at 524°C, grown at 600°C; magnification x 200

Bottom: 2 hours at 552°C, grown at 600°C; magnification x50

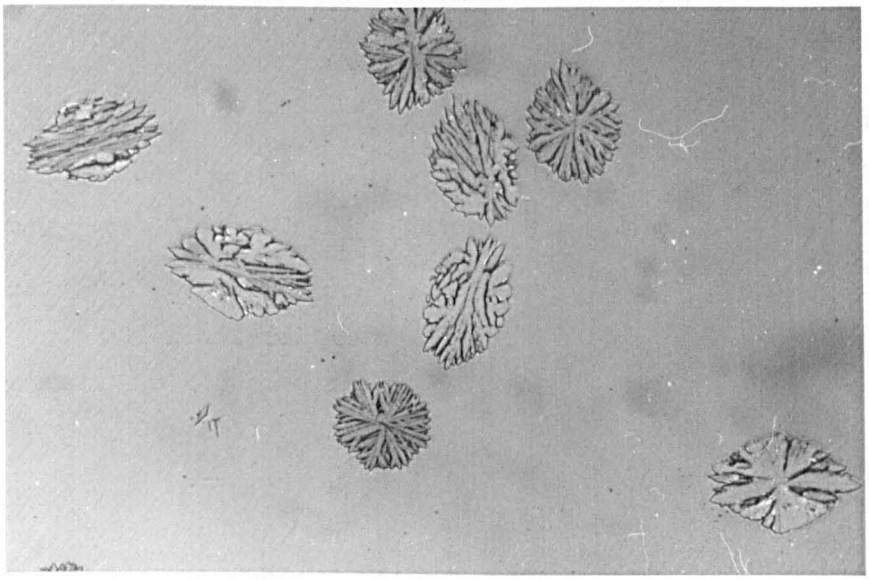

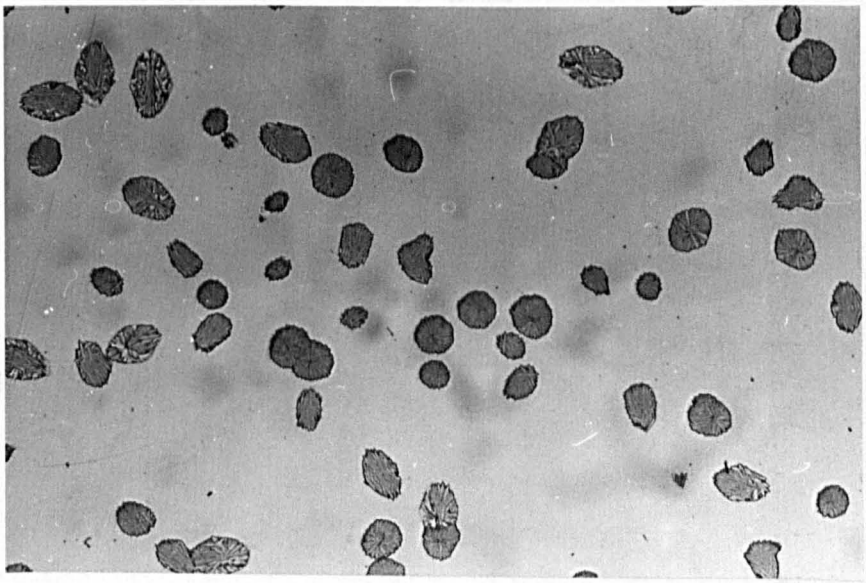

TABLE 3.5

NUCLEATION DATA AS A FUNCTION OF TIME AND NUCLEATION TEMPERATURE FOR THE COMPOSITION $90^{m}/o\ Li_2Si_2O_5$-$10^{m}/o\ BaSi_2O_5$ (CODE 90:10)

T(°C)	time(hrs)	N_v (cm^{-3}) x 10^{-5}	I($cm^{-3}sec^{-1}$)
Full analysis:-			
476	1	2.22	56.0
	2	4.24	
501	1	2.36	51.9
	2	4.23	
524	1	2.45	10.2
	2	2.82	
552	1	0.96	8.3
	2	1.26	
554	5.96	1.20	6.2
	8.88	1.85	
578	2.62	0.49	1.4
	3.82	0.55	
599	1	0.26	2.2
	2	0.34	
600	0.67	0.27	0
	1.00	0.27	
	1.33	0.27	
Simple analysis:-			
462	1	0.49	41.1
	2	1.97	
486	1	2.25	71.9
	2	4.84	
516	1	2.65	42.3
	2	4.17	
539	1	1.24	39.0
	2	2.64	

FIG. 3.44. NUCLEATION RATE AS A FUNCTION OF TEMPERATURE FOR THE COMPOSITION 90 m/o $Li_2Si_2O_5$ - 10 m/o $BaSi_2O_5$ (CODE 90:10)

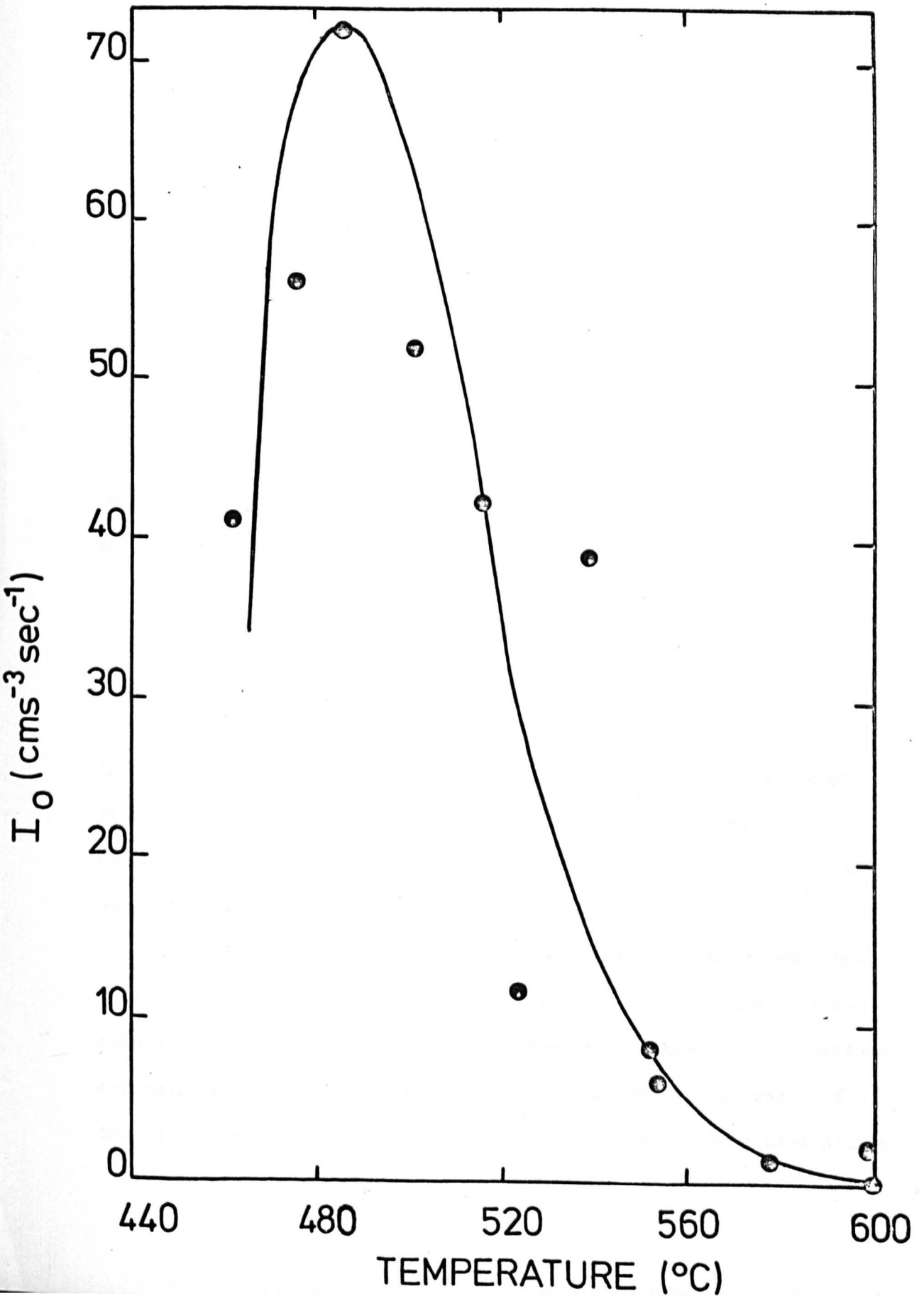

It should also be mentioned that whereas the 100 ^{m}/o $Li_2Si_2O_5$ composition generally required a 3 minute etch in 1% etching solution in order to reveal the spherulites under the microscope, the 90:10 composition only required 30 secs in 0.5% etching solution. This is probably because BaO increases the durability of the glass relative to that of crystalline $Li_2Si_2O_5$. Thus a lighter etch would be required to achieve the same contrast between glass and crystal.

Crystal growth rates were obtained in the temperature range 554 to 675°C. All measurements were made on the surface layer, the growth rates being constant with time (see Figure 3.45). The growth rate curve is shown in Figure 3.46. Typically large 'spikes' of $Li_2Si_2O_5$ were observed, separated in places by much smaller crystallised regions (see Figure 3.47). These smaller regions were probably $BaSi_2O_5$-$Li_2Si_2O_5$ eutectic. The growth rates obtained refer to the spikes. This morphology is different from that observed for the 100 ^{m}/o $Li_2Si_2O_5$ composition, where the crystalline layer had an almost smooth crystal-glass interface, faceted only on a small scale at x 500 (see Figure 3.41(c)). This is presumably because the spikes occur on a much finer scale for the 100 ^{m}/o $Li_2Si_2O_5$ composition, and they are not separated by any eutectic growth as in the 90:10 composition. The difference in morphology between the two compositions can also be seen for the internal spherulites, although they have the same shape in both cases.

Crystal growth rates of internal nuclei were not measured. However, it was always found that the major axes of the largest internal spherulites were equal in length to twice the thickness of the surface crystalline layer (see Figure 3.47(a)). Hence the growth rates of the major axes of the internal spherulites and the surface crystalline

FIG. 3.45. GROWTH RATE MEASUREMENTS FOR THE COMPOSITION 90m/o $Li_2Si_2O_5$ - 10m/o $BaSi_2O_5$ (CODE 90 : 10)

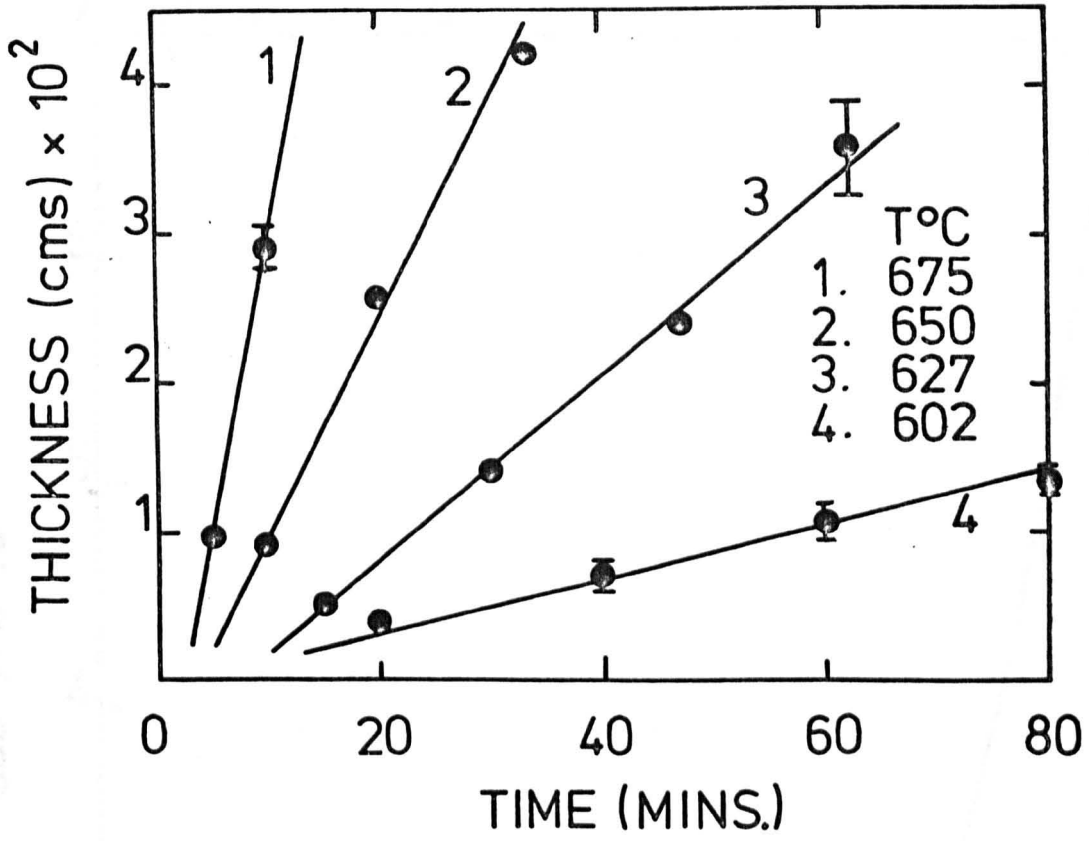

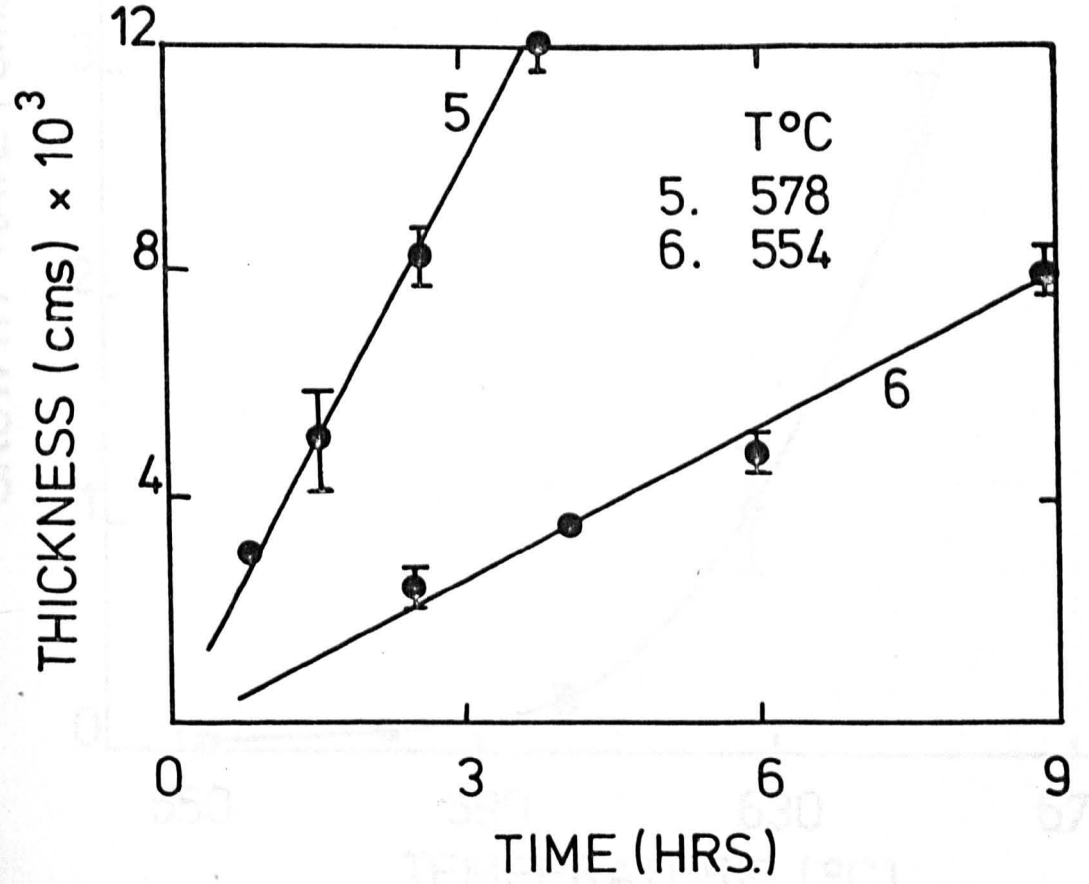

FIG. 3.46. CRYSTAL GROWTH RATE AS A FUNCTION OF TEMPERATURE FOR THE COMPOSITION 90 m/o $Li_2Si_2O_5$ - 10 m/o $BaSi_2O_5$ (CODE 90:10)

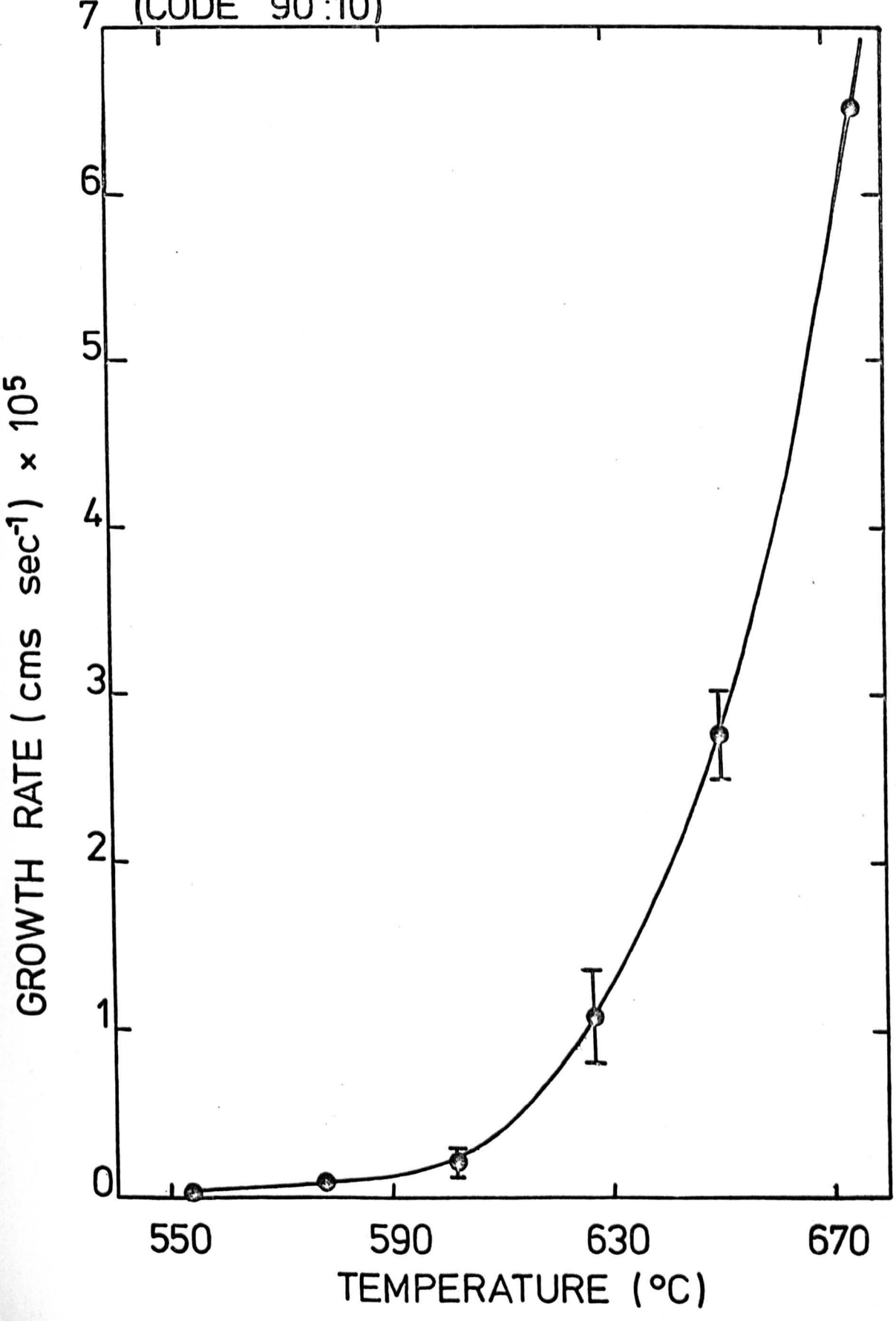

Fig. 3.47 Optical micrographs of the composition 90 ^{m}/o $Li_2Si_2O_5$-10 ^{m}/o $BaSi_2O_5$ heated at 602°C for 80 minutes

(a) Top: Magnification x200

(b) Bottom: Magnification x500

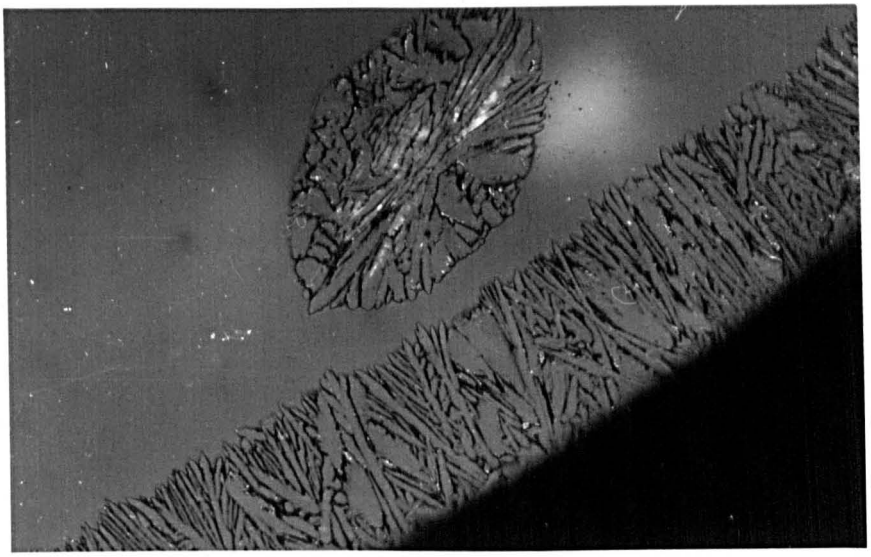

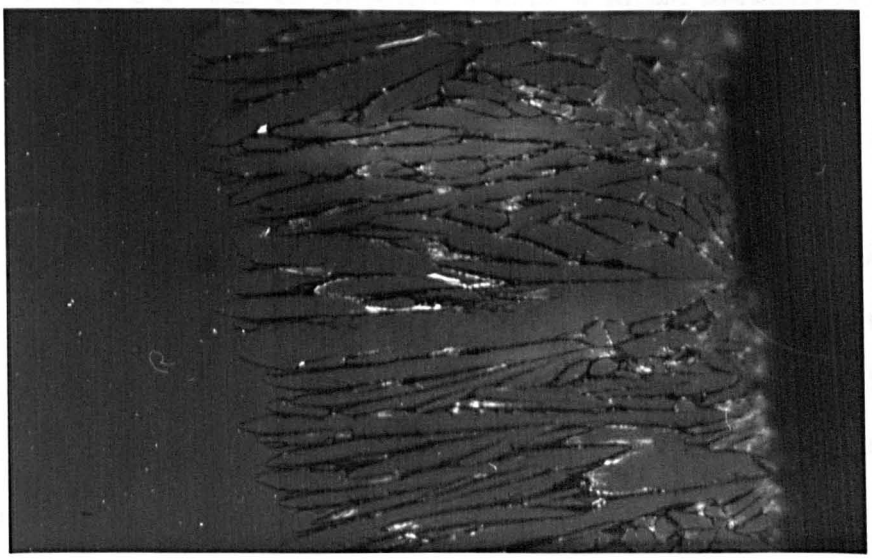

layer are equal. The growth rate of the minor axes were less than that of the surface layer by a factor equal to the axial ratio. This difference in crystal growth rate between the minor and major axes has also been observed for the 100 $^{m}/_{o}$ $Li_2Si_2O_5$ composition, as mentioned earlier.

3.2.3 80 $^{m}/_{o}$ $Li_2Si_2O_5$-20 $^{m}/_{o}$ $BaSi_2O_5$, Code 80:20 (T_L = 1000°C)

This composition crystallised rapidly above 680°C. Thus at 680°C after 25 minutes specimens were almost completely crystalline due to the presence of internal spherulites which had grown and coalesced. The major crystalline phase was $Li_2Si_2O_5$. $BaSi_2O_5$ was present in a larger quantity than for the 90:10 composition, but again it was not possible to determine which modification was present.

A standard D.T.A. run at 10°C min^{-1} gave a broad crystallisation exotherm in the temperature range 575°C to 657°C and 'D.T.A. T_g' was found to be 470°C. As for the 90:10 composition, a point of inflection occurred on the low temperature side of the crystallisation peak, in this case at 605°C, implying the presence of more than one peak. In order to separate the peaks a second D.T.A. run at 4°C min^{-1} was made. However, in this case two points of inflection occurred, in addition to the apparent main peak (see Figure 3.48). Also, the crystallisation exotherm occurs at slightly lower temperatures. The actual peak positions were located with the aid of a Du Pont 310 Curve Resolver. Surprisingly, the main peak is at 605°C, between two smaller peaks at 571°C and 618°C. To determine the cause of these exothermic peaks, powdered specimens of the 80:20 composition were heat treated at 5°C min^{-1} up to the appropriate temperature and then removed from the furnace for x-ray analysis. This is just a slightly

FIG. 3.48. DTA CRYSTALLISATION EXOTHERM AS A FUNCTION OF HEATING RATE FOR THE COMPOSITION 80 : 20.

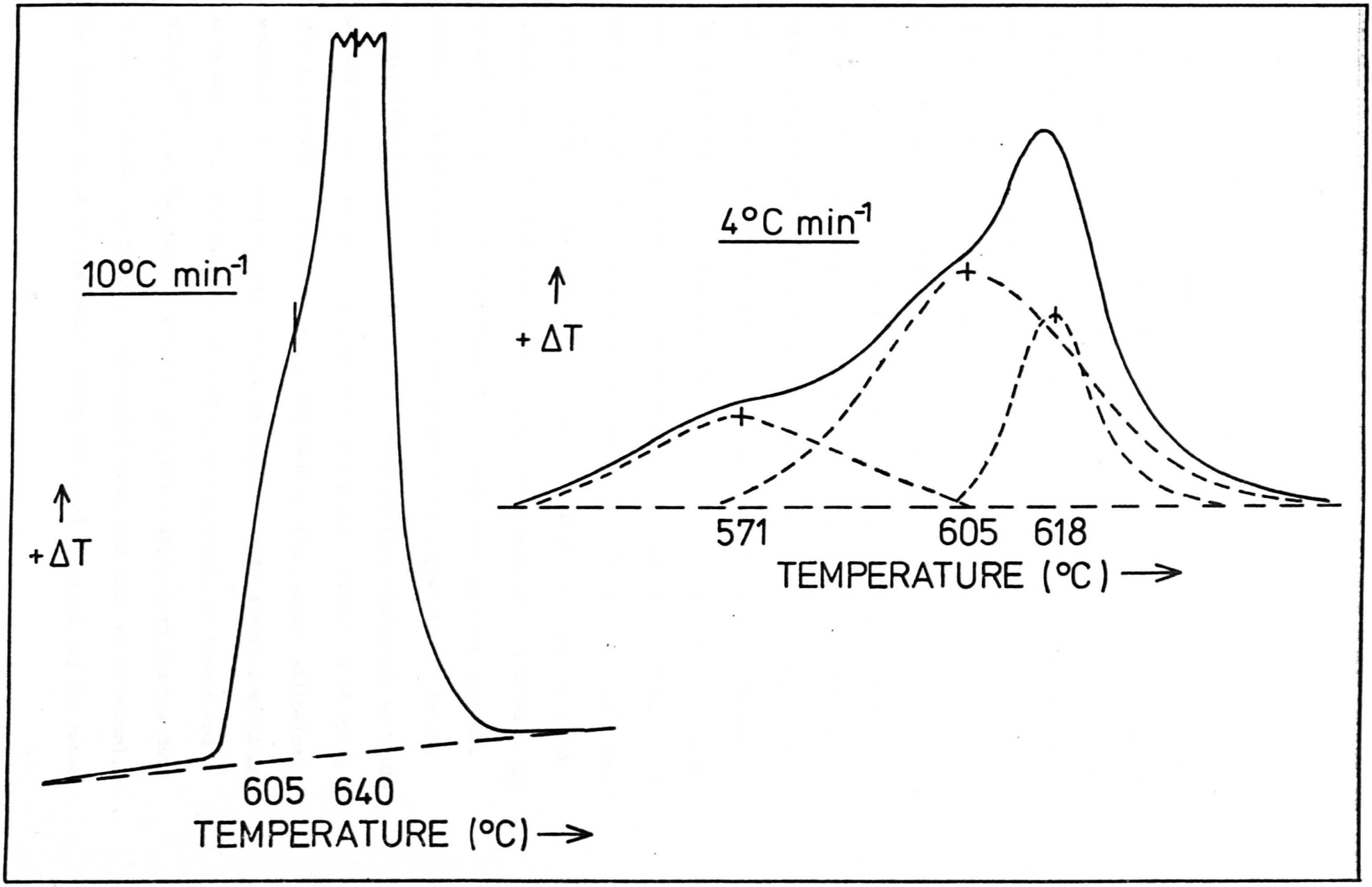

higher heating rate than employed for the slow D.T.A. runs. At 571°C the amount of crystallinity was low, $Li_2Si_2O_5$ being the only phase present. At 605°C the percentage crystallinity was higher, but again only $Li_2Si_2O_5$ could be detected. However, at 630°C $BaSi_2O_5$ was present as well as $Li_2Si_2O_5$, the amount of crystallinity being further increased. Thus it would appear that the peak at 618°C is in some way associated with the crystallisation of both $BaSi_2O_5$ and $Li_2Si_2O_5$, whereas the lower two peaks are concerned only with the crystallisation of $Li_2Si_2O_5$. The exact processes responsible for these peaks could not be identified.

The nucleation curve was investigated by measuring the difference in nucleation densities between 1 and 2 hour heat treatments in the temperature range 450°C to 575°C. Initially, a growth treatment of about 2 hrs at 600°C was given to all nucleated specimens. However for specimens nucleated at 450°C and 476°C, where the nucleation rate was very low, a further growth treatment of 15 mins at 650°C was required. As for the 90:10 composition the same growth treatment was given to specimens nucleated at the same temperature. Typical micrographs are shown in Figure 3.49. It was not possible to determine the geometric shape of the spherulites, although they are certainly not prolate ellipsoids as in the case of the 90:10 composition. If the spherulites for the 80:20 composition were prolate ellipsoids we would expect to see some circular sections, the largest diameters of which would be equal in length to the minor axes of the largest elliptical sections. In practice very few, even approximately circular sections, were observed. Furthermore, according to the graphs of DeHoff and Rhines[39], as the axial ratio of a prolate ellipsoid approaches zero (i.e. it becomes increasingly elongated along its axis of rotation), the average value of the axial ratio, obtained by measuring the minor

Fig. 3.49 Optical micrographs of the composition 80 ^{m}/o $Li_2Si_2O_5$-20 ^{m}/o $BaSi_2O_5$ nucleated for 2 hours at

Top: 524°C and grown at 600°C; magnification x50, x100

Bottom: 476°C and grown at 600°C then 650°C; magnification x50

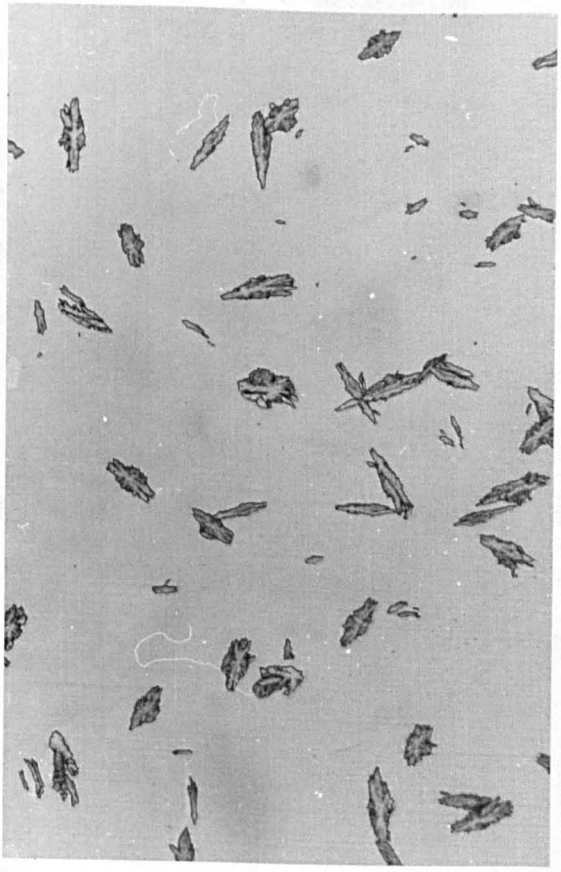

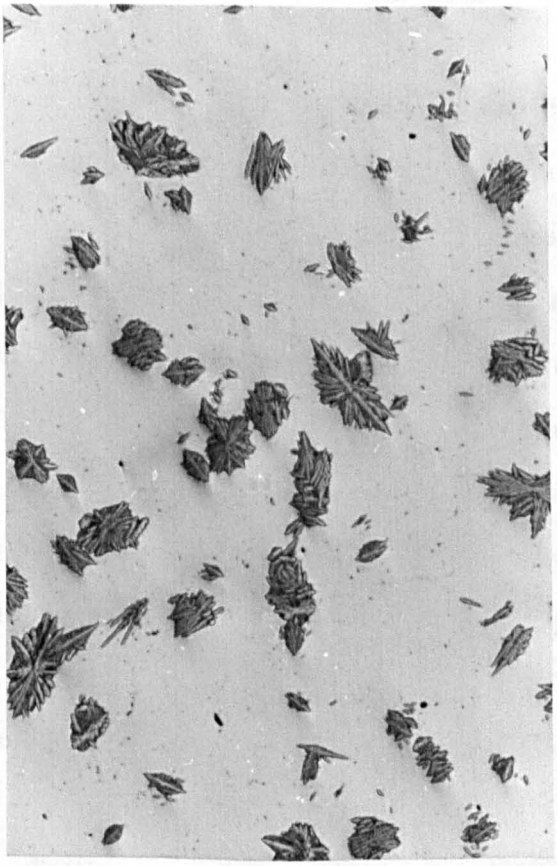

and major axes of all sections observed through such ellipsoids, approaches 0.50. For the 80:20 composition, assuming each spherulite section to have a minor and major axis, an average value of 0.39 was obtained for those specimens grown at 600°C only (see Table 3.6), implying that the spherulites grown at this temperature could not be prolate ellipsoids in shape. It is interesting to note that specimens given an additional growth treatment at 650°C had a larger average axial ratio of 0.51. An increase in the axial ratio with growth temperature has also been observed for the 100 $^{m}/_{o}$ $Li_2Si_2O_5$ composition.

Without knowing the shape of the spherulites it was not possible to calculate actual nucleation densities, since the shape factors were unknown. However, from equation (2.7), which is a general equation independent of shape, we can write

$$N_V k_1 = \frac{2}{\pi} N_A \bar{Z} \qquad (3.7)$$

where k_6 has been assumed equal to $\frac{\pi}{2}$, k_1 is some unspecified shape factor, and $\bar{Z}$ is the average value of the measured minor axes. Table 3.6 gives the values of $N_V k_1$ for the 1 and 2 hour heat treatments estimated from equation (3.7). Hence Ik_1 could be calculated by difference. Since the average value of the axial ratio was found to be only dependent on the growth temperature (see Table 3.6), k_1 was assumed to be independent of the nucleation treatment. Figure 3.50 shows the normalised nucleation rate I_o/I_{max} as a function of temperature. The unknown factor k_1 could be eliminated because the same growth treatment was used for those nucleation temperatures at which appreciable nucleation occurred. Also shown in Figure 3.50 are the normalised nucleation curves for the compositions 100 $^{m}/_{o}$ $Li_2Si_2O_5$ and 90:10. As the molar

TABLE 3.6

NUCLEATION DATA AS A FUNCTION OF TIME AND NUCLEATION TEMPERATURE FOR THE COMPOSITION $80^{m}/o\ Li_2Si_2O_5$-$20^{m}/o\ BaSi_2O_5$ (CODE 80:20)

T(°C)	time(hrs)	average axial ratio	$k_1N_v(cm^{-3})$ x 10^{-5}	$k_1I(cm^{-3}sec^{-1})$
Grown at 600°C, then 650°C:-				
450	1	0.483	2.21	~ 0
	2	0.479	1.68	
476	1	0.516	2.25	~ 0
	2	0.559	2.28	
Grown only at 600°C:-				
501	1	0.414	2.49	92.1
	2	0.376	5.80	
524	1	0.365	4.05	398.6
	2	0.390	18.40	
551	1	0.397	6.19	314.2
	2	0.381	17.50	
575	1	-	3.14	~ 0
	2	-	3.85	

(Full analysis used to calculate k_1N_v)

FIG. 3.50. NORMALISED STEADY STATE NUCLEATION RATE AS A FUNCTION OF TEMPERATURE FOR THE COMPOSITIONS 100m/o $Li_2Si_2O_5$ (A), 90 : 10 (B), AND 80 : 20 (C).

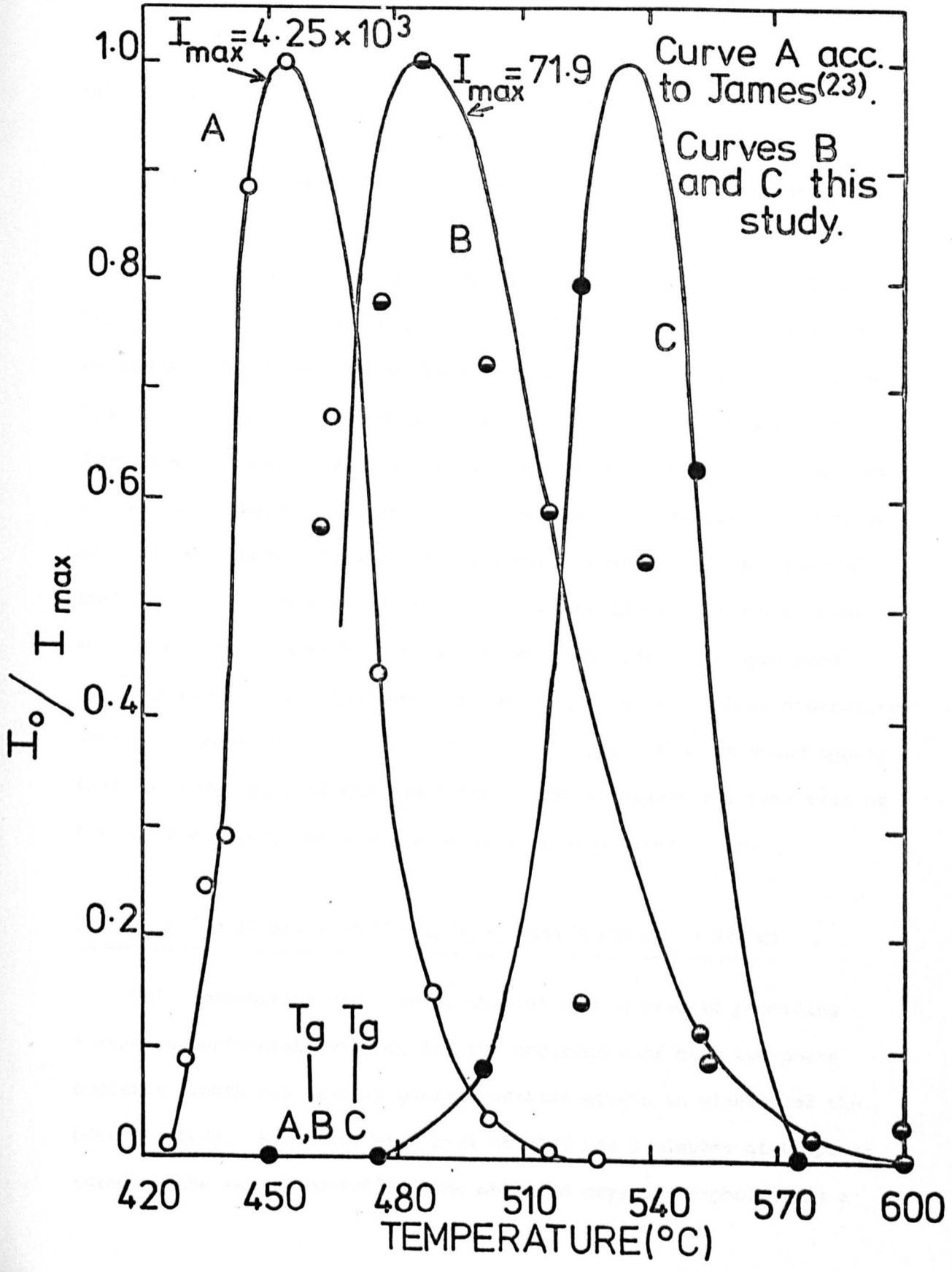

percentage of $Li_2Si_2O_5$ decreases, the maximum nucleation rate becomes smaller, whilst the nucleation curve moves to a higher temperature range. Unfortunately, I_{max} could not be calculated absolutely for 80:20 because k_1 is unknown. Considering the elongated shape of the spherulites, k_1 could be much greater than unity. Thus according to DeHoff and Rhines[39] k_1 for prolate ellipsoids increases rapidly as the axial ratio decreases, i.e. as the ellipsoid becomes elongated along its axis of rotation.

Crystal growth rates were obtained for the surface crystalline layer in the temperature range 584 to 700°C. The layer consists of large faceted spikes, perpendicular to the glass surface and separated from each other by eutectic-like growth (Figure 3.51). These spikes grew at a constant rate. The growth measurements and growth rate curve are shown in Figures 3.52 and 3.53 respectively. Crystal growth rates of internal spherulites were not measured. However, it was observed that the semi-minor axes of the largest spherulites were always smaller than the surface layer by a factor of about 3, for those specimens grown at 600°C. In comparison, the semi-major axes of these spherulites were only about 10% less than the surface layer. Thus it would appear that the major axes of the spherulites grow at almost the same rate as the surface layer, the minor axes growing at a slower rate.

3.2.4 70 $^m/_o$ $Li_2Si_2O_5$-30 $^m/_o$ $BaSi_2O_5$, Code 70:30 (T_L = 975°C)

This composition was briefly studied with a view to providing further experimental evidence for the occurrence of both two-phase eutectic growth and primary phase dendritic growth in glasses of the present study. Specimens were heat treated for 5 minutes at temperatures in the range 800-975°C. The observed crystal morphology as a

Fig. 3.51 Optical micrographs of the composition 80 $^{m}/_{o}$ $Li_2Si_2O_5$-20 $^{m}/_{o}$ $BaSi_2O_5$ heated at

Top: 584°C for 8 hours;
magnification x200, x500

Bottom: 639°C for 1½ hours;
magnification x200, x500

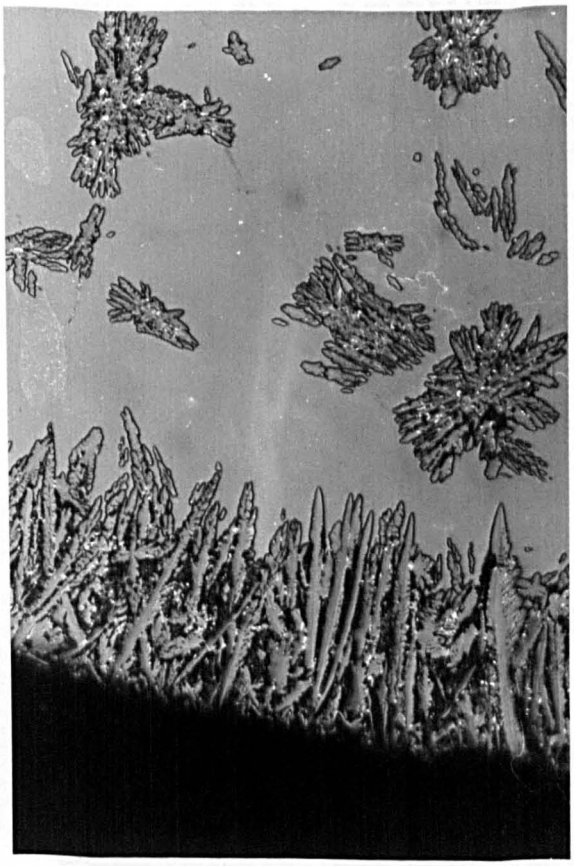

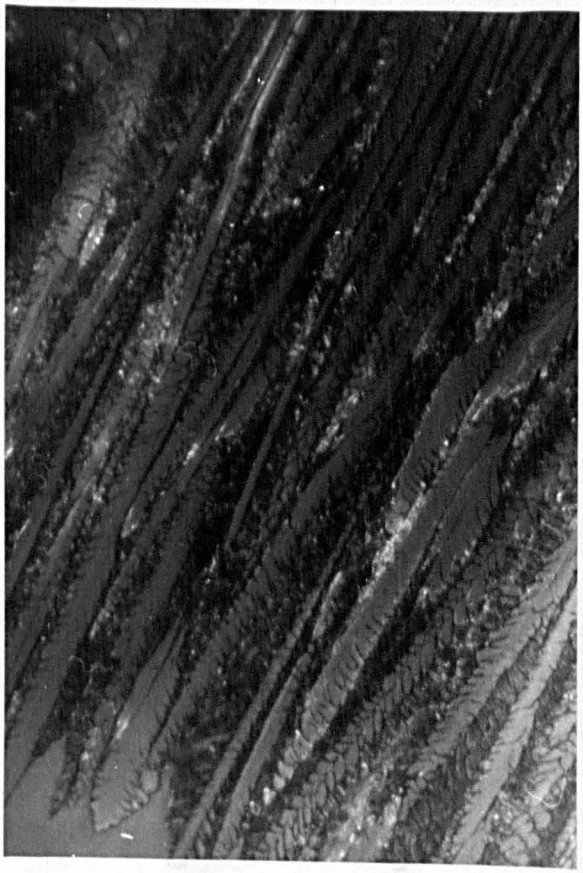

FIG. 3.52. GROWTH RATE MEASUREMENTS FOR THE COMPOSITION 80 m/o $Li_2Si_2O_5$ - 20 m/o $BaSi_2O_5$ (CODE 80 : 20)

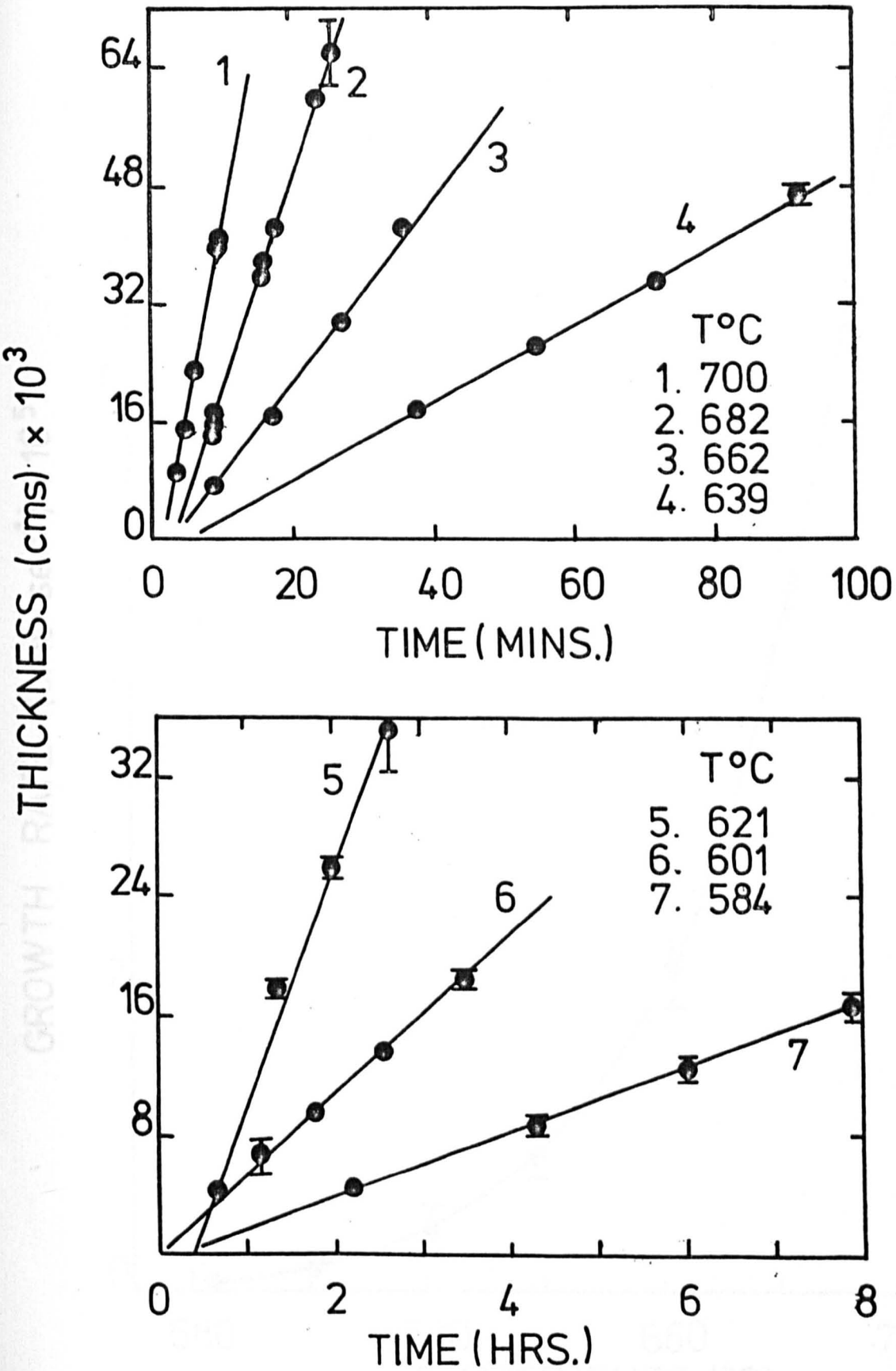

FIG. 3. 53. CRYSTAL GROWTH RATE AS A FUNCTION OF TEMPERATURE FOR THE COMPOSITION 80 m/o $Li_2Si_2O_5$ - 20 m/o $BaSi_2O_5$ (CODE 80 : 20)

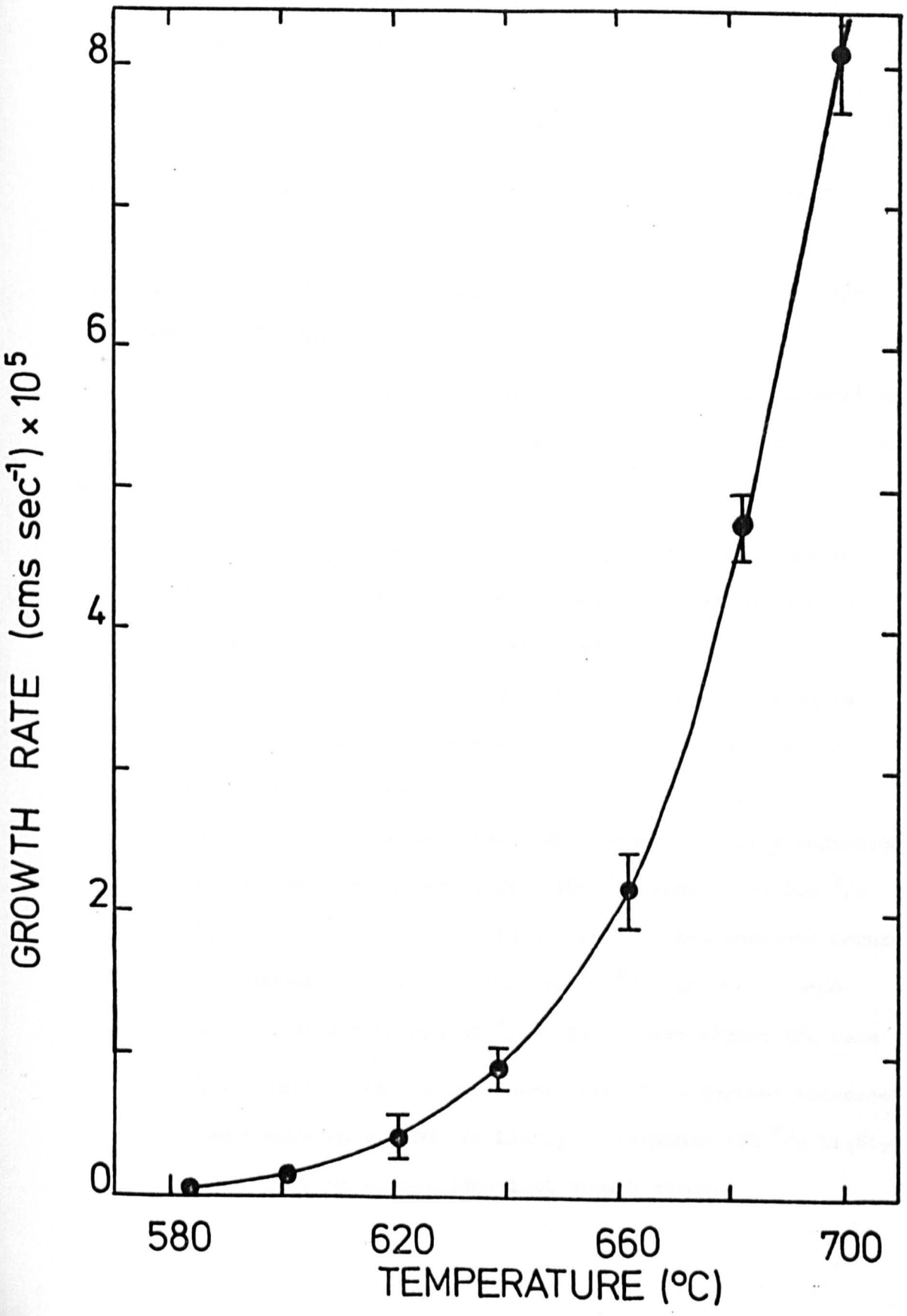

function of temperature is shown in Figure 3.54. As for the 50L:50 and 60:40 compositions, it is possible to distinguish a eutectic layer and a dendritic layer. The thickness of these two layers as a function of temperature is shown in Figure 3.55. Whereas the eutectic layer has a maximum growth rate at about 850°C, becoming zero at the eutectic temperature, the dendritic layer has a much higher maximum growth rate at 900°C, which becomes zero at the liquidus temperature.

3.3 Summary - Internal nucleation and crystal growth in the system $Li_2Si_2O_5$-$BaSi_2O_5$

The internal nucleation and crystal growth curves of compositions in the system $Li_2Si_2O_5$-$BaSi_2O_5$ are shown together in Figure 3.56. The major trends are

1. The addition of $BaSi_2O_5$ to $Li_2Si_2O_5$ causes a decrease in the internal nucleation rate of $Li_2Si_2O_5$, the nucleation curve moving to higher temperatures.
2. The addition of $Li_2Si_2O_5$ to $BaSi_2O_5$ causes a decrease in the internal nucleation rate of $BaSi_2O_5$, the nucleation curve moving to lower temperatures.
3. The growth rate at any given temperature generally increases as the composition varies from 100 $^m/_o$ $BaSi_2O_5$ to 100 $^m/_o$ $Li_2Si_2O_5$. However, the largest part of that increase occurs for compositions between 100 and 90 $^m/_o$ $BaSi_2O_5$. Compositions between 90 and 40 $^m/_o$ $BaSi_2O_5$ have almost the same growth rates within experimental error. A further increase then occurs up to 100 $^m/_o$ $Li_2Si_2O_5$, although 100 $^m/_o$ $Li_2Si_2O_5$ and 90:10 have almost identical growth rates.

Fig. 3.54 Optical micrographs of the composition 70 ^{m}/o $Li_2Si_2O_5$-30 ^{m}/o $BaSi_2O_5$ heated for 5 minutes at

Top left: 800°C; magnification x100

Top right: 850°C; magnification x50

Bottom left: 900°C, showing dendrite/glass interface; magnification x100

Bottom right: 900°C, showing eutectic layer; magnification x100

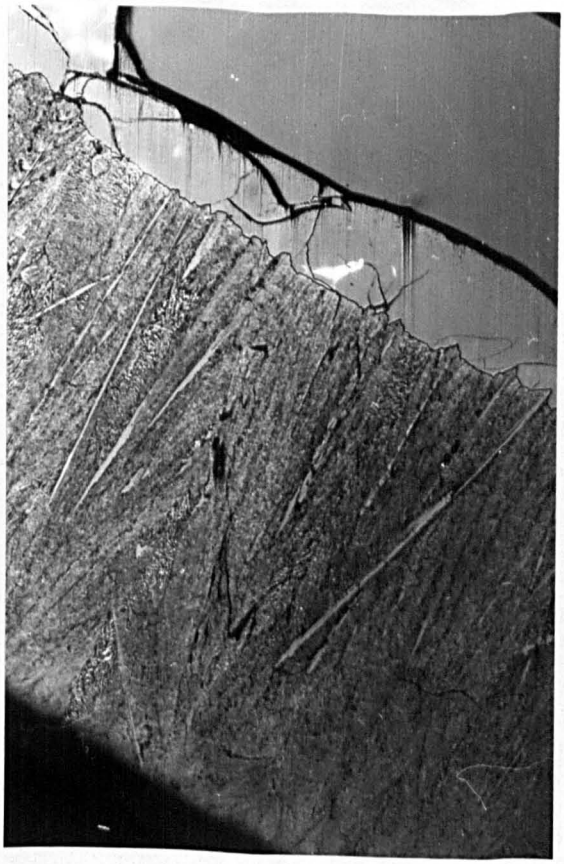

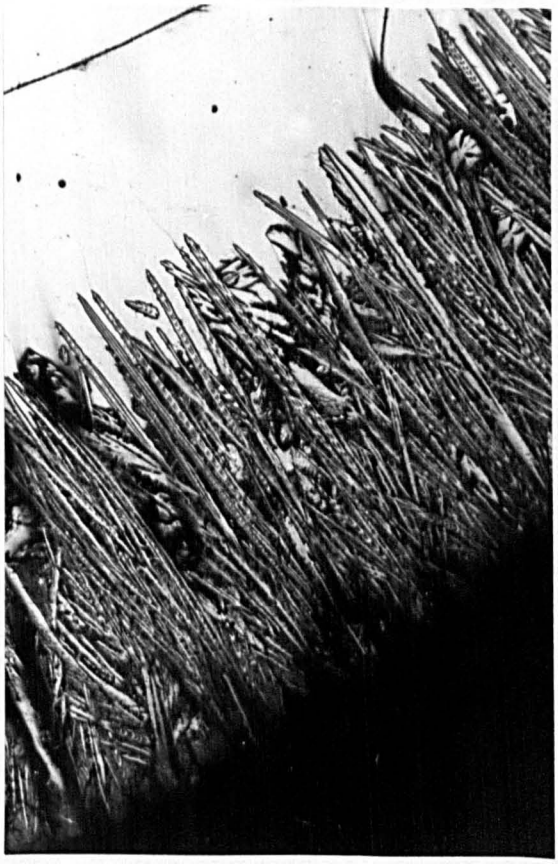

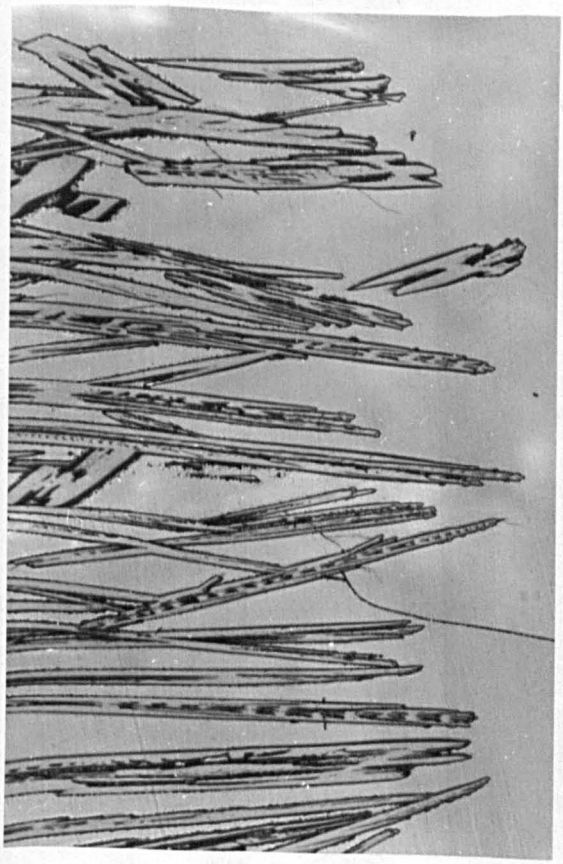

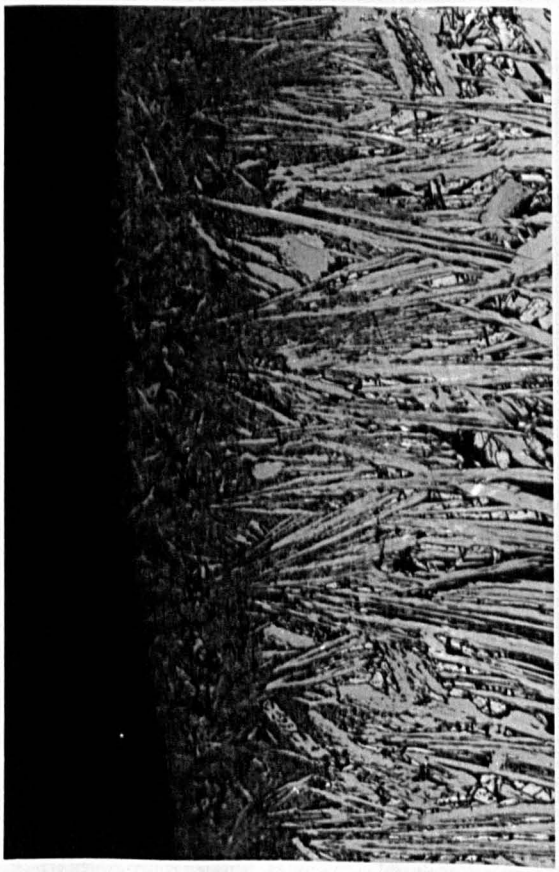

Fig. 3.54 contd/...

Top left: 935°C, magnification x32

Top right: 935°C, showing dendrite/glass interface; magnification x100

Bottom: 935°C, showing eutectic layer; magnification x100

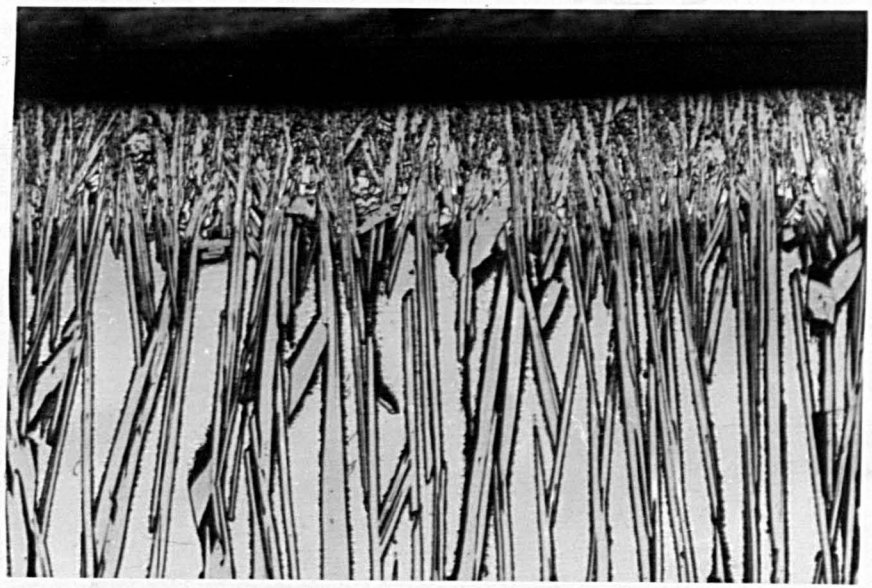

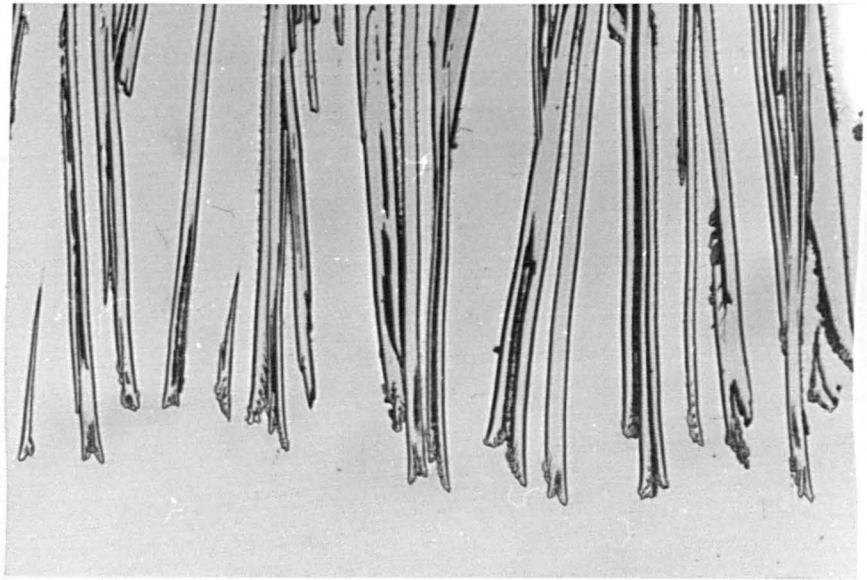

FIG. 3.55. THICKNESS OF SURFACE CRYSTALLINE LAYER AFTER 5 MINUTES AS A FUNCTION OF TEMPERATURE FOR THE COMPOSITION 70 m/o $Li_2Si_2O_5$ - 30 m/o $BaSi_2O_5$ (CODE 70 : 30)

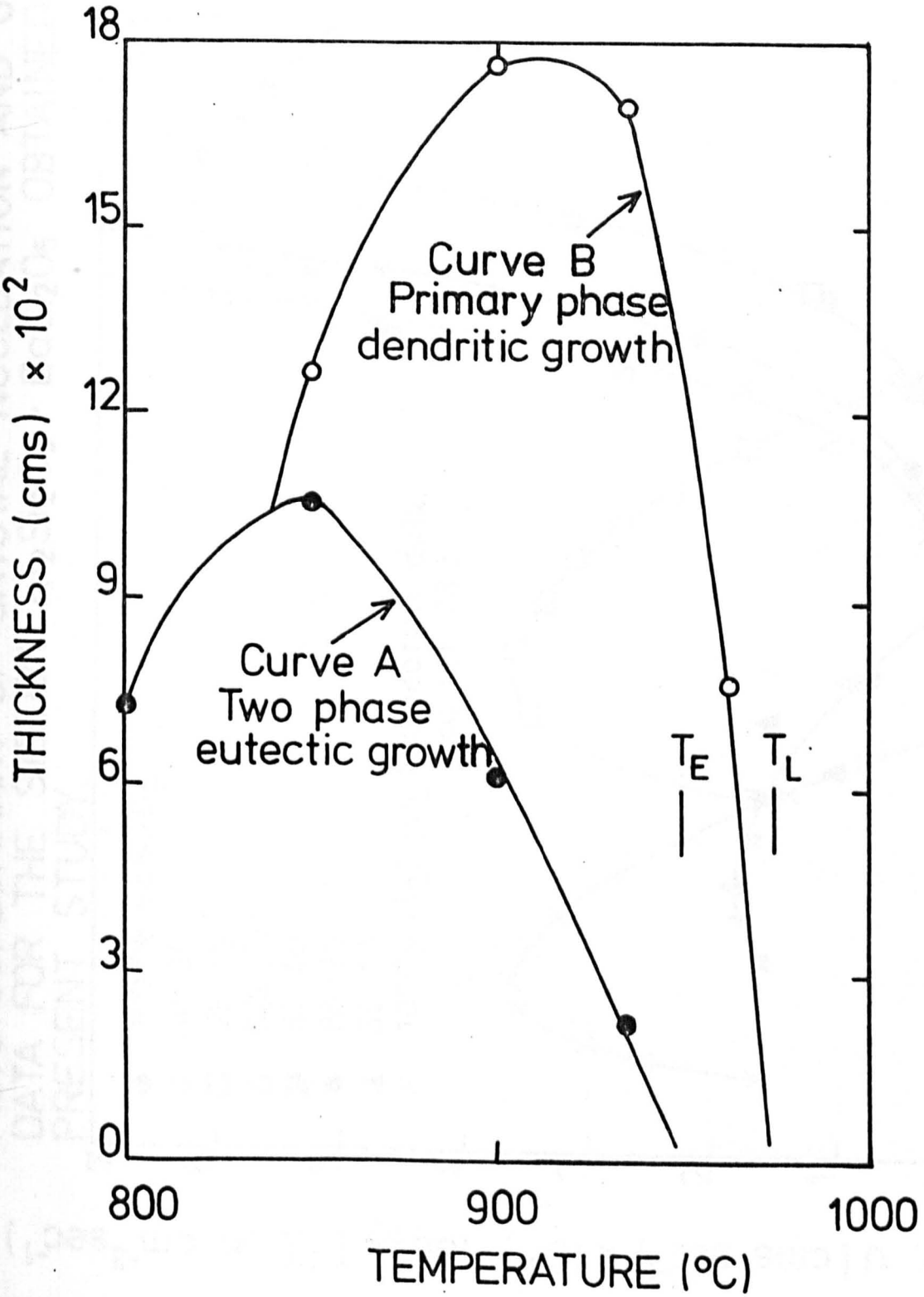

FIG. 3.56. SUMMARY OF CRYSTAL NUCLEATION AND GROWTH RATE DATA FOR THE SYSTEM $Li_2Si_2O_5$ - $BaSi_2O_5$ OBTAINED IN THE PRESENT STUDY.

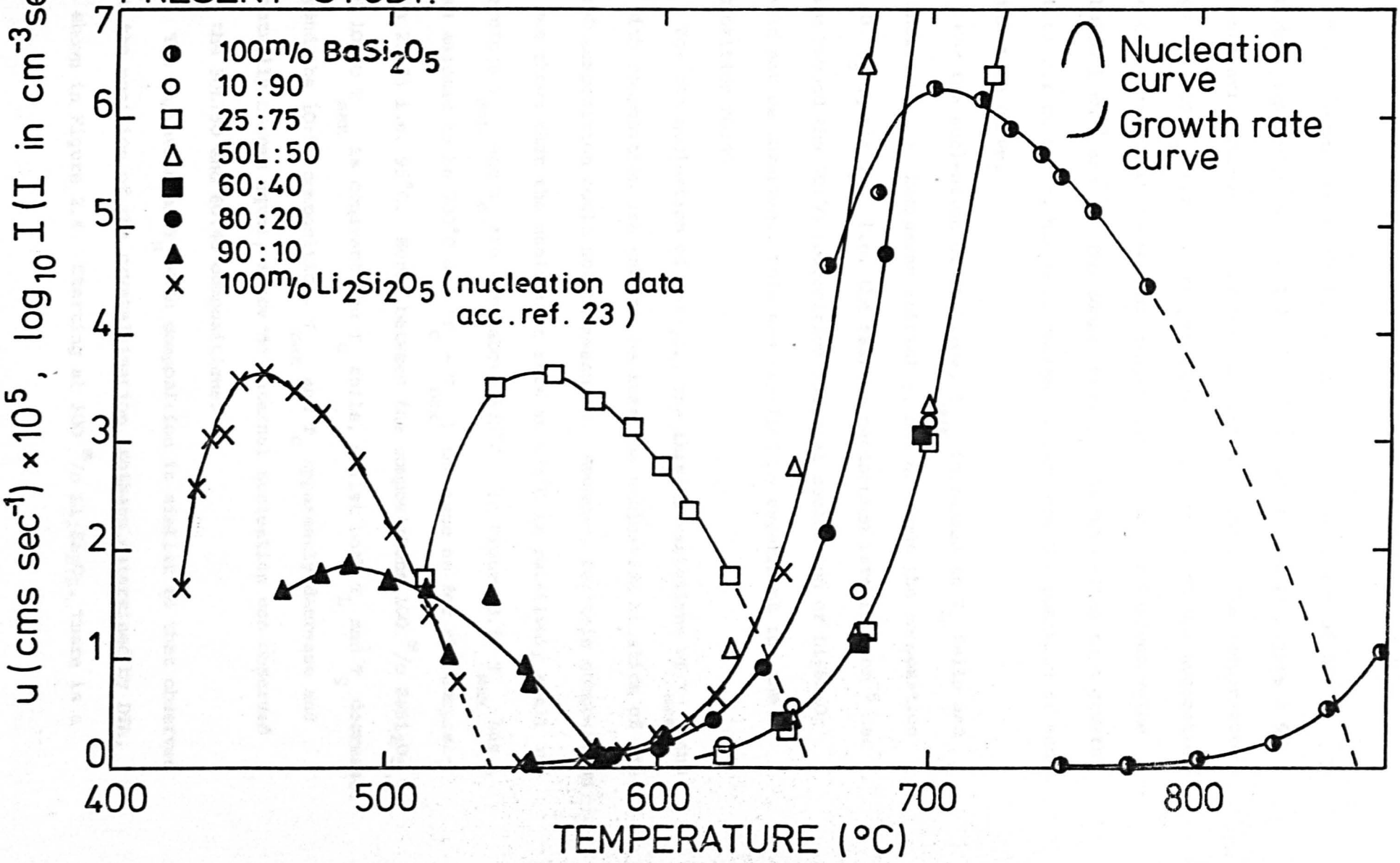

These trends are shown in relation to the variation of the liquidus temperature and 'D.T.A. T_g' with composition in Figure 3.57. The nucleation curves have been expressed in terms of the temperature range T_{max} to T_c, i.e. the temperature range over which the nucleation rate decreases (with increasing temperature) from its maximum value to below 1 cm^{-3} sec^{-1}. The temperature T_u, corresponding to a growth rate of 0.1 μm sec^{-1}, has been chosen to indicate the position of each growth rate curve.

For the nucleation of $Li_2Si_2O_5$, T_{max} increases as T_L falls and T_g increases. T_c increases initially, but at about the composition 70:30, T_c equals T_{max} i.e. the maximum nucleation rate is 1 cm^{-3} sec^{-1}. Hence beyond the 70:30 composition internal nucleation of $Li_2Si_2O_5$ should not be observed. This was verified by experiment for the composition 60:40.

For the nucleation of $BaSi_2O_5$, the initial variations of T_{max} and T_c with composition are unknown because the nucleation kinetics of the 10:90 composition could not be measured. However, for this composition it was shown that the nucleation rate at 675°C is relatively small and therefore T_{max} and T_c are both above 675°C. In Figure 3.57 T_{max} has been assumed to be 700°C and (T_c - T_{max}) the same as for the composition 25:75 i.e. 95°C. Hence between the compositions 100 $^m/_o$ $BaSi_2O_5$ and 10:90 T_{max} is constant and T_c falls, whilst both T_L and T_g decrease. Beyond the 10:90 composition, T_{max} and T_c apparently decrease and eventually become equal, since no internal nucleation was observed for the 50L:50 and 60:40 compositions.

The variation of T_u with composition is similar to that observed for the position of the crystallisation exotherm determined by DTA, as shown in Figure 2.4. Starting at 100 $^m/_o$ $Li_2Si_2O_5$, there is a

FIG. 3.57. THE VARIATION OF T_L, 'DTA' T_g, T_c, T_{max}, AND T_u WITH COMPOSITION IN THE SYSTEM $Li_2Si_2O_5$-$BaSi_2O_5$.

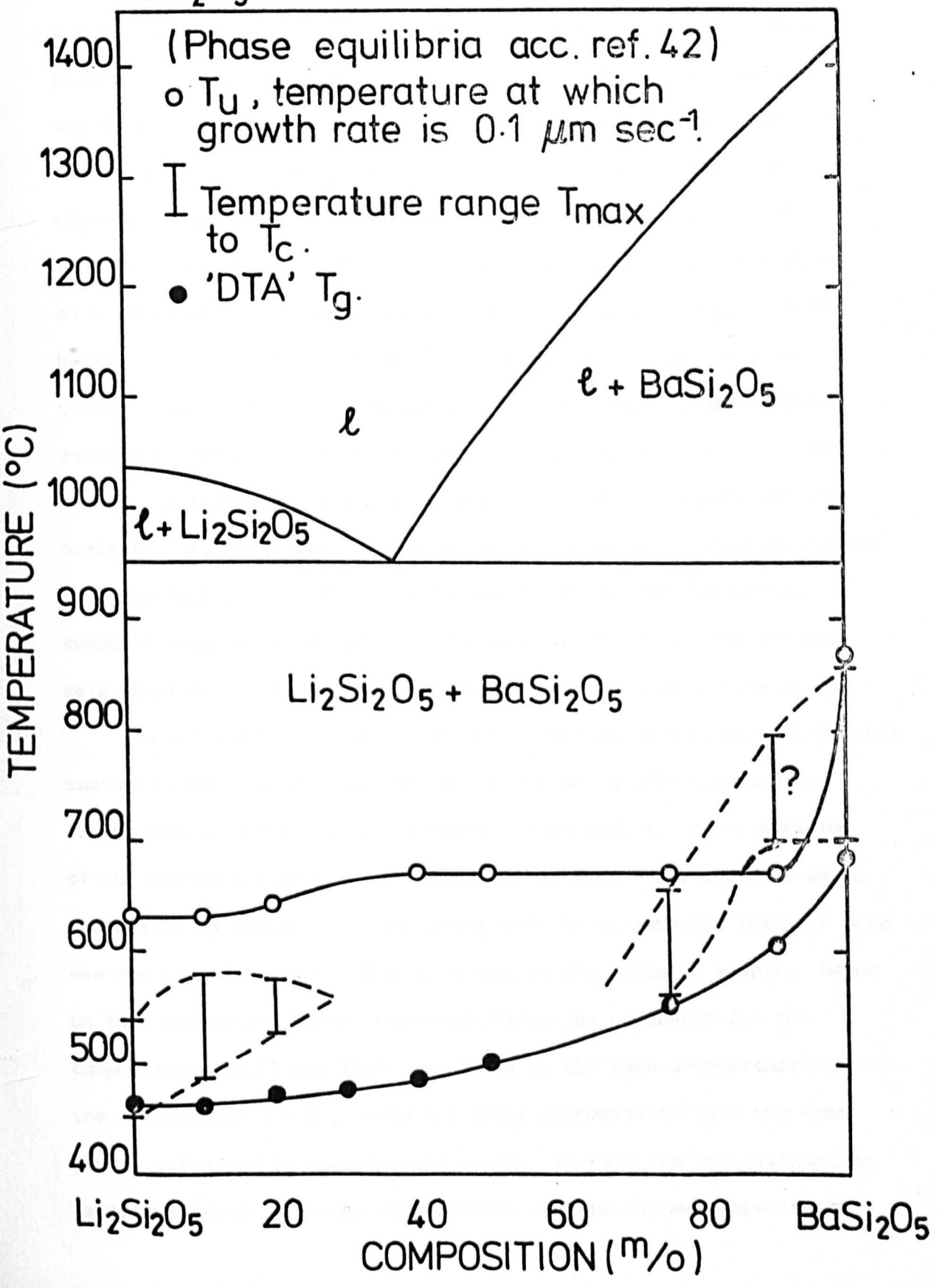

gradual rise in T_u up to the composition 60:40, followed by a plateau region of constant T_u up to the 10:90 composition, and then a rapid rise in T_u between the compositions 10:90 and 100 $^m/_o$ $BaSi_2O_5$. The D.T.A. crystallisation exotherm, however, does not show as wide a plateau region, but exhibits a marked rise in temperature between the 60:40 and 10:90 compositions. Thus the crystallisation exotherm tends to 'follow' the T_g curve, whereas T_u does not 'follow' as closely. The difference in behaviour between 'D.T.A. T_g' and T_u is emphasised in Figure 3.58 where the growth rate curves are shown as a function of $(T - T_g)$. It is interesting to note that on this basis 100 $^m/_o$ $Li_2Si_2O_5$ and 100 $^m/_o$ $BaSi_2O_5$ have almost the same growth rates. Also, the composition 10:90 has much higher growth rates than other compositions, for a given value of $(T - T_g)$. This partly contributes to the experimental difficulty of measuring the nucleation kinetics for that composition. Even if T_{max} was concurrent with the 'D.T.A. T_g', as it is for the 25:75 and 100 $^m/_o$ $BaSi_2O_5$ compositions, the high growth rates would still hinder the accurate determination of the nucleation kinetics for the composition 10:90.

The difference in 'behaviour' of T_u and the D.T.A. crystallisation exotherm would suggest that the latter is not solely governed by growth rate considerations. However, in section 3.1.4 the position of the exothermic peak for the composition 50L:50 was shown to be in reasonable agreement with the growth rate data, assuming that the peak was due to the surface crystallisation of the powdered sample. Based on this assumption alone, the crystallisation exotherms for the compositions 25:75 and 10:90 should be at the same temperatures as for the composition 50L:50, since all these compositions have the same growth rates within experimental error. In fact the crystallisation exotherms occur at higher temperatures for the former compositions

FIG. 3.58. GROWTH RATE DATA FOR COMPOSITIONS IN THE SYSTEM $Li_2Si_2O_5$ - $BaSi_2O_5$ AS A FUNCTION OF $(T - T_g)$.

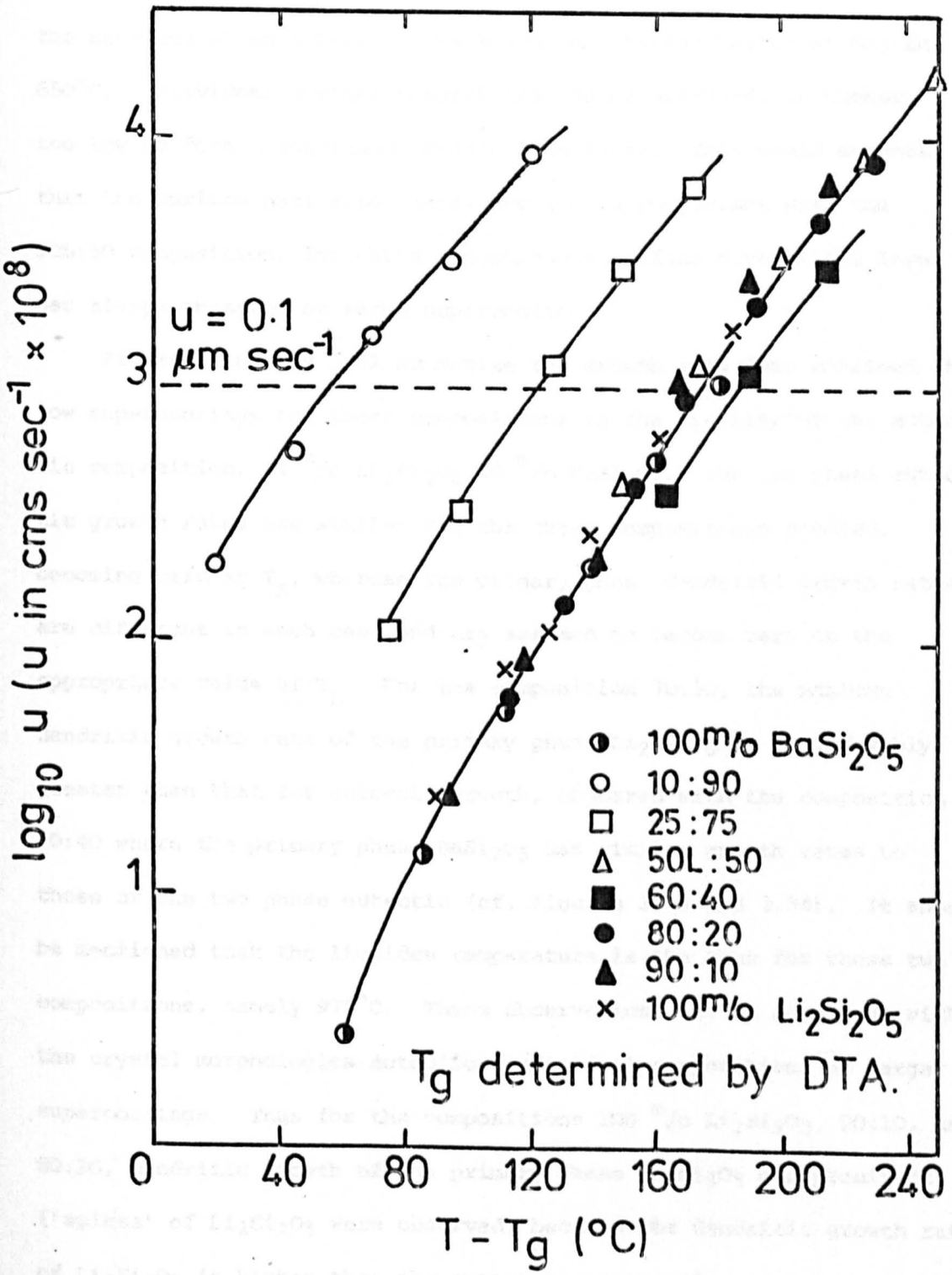

and for the 10:90 composition it is 85°C higher. A possible explanation for this anomalous behaviour is that the surface nucleation rates for the composition 50L:50 are higher than those for the 25:75 and 10:90 compositions at the same temperature. Figure 3.59 shows the surfaces of specimens of the 10:90 composition heated at 625 and 650°C. Individual surface spherulites can be observed, in numbers too low to form a continuous crystalline layer. This would suggest that the surface nucleation rates are low in comparison with the 50L:50 composition, for which a continuous surface crystalline layer was always observed at large supercoolings.

Figures 3.60 and 3.61 summarize the growth rate data obtained at low supercoolings for those compositions in the vicinity of the eutectic composition, 64 $^{m}/_{o}$ $Li_2Si_2O_5$ 36 $^{m}/_{o}$ $BaSi_2O_5$. The two phase eutectic growth rates are similar for the three compositions studied, becoming zero at T_E, whereas the primary phase dendritic growth rates are different in each case and are assumed to become zero at the appropriate value of T_L. For the composition 70:30, the maximum dendritic growth rate of the primary phase $Li_2Si_2O_5$ is considerably greater than that for eutectic growth, compared with the composition 60:40 where the primary phase $BaSi_2O_5$ has similar growth rates to those of the two phase eutectic (cf. Figures 3.55 and 3.34). It should be mentioned that the liquidus temperature is the same for these two compositions, namely 975°C. These observations are in agreement with the crystal morphologies noted for individual compositions at larger supercoolings. Thus for the compositions 100 $^{m}/_{o}$ $Li_2Si_2O_5$, 90:10, and 80:20, dendritic growth of the primary phase $Li_2Si_2O_5$ was prominent ('spikes' of $Li_2Si_2O_5$ were observed) because the dendritic growth rate of $Li_2Si_2O_5$ is higher than the eutectic growth rate. However, for the

Fig. 3.59 Optical micrographs of the composition 10 m/o $Li_2Si_2O_5$-90 m/o $BaSi_2O_5$ heated at

Top: 650°C for 1 hour; magnification x100

Bottom: 625°C for 4 hours; magnification x50

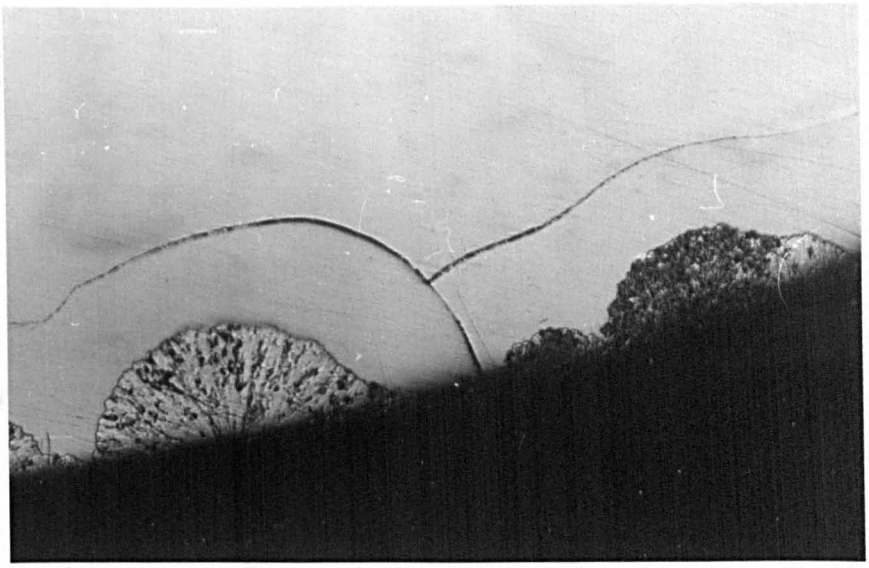

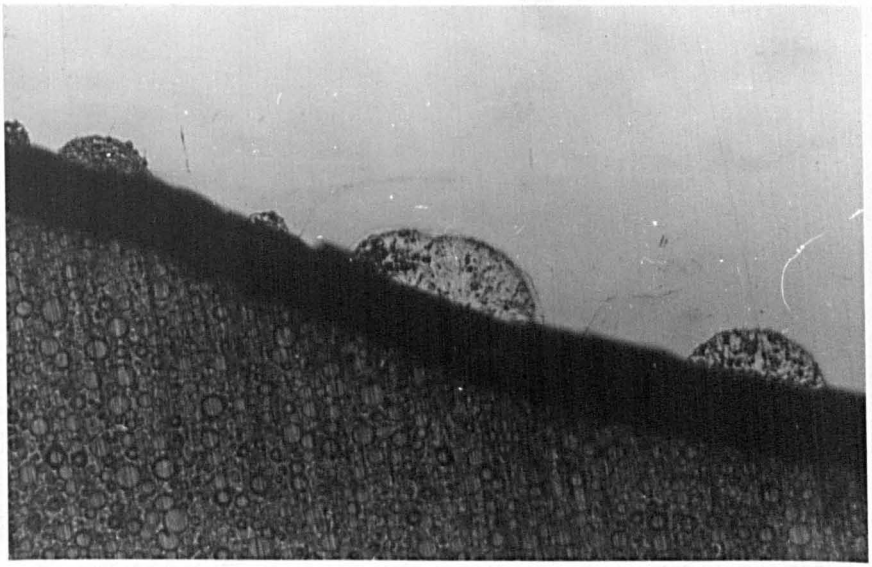

FIG. 3.60. EXTENT OF TWO PHASE EUTECTIC GROWTH AFTER 5 MINUTES AS A FUNCTION OF TEMPERATURE FOR THE COMPOSITIONS 70:30, 60:40, AND 50L:50.

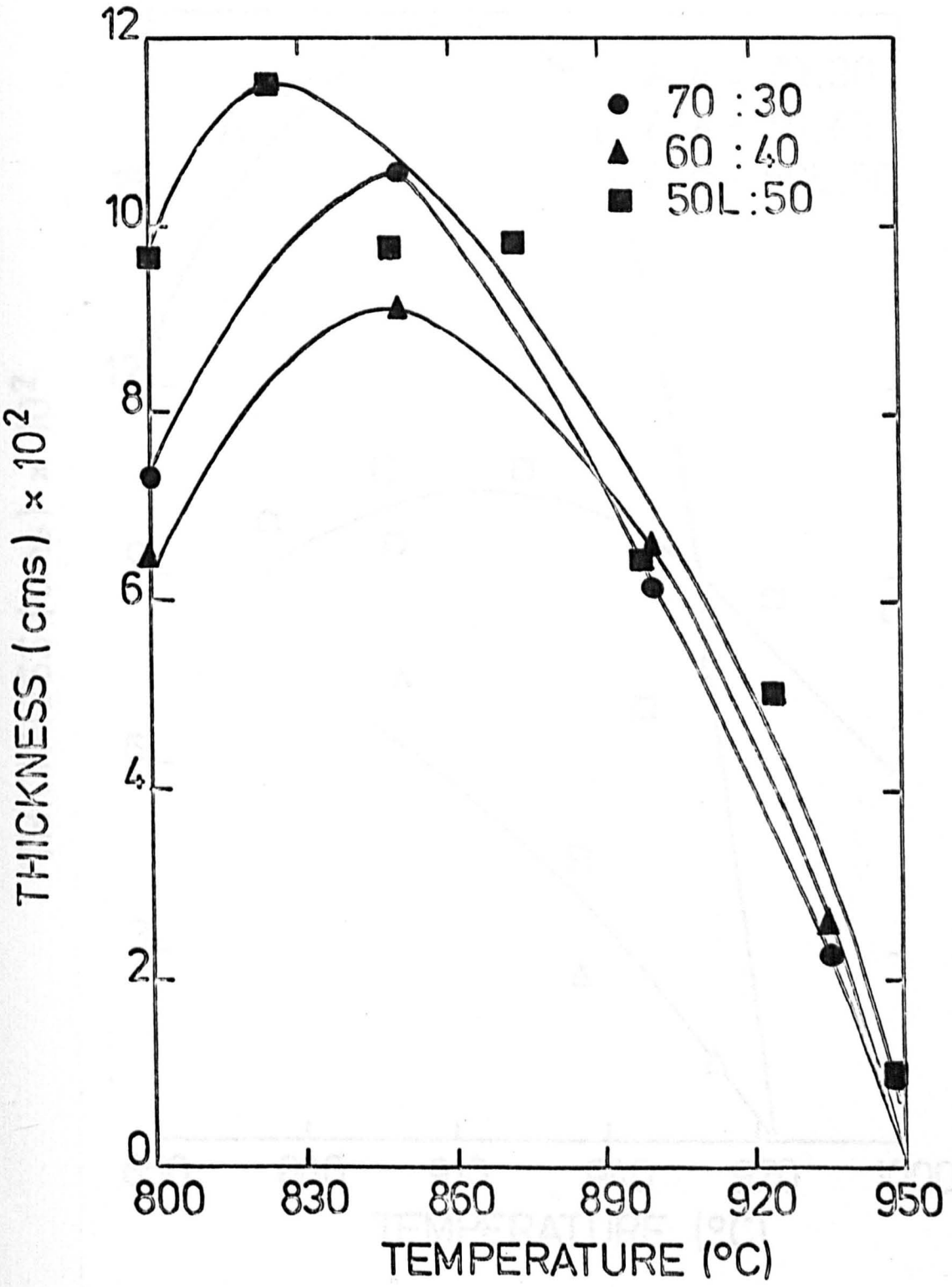

FIG. 3.61. EXTENT OF PRIMARY PHASE DENDRITIC GROWTH AFTER 5 MINUTES AS A FUNCTION OF TEMPERATURE FOR THE COMPOSITIONS 70:30, 60:40, AND 50L:50

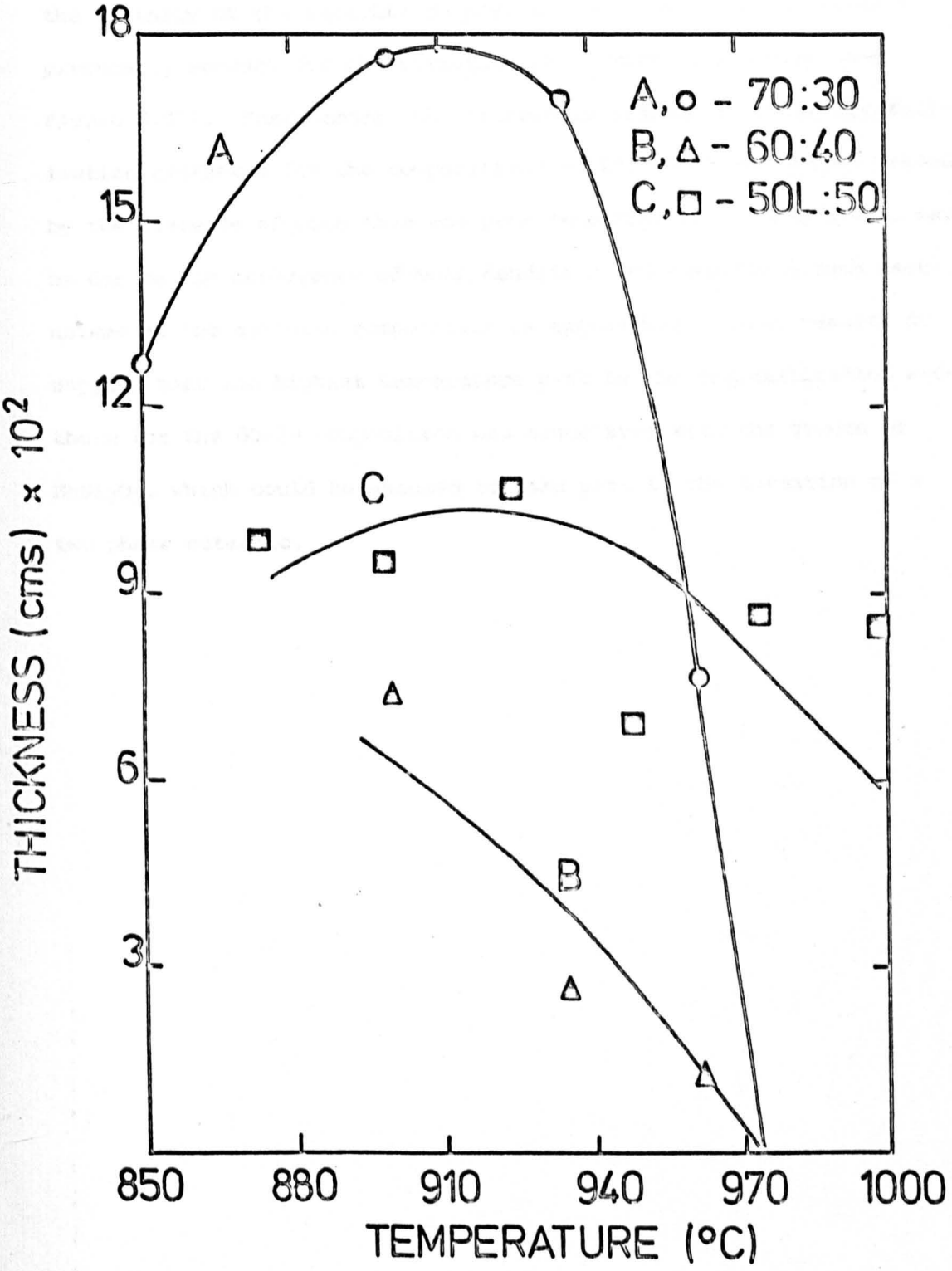

compositions 60:40 to 10:90 only eutectic growth was apparent, since the primary phase, which is now $BaSi_2O_5$, has the lower growth rate. Only in the composition 100 $^m/_o$ $BaSi_2O_5$ is the primary phase $BaSi_2O_5$ observed to grow as dendrites. These changes in growth mechanism in the vicinity of the eutectic composition and the 10:90 composition presumably account for the variation of T_u with composition (see Figure 3.57). Furthermore, the increasing broadness of the crystallisation exotherms for the compositions 90:10, 80:20 and 70:30, caused by the presence of more than one peak (see Figures 2.4 and 3.48), may be due to the occurrence of both dendritic and eutectic growth mechanisms as the eutectic composition is approached. X-ray results do suggest that the highest temperature peak in the crystallisation exotherm for the 80:20 composition was associated with the growth of $BaSi_2O_5$, which could be assumed to take part in the formation of a two phase eutectic.

CHAPTER 4

THEORETICAL ANALYSIS OF EXPERIMENTAL RESULTS FOR THE SYSTEMS $Li_2Si_2O_5$-$BaSi_2O_5$ AND $Na_2Si_2O_5$-$BaSi_2O_5$

Chapter 4

In this Chapter a detailed analysis is given of the results presented in Chapter 3. This is based on nucleation and growth theory reviewed in Chapter 1. First, an estimate of the heat of fusion of $BaSi_2O_5$ is obtained, thus enabling a complete analysis to be made of the nucleation kinetics of the 100 ^{m}/o $BaSi_2O_5$ composition. It is also shown that the thermodynamic driving force for cyrstal nucleation and growth in the systems $R_2Si_2O_5$-$BaSi_2O_5$ (R ≡ Na,Li) can be calculated from available liquidus data. Secondly, a critical assessment is given of the various methods of analysing nucleation kinetics, based on the accurate nucleation data available for $Li_2Si_2O_5$. One of these methods is chosen to analyse nucleation kinetics in the systems $R_2Si_2O_5$-$BaSi_2O_5$. Finally, the analysis of growth rates at large supercoolings is considered and applied to growth rate data obtained in this study. It is also shown that a previous analysis of growth rates for the $Na_2Si_2O_5$-$BaSi_2O_5$ system should be corrected to allow for the thermodynamic term.

4.1 Calculation of the thermodynamic driving force, ΔG, using phase diagram data

The importance of ΔG in determining nucleation and growth kinetics was discussed in Chapter 1. There are two problems in calculating ΔG in glassforming systems. First, accurate heats of fusion of the crystallising phases may not be known. Secondly, such systems are generally multicomponent and experimental activity data is often unavailable. However, as shown in Chapter 1, liquidus data can be used to estimate the heat of fusion of a crystalline phase, and furthermore, calculate its activity as a function of composition.

In this section liquidus data is used to calculate the heat of fusion of $BaSi_2O_5$, for which a calorimetrically determined value is unavailable. It is also shown that this compound can exhibit ideal behaviour in the systems Na_2O-BaO-SiO_2 and Li_2O-BaO-SiO_2. Thus it has been possible to quantitatively analyse the nucleation of $BaSi_2O_5$ from stoichiometric $BaSi_2O_5$ glass, and also from several ternary compositions.

4.1.1 The system sodium disilicate-barium disilicate

Crystal nucleation and growth have been studied in detail for the system Na_2O-BaO-SiO_2 [20]. Internal nucleation was found to occur only in a region near to the stoichiometric $BaSi_2O_5$ composition, the nucleating phase being $BaSi_2O_5$. Although critical nucleation temperatures were measured, including for one composition the whole nucleation curve, no quantitative analysis of the results was made due to the lack of thermodynamic data for $BaSi_2O_5$.

Whilst the thermodynamic properties of a ternary system are generally expressed in terms of the activities of the three basic

components, in this case a_{Na_2O}, a_{BaO} and a_{SiO_2}, it is also possible to use the activities of compounds formed within the system for the same purpose. Of particular interest are compositions in the system Na_2O-BaO-SiO_2 which lie on the constant $66^2/_3$ mole % SiO_2 section. These can be considered in terms of the activities of $Na_2Si_2O_5$ (a_{NS_2}) and $BaSi_2O_5$ (a_{BS_2}). Since $BaSi_2O_5$ is a primary phase on this section, it is possible to estimate a_{BS_2} from liquidus data.

Phase equilibria on the $Na_2Si_2O_5$-$BaSi_2O_5$ section were studied by Greene and Morgan[51], and subsequently by Gunawardane and Glasser[52]. Greene and Morgan found the section to be a simple binary eutectic system of the components $Na_2Si_2O_5$ and $BaSi_2O_5$. This was modified by Gunawardane and Glasser who found an incongruently melting compound at 80 mole % $BaSi_2O_5$, causing the primary phase field of $Ba_2Si_2O_5$ to be reduced by about 35 mole %. They also verified the reversible high-low transition of $BaSi_2O_5$ at 1360°C. Figure 4.1 shows the phase equilibria according to Gunawardane and Glasser, including the experimental points of Greene and Morgan.

According to equation (1.19) the activity of a component in solution at the liquidus temperature, with respect to the pure liquid component at the same temperature, is given by

$$\ln a^{\ell} = -\frac{\Delta H_f}{R}\left(\frac{1}{T_L} - \frac{1}{T_m}\right) \qquad (1.19)$$

This is exact, apart from the neglect of specific heat contributions. In an ideal system $a^{\ell} = x$, the mole fraction of the component in

FIG. 4.1. PHASE DIAGRAM FOR THE SYSTEM $Na_2Si_2O_5$—$BaSi_2O_5$.

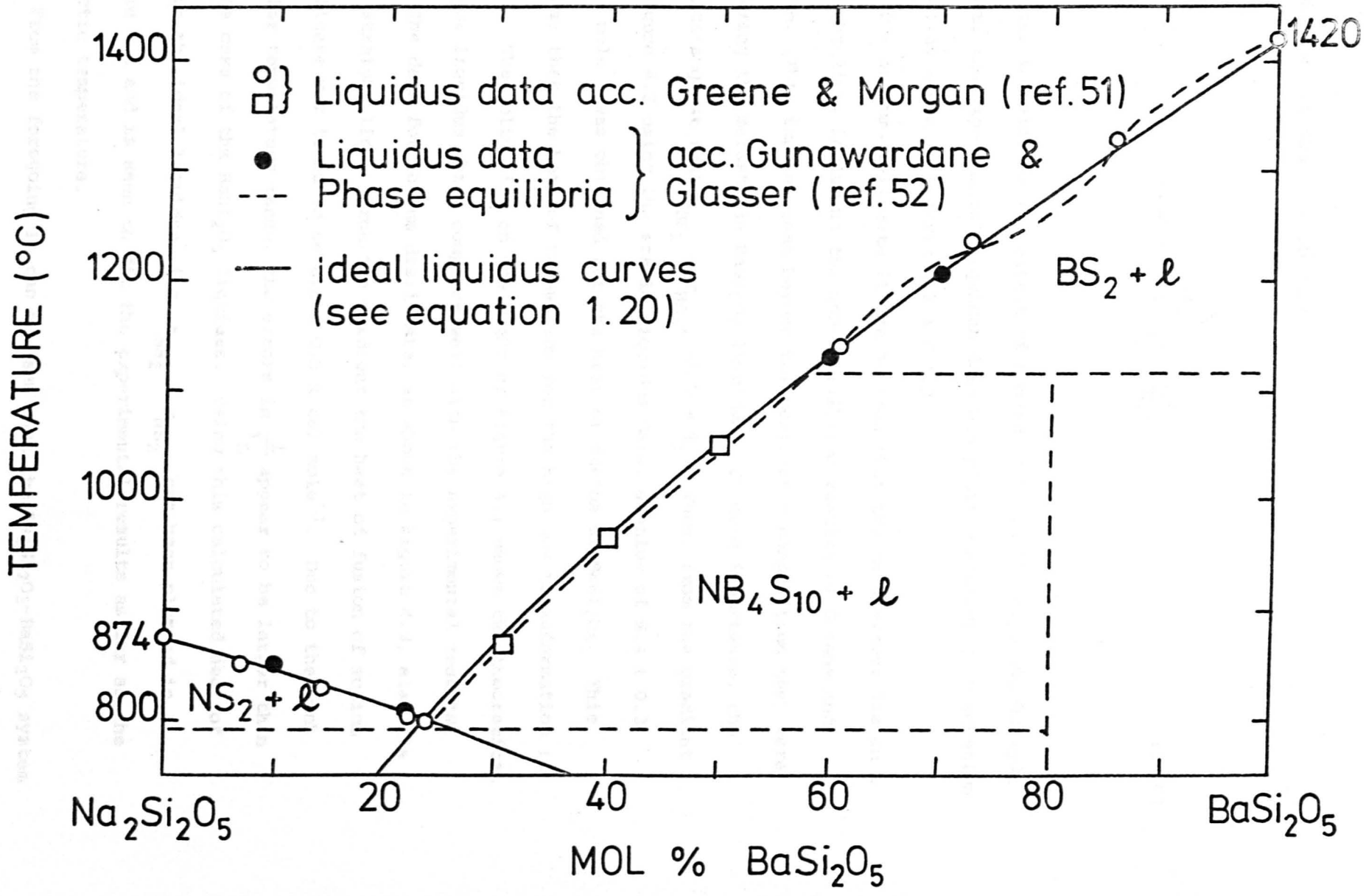

solution, so that one obtains

$$\ell n\ x = -\frac{\Delta H_f}{R}\left(\frac{1}{T_L} - \frac{1}{T_m}\right) \qquad (1.20)$$

In order to estimate the extent of non-ideality in the $Na_2Si_2O_5$-$BaSi_2O_5$ system, the experimental liquidus data was plotted according to equation (1.20) as shown in Figures 4.2 and 4.3.

For barium disilicate it can be seen that the data almost lie on a straight line, including the non-equilibrium results of Greene and Morgan. This implies that beyond the peritectic composition they were measuring the metastable $BaSi_2O_5$ liquidus. Of more importance, the results suggest that $a_{BS_2} = x_{BS_2}$, at $T = T_L$. Thus, from the gradient of Figure 4.2, using the stable liquidus data, a value of 8.4 ± 0.3 k cal mole^{-1} was obtained for the heat of fusion of $BaSi_2O_5$. This assumes that the heat of transition for the high-low transformation is small. The solid line on the right of Figure 4.1 shows the theoretical $BaSi_2O_5$ liquidus which compares well with the experimental results.

The data for sodium disilicate, as shown in Figure 4.3, also lie on a straight line. From the gradient the heat of fusion of sodium disilicate was found to be 8.8 ± 0.5 k cal mole^{-1}. Due to the much smaller temperature range, the errors in $\frac{1}{T_L}$ appear to be larger than in the case of the $BaSi_2O_5$ liquidus. Using this calculated heat of fusion the ideal liquidus, i.e. $a_{NS_2} = x_{NS_2}$, has been plotted in Figure 4.1 and is seen to fit the experimental results as far as the eutectic temperature.

From the foregoing it can be seen that the $Na_2Si_2O_5$-$BaSi_2O_5$ system is, within experimental error, ideal at the liquidus temperatures in

FIG. 4.2. $BaSi_2O_5$ LIQUIDUS DATA PLOTTED ACC. EQUATION 1.20 FOR THE SYSTEM $Na_2Si_2O_5 - BaSi_2O_5$.

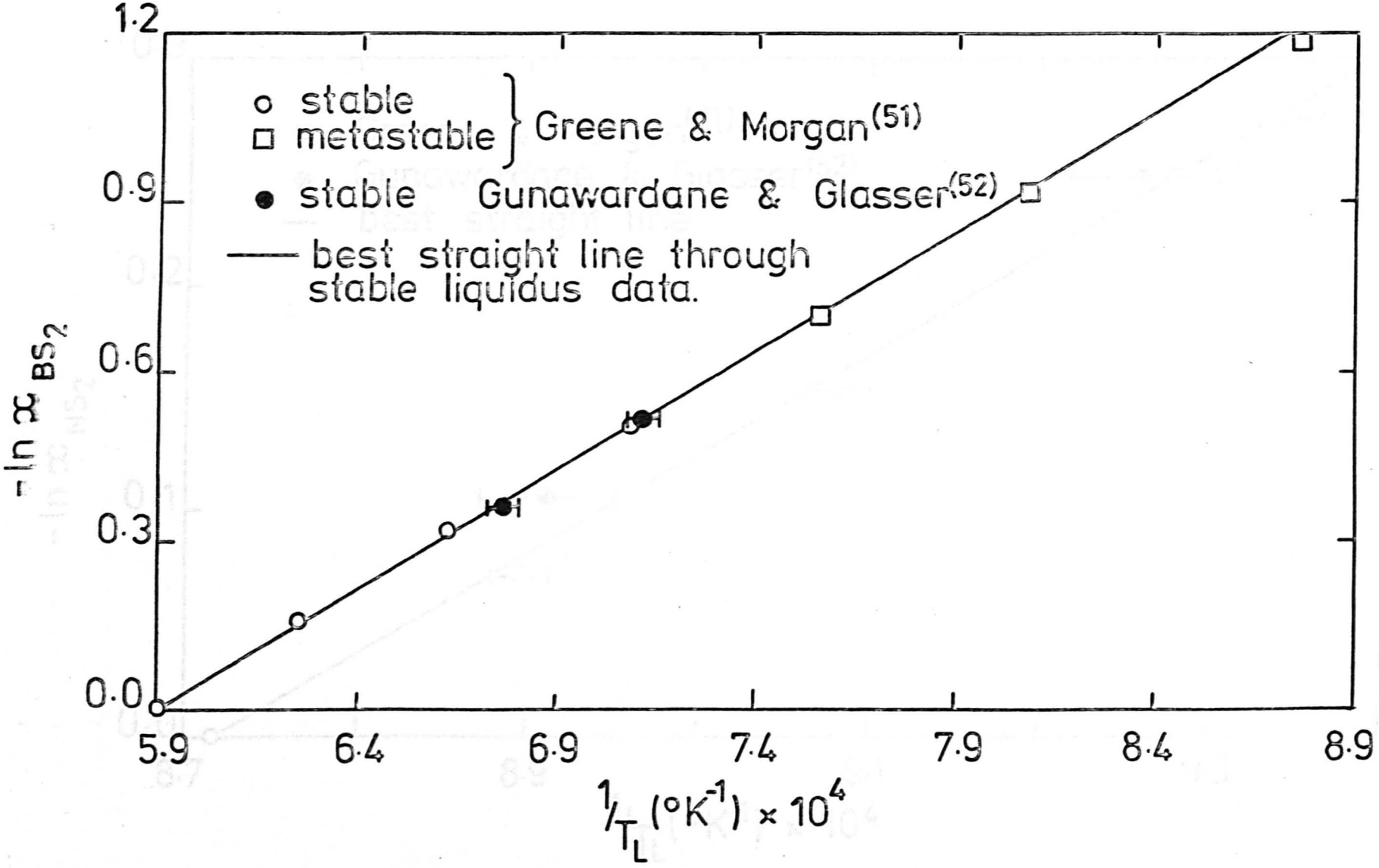

FIG. 4.3. $Na_2Si_2O_5$ LIQUIDUS DATA PLOTTED ACC. EQUATION 1.20. FOR THE SYSTEM $Na_2Si_2O_5 - BaSi_2O_5$.

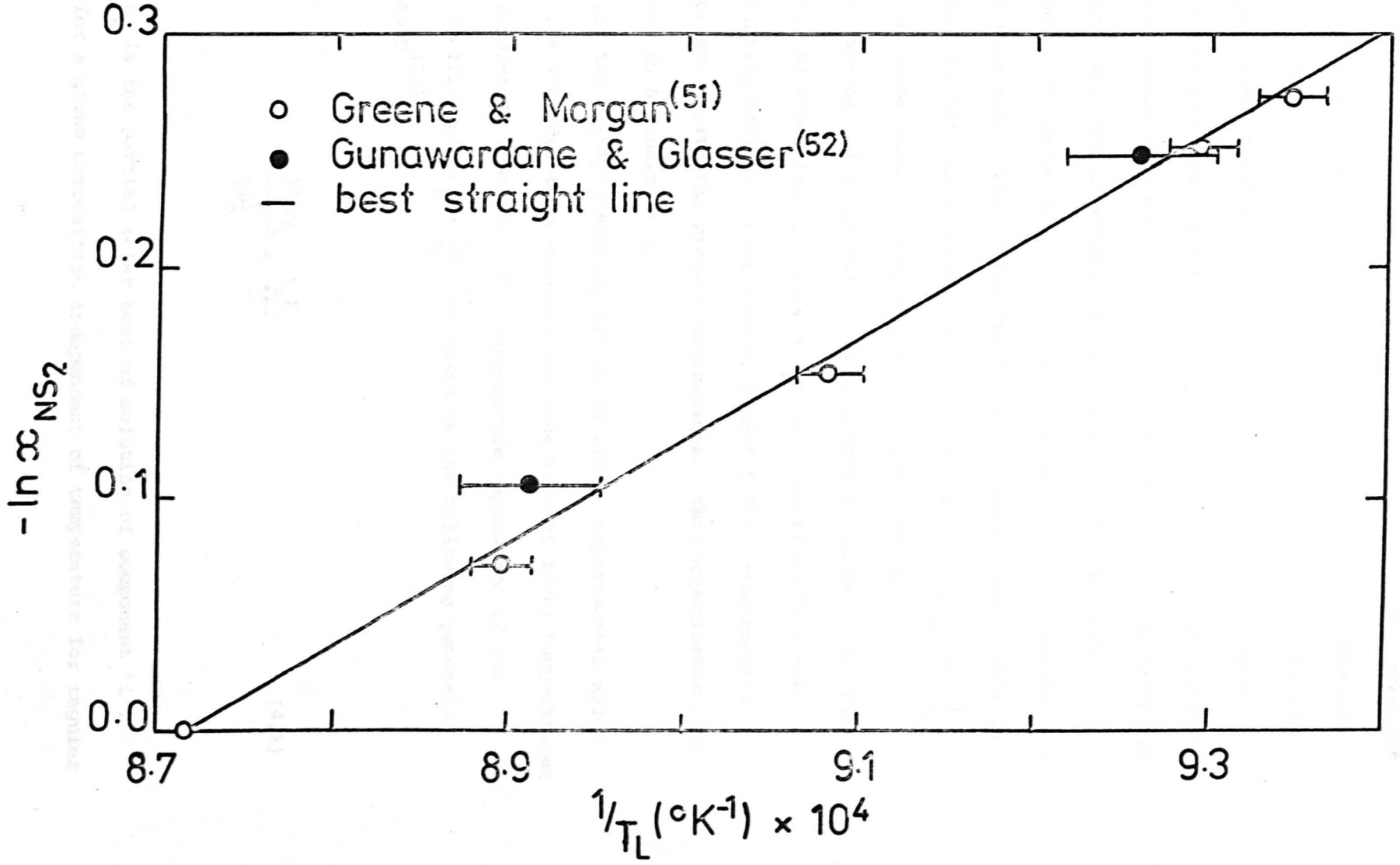

terms of the estimated heats of fusion. Confirmation of this requires an independent estimate of the heats of fusion for the two compounds. According to J.A.N.A.F. Thermochemical Tables[5] the heat of fusion of $Na_2Si_2O_5$ is 8.5 k cal mole^{-1}. This is based on four different kinds of measurement viz. phase diagram (as above), solution calorimetry, high temperature solution calorimetry, and dynamic differential calorimetry. Thus the experimental value can be taken as being well established. The value of 8.8 ± 0.5 k cal mole^{-1} is in excellent agreement with this. For barium disilicate no thermodynamic data is tabulated. However, considering the linearity of the $\ln x_{BS_2}$ vs. $\frac{1}{T_L}$ plot and the wide range of compositions covered, one may reasonably assume 8.4 k cal mole^{-1} to be a good estimate of the heat of fusion. As shown later, a similar value is obtained from the system $Li_2Si_2O_5$-$BaSi_2O_5$. Furthermore, recent D.T.A. measurements are in agreement with the present estimations. This unpublished work is reviewed in Appendix A4.1.

Whilst the $Na_2Si_2O_5$-$BaSi_2O_5$ system is within experimental error ideal at its liquidus temperatures, its behaviour at lower temperatures is not immediately apparent. The temperature dependence of the activity coefficient, $\gamma_i = \frac{a_i}{x_i}$, is given by the following general relationship[53]

$$\frac{\partial \ln \gamma_i}{\partial (\frac{1}{T})} = \frac{\Delta_m H_i}{R} \qquad (4.1)$$

where $\Delta_m H_i$ is the partial molar heat of solution of component 'i'. $\Delta_m H_i$ is for a given composition independent of temperature for regular

type (and ideal) model solutions. Since such models have been used with moderate success to estimate immiscibility regions in silicate systems[40,54,55], it is reasonable to assume that the system $Na_2Si_2O_5$-$BaSi_2O_5$ can be described similarly. Hence $\Delta_m H_i$, which is zero at the liquidus temperatures in the $Na_2Si_2O_5$-$BaSi_2O_5$ system, will remain almost zero, even for large supercoolings. Thus γ_{NS_2} and γ_{BS_2} will be very close to unity at all temperatures, and a = x for both components.

Thus the thermodynamic driving force for the crystallisation of $BaSi_2O_5$ (or $Na_2Si_2O_5$) in the $Na_2Si_2O_5$-$BaSi_2O_5$ system is given by

$$\Delta G = - \frac{\Delta H_f}{T_L} (T_L - T) \qquad (1.21)$$

where ΔH_f is the heat of fusion of $BaSi_2O_5$ and T_L is the liquidus temperature for $BaSi_2O_5$.

Whilst the present analysis has been concerned with providing thermodynamic data for crystallisation studies, it should be mentioned that the analysis also gives indirect information concerning the thermodynamics of mixing in the $Na_2Si_2O_5$-$BaSi_2O_5$ system and suggests a possible atomistic model of the mixing process involved. Thus the liquidus data has indicated that the entropy of mixing is ideal. Hence any proposed 'structural' model for liquids (glasses) in the $Na_2Si_2O_5$-$BaSi_2O_5$ system must predict ideality for all compositions. This aspect is considered separately in Appendix A4.2.

4.1.2 The system lithium disilicate-barium disilicate

The present study of the Li_2O-BaO-SiO_2 system has shown that both $Li_2Si_2O_5$ and $BaSi_2O_5$ can nucleate internally without the aid of

any intentional nucleating agent. Thus liquidus data in the $Li_2Si_2O_5$-$BaSi_2O_5$ system was analysed to obtain activity data for $Li_2Si_2O_5$ and $BaSi_2O_5$ and thereby calculate the thermodynamic driving force for the crystallisation of these phases in ternary compositions containing $66^2/_3$ mole % SiO_2. As in the previous analysis of the $Na_2Si_2O_5$-$BaSi_2O_5$ system, the liquidus curves were compared with those expected for an ideal solution.

The phase equilibria of the system were studied by Dietzel et al[42]. Lithium disilicate melts incongruently at 1033°C to give lithium metasilicate and liquid, the liquidus temperature being 1034°C. As barium disilicate is added to lithium disilicate the primary phase rapidly changes from lithium metasilicate to disilicate. The system is otherwise a simple eutectic. Since the hypothetical melting point must lie between 1033 and 1034°C, the system can be analysed in terms of mole fractions of $Li_2Si_2O_5$ and $BaSi_2O_5$ and the corresponding liquidus temperatures. The experimental data is shown in Figure 4.4 and this was plotted according to equation (1.20), as shown in Figures 4.5 and 4.6. The data for $BaSi_2O_5$ lie on a straight line, the gradient giving a value of 8.8 ± 0.2 k cal $mole^{-1}$ per mole for the heat of fusion of barium disilicate. This is in good agreement with the estimate of 8.4 ± 0.3 k cal $mole^{-1}$ obtained earlier and leads to an overall average value of 8.6 k cal $mole^{-1}$. The solid line on the right of Figure 4.4 shows the ideal liquidus which compares well with the experimental data.

The results for $Li_2Si_2O_5$ plotted in Figure 4.6 show a deviation from ideality, since any curve drawn must pass through the theoretical melting point. J.A.N.A.F. Tables[5] give a value of 12.86 k cal $mole^{-1}$ for the heat of fusion, as determined by the difference in enthalpy of

FIG. 4.4. PHASE DIAGRAM FOR THE SYSTEM $Li_2Si_2O_5$ - $BaSi_2O_5$.

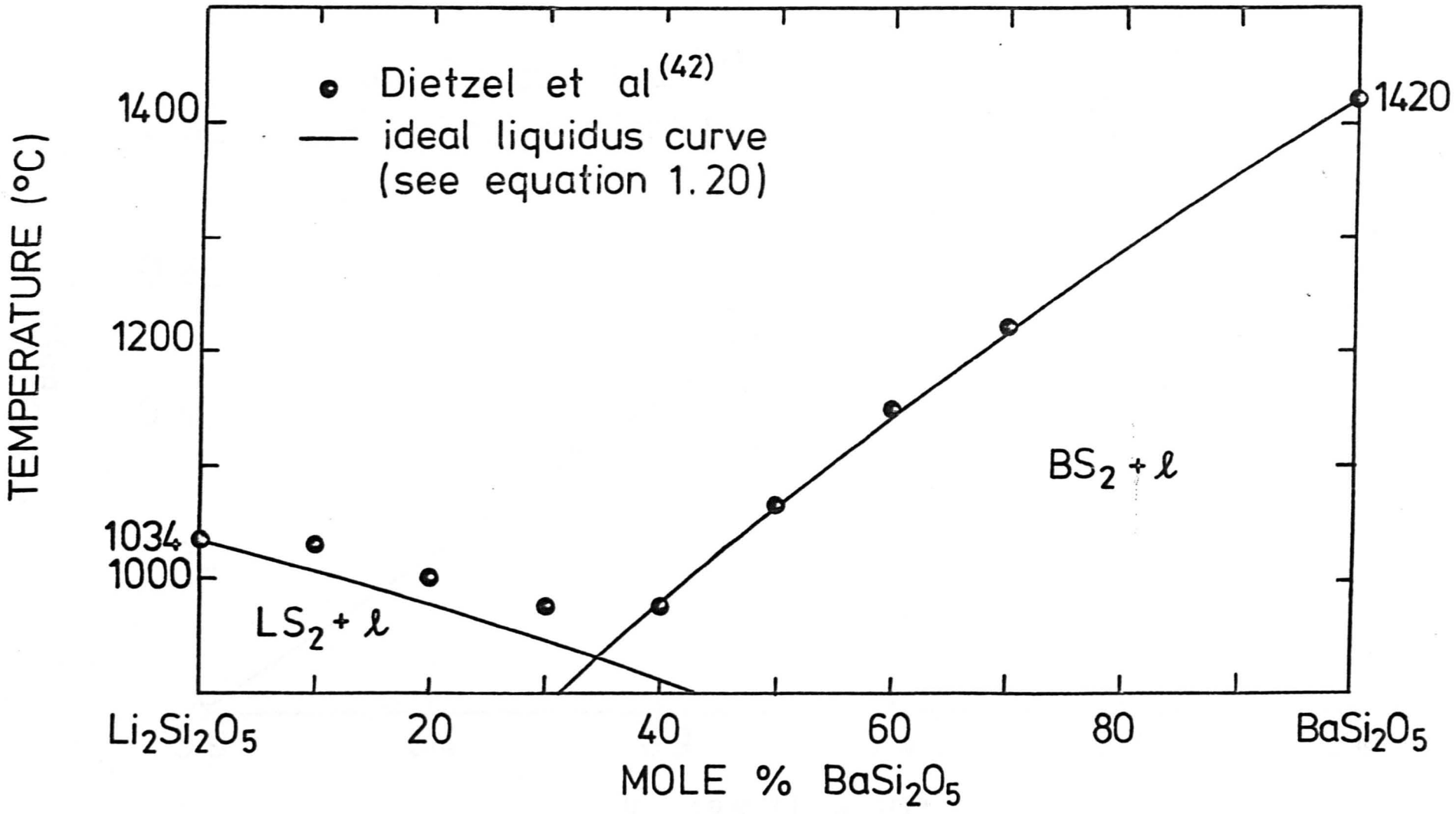

FIG. 4.5. $BaSi_2O_5$ LIQUIDUS DATA PLOTTED ACC. EQUATION 1.20. FOR THE SYSTEM $Li_2Si_2O_5 - BaSi_2O_5$.

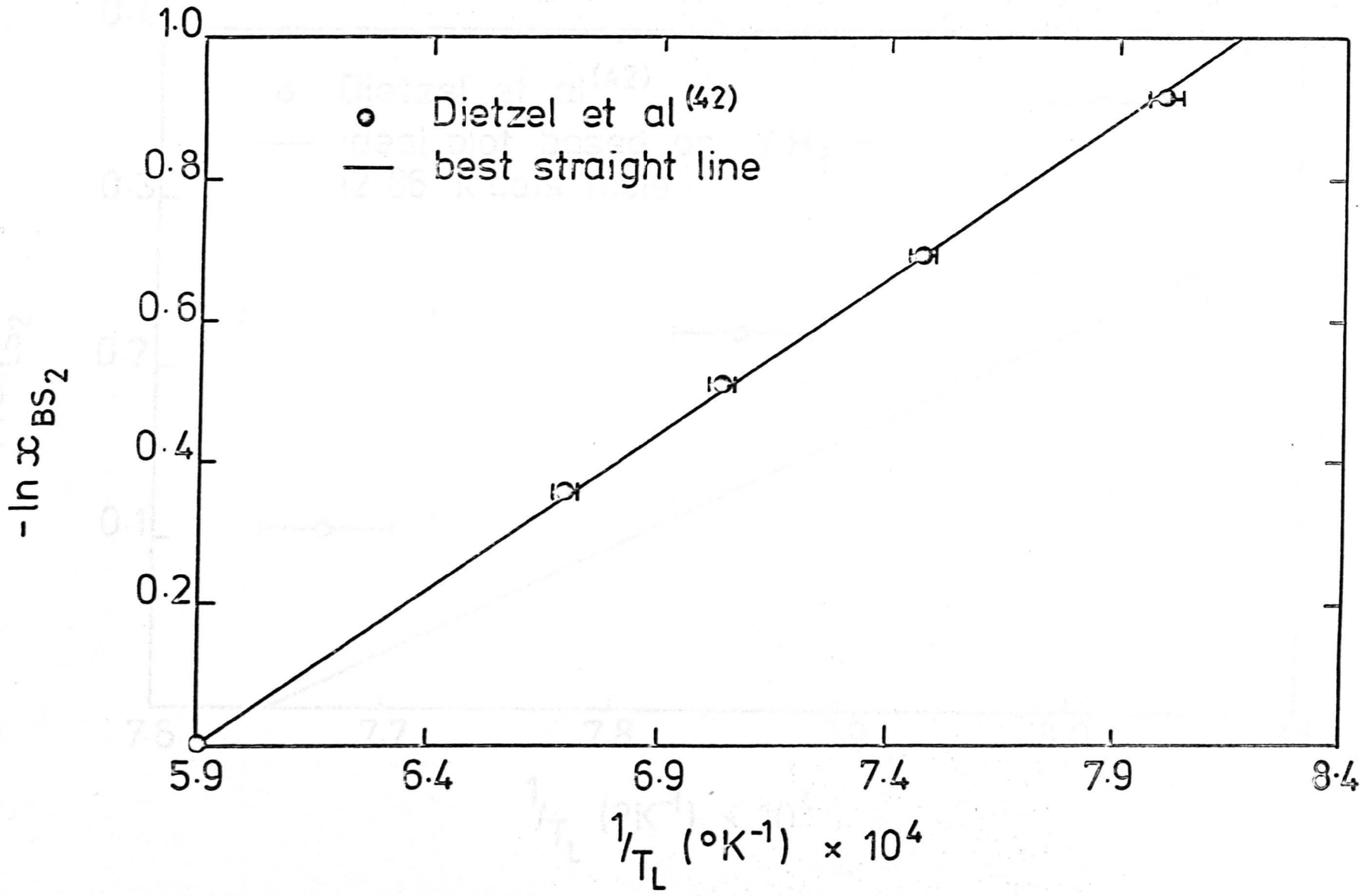

FIG. 4.6. $Li_2Si_2O_5$ LIQUIDUS DATA PLOTTED ACC. EQUATION 1.20. FOR THE SYSTEM $Li_2Si_2O_5 - BaSi_2O_5$.

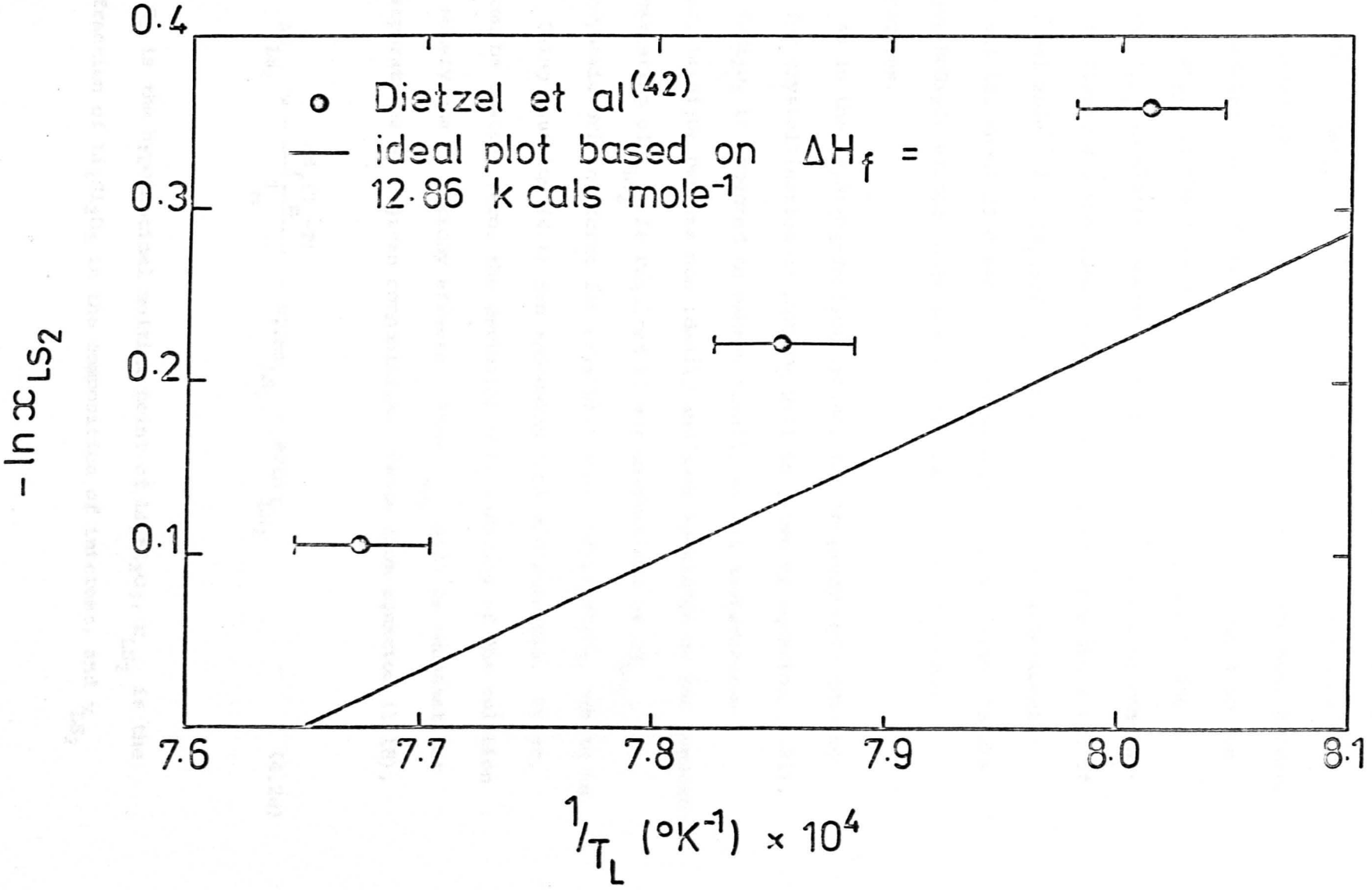

formation between lithium disilicate crystal and glass. The theoretical curve of $\ln x_{LS_2}$ vs. $\frac{1}{T_L}$ is shown in Figure 4.6. It can be seen that the deviations from ideality are positive, the difference between the theoretical plot and the experimental points being equal to the value of $\ln\gamma_{LS_2}$ at the liquidus temperature. It is interesting to note that γ_{LS_2} is almost constant, about 1.1, independent of composition. In Figure 4.4 the ideal liquidus is plotted using the value of 12.86 k cal mole^{-1} for ΔH_f and T_m equals 1034°C. The experimental points all lie about 25°C above the theoretical curve. Hence in the $Li_2Si_2O_5$-$BaSi_2O_5$ system, only $BaSi_2O_5$ is ideal at its liquidus temperatures.

As in the $Na_2Si_2O_5$-$BaSi_2O_5$ system, the thermodynamic driving force for crystallisation of $BaSi_2O_5$ will be given by equation (1.21), since $BaSi_2O_5$ is expected to behave ideally at all temperatures. However, $Li_2Si_2O_5$ behaves non ideally and some knowledge of the temperature variation of γ_{LS_2} is required if any estimations of ΔG_{LS_2}, the thermodynamic driving force for crystallisation of $Li_2Si_2O_5$, are to be made. Using equation (4.1) two approximations are possible. First, $\Delta_m H_i$ can be assumed zero, the deviation from ideality of the solution being solely due to entropy effects. Thus γ_{LS_2} will be constant for all temperatures at a given composition. Hence from equation (1.18),

$$\Delta G_{LS_2} = -\frac{\Delta H_f(T_m - T)}{T_m} - RT\ln x_{LS_2} - RT\ln\gamma_{LS_2} \qquad (4.2a)$$

where T_m is the hypothetical melting point of $Li_2Si_2O_5$, x_{LS_2} is the mole fraction of $Li_2Si_2O_5$ in the composition of interest, and γ_{LS_2}

(equals a_{LS_2}/x_{LS_2}) is calculated from liquidus data. Since γ_{LS_2} was found to be almost constant, except near pure $Li_2Si_2O_5$, the correction to ΔG_{LS_2} as compared with the ideal case (equals $RT\ln\gamma_{LS_2}$) is not only directly proportional to the temperature, but also independent of composition.

Secondly, $\Delta_m H_i$ can be assumed constant and γ_{LS_2} to approach unity at high temperatures. This assumption, also made by Charles[55], is equivalent to a regular solution model and implies ideal entropy of mixing. In this case ΔG_{LS_2} is given by

$$\Delta G_{LS_2} = -\frac{\Delta H_f (T_m - T)}{T_m} - RT\ln x_{LS_2} - RT\ln\gamma_{LS_2} \qquad (4.2b)$$

The correction to ΔG as compared with the ideal case is now independent of temperature, but not composition. Which of these approximations is the more exact can only be decided by obtaining further thermodynamic data. Further discussion as to the reason why the $Li_2Si_2O_5$ liquidus curve is non-ideal is given in Appendix M4.2, where the two systems $Na_2Si_2O_5$-$BaSi_2O_5$ and $Li_2Si_2O_5$-$BaSi_2O_5$ are compared from a structural viewpoint.

4.2 Methods of analysing nucleation rates

A quantitative analysis of nucleation rates involves the evaluation of the parameters $\bar{\sigma}$, ΔG_D and A. Only the pre-exponential factor can be calculated from nucleation theory. Unfortunately $\bar{\sigma}$ and ΔG_D cannot readily be obtained from independent experiments unrelated to nucleation kinetics.

Earlier in this thesis both $\bar{\sigma}$ and ΔG_D were tacitly assumed to be constants. However, these parameters are strictly free energy terms which contain both enthalpy and entropy contributions. The surface free energy is often expressed as

$$\bar{\sigma} = \bar{\sigma}_o - bT \qquad (4.3)$$

$\bar{\sigma}_o$ and b being the surface enthalpy and entropy respectively. Theoretically, it is not possible to estimate the magnitude or sign of b. Since $W^* \alpha \bar{\sigma}^3$ (equation (1.24)) even small values of b may affect nucleation kinetics.

Similarly, ΔG_D can be expressed as

$$\Delta G_D = \Delta H_D - T\Delta S_D \qquad (4.4)$$

where ΔH_D and ΔS_D are the activation enthalpy and entropy for diffusion respectively. Again it is not theoretically possible to estimate the magnitude or sign of the entropy term.

Substituting equations (4.3) and (4.4) into equation (1.28), assuming the respective enthalpy and entropy terms to be independent of temperature, we obtain

$$I = A_D \exp\left\{-\frac{k_5(\bar{\sigma}_o - bT)^3}{\Delta G_v^2\, kT}\right\} \exp\left(-\frac{\Delta H_D}{kT}\right) \qquad (4.5)$$

where $A_D = A \exp\left(\frac{\Delta S_D}{k}\right)$

An analysis of the temperature dependence of nucleation kinetics is therefore unaffected by the value of ΔS_D, although only A_D can be obtained. On the other hand, the temperature coefficient of $\bar{\sigma}$ cannot be simply separated in this way. However since nucleation is generally only observable over a range of about 100°C, it will be assumed that $\bar{\sigma}$ is constant for the purposes of analysis. It is obviously an advantage to avoid any additional unspecified parameters, unless the simpler nucleation equation fails to account for the experimental results.

In the following discussion we systematically consider the various methods of analysing nucleation data. These methods are applied to the results for $Li_2Si_2O_5$ in order to demonstrate that the parameters obtained are very dependent on the method chosen.

4.2.1 Method 1

A simple approach is to consider the nucleation curve as being divided into two parts. In the temperature range lower than the temperature T_{max} corresponding to the maximum nucleation rate

$$I = A \exp -\left(\frac{\Delta G_D}{kT}\right) \qquad (4.6)$$

and in the temperature range higher than that

$$I = A \exp\left(-\frac{W^*}{k\Phi}\right) \qquad (4.7)$$

Thus from Arrhenius plots of equations (4.6) and (4.7) ΔH_D, ΔS_D, $\bar{\sigma}$,

and A may be estimated. This method has been used by several workers, namely Ito et al[24], Rogers and Williamson[56], Burnett and Douglas[20], and Strnad and Douglas[26]. It is particularly useful when the thermodynamic data is unavailable, since ΔH_D can still be simply estimated. Unfortunately, equations (4.6) and (4.7) are probably based on incorrect assumptions viz.

$$\text{for } T > T_{max},\ W^* >> \Delta G_D$$

$$T < T_{max},\ \Delta G_D >> W^*$$

Implicit in these assumptions is that the hump-shaped nucleation curve results from a combination of two factors, one of which is dominant for $T > T_{max}$ i.e. W^*, the other being dominant for $T < T_{max}$ i.e. ΔG_D. Thus according to MacMillan[15]:- "For small degress of supercooling, W^* is large since the value of the volume free energy ΔG_v is very small and consequently the nucleation rate is low. With further supercooling ΔG_v increases markedly until W^* becomes comparable in magnitude with ΔG_D; under these conditions the maximum nucleation rate is achieved. The nucleation rate diminishes with further supercooling when W^* becomes negligible in comparison with ΔG_D." This reasoning overstates the role of ΔG_D, since if ΔG_D were zero, a hump-shaped nucleation curve would still be observed, with a maximum at $\frac{T_m}{3}$, where T_m is the melting point.

The effect of the diffusion term in the nucleation equation (i.e. a non zero ΔG_D) is to raise the temperature T_{max} and to cause an overall decrease in the observed nucleation rates. ΔG_D can be expressed in terms of the value of W^*_{max}, the value of W^* at T_{max}.

From equation (1.28)

$$\frac{d\ln I}{dT} = \frac{1}{I}\frac{dI}{dT} = -\left[\frac{kT\left(\frac{d\Delta G_D}{dT} + \frac{dW^*}{dT}\right) - k(\Delta G_D + W^*)}{k^2T^2}\right] \qquad (4.8)$$

ignoring the slight temperature dependence of A. Thus at $T = T_{max}$, expressing ΔG_D as $(\Delta H_D - T\Delta S_D)$, we obtain

$$\Delta G_D = T_{max}\left(\frac{dW^*}{dT}\right)_{max} - W^*_{max} - T_{max}\,\Delta S_D \qquad (4.9)$$

since $\frac{dI}{dT} = 0$. ΔH_D and ΔS_D are assumed to be constants.

From equation (1.24)

$$W^* = \frac{k_5\bar{\sigma}^3}{\Delta T^2}\left(\frac{V_m T_m}{\Delta H_f}\right)^2$$

$$\therefore \qquad \frac{dW^*}{dT} = \frac{2k_5\bar{\sigma}^3}{\Delta T^3}\left(\frac{V_m T_m}{\Delta H_f}\right)^2$$

$$= \frac{2W^*}{\Delta T} \qquad (4.10)$$

where ΔT is the supercooling below the melting point T_m. Thus equation (4.9) becomes

$$\Delta G_D = \frac{2T_{max}W^*_{max}}{T_m - T_{max}} - W^*_{max} - T_{max}\,\Delta S_D$$

and since $\Delta H_D = \Delta G_D + T\Delta S_D$ we obtain

$$\left(\frac{\Delta H_D}{W^*}\right)_{max} = \frac{3T_r - 1}{1 - T_r} \tag{4.11}$$

where $T_r = \frac{T_{max}}{T_m}$, the reduced maximum nucleation temperature.

Table 4.1 gives several values of $\left(\frac{\Delta H_D}{W^*}\right)$ vs. T_r. This clearly shows that at the maximum nucleation temperature W* may or may not be comparable with ΔH_D (or with ΔG_D).

Let us assume that $\left(\frac{\Delta H_D}{W^*}\right)_{max} = 1$, i.e. $T_m = 2T_{max}$. In the vicinity of W^*_{max}

$$W^* = W^*_{max} - (T_{max} - T)\left(\frac{dW^*}{dT}\right)_{max}$$

$$= W^*_{max} - \left(\frac{T_{max} - T}{T_m - T_{max}}\right) 2W^*_{max}$$

$$\therefore \quad W^* = W^*_{max}\left(\frac{T - \Delta T_{max}}{T_{max}}\right) \tag{4.12}$$

where $\Delta T_{max} = T_{max} - T$

$$\therefore \quad W^* = \Delta H_D\left(\frac{T - \Delta T_{max}}{T_{max}}\right) \tag{4.13}$$

Thus if W* is comparable with ΔH_D at T_{max}, then this will be the case for appreciable values of ΔT_{max}, where $T_{max} > T$. In silicate systems observable nucleation rates decrease quite rapidly for $T < T_{max}$ i.e. experimental data for $T < T_{max}$ are for small + ΔT_{max} values.

TABLE 4.1

$\left(\frac{\Delta H_D}{W^*}\right)_{max}$ AS A FUNCTION OF T_r

$\left(\frac{\Delta H_D}{W^*}\right)_{max}$	T_r
0	0.33
1	0.50
2	0.60
5	0.75
10	0.86

Since T_r in these systems is usually between 0.5 and 0.6, i.e. $1 \leq \left(\frac{\Delta H_D^r}{W^*}\right)_{max} \leq 2$, W* cannot be neglected for $T < T_{max}$ over the range where experimental data are available.

In conclusion it may be stated that equations (4.6) and (4.7) are probably incorrect approximations for silicate systems.

4.2.2 Method 2

Perhaps the most obvious plot is that given by

$$kT(\ln A_D - \ln I) \text{ vs. } \frac{k_5}{\Delta G_v^2} \qquad (4.14)$$

which has a gradient $\bar{\sigma}^3$ and an intercept ΔH_D. There are, however, two problems in calculating $\ln A_D$. First, ΔS_D is unknown and secondly A is a function of $\bar{\sigma}$. A good approximation to the value of A is given by[4]

$$A = k_A \bar{\sigma}^{3/2} \qquad (4.15)$$

where k_A is almost constant with temperature and can be calculated from theory. For $Li_2Si_2O_5$, A is between 6.5×10^{34} and 7.3×10^{35} cm^{-3} sec^{-1} for values of $\bar{\sigma}$ in the range 50 to 250 ergs cm^{-2}. The variation in ln A is therefore about 2.4, which is large when compared with the values of ln I for $Li_2Si_2O_5$. Thus an estimate of A is expected to be unsatisfactory and even ignoring ΔS_D, equation (4.14) cannot be used to calculate $\bar{\sigma}^3$.

However, taking two points on the nucleation curve we can write

$$\frac{T \ln I - T' \ln I'}{T - T'} = \ln A_D - \frac{k_5 \bar{\sigma}^3}{k(T-T')} \left\{ \frac{1}{\Delta G_v^2} - \frac{1}{\Delta G_v'^2} \right\} \qquad (4.16)$$

where I' and $\Delta G_v'$ are the values of I and $\Delta G_v (= \frac{\Delta G}{V_m})$ at the temperature T'. If ΔS_D is zero, $A_D (= A)$ is given by equation (4.15), and for convenience equation (4.16) can then be expressed as

$$f(\bar{\sigma}) = a\bar{\sigma}^3 + b\ln\bar{\sigma} + c = 0 \qquad (4.17)$$

An approximate solution to this equation, using Newton's method is given by

$$\bar{\sigma}_2 = \bar{\sigma}_1 - \frac{f(\bar{\sigma}_1)}{f'(\bar{\sigma}_1)} \qquad (4.18)$$

where $\bar{\sigma}_1$ is the first guessed approximation, $\bar{\sigma}_2$ is a better approximation, and $f'(\bar{\sigma}_1)$ is the first derivative of $f(\bar{\sigma})$ with respect to $\bar{\sigma}$, evaluated at $\bar{\sigma}_1$. By repeatedly using equation (4.18), a value of $\bar{\sigma}$ satisfying equation (4.17) can be obtained. The method is sensitive to errors in the values of T' and $\ln I'$, hence the calculation

should be repeated for various T′ values. ΔG_D can be obtained by substituting back into the nucleation equation. Since we ignored ΔS_D in calculating $\bar{\sigma}$, the values of $\bar{\sigma}$ and ΔG_D will be in error.

A modification of this method is to use equation (4.16) directly, without specifying the values of A and ΔS_D, but assuming that they are both constant with temperature. From a plot of

$$\frac{T \ln I - T' \ln I'}{T-T'} \quad \text{vs.} \quad \frac{1}{T-T'} \left\{ \frac{1}{\Delta G_v^2} - \frac{1}{\Delta G_v'^2} \right\}$$

$\bar{\sigma}$ and $\ln A_D$ may be obtained from the gradient and intercept respectively. All points should lie on the same straight line independent of the (T′, ln I′) values. ΔH_D is then obtained by substituting back into the nucleation equation.

4.2.3 Method 3

In Method 2 the value of I(I′) at a specific value of T(T′) was used as a means of eliminating one of the parameters $\bar{\sigma}$ or ΔH_D. For convenience ΔH_D was eliminated. Method 3, however, utilises the fact that $\frac{d \ln I}{dT}$ is zero at T_{max} in order to eliminate one of the unknowns, $\bar{\sigma}$ or ΔH_D. Thus from equation (4.9)

$$\Delta H_D = T_{max} \left(\frac{dW^*}{dT}\right)_{max} - W^*_{max} \qquad (4.9)$$

Expressing W* in terms of ΔG, we can substitute for ΔH_D in the nucleation equation and obtain

$$\ln I = \ln A_D + \frac{k_5 \bar{\sigma}^3 V_m^2}{kT} \left\{ \frac{1}{\Delta G^2_{max}} + \frac{2T_{max}}{\Delta G^3_{max}} \left(\frac{d\,\Delta G}{dT}\right)_{max} - \frac{1}{\Delta G^2} \right\}$$

$$= \ln A_D + \frac{k_5 \bar{\sigma}^3 V_m^2}{k} \frac{\phi'(T)}{T} \qquad (4.19)$$

Hence from a plot of ln I vs. $\frac{\phi'(T)}{T}$, $\bar{\sigma}$ and ln A_D may be estimated. ΔH_D is then calculated from equation (4.11).

4.2.4 Method 4

This method is basically different from the methods previously discussed in that one of the parameters, specifically ΔG_D, is effectively estimated independently from nucleation measurements.

The diffusion process which occurs in nucleation can be expressed in terms of a diffusion coefficient given by

$$D = D_o \exp\left(-\frac{\Delta G_D}{kT}\right) \qquad (4.20)$$

Substituting back into the nucleation equation, we obtain

$$I = \frac{AD}{D_o} \exp\left(-\frac{W^*}{kT}\right) \qquad (4.21)$$

If diffusion and viscous flow occur by a similar mechanism, we can relate D to the viscosity of the liquid via the Stokes-Einstein equation given by

$$D = \frac{kT}{3\pi\lambda\eta} \qquad \text{(cf 1.56)}$$

Thus equation (4.21) becomes

$$I = \frac{A_\eta T}{\eta} \exp(-\frac{W^*}{kT}) \qquad (4.22)$$

Hence by plotting $\ln(\frac{I\eta}{T})$ vs. $\frac{1}{T\Delta G_v^2}$, we can obtain $\bar{\sigma}$ from the slope and $\ln A_\eta$ from the intercept. A_η is given by

$$A_\eta = \frac{Ak}{3\pi\lambda D_o}$$

and since $D_o \sim \nu_o\lambda^2 \sim \frac{kt}{h}\ \lambda^2$ (ν_o is the 'atomic' vibrational frequency and λ the jump distance - approximately the atomic diameter) we obtain

$$A_\eta \simeq \frac{Ah}{3\pi\lambda^3 T} = \frac{kN_v}{3\pi\lambda^3} \qquad \ldots\ (4.23)$$

Thus it is possible to calculate the value of A within a few orders of magnitude, assuming an average value for T, and λ say 1 - 10 Å.

Method 4 is the only analysis considered which can be used to compare the magnitude of the experimental rates with those predicted by theory. In Methods 1, 2 and 3, ΔS_D is unknown and A cannot be calculated from A_D. The possible disadvantage of Method 4 is that the diffusion process required for nucleation is assumed to be closely related to the process of viscous flow.

4.2.5 A comparison of Methods 1-4 using experimental data for $Li_2Si_2O_5$

One of the most detailed studies of crystal nucleation in silicate systems is that of James[23], who studied the nucleation of lithium disilicate from a glass of almost the same composition. Non-steady state nucleation rates were carefully distinguished from steady state rates and the various factors which affect the accuracy of measured nucleation kinetics were considered. These results were therefore used to compare the various methods which may be employed when analysing nucleation kinetics. The thermodynamic data for $Li_2Si_2O_5$ was readily available from tables[5], thus enabling ΔG to be accurately calculated. As already mentioned, $Li_2Si_2O_5$ melts incongruently but can be considered to have a theoretical congruent melting point at 1034°C. For the present purposes it has been assumed that the critical nuclei are spherical in shape. Thus $\bar{\sigma} = \sigma$ i.e. the surface energy is assumed to be isotropic and $k_5 = \frac{16\pi}{3}$. Also, in order to facilitate the calculations involved in each analysis, ΔG was expressed in terms of an effective heat of fusion

ΔH_x and an effective melting point T_x (see Chapter 1.1). Using these parameters it is possible to express ΔG in terms of an effective supercooling $\Delta T_x (= T_x - T)$ without neglecting the difference in specific heat between the crystalline and liquid phases. Thus over the temperature range where nucleation occurs, ΔG is equal to $\Delta G^{\sim}$ in Table 1.1.

The maximum nucleation rate for $Li_2Si_2O_5$ occurs at 450°C and the reduced maximum nucleation temperature $(\frac{T_{max}}{T_x})$ is therefore 0.52. From equation (4.11) the ratio $(\frac{\Delta H_D}{W^*})_{max}$ is found to be 1.21. From the previous discussion, it is apparent that Method 1 is not applicable in this case. Hence the values of σ and ΔG_D calculated by Ito et al[24] will not be correct.

Method 2 was first tried by calculating k_A from theory and ignoring ΔS_D (see equation (4.17)). Several pairs of points on the nucleation curve were taken and the value of σ was estimated in each case. A consistent value could only be obtained if both T and T′ were greater than T_{max}. Thus for $T, T' \geq T_{max}$, $\sigma = 160 \pm 5$ ergs cm^{-2} whereas, for example, T = 454°C, T′ = 435°C, $\sigma = 95$ ergs cm^{-2}. Assuming $\sigma = 160$ ergs cm^{-2}, ΔG_D was found to be 27 k cal $mole^{-1}$. The average value of ln A over the temperature range where nucleation occurs was 81.8 (A in cm^{-3} sec^{-1}). Figure 4.7 compares the experimental nucleation curve with that calculated using the values of ln A, ΔG_D, and σ given above. For $T \geq T_{max}$ the agreement is reasonable, but for $T < T_{max}$ the theoretical nucleation rates are much greater than those observed by experiment. It should be emphasised that the experimnetal data refer to steady state values. Thus the discrepancy between theory and experiment cannot be attributed to non-steady state behaviour.

Method 2 was then tried without specifying the values of A or ΔS_D. Figure 4.8 shows a plot of

FIG. 4.7. ln I AS A FUNCTION OF TEMPERATURE FOR THE COMPOSITION 100 m/o $Li_2Si_2O_5$.

Curve 1 Calculated (method 2, equation 4·17)

Curve 2 Experimental data acc. ref. 23

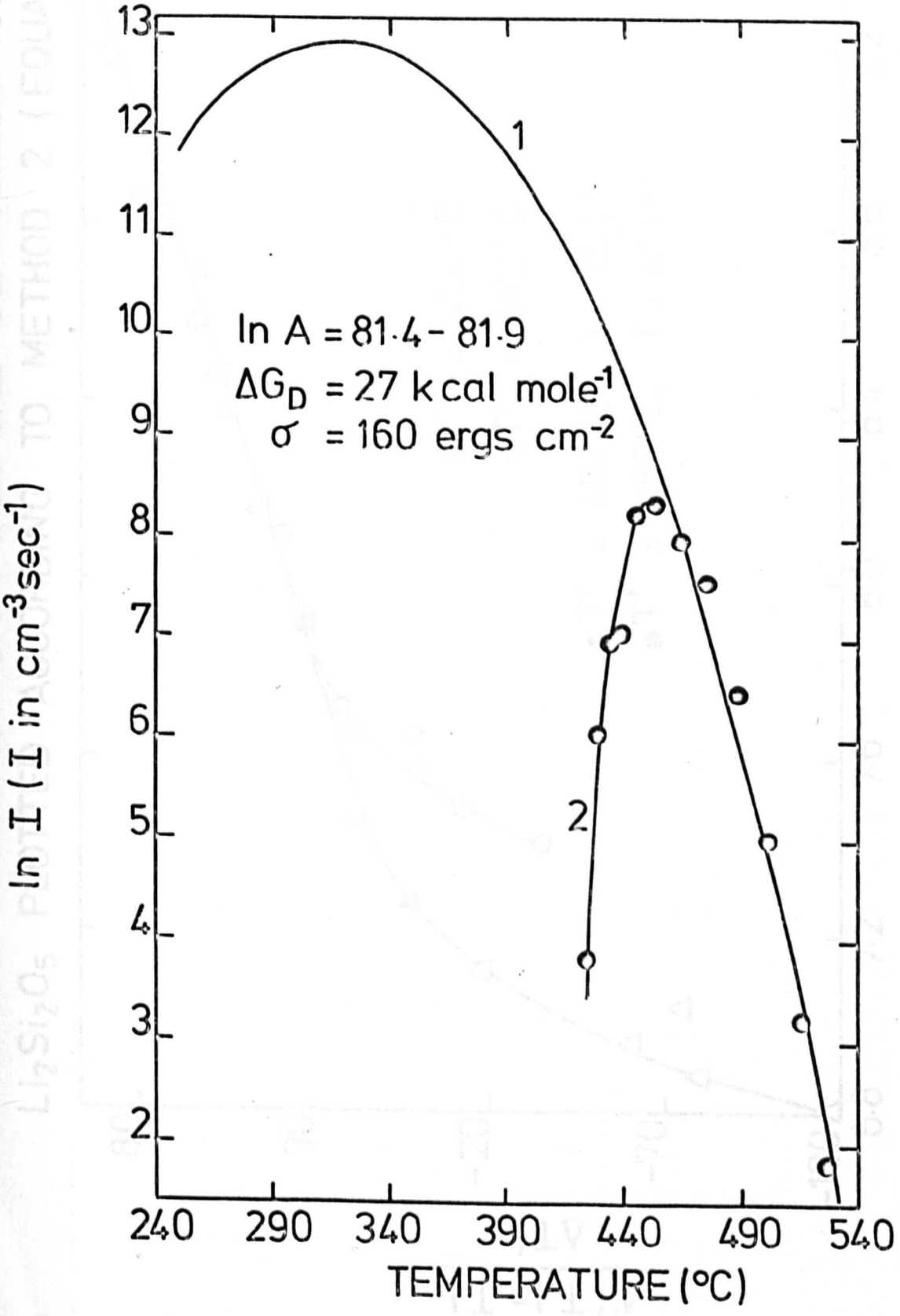

FIG. 4.8. NUCLEATION DATA FOR THE COMPOSITION 100 m/o $Li_2Si_2O_5$ PLOTTED ACCORDING TO METHOD 2 (EQUATION 4·16)

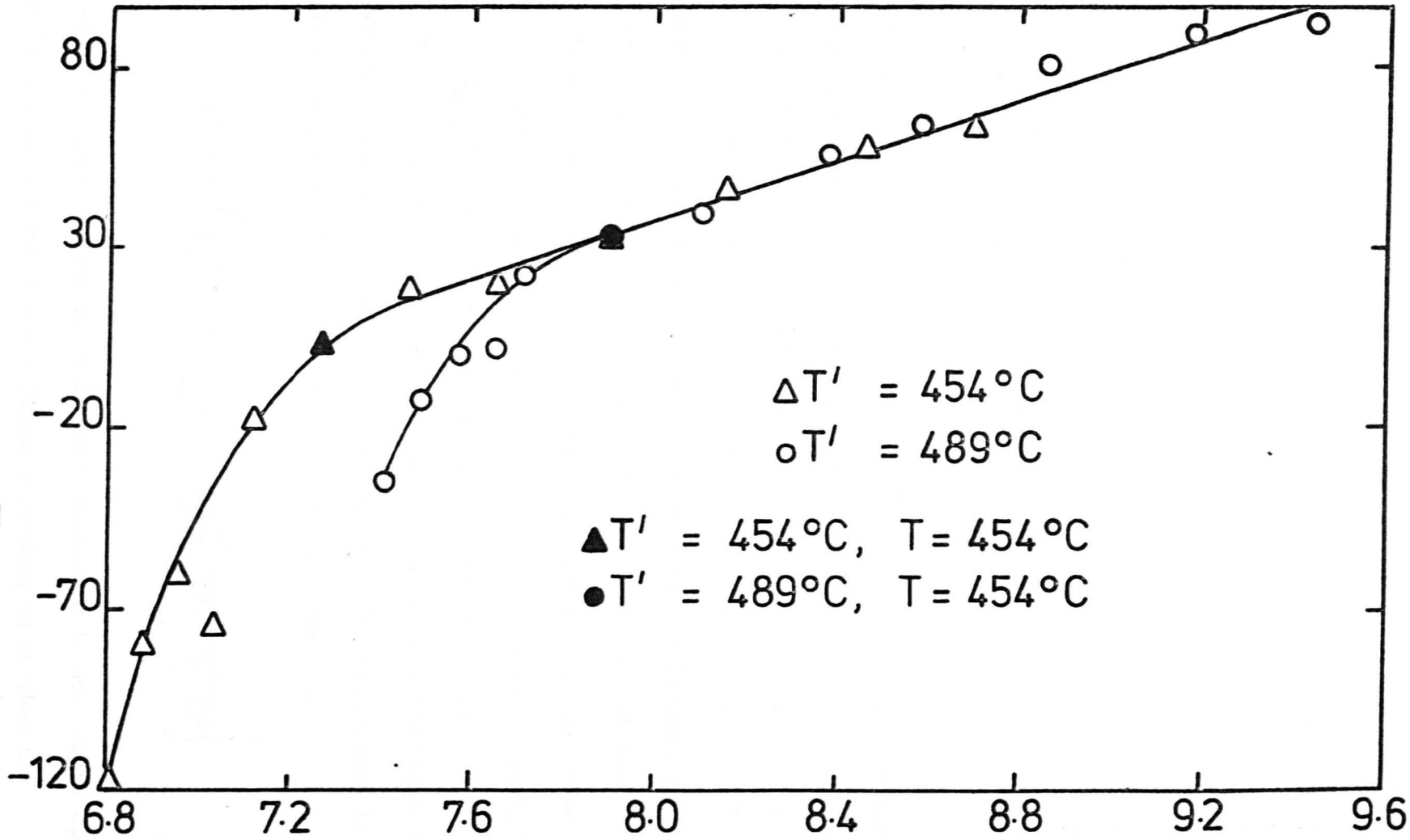

$$\frac{\Delta'(T \ln I)}{\Delta T'} \quad \text{vs.} \quad \frac{\Delta'(\frac{1}{\Delta T_x})^2}{\Delta T'}$$

where $\Delta T' = T - T'$,

$$\Delta'(T \ln I) = T \ln I - T' \ln I'$$

and $$\Delta'(\frac{1}{\Delta T_x})^2 = (\frac{1}{\Delta T_x})^2 - (\frac{1}{\Delta T_x'})^2 .$$

for T' values 454°C and 489°C. For $T > T_{max}$ the results can be fitted to a straight line (see also Figure 4.9). Below T_{max} the two plots diverge. From a straight line through the results for $T > T_{max}$, σ and ln A_D were found to be 222 ergs cm^{-2} and 291 (A_D in cm^{-3} sec^{-1}). respectively. Substituting these values into the nucleation equation, ΔH_D was found to be 215 k cal $mole^{-1}$. Figure 4.10 compares the experimental nucleation curve with that calculated using the values of ln A_D, ΔH_D and σ given above. For $T \geq T_{max}$ the agreement is good, but for $T < T_{max}$ the theoretical nucleation rates are too high.

Figure 4.11 shows the experimental nucleation data plotted according to Method 3, whereby the position of the maximum nucleation rate is utilised (equation (4.19)). $\phi'(T)$ has been expressed as

$$\phi'(T) = \left(\frac{T_x}{\Delta H_x}\right)^2 \left\{ \frac{1}{(T_x - T_{max})^2} - \frac{2T_{max}}{(T_x - T_{max})^3} - \frac{1}{(T_x - T)^2} \right\}$$

in order to allow for the specific heat correction to ΔG. Again the results may be divided into two groups depending on whether the temperature is above or below T_{max}. From the results above T_{max},

FIG. 4.9. NUCLEATION DATA FOR THE COMPOSITION 100 m/o $Li_2Si_2O_5$ PLOTTED ACCORDING TO METHOD 2. (EQUATION 4.16.)

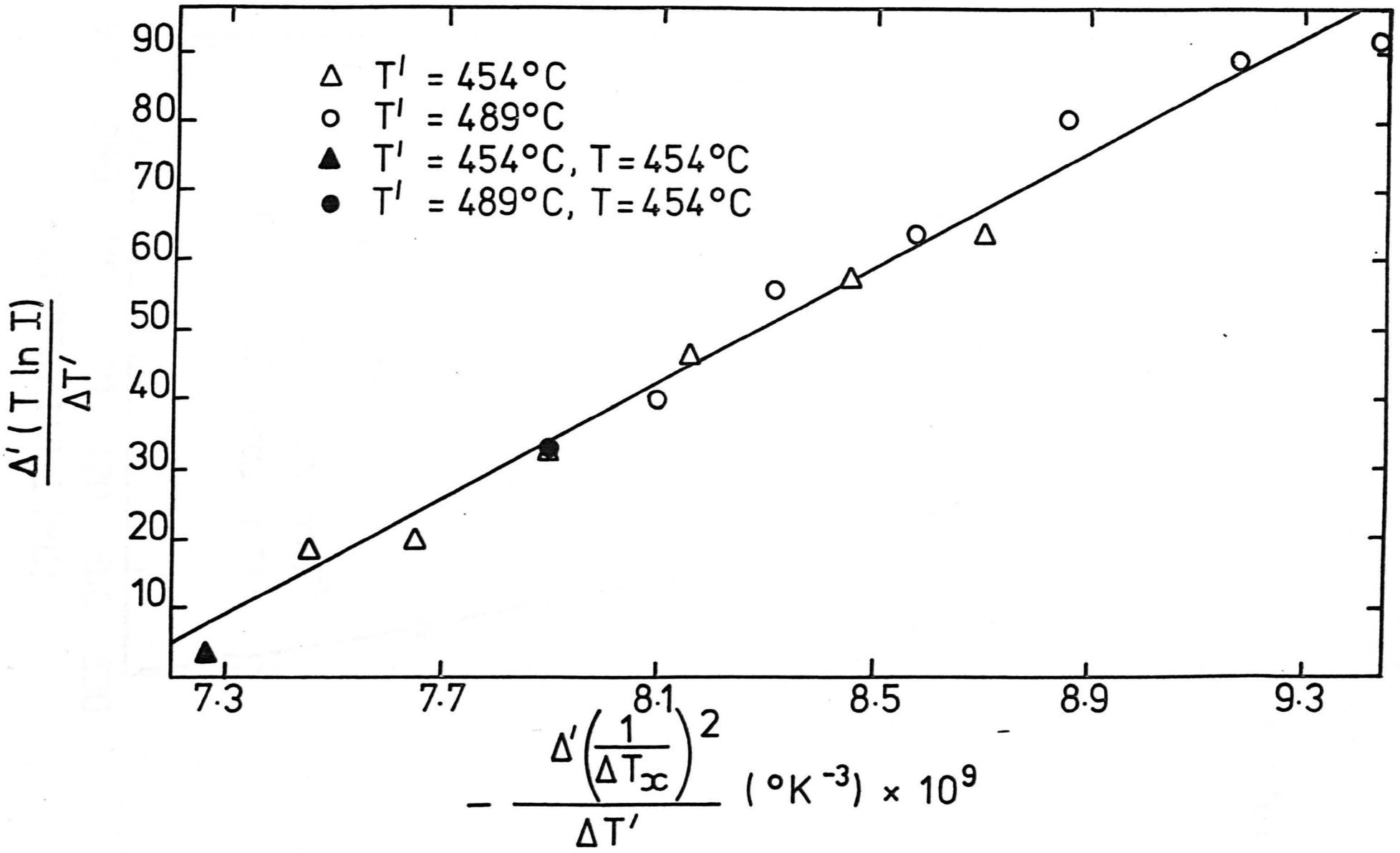

FIG. 4.10. ln I AS A FUNCTION OF TEMPERATURE FOR THE COMPOSITION 100 m/o $Li_2Si_2O_5$:–

curve 1. calculated (method 2, equation 4.16)

curve 2. experimental data acc. ref. 23

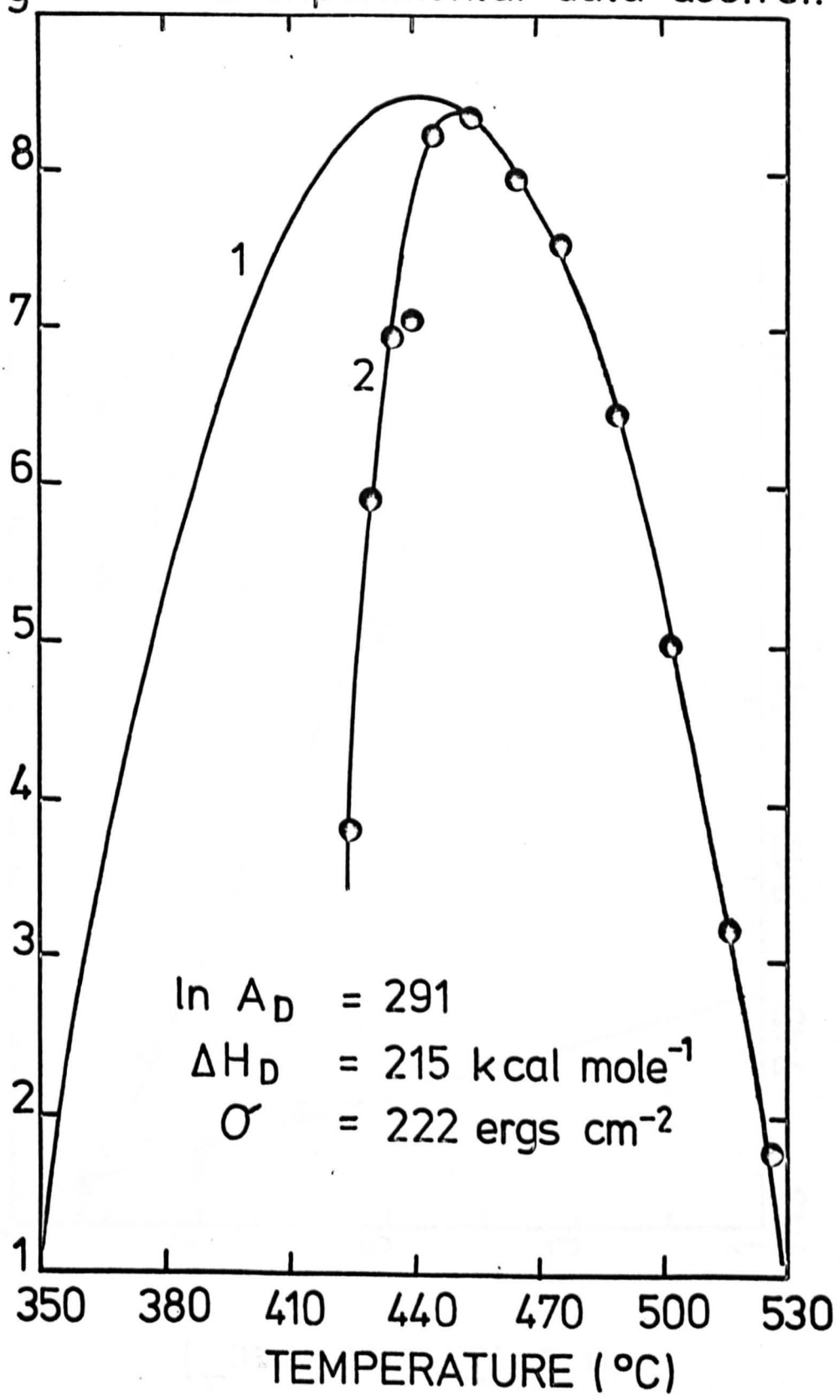

FIG. 4.11. NUCLEATION DATA FOR THE COMPOSITION 100 m/o $Li_2Si_2O_5$ PLOTTED ACCORDING TO METHOD 3 (EQUATION 4·19.)

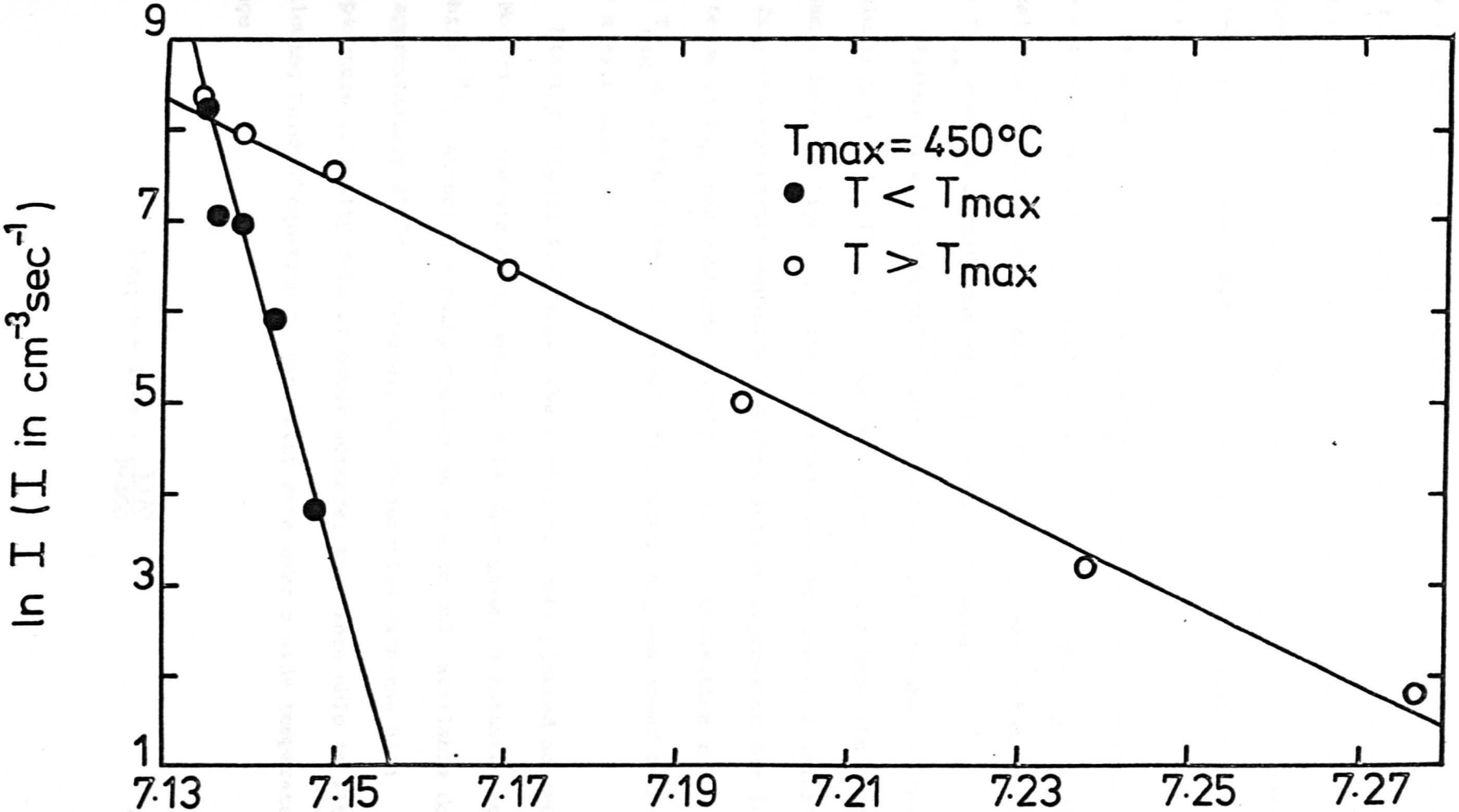

σ = 230 ergs cm^{-2} and ln A_D = 338 (A_D in cm^{-3} sec^{-1}). From equation (4.11) ΔH_D was found to be 260 k cal $mole^{-1}$. Figure 4.12 compares the experimental nucleation curve with that calculated using the values of ln A_D, ΔH_D and σ given above. For $T \gtrsim T_{max}$ the agreement is fair, but at lower temperatures the theoretical nucleation rates are too high.

If we use the results for $T < T_{max}$ in Figure 4.11 we obtain σ = 434 ergs cm^{-2}, ln A_D = 2211 (A_D in cm^{-3} sec^{-1}), and ΔH_D = 1732 k cal $mole^{-1}$. These values are much higher than those obtained for $T > T_{max}$ and are larger than might be reasonably expected.

Filipovich and Kalinina[22] also used Method 3 to analyse their nucleation data for $Li_2Si_2O_5$. However, they did not have the thermodynamic data for $Li_2Si_2O_5$. They overcame this problem by eliminating σ from the nucleation equation and obtaining an expression for ln I in terms of ΔG_D (see equation (1.59)). Only the nucleation rates for $T > T_{max}$ could be fitted to theory, from which ΔH_D was found to be 152 k cals $mole^{-1}$.

Finally, Figure 4.13 shows the nucleation data plotted according to Method 4. The viscosity data used is that given by Matusita and Tashiro[36]. Actual viscosity measurements were only available down to approximately 450°C. However, in conjunction with the high temperature viscosity data of other workers, they were able to fit the following Fulcher equation to viscosity data over a wide temperature range

$$\log_{10}\eta = 1.44 + \frac{3370}{T-460} \qquad (4.24)$$

FIG. 4.12. ln I AS A FUNCTION OF TEMPERATURE FOR THE COMPOSITION 100 m/o $Li_2Si_2O_5$:-
curve 1. calculated (method 3, equation 4·19)
curve 2. experimental data acc. ref. 23.

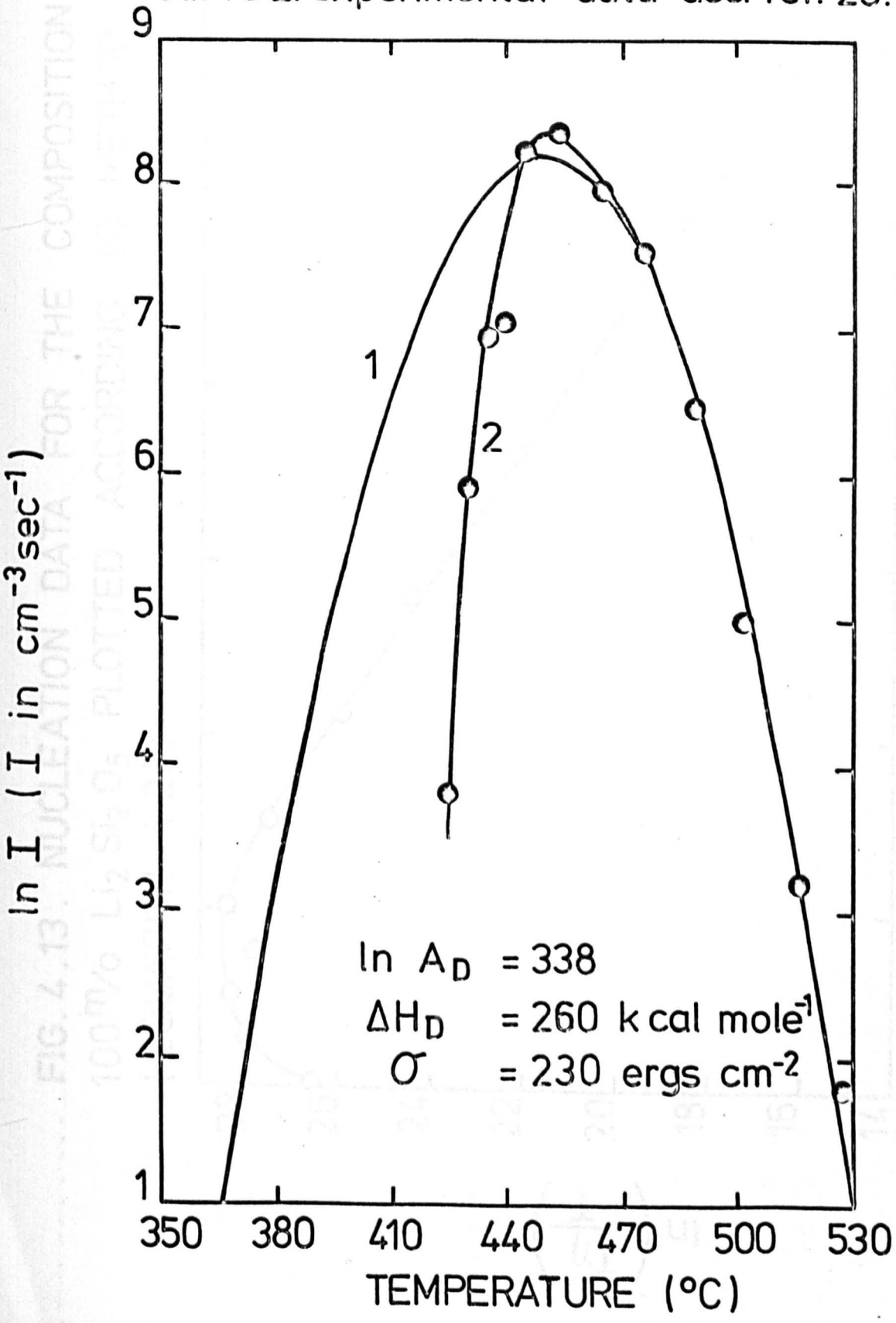

FIG. 4.13. NUCLEATION DATA FOR THE COMPOSITION 100 m/o $Li_2Si_2O_5$ PLOTTED ACCORDING TO METHOD 4. (EQUATION 4·22)

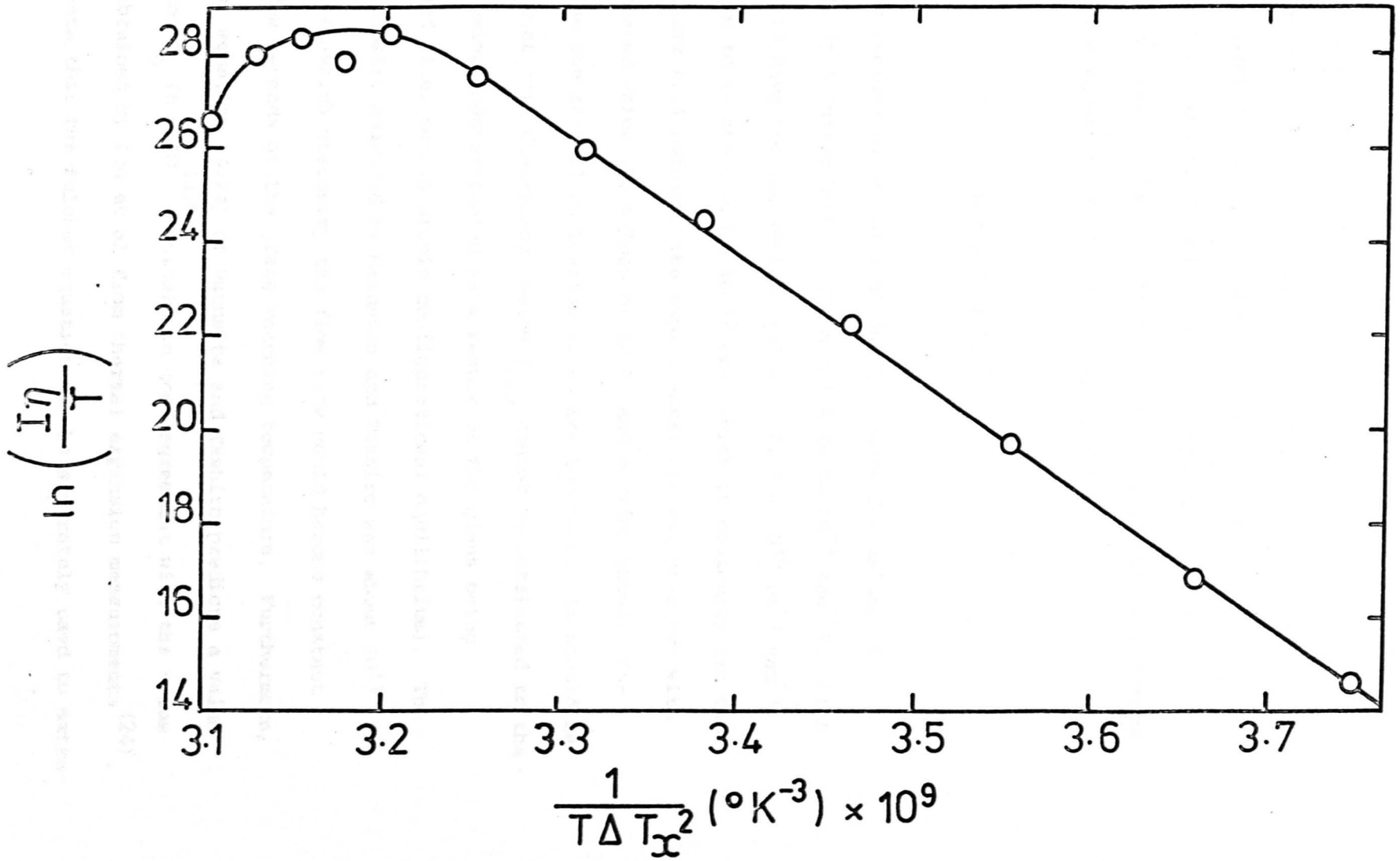

where η is in poise and T is in °K. This equation was used to extrapolate viscosity data down to 425°C, the lowest nucleation temperature considered. From Figure 4.13 it can be seen that Method 4 provides a good fit to the experimental data for $T > T_{max}$. Using only these results we obtain $\sigma = 185$ ergs cm^{-2} and $\ln A_\eta = 113$ (A_η in cm^{-3} sec^{-1} p $°K^{-1}$). It is of interest to obtain the value of ln A. From equation (4.23), substituting for A_η

$$A = 1.22 \times 10^{79} \lambda^3$$

assuming an average value for T of 490°C. Hence for values of λ 1Å ~ 10Å, ln A varies between 127 and 134 (A in cm^{-3} sec^{-1}). If A is assumed to have the theoretical value of 4.53×10^{35} cm^{-3} sec^{-1}, λ would have to be about 3.3×10^{-15} cms, which is obviously far too small. Figure 4.14 compares the experimental nucleation curve with that calculated using the values of ln A_η and σ given above. For $T > T_{max}$ the theoretical nucleation rates are too high. It should be mentioned that this discrepancy below T_{max} cannot be attributed to the viscosity being underestimated as a result of the glass being unstabilised (i.e. not in atomic configurational equilibrium). The highest viscosity measured by Matusita and Tashiro was about 10^{11} poise[36], at which viscosity the flow rate would become constant within a few seconds of the glass reaching temperature. Furthermore, the Fulcher equation (4.24) of Matusita and Tashiro predicts a value of 411°C for T_g ($\eta = 10^{13.6}$ poise), in good agreement with the value of 410°C obtained by Ito et al from thermal expansion measurements[24]. This suggests that the Fulcher equation can be accurately used to extra-

FIG. 4.14. ln I AS A FUNCTION OF TEMPERATURE FOR THE COMPOSITION 100m% $Li_2Si_2O_5$:-
curve 1. calculated (method 4, equation 4·22)
curve 2. experimental data acc. ref. 23.

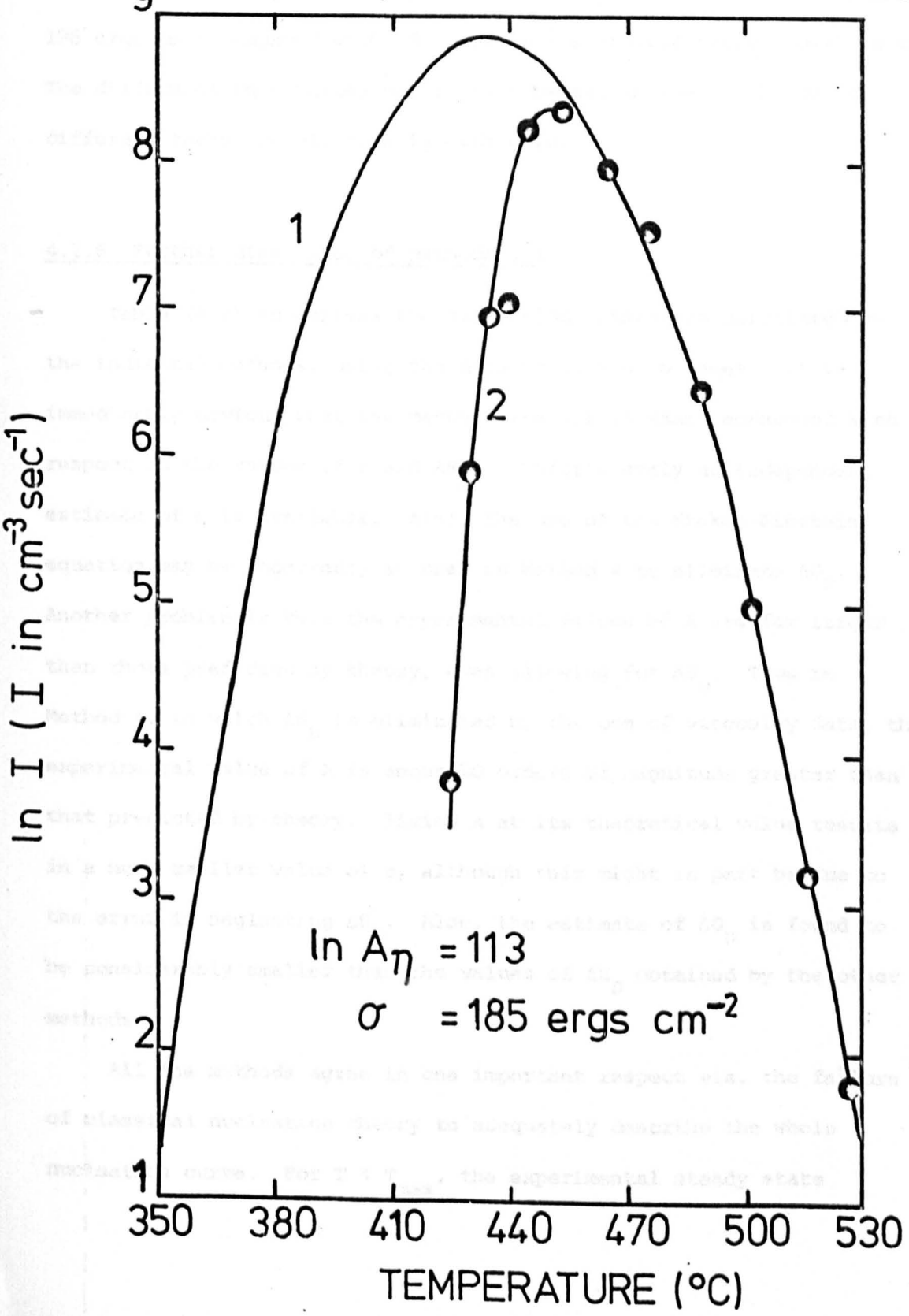

polate viscosity data to temperatures below 450°C.

Matusita and Tashiro also used Method 4 to analyse their nucleation kinetics for $Li_2Si_2O_5$ [25]. They obtained a good fit to their data, although they only covered $T > T_{max}$. σ was found to be 196 ergs cm^{-2} compared with 185 ergs cm^{-2} estimated using James' data. The difference in σ values may in part be attributed to the use of different thermodynamic data in each case.

4.2.6 Further discussion of Methods 1-4

Table (4.2) summarises the nucleation parameters calculated by the indicated methods, using the data according to James. It is immediately obvious that the methods are not in exact agreement with respect to the values of σ and ΔH_D. Unfortunately no independent estimate of σ is available. Also, the use of the Stokes-Einstein equation may be incorrect, as used in Method 4 to eliminate ΔG_D. Another problem is that the experimental values of A are far larger than those predicted by theory, even allowing for ΔS_D. Thus in Method 4, in which ΔS_D is eliminated by the use of viscosity data, the experimental value of A is about 20 orders of magnitude greater than that predicted by theory. Fixing A at its theoretical value results in a much smaller value of σ, although this might in part be due to the error in neglecting ΔS_D. Also, the estimate of ΔG_D is found to be considerably smaller than the values of ΔH_D obtained by the other methods.

All the methods agree in one important respect viz. the failure of classical nucleation theory to adequately describe the whole nucleation curve. For $T < T_{max}$, the experimental steady state

TABLE 4.2

THE NUCLEATION PARAMETERS OBTAINED FOR $Li_2Si_2O_5$ USING METHODS 1-4

Method of Analysis	ln A or ln A_D (A or A_D in cm^{-3} sec^{-1})	ΔH_D (or ΔG_D) k cal $mole^{-1}$	σ ergs cm^{-2}
2(a)	81.4 - 81.9	27 (ΔG_D)	160 ±5
2(b)	291 ±15	215	222 ±7
3	338 ±12	260	230 ±6
4	127 - 134 (±3)	-	186 ±2

Notes:-

(i) Method 2(a) A calculated from theory. $A = k_A \sigma^{3/2}$.

Method 2(b) A_D obtained by experiment

Method 3 A_D obtained by experiment

Method 4 A_η obtained by experiment

$$A = \frac{3\pi\lambda^3 T}{h} A_\eta \ , \ \lambda = 1 - 10 \ \text{Å} \ , \ \Delta G_D = \Delta G_\eta$$

(ii) σ calculated assuming $k_5 = \frac{16\pi}{3}$

(iii) 95% confidence limits quoted for ln A_D and σ.

ΔH_D (or ΔG_D) calculated assuming mean values for ln A_D and σ.

nucleation rates are lower than would be predicted from the rates for $T > T_{max}$. Again it should be emphasised that this is not due to transitory or non-steady state effects. There are two possible explanations. The first is that σ increases as the temperature decreases below T_{max}. Alternatively, or in addition to the first possibility, ΔG_D is not linear with T, as in equation (4.4), with ΔH_D and ΔS_D constants independent of temperature, but increases much more rapidly with fall in temperature. Unfortunately, the physical significance of the nucleation equation would be lost if we introduced further disposable parameters for which there are no experimental values.

Method 4, in which viscosity data is used, intrinsically allows for the temperature variation of ΔG_D. Viscosity data is often expressed as an Arrhenius equation

$$\eta = \eta_o \exp\left(\frac{\Delta G_\eta}{RT}\right) \qquad (4.25)$$

where $\Delta G_\eta = \Delta H_\eta - T\Delta S_\eta$, the activation free energy for viscous flow, and η_o is a constant. From the Stokes-Einstein equation, $\Delta G_\eta = \Delta G_D$. For many glassforming systems, equation (4.25) is only true if ΔG_η increases rapidly at a non linear rate with decreasing temperature such that either one or both of the parameters ΔH_η and ΔS_η cannot be considered as constants. However, values of ΔH_η and $\eta_o \exp\left(-\frac{\Delta S_\eta}{R}\right)$ are often quoted for a given temperature range. Thus for $Li_2Si_2O_5$ glass between 450 and 550°C, ΔH_η = 109 k cal $mole^{-1}$ and $\eta_o \exp\left(-\frac{\Delta S_\eta}{R}\right)$ = 2.1 x 10^{-22} poise[57]. The value of η_o according to the Eyring theory is about 10^{-6} poise[58], hence ΔS_η should be about 72 cal $mole^{-1}$ K^{-1}. Expressing the viscosity data in this way, there is a

tendency to forget that ΔH_η and ΔS_η may both be functions of temperature. Comparing equation (4.24) with (4.25)

$$\eta_o = 10^{-1.44}$$

$$\Delta G_\eta = 2.303R\left(\frac{3370T}{T-460}\right)$$

and since

$$\Delta H_\eta = \left[\frac{\partial\left(\frac{\Delta G_\eta}{T}\right)}{\partial\frac{1}{T}}\right]_p \qquad \Delta S_\eta = -\left[\frac{\partial \Delta G_\eta}{\partial T}\right]_p$$

we obtain

$$\Delta H_\eta = 2.303R \times 3370 \left(\frac{T}{T-460}\right)^2$$

$$\Delta S_\eta = 2.303R \times 3370 \left\{\frac{460}{(T-460)^2}\right\}$$

The experimental value of η_o derived from the Fulcher equation is in reasonable agreement with the theoretical value of 10^{-6} poise. At 500°C ΔG_η ΔH_η and ΔS_η have values of 38.1 k cal mole^{-1}, 94.1 k cal mole^{-1} and 72.4 cal mole^{-1} k^{-1} respectively, compared with the average value of ΔH_η of 109 k cal obtained from the Arrhenius plot, assuming ΔH_η and ΔS_η to be constants. Thus ΔG_η is much smaller than ΔH_η. It is interesting to note that when Method 2 was used to

analyse the nucleation data, whereby the value of A was calculated from theory, the estimate of ΔG_D was considerably smaller than the values of ΔH_D obtained by the other methods.

The temperature dependence of ΔG_η can be expressed indirectly in terms of viscosity. Rearranging equation (4.24)

$$\ln \eta = - 3.316 + \frac{1}{T} (9.287 \times 10^3 + 460 \ln \eta)$$

By comparison with equation (4.24)

$$\eta_o = 10^{-1.44}$$

$$\Delta G_\eta = 9.287 \times 10^3 + 460 \ln \eta \qquad (4.26)$$

Since the viscosity rises rapidly as T_g is approached which for $Li_2Si_2O_5$ glass is about 410°C, equation (4.26) predicts a rapid rise in $\Delta G_\eta (= \Delta G_D)$ as the temperature falls.

Filipovich and Kalinina[22] suggested that a rapid rise in ΔG_η was sufficient to explain the rapid fall off in steady state nucleation rates below T_{max}. However, as Method 4 showed, there is still an unexplainable discrepancy between theory and experiment at lower temperatures. It should be mentioned that Filipovich and Kalinina came to their conclusion by assuming that T_g was 450°C i.e. $T_g = T_{max}$. They measured T_g by D.T.A. However, for $Li_2Si_2O_5$ the endothermic dip which is commonly associated with T_g, or $\eta = 10^{13.6}$ poise,

actually occurs at a temperature where the viscosity is about $10^{11.0}$ poise. Thus they overestimated the rate of change of ΔG_η in the vicinity of T_{max}. Also, their longest heat treatment time was 48 hrs. Since at 430°C the nucleation induction time is about 36 hrs the results of Filipovich and Kalinina below 440°C are not the steady state values.

It should be stressed that the physical significance of a non-linear temperature dependent ΔG_D or ΔG_η is uncertain. In the case of viscosity it has been suggested that non-Arrhenius behaviour may be explained if the free volume of the liquid is considered in addition to the activation energy for viscous flow[58].

There are several points which have not been discussed so far. First, the nucleation results for $Li_2Si_2O_5$ have been analysed in terms of homogeneous nucleation theory. However, the nucleation of $Li_2Si_2O_5$ may involve a heterogeneous mechanism. It is of interest to consider whether this accounts for the large pre-exponential factor obtained assuming homogeneous nucleation theory. A comparison of equations (1.28) and (1.29) with (1.42) shows that the pre-exponential factors are approximately in the ratio $N_v : {}^vN_s$ for homogeneous and heterogeneous nucleation respectively, where N_v is the number of 'molecules' or 'formula units' of the nucleating component and ${}^vN_s$ is the number of surface substrate 'atoms', both per unit volume of the liquid. ${}^vN_s$ will obviously depend on the volume fraction of substrate particles (the substrate will generally be dispersed throughout the liquid) and their size. However, unless we consider unrealistically large volume fractions of very small substrate particles, $N_v >> {}^vN_s$. Therefore the pre-exponential factor for homogeneous

nucleation will be greater than that for heterogeneous nucleation. Hence the occurrence of heterogeneous nucleation would lead to a greater discrepancy between theory and experiment with regard to the magnitude of the pre-exponential factor.

Secondly it has been suggested, as discussed in the next chapter, that larger values of the pre-exponential factor may be possible than would be expected from classical theory. This is because classical theory neglects rotational and translational energies when considering the thermodynamic properties of small clusters of atoms or molecules.

Finally, it has been assumed that critical nuclei are spherical and therefore that σ is isotropic i.e. $\bar{\sigma} = \sigma$. The temperature dependence of σ can then be described by just one equation (e.g. equation (4.3)). However, as discussed in the next chapter, σ is generally not isotropic and critical nuclei are not necessarily spherical. Thus in the early stages of nucleation and crystal growth of $Li_2Si_2O_5$, it has been found that the internally nucleated crystals consist of small faceted single crystal plates parallel to (010) planes and elongated along [001] [59]. In general there will be 'i' equations of the type equation (4.3) for a crystal exhibiting 'i' faces. Hence the temperature dependence of $\bar{\sigma}$ will be a complex function of the temperature variation of each σ_i. It is also important to emphasise that unless the shape of the critical nucleus is known, we are only able to estimate the value of $\sqrt[3]{k_5}\ \bar{\sigma}$ from nucleation kinetics.

In conclusion we have considered several methods of analysing steady state nucleation data. Method 1 is almost certainly incorrect for silicate systems. The other three methods which may be used do

not yield exactly the same values for the nucleation parameters and none of them are able to describe the whole nucleation curve. No independent estimates of the nucleation parameters are available, hence the choice of method is optional. However, viscosity data as required in Method 4 is seldom available and hence Methods 2 and 3 are of more general use. Since T_{max} appears to be the temperature below which the nucleation parameters may not be treated as constants, the use of T_{max} to define the ratio $\Delta H_D/\sigma^3$, as in Method 3, is perhaps unsatisfactory. Hence it is suggested that Method 2 should be used, preferably without specifying the value of A. This avoids any error due to the neglect of ΔS_D. It is shown in Chapter 5 that this method does give a value of σ in close agreement with that predicted from a semi-quantitative model of the solid-liquid interface.

4.3 Analysis of nucleation data for the composition 100 $^m/_o$ $BaSi_2O_5$, 25:75, 50N:50 and 90:10

Composition 100 $^m/_o$ $BaSi_2O_5$

The maximum nucleation rate for this composition occurs at 700°C (see Figure 3.4). Hence T′ values of 700, 740 and 780°C were used in order to analyse the nucleation data according to Method 2, equation (4.16). This is shown in Figure 4.15. The thermodynamic driving force was calculated according to equation (1.8), using the value of ΔH_f estimated in section 4.1. Assuming $k_5 = \frac{16\pi}{3}$, σ and $\ln A_D$ were found to be 132 ergs cm^{-2} and 172 (A_D in cm^{-3} sec^{-1}) respectively. Substituting these values into the nucleation equation a value of 177 k cal $mole^{-1}$ is obtained for ΔH_D.

Figure 4.16 compares the calculated nucleation curve, based on the parameters given above, with the nucleation curve obtained by experiment. As expected, there is good agreement between the calculated

FIG. 4.15. NUCLEATION DATA FOR THE COMPOSITION 100 m/o $BaSi_2O_5$ PLOTTED ACCORDING TO METHOD 2. (EQUATION 4.16)

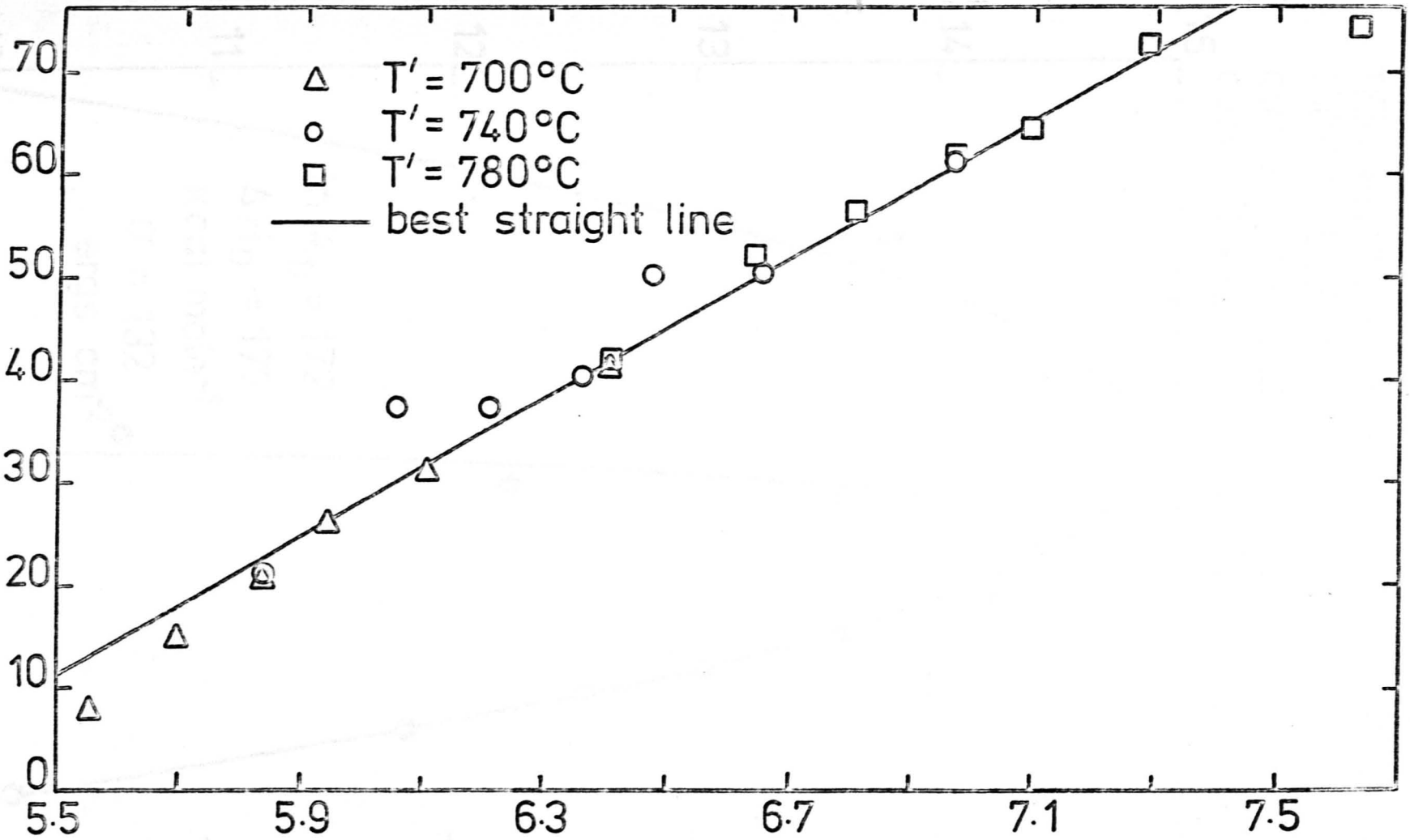

FIG. 4.16. ln I AS A FUNCTION OF TEMPERATURE FOR THE COMPOSITION 100 m/o $BaSi_2O_5$:-
curve 1. calculated (method 2, equation 4.16)
curve 2. experimental data acc. present study.

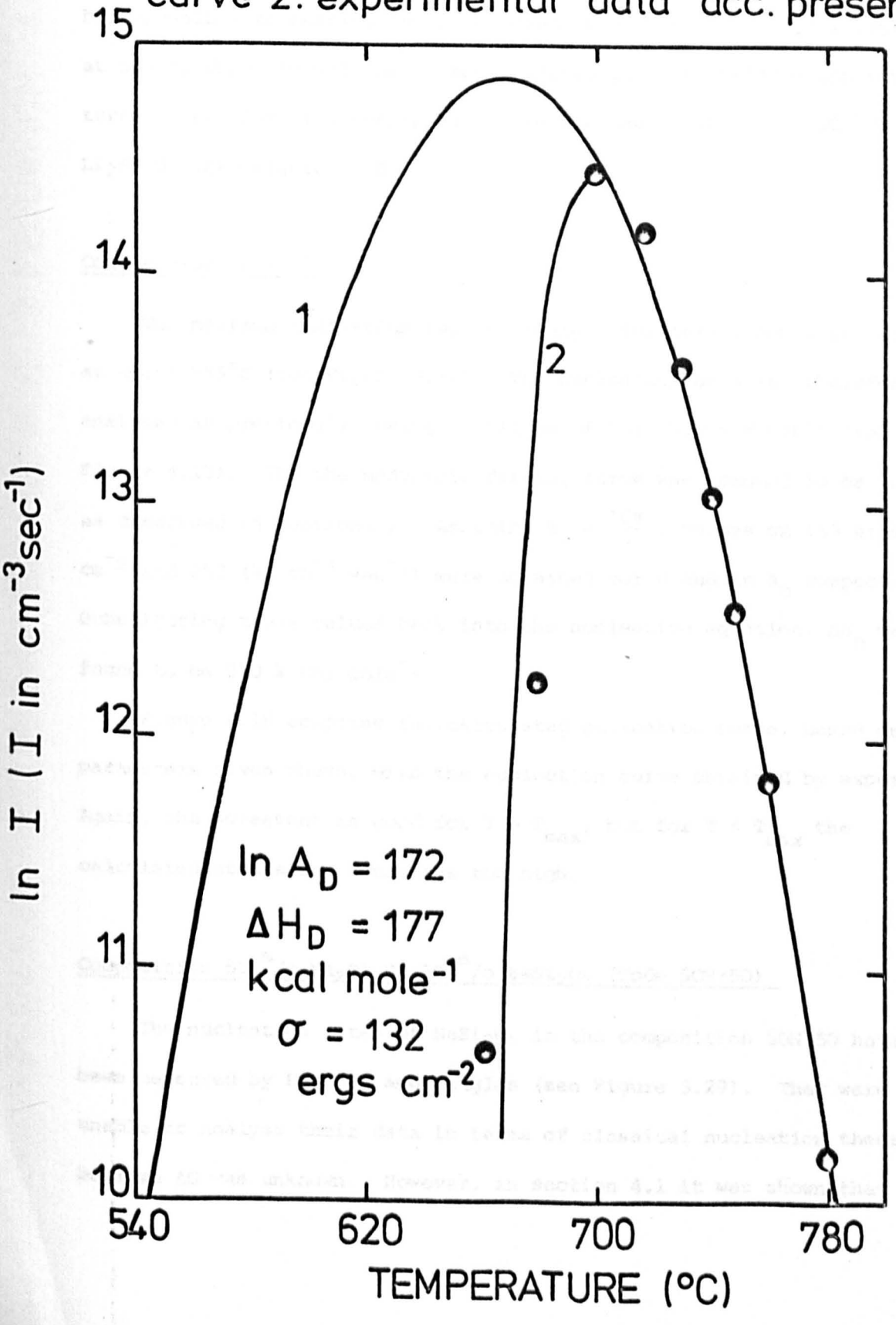

and experimentally determined curves for $T \geq T_{max}$, but at lower temperatures the calculated nucleation rates are far too large. Even allowing for possible error in the values of I for $T < T_{max}$, it would be impossible to observe the large predicted value of I, for example, at 550°C, which is well below the expected glass transformation temperature. A similar discrepancy was found for the composition 100 $^{m}/_{o}$ $Li_2Si_2O_5$ (see Figure 4.10).

Composition 25 : 75

The maximum nucleation rate of $BaSi_2O_5$ for this composition occurs at about 555°C (see Figure 3.18). The nucleation data was therefore analysed as previously, using T′ values of 561, 590 and 626°C (see Figure 4.17). The thermodynamic driving force was assumed to be ideal, as discussed in section4.1. Assuming $k_5 = \frac{16\pi}{3}$, values of 153 ergs cm^{-2} and 253 (A_D cm^{-3} sec^{-1}) were obtained for σ and ln A_D respectively. Substituting these values back into the nucleation equation, ΔH_D was found to be 210 k cal $mole^{-1}$.

Figure 4.18 compares the calculated nucleation curve, based on the parameters given above, with the nucleation curve obtained by experiment. Again, the agreement is good for $T \geq T_{max}$, but for $T < T_{max}$ the calculated nucleation rates are too high.

Composition 50 $^{m}/_{o}$ $Na_2Si_2O_5$ 50 $^{m}/_{o}$ $BaSi_2O_5$ (Code 50N:50)

The nucleation rates of $BaSi_2O_5$ in the composition 50N:50 have been measured by Burnett and Douglas (see Figure 3.29). They were unable to analyse their data in terms of classical nucleation theory because ΔG was unknown. However, in section 4.1 it was shown that ΔG

FIG. 4.17. NUCLEATION DATA FOR THE COMPOSITION 25 : 75 PLOTTED ACCORDING TO METHOD 2 (EQUATION 4·16)

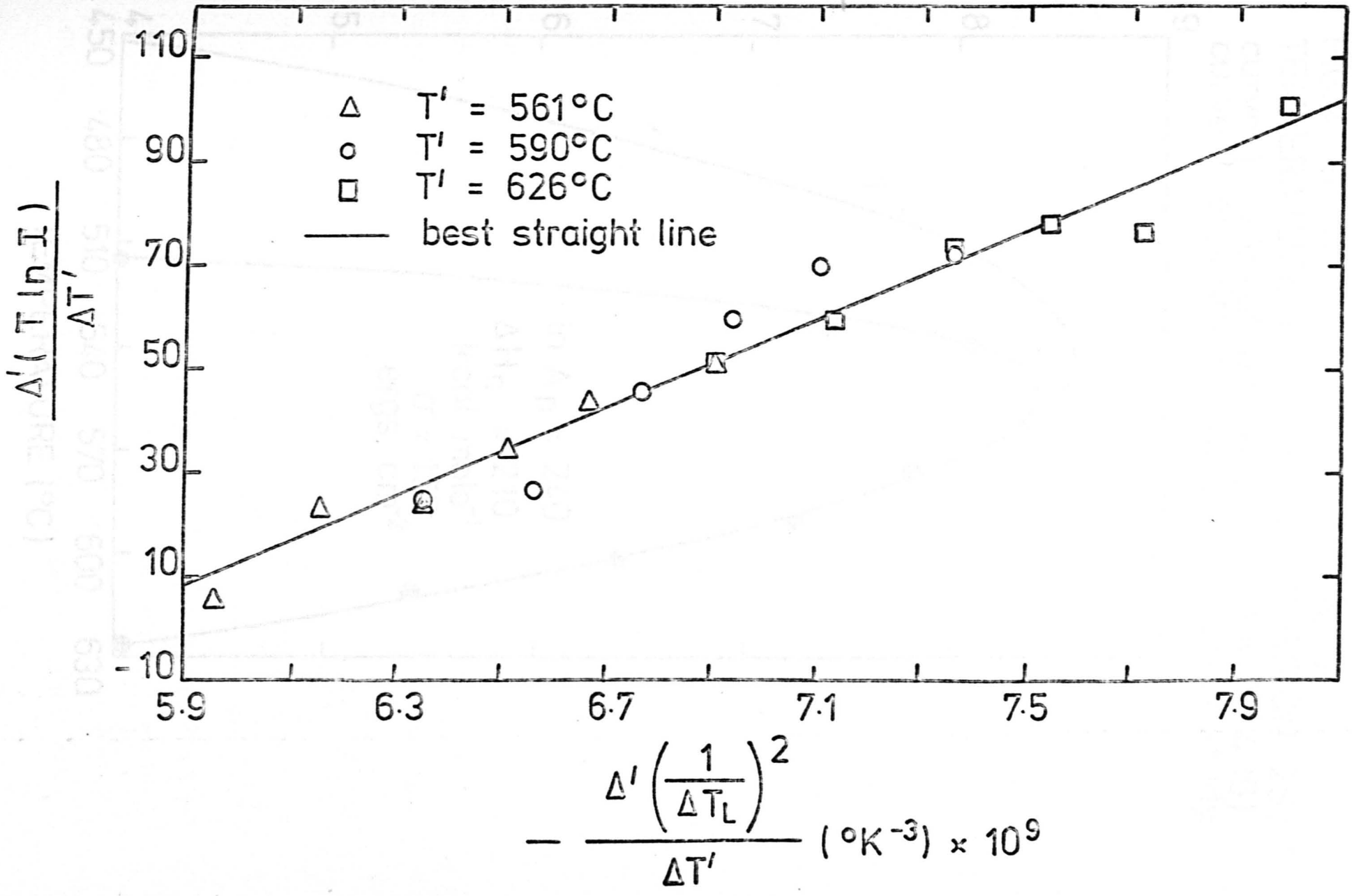

FIG. 4.18. ln I AS A FUNCTION OF TEMPERATURE FOR THE COMPOSITION 25:75.
curve 1. calculated (method 2, equation 4.16)
curve 2. experimental data acc. present study.

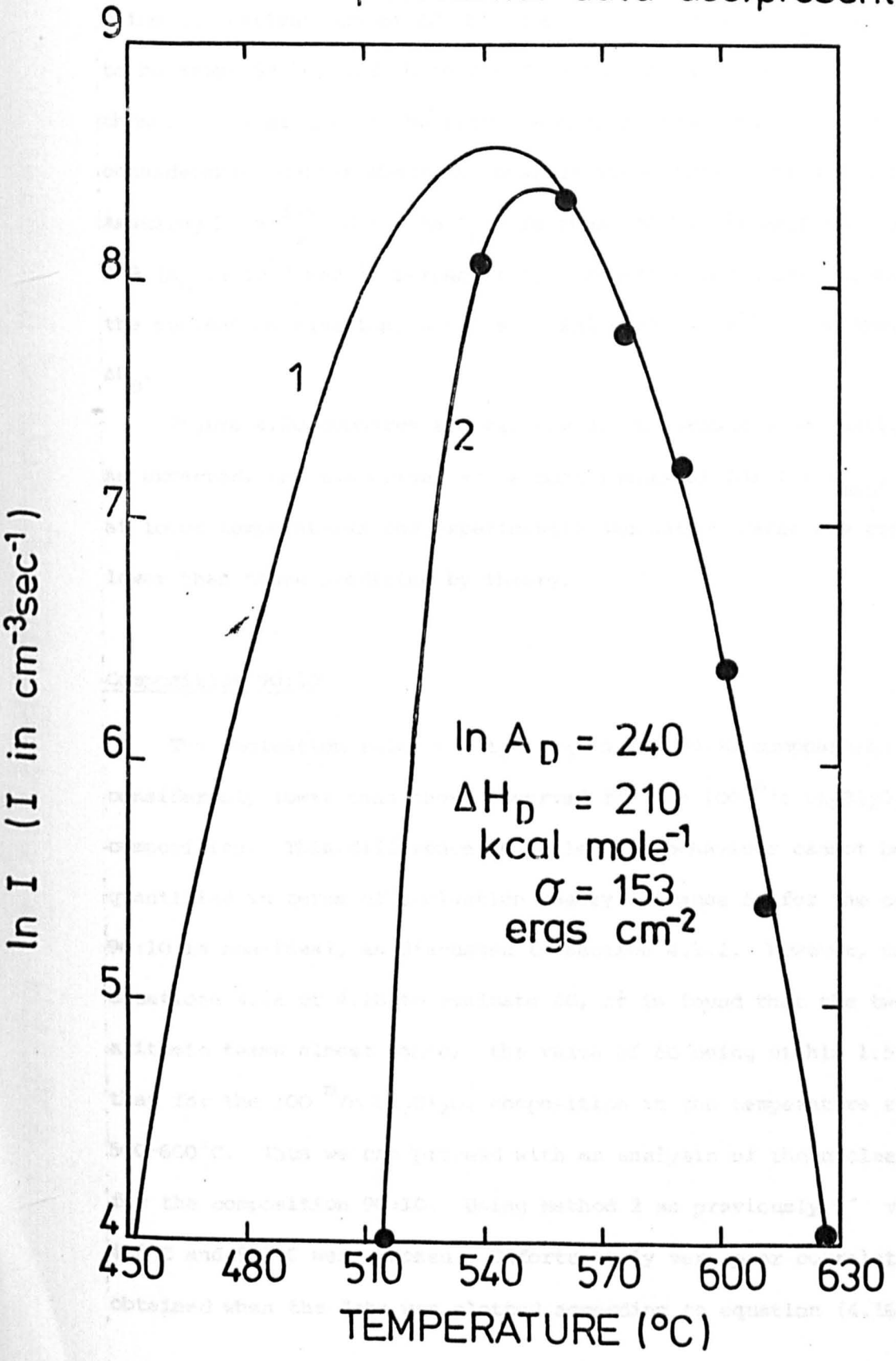

could be estimated from available liquidus data. Figure 4.19 shows the data of Burnett and Douglas plotted as for the previous compositions, using the estimations of ΔG obtained in this study. T_{max} was assumed to be about 535°C, and therefore T' values of 535, 560 and 600°C were chosen. Compared with the previous compositions analysed, there is considerable scatter about the best straight line in Figure 4.19. Assuming $k_5 = \frac{16\pi}{3}$, σ and $\ln A_D$ were found to be 126 ergs cm^{-2} and 238 (A_D in cm^{-3} sec^{-1}) respectively. Substituting these values into the nucleation equation, a value of 233 k cal $mole^{-1}$ is obtained for ΔH_D.

Figure 4.20 compares the calculated and measured nucleation curves. As expected, the two curves are almost identical for $T > T_{max}$, but at lower temperatures the experimental nucleation rates are considerably lower than those predicted by theory.

Composition 90:10

The nucleation rates of $Li_2Si_2O_5$ in the 90:10 composition are considerably lower than those observed for the 100 $^m/_o$ $Li_2Si_2O_5$ composition. This difference in nucleation behaviour cannot be simply quantified in terms of nucleation theory, because ΔG for the composition 90:10 is non-ideal, as discussed in section 4.1.2. However, using equations 4.2a or 4.2b to evaluate ΔG, it is found that the two logarithmic terms almost cancel, the value of ΔG being within 1.5% of that for the 100 $^m/_o$ $Li_2Si_2O_5$ composition in the temperature range 500-600°C. Thus we can proceed with an analysis of the nucleation rates for the composition 90:10. Using Method 2 as previously T' values of 486°C and 552°C were chosen. Unfortunately very poor correlation was obtained when the data was plotted according to equation (4.16), due

FIG. 4.19. NUCLEATION DATA FOR THE COMPOSITION 50N:50 (AFTER REF. 20) PLOTTED ACCORDING TO METHOD 2 (EQUATION 4.16)

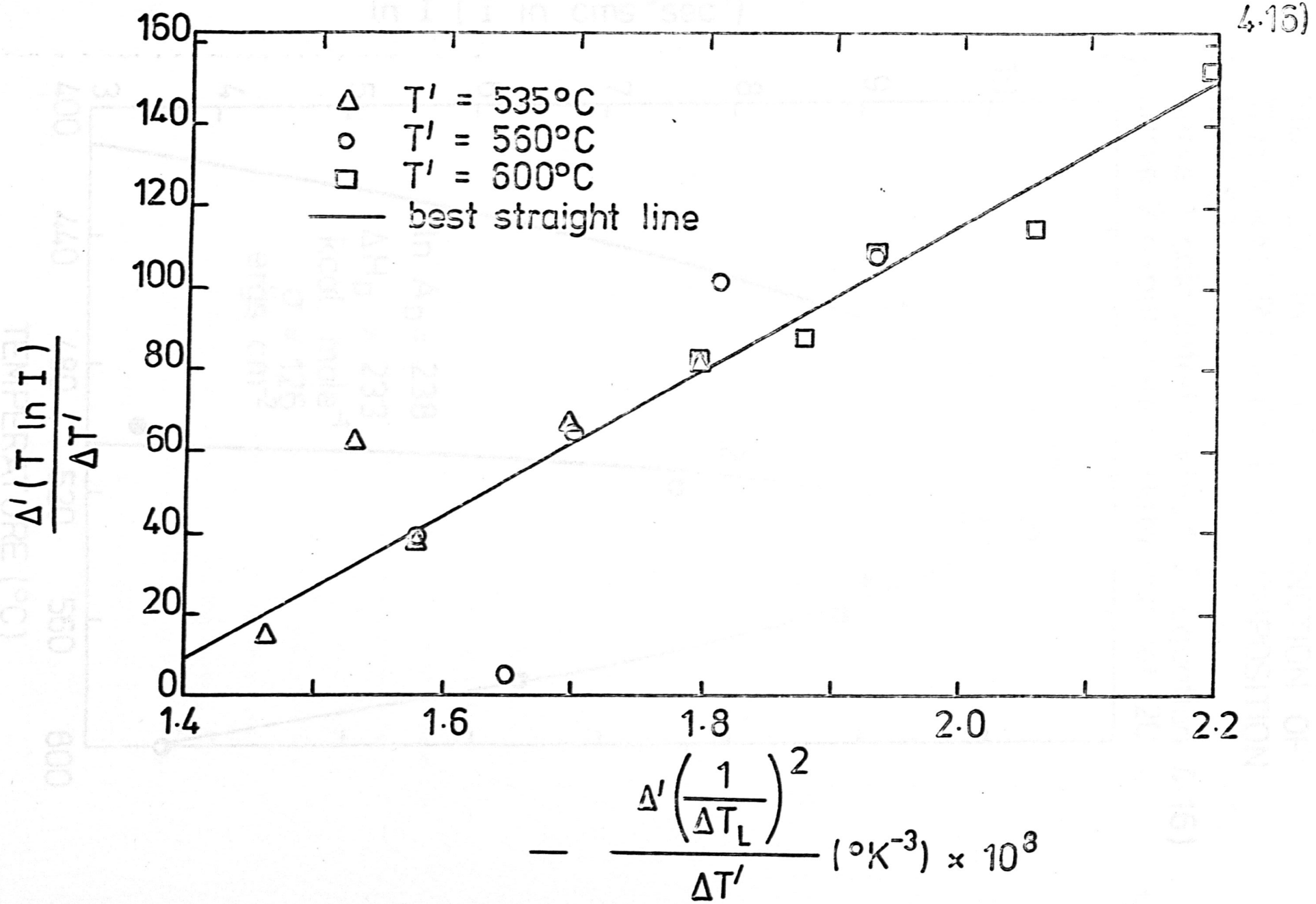

FIG. 4.20. ln I AS A FUNCTION OF TEMPERATURE FOR THE COMPOSITION 50N:50.
curve 1. calculated (method 2, equation 4·16)
curve 2. experimental data acc. ref. 20.

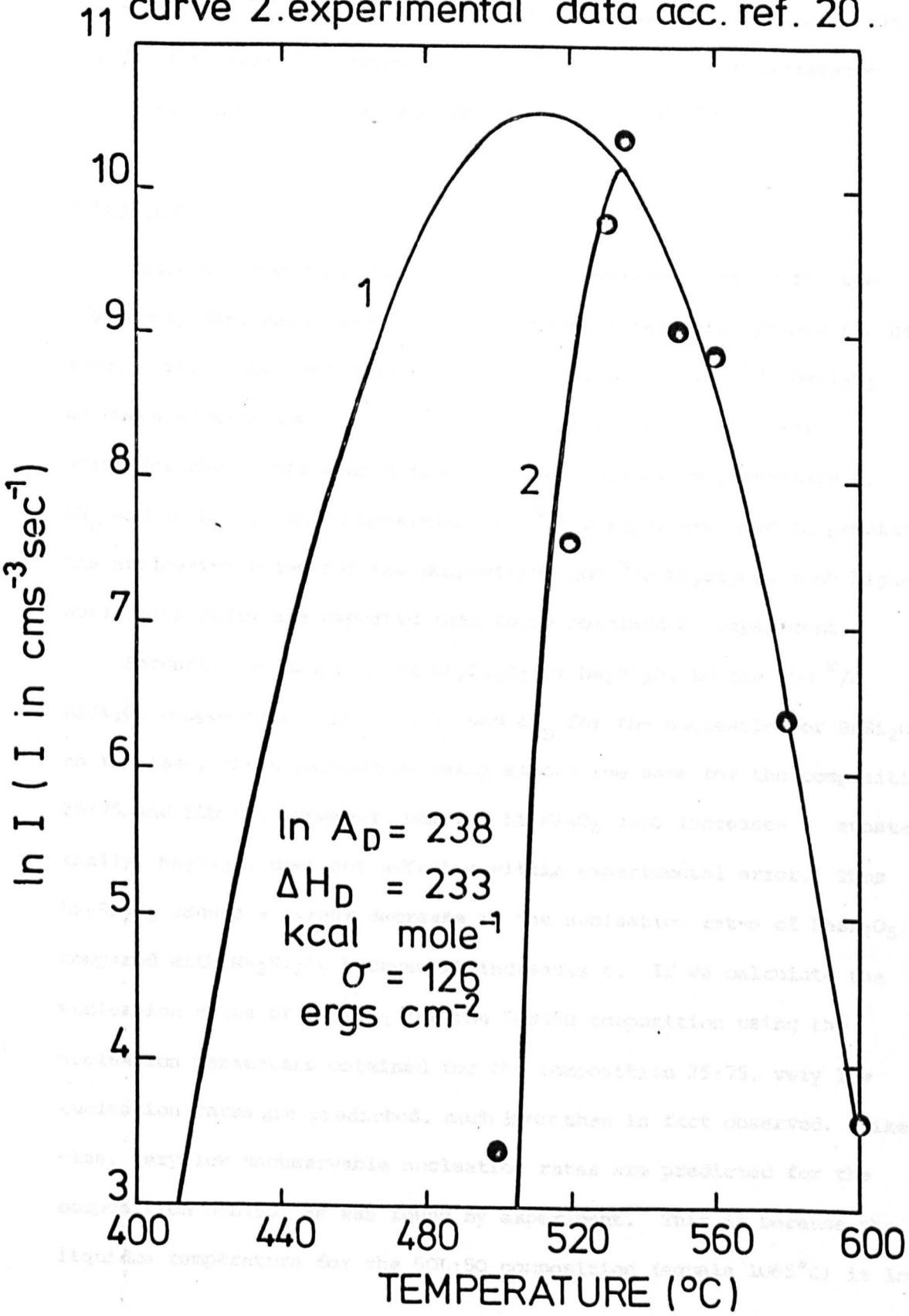

to the relatively large experimental error in determining low nucleation rates. Hence values of σ and ln A_D were not estimated. It should be mentioned that ΔG for the 80:20 composition is also nearly identical to that for composition 100 ^{m}/o $Li_2Si_2O_5$, the difference being less than 5% in the temperature range 500-600°C.

Discussion

Table 4.3 compares the nucleation parameters obtained for the previously discussed compositions. Several interesting points can be made. First, the much higher nucleation rates for 100 ^{m}/o $BaSi_2O_5$ as compared with 100 ^{m}/o $Li_2Si_2O_5$, is mainly due to the lower σ value for the former composition. If the nucleation parameters σ, ΔH_D and ln A_D for the composition 100 ^{m}/o $BaSi_2O_5$ are used to predict the nucleation rates for the composition 100 ^{m}/o $Li_2Si_2O_5$, much higher nucleation rates are expected than those obtained by experiment.

Secondly the addition of $Li_2Si_2O_5$ or $Na_2Si_2O_5$ to the 100 ^{m}/o $BaSi_2O_5$ composition causes ln A_D and ΔH_D for the nucleation of $BaSi_2O_5$ to increase, these parameters being almost the same for the compositions 25:75 and 50N:50. However, whereas $Li_2Si_2O_5$ also increases σ substantially, $Na_2Si_2O_5$ does not affect σ within experimental error. Thus $Li_2Si_2O_5$ causes a larger decrease in the nucleation rates of $BaSi_2O_5$ compared with $Na_2Si_2O_5$ because it increases σ. If we calculate the nucleation rates of $BaSi_2O_5$ for the 50N:50 composition using the nucleation parameters obtained for the composition 25:75, very low nucleation rates are predicted, much lower than in fact observed. Likewise, very low unobservable nucleation rates are predicted for the composition 50L:50, as was found by experiment. This is because the liquidus temperature for the 50L:50 composition (equals 1065°C) is low

TABLE 4.3

THE NUCLEATION PARAMETERS OBTAINED FOR COMPOSITIONS 100 ^{m}/o $Li_2Si_2O_5$, 100 ^{m}/o $BaSi_2O_5$, 25:75 AND 50N:50 USING METHOD 2, EQUATION (4.16)

Composition	ln A_D (A_D in cm^{-3} sec^{-1})	ΔH_D k cal $mole^{-1}$	σ ergs cm^{-2}	ΔT °C	Nucleating phase
100 ^{m}/o $Li_2Si_2O_5$	291 ±15	215	222 ±7	454 - 527	$Li_2Si_2O_5$
100 ^{m}/o $BaSi_2O_5$	172 ±20	177	132 ±4	700 - 780	$BaSi_2O_5$
25:75	240 ±45	210	153 ±8	561 - 626	$BaSi_2O_5$
50N:50	238 ±88	233	126 ±12	535 - 600	$BaSi_2O_5$

Notes:-

(i) σ calculated assuming $k_5 = \frac{16\pi}{3}$

(ii) 95% confidence limits quoted for ln A_D and σ.
ΔH_D calculated assuming mean values for ln A_D and σ.

(iii) Parameters calculated for the temperature range ΔT.

and therefore ΔG is not large enough to give observable nucleation rates. Using the nucleation parameters obtained for the composition 25:75, we can calculate that a liquidus temperature of 1202°C is required if the critical nucleation temperature, T_c is to be at 500°C, the D.T.A. estimate of T_g. Likewise, nucleation of $BaSi_2O_5$ was not observed for the composition 60:40 because its liquidus temperature (equals 975°C) is also too low. In this case the liquidus temperature would have to be increased to 1205°C for T_c to occur at 485°C, the D.T.A. estimate of T_g for the 60:40 composition. A similar calculation for the nucleation of $Li_2Si_2O_5$ in the composition 70:30, using the nucleation parameters obtained for the 100 ^{m}/o $Li_2Si_2O_5$ composition, would suggest that the liquidus temperature for the 70:30 composition should be too low for nucleation of $Li_2Si_2O_5$ to be observed. Although the nucleation kinetics of this composition were not investigated, no internal spherulites were observed during the brief growth rate study referred to in Chapter 3.

Thirdly if we calculate the nucleation rates of $BaSi_2O_5$ for the compositions 25:75 and 50N:50 using the nucleation parameters obtained for the composition 100 ^{m}/o $BaSi_2O_5$, no observable nucleation is expected for either 25:75 or 50N:50. The fact that nucleation is observed is due solely to the large increase in ln A_D for these two compositions, brought about by adding $Li_2Si_2O_5$ or $Na_2Si_2O_5$ respectively. It should be mentioned that, as for the 100 ^{m}/o $Li_2Si_2O_5$ discussed earlier, the values of ln A_D in Table 4 are all far larger than that predicted by theory. Although the nucleation parameters for $BaSi_2O_5$ do change with composition, the values of T_c predicted for the 10:90 composition using the parameters obtained for the compositions 100 ^{m}/o $BaSi_2O_5$ and 25:75 are similar, viz. 776 and 791°C respectively.

In Figure 3.57 a value of 795°C was assumed.

Finally, it is of interest to compare the nucleation parameters for $BaSi_2O_5$ obtained for the compositions 50N:50 and 100 $^m/_o$ $BaSi_2O_5$ with those which may be estimated from the critical nucleation temperatures given by Burnett and Douglas in their study of the $Na_2Si_2O_5$-$BaSi_2O_5$ system[20]. Assuming that their values of T_c correspond to a constant low nucleation rate, independent of composition, we can express the nucleation equation as

$$k\,T_c\,\ln I_c = k\,T_c\,\ln A_D - \left\{\Delta H_D + \frac{k_5 V_m^{\,2}\sigma^3}{\Delta H_f^{\,2}}\left(\frac{T_L}{\Delta T_c}\right)^2\right\}$$

$$\therefore \qquad T_c = \frac{\Delta H_D}{k\,\ln\left(\frac{A_D}{I_c}\right)} + \frac{k_5 V_m^{\,2}\sigma^3}{\Delta H_f^{\,2} k\,\ln\left(\frac{A_D}{I_c}\right)}\left(\frac{T_L}{\Delta T_c}\right)^2 \qquad (4.27)$$

where $I = I_c$ at $T = T_c$, $\Delta T_c = T_L - T_c$, and ΔG has been assumed ideal. Thus if the nucleation parameters are constant, independent of composition, a plot of T_c vs $\left(\frac{T_L}{\Delta T_c}\right)^2$ should be linear. If $I_c = 1$ and A_D is known we can calculate ΔH_D and σ from the intercept and slope respectively. In general, however, we can only obtain the value of the ratio $\frac{\Delta H_D}{\sigma^3}$. Figure 4.21 shows the values of T_c measured by Burnett and Douglas plotted according to equation (4.27) for the compositions containing 50, 60 and 70 $^m/_o$ $BaSi_2O_5$ respectively. The fit is reasonable and we obtain $\Delta H_D = 0.198\,\sigma^3$, where ΔH_D is in k cal $mole^{-1}$ and σ is in ergs cm^{-2}. Using the results of the previous analysis of the whole nucleation curve for the 50N:50 composition we find that $\Delta H_D = 0.117\,\sigma^3$. Although the agreement is not very good, it should

FIG. 4.21. T_C vs. $(T_L / \Delta T_C)^2$ FOR THE NUCLEATION OF $BaSi_2O_5$ IN THE SYSTEM $Na_2Si_2O_5$ - $BaSi_2O_5$.
(T_C VALUES ACC. REF. 20)

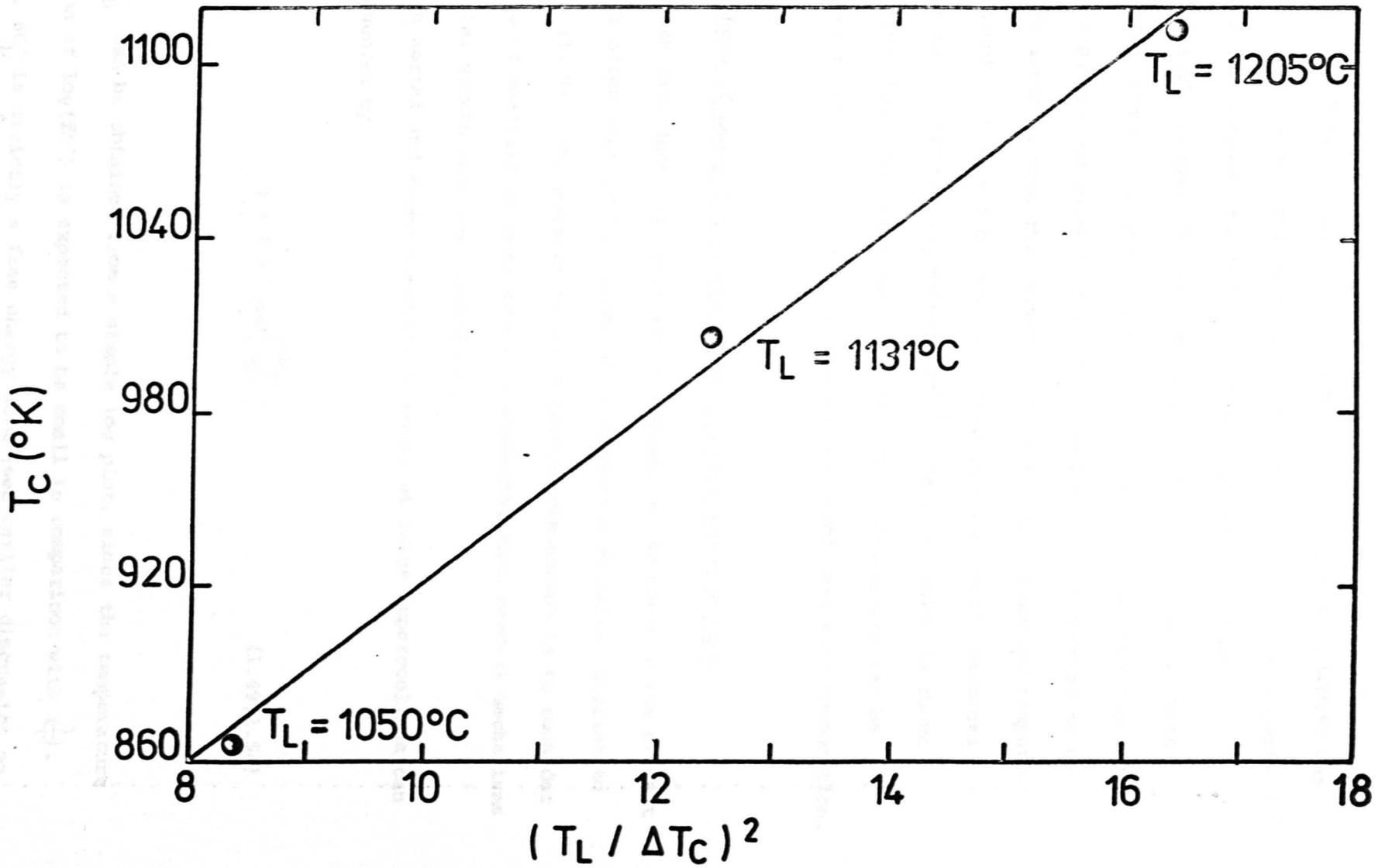

be remembered that the nucleation curve for the composition 50N:50 was determined much more accurately than the critical nucleation temperatures for the compositions 50N:50, 40N:60, and 30N:70. Also, equation (4.27) assumes the nucleation parameters are constant with composition, which is probably incorrect. Hence the analysis based on the whole nucleation curve of the 50N:50 composition is thought to be much more accurate than that based on the critical nucleation temperature concept. It should be mentioned that equation (4.27) predicts T_c to be 1073°C for the composition 100 $^{m}/_{o}$ $BaSi_2O_5$, which is about 200°C higher than the experimental value. This discrepancy can be attributed to the variation of the nucleation parameters with composition.

4.4 Methods of analysing growth rates at large supercoolings

Growth rate data for large supercoolings, as obtained in the present study, is often expressed in terms of an Arrhenius equation, similar to equation (1.49). The purpose of the following discussion is to consider this kind of analysis in more detail, remembering that several mechanisms for crystal growth have been postulated.

Both normal and screw dislocation models at large supercoolings can be represented by

$$u = f A' \exp\left(\frac{\Delta G_D'}{RT}\right) \qquad (1.49,1.54)$$

Thus $\Delta G_D'$ can be obtained from a simple log plot, since the temperature variation of $\log(fA')$ is expected to be small in comparison with $(\frac{1}{T})$. However, $\Delta G_D'$ is strictly a free energy term (see earlier discussion on

crystal nucleation) which can be expressed as

$$\Delta G'_D = \Delta H'_D - T\Delta S'_D \qquad (4.28)$$

Thus the expression for u becomes

$$u = f\, A'_D \exp\left(-\frac{\Delta H'_D}{RT}\right) \qquad (4.29)$$

where

$$A'_D = A' \exp\left(\frac{\Delta S'_D}{R}\right)$$

Hence $\Delta H'_D$ can be estimated from experiment, but the theoretical value of A' cannot be verified, since $\Delta S'_D$ is unknown. According to theory f is unity for materials of $\Delta S_f < 2R$, but for materials of $\Delta S_f > 4\text{-}6R$ f is given by equation (1.52). The value of f should be in agreement with the crystal morphology observed, as discussed in section 1.3.

While the surface nucleation model has not generally been found applicable in inorganic glass forming systems, it is of interest to consider the method of analysis required. As in crystal nucleation, it is possible to determine the interfacial surface energy (in this case σ_E) by normalising the kinetic data (see equations (1.50), (1.51) and (4.16)). Thus a plot of

$$\frac{T \ln u - T' \ln u'}{T - T'} \text{ vs. } \frac{1}{T - T'} \left\{ \frac{1}{\Delta G_v} - \frac{1}{\Delta G'_v} \right\} \qquad (4.30)$$

should be linear, and σ_E and $\ln \left\{ A'' \exp\left(\frac{\Delta S'_D}{k}\right) \right\}$

may be obtained from the gradient and intercept respectively. Furthermore, this plot should be applicable at all supercoolings. Since $\Delta S'_D$ is unknown, it is not possible to obtain A'' by experiment.

The diffusion coefficent for growth, given by

$$D' = D'_o \exp\left(- \frac{\Delta G'_D}{RT}\right) \qquad (1.57)$$

is often related to viscosity data via the Stokes-Einstein equation

$$D' = \frac{kT}{3\pi\lambda\eta} \qquad (1.56)$$

Thus substituting for $\Delta G'_D$ in the growth equations, we obtain for the normal and screw dislocation models at large supercoolings

$$u = \frac{f A'_\eta T}{\eta} \qquad (4.31a)$$

where $A'_\eta = \frac{A\,h}{3\pi\lambda^3 T}$ (c.f. equation (4.23)).

Since $A' = \lambda \nu_o \approx \lambda \frac{kT}{h}$, A'_η can also be expressed as

$$A'_\eta = \frac{k}{3\pi\lambda^2}$$

As mentioned in Chapter 1, we can define a reduced growth rate, u_R given by

$$u_R = \frac{u\eta}{1 - \exp\left(-\frac{|\Delta G|}{kT}\right)} \qquad (1.55)$$

Thus at large supercoolings $u_R = u\eta$. Hence equation (4.31a) becomes

$$u_R = f A'_\eta T \qquad (4.31b)$$

Thus if the use of viscosity data is correct, we can determine f as a function of temperature and therefore decide which model is more applicable. Knowing f we can also obtain A'.

As far as the author is aware, there is no quantitative model describing eutectic growth as a function of the supercooling, $T_E - T$. As indicated in Chapter 1, the growth rate is expected to be proportional to $\frac{D'}{y_{AB}}$, where y_{AB} is the interlamellar spacing and D' is the diffusion coefficient for the slowest of the diffusion processes required for growth to occur. Figure 4.22 shows the possible diffusion paths for A atoms during the growth of a two phase A-B eutectic into a

FIG. 4.22. POSSIBLE DIFFUSION PATHS FOR A ATOMS DURING EUTECTIC GROWTH OF A BINARY EUTECTIC A-B.

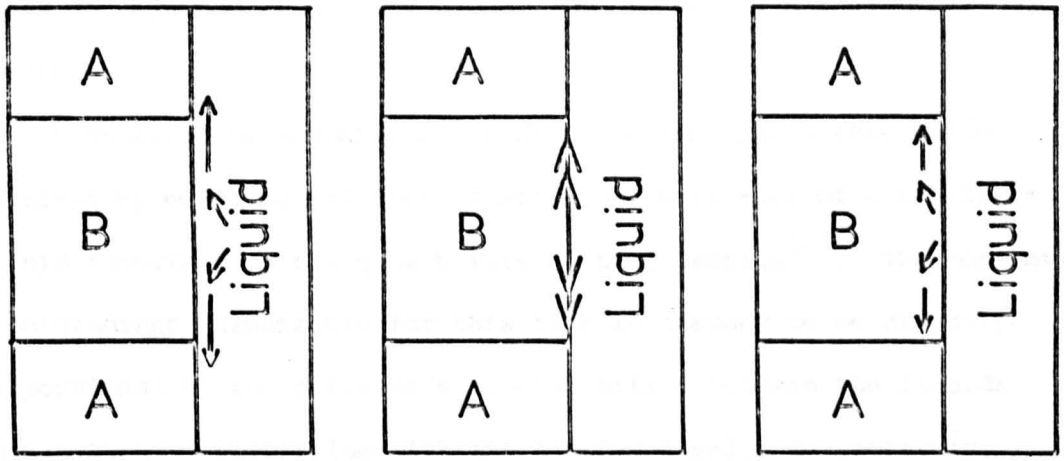

FIG. 4.23. CONSTRUCTION REQUIRED TO OBTAIN THE COMPOSITIONS OF THE LIQUID, x_A AND x_B, OPPOSITE THE CENTRES OF A AND B LAMELLAE RESPECTIVELY IN A BINARY EUTECTIC A-B.

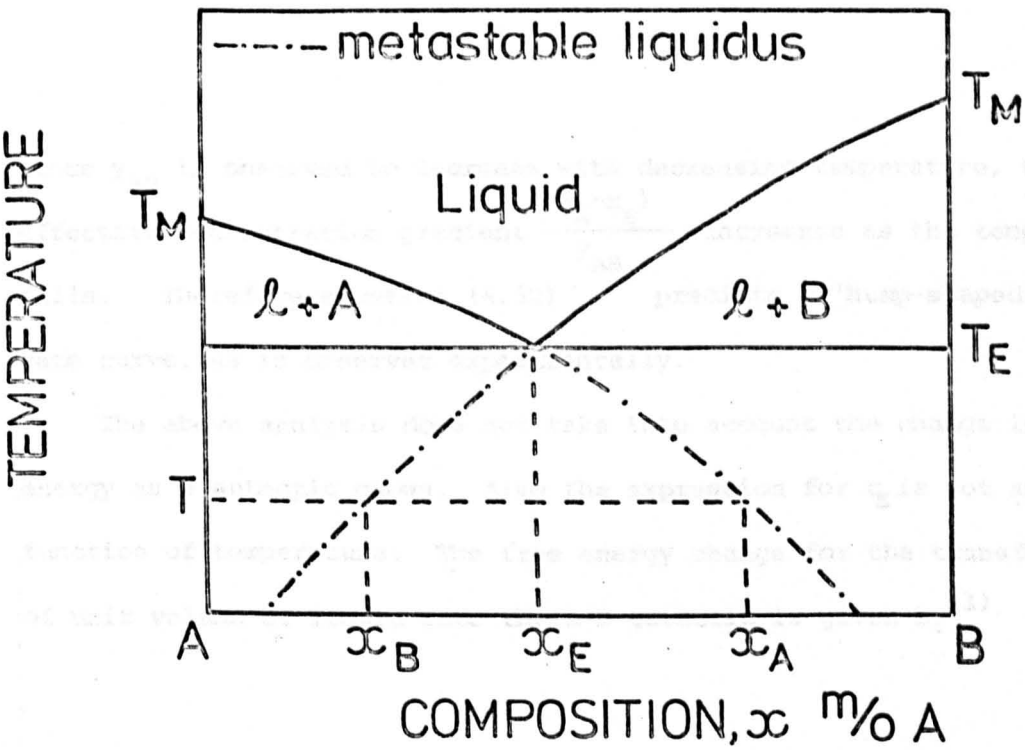

liquid. In this case it is reasonable to assume that almost all diffusion of A atoms will occur through the liquid phase. B atoms would be required to diffuse through the liquid in the opposite direction.

A qualitative expression for the eutectic growth rate can be obtained by equating the flux of atoms per unit area of a lamellar-liquid interface to the growth rate of that lamella[1]. The concentration gradient responsible for this flux is assumed to be directly proportional to the difference in composition between the liquids in metastable equilibrium with the A and B lamella respectively. Figure 4.23 shows how this difference is estimated from the phase diagram. As the temperature falls $(x_A - x_B)$ is effectively the driving force for growth and gives a measure of the supercooling below T_E. The growth rate is given by

$$u_E = \frac{D'(x_A - x_B)}{y_{AB}} \qquad (4.32)$$

Since y_{AB} is observed to decrease with decreasing temperature, the effective concentration gradient $\frac{(x_A - x_B)}{y_{AB}}$ increases as the temperature falls. Therefore equation (4.32) predicts a 'hump-shaped' growth rate curve, as is observed experimentally.

The above analysis does not take into account the change in surface energy as a eutectic grows. Also the expression for u_E is not an explicit function of temperature. The free energy change for the transformation of unit volume of liquid into the A-B eutectic is given by[1]

$$W_E = \Delta G_v + \sigma_{AB} A = \Delta G_v + \frac{2\sigma_{AB}}{y_{AB}} \qquad (4.33)$$

where ΔG_v is the change in volume free energy, A is the increase in A-B interfacial area, and σ_{AB} is the interfacial surface energy between phases A and B. Since a unit volume of eutectic will contain $\frac{1}{y_{AB}}$ lamellae, each having two surfaces of unit area, $A = \frac{2}{y_{AB}}$. For growth to occur W_E has to be negative. Thus we can define a minimum spacing y'_{AB}, which corresponds to $W_E = 0$, and $|\Delta G_v|$ can be expressed as $\frac{2\sigma_{AB}}{y'_{AB}}$. However, the maximum negative value of W_E, corresponding to the maximum value of y_{AB}, is limited by the necessity for diffusion to occur. At a given temperature there is thus an optimum value of y_{AB} for which u_E is a maximum. This can be brought into the expression for u_E by tentatively assuming that the driving force for eutectic growth is directly proportional to W_E and since $u_E \propto \frac{D}{y_{AB}}$ we obtain

$$u_E = \frac{c|W_E|D}{y_{AB}} = \frac{2c\sigma_{AB}(y_{AB}-y'_{AB})D}{y^2_{AB}\, y'_{AB}} \qquad (4.34)$$

where c is a constant. Defining y''_{AB} as the spacing corresponding to maximum u and differentiating equation (4.34) with respect to y_{AB} it can be shown that $y''_{AB} = 2y'_{AB}$. Therefore

$$y''_{AB} = \frac{4\sigma_{AB}}{|\Delta G_v|} = \frac{4\sigma_{AB}}{|\Delta G_v|\Delta T} \qquad (4.35)$$

where ΔS_v is the change in volume entropy and $\Delta T = T_E - T$. Thus the observed spacing should be a linear function of the reciprocal supercooling. Evaluating equation (4.34) for $y_{AB} = y''_{AB}$ we finally obtain

$$u_E \simeq A_E \, \Delta T^2 \exp(-\frac{\Delta H'_D}{RT}) \qquad (4.36)$$

where A_E is a constant and D' has been expressed in terms of equations (1.57) and (4.28). Thus a plot of $\ln(\frac{u_E}{\Delta T^2})$ vs. $\frac{1}{T}$ should be linear, with slope $\frac{-\Delta H'_D}{R}$.

4.5 Analysis of growth rate data for systems $R_2Si_2O_5$-$BaSi_2O_5$

4.5.1 The system $Li_2Si_2O_5$-$BaSi_2O_5$

Composition 100 ^{m}/o $Li_2Si_2O_5$

Figure 4.24 shows the data for the 100 ^{m}/o $Li_2Si_2O_5$ composition in the temperature range 551-646°C plotted in three ways as a function of $\frac{1}{T}$, assuming either the normal or screw dislocation growth model to be applicable. First the data was plotted according to equation (4.29), assuming f to be unity and ignoring the relatively slight temperature dependence of A'_D. The second plot is according to equation (1.47) for the normal growth model, assuming $A' = \lambda \nu_o = \lambda \frac{kT}{h}$, and using J.A.N.A.F. Tables[5] to calculate $[1 - \exp(-\frac{|\Delta G|}{RT})]$. Thirdly, the data was plotted according to equation (1.53) for the screw dislocation model, in which $f \propto \Delta T$. A' and the thermodynamic term were calculated as in the second method. These three plots fit the data

FIG. 4.24. GROWTH RATE DATA FOR THE COMPOSITION 100 m/o $Li_2Si_2O_5$ PLOTTED AS A FUNCTION OF $1/T$.

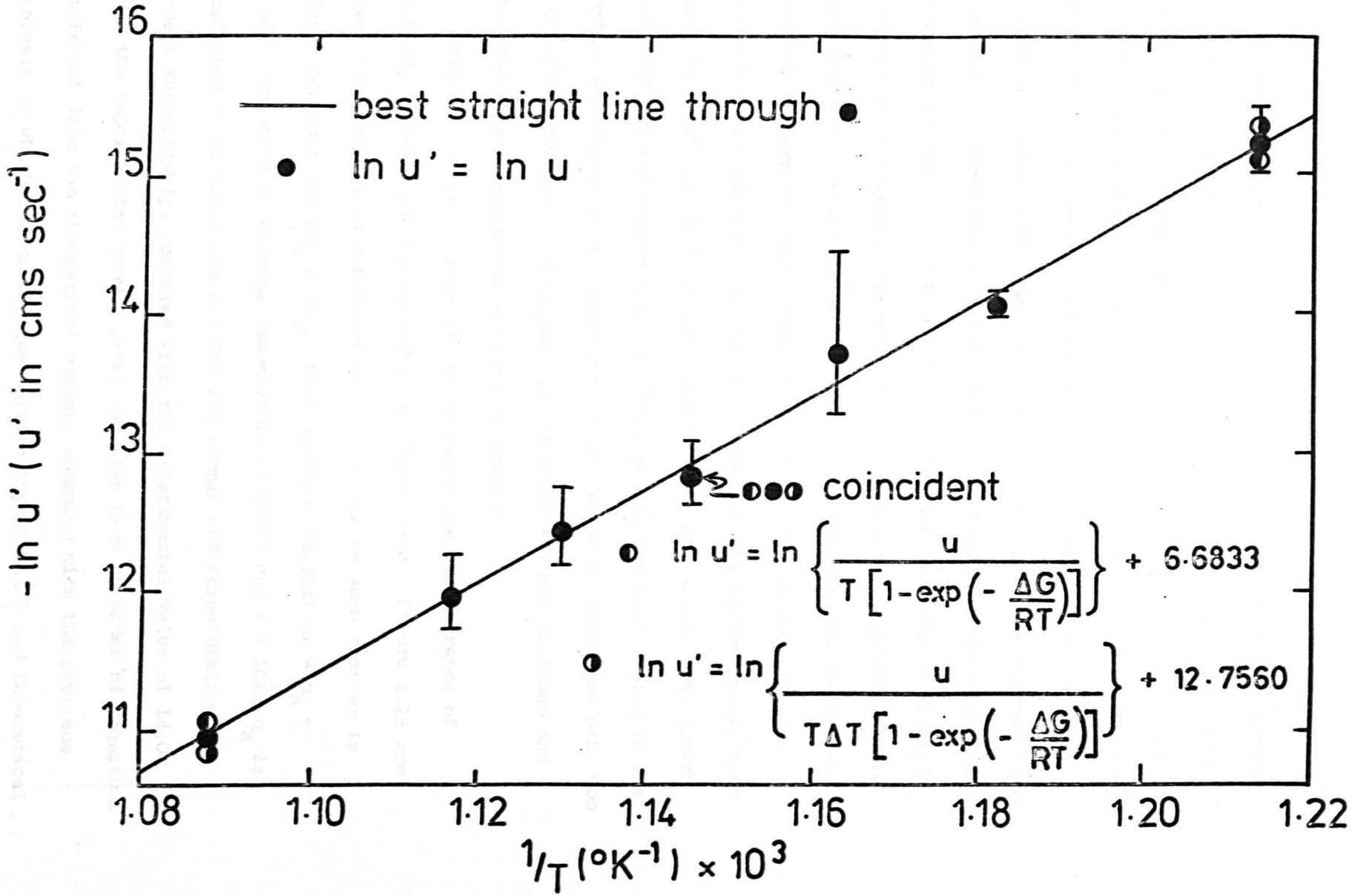

equally well and have almost identical slopes. Table (4.4) compares the intercept and $\Delta H_D'$ values obtained. The experimental intercepts are considerably larger than those calculated from theory ignoring $\Delta S_D'$, the experimental growth rates being 5-7 orders of magnitude too great. It can be concluded that it is not possible to distinguish between the normal and screw dislocation models at large supercoolings from kinetic measurements alone. However, considering the high entropy of fusion of $Li_2Si_2O_5$ ($\simeq$ 5R) and the small scale faceting of $Li_2Si_2O_5$ observed in this study, the screw dislocation model is probably more appropriate in the present case. The above analysis also indicates that the temperature dependence of A' can be ignored and $\Delta H_D'$ can be calculated from a simple lnu plot, ignoring the thermodynamic term which is about 0.88-0.95 at the temperatures considered. The growth rate data for the composition 100 $^m/_o$ $Li_2Si_2O_5$ was also fitted to the surface nucleation model (equation (4.30)) using T' values of 646, 600 and 551°C. However, a straight line relation was not obtained and the growth rate parameters were not estimated.

Finally, it is of interest to consider the growth rates of $Li_2Si_2O_5$ in terms of the available viscosity data. Figure 4.25 compares -lnu and lnη as functions of $\frac{1}{T}$. It can be seen that uη is almost constant and $\Delta H_D' = \Delta H_\eta$. From equation (4.31b) $u_\eta = u_R = f A_\eta' T$. Assuming an average temperature of 600°C and $\lambda \simeq 10\mathring{A}$, u_R is predicted to be 127.8 and 6.8 for the normal and screw dislocation models respectively, compared with the experimental value of 14.0. Thus the experimental growth rates are less than an order of magnitude different from the theoretical values, compared with the previous analysis in which the difference between experimental and theoretical

TABLE 4.4

GROWTH RATE PARAMETERS OBTAINED FOR THE COMPOSITION $Li_2Si_2O_5$ USING VARIOUS METHODS

Method of Analysis	Experimental intercept, $\ln(cm\ sec^{-1})$	$\Delta H_D'$ k cal $mole^{-1}$	Theoretical intercept, $\ln(cm\ sec^{-1})$
1	26.0 ±3.2	67.6 ±5.4	≈ 14.4
2	19.0 ±3.2	67.0 ±5.5	≈ 7.6
3	15.0 ±3.2	70.5 ±5.6	≈ -1.4

Notes:-

(i) Method 1. Simple Arrhenius plot (equation (4.29) f = 1)

$$\text{Intercept} = \ln A_D' = \ln\left(\frac{\lambda k T}{h}\right)$$

Method 2. Normal model (equation (1.47))

$$\text{Intercept} = \ln\left(\frac{A_D'}{T}\right) = \ln\left(\frac{\lambda k}{h}\right)$$

Method 3. Screw dislocation model (equation (1.53))

$$\text{Intercept} = \ln\left(\frac{f\ A_D'}{T\ \Delta T}\right) = \ln\left(\frac{\lambda k}{2\pi h T_m}\right)$$

(ii) Theoretical intercepts calculated assuming $\Delta S_D' = 0$ and $\lambda = 10$ Å

(iii) Parameters calculated for the temperature range 551-646°C

FIG. 4.25. A COMPARISON OF CRYSTAL GROWTH RATE DATA AND VISCOSCITY DATA AS A FUNCTION OF $1/T$ FOR THE COMPOSITION 100m% $Li_2Si_2O_5$.

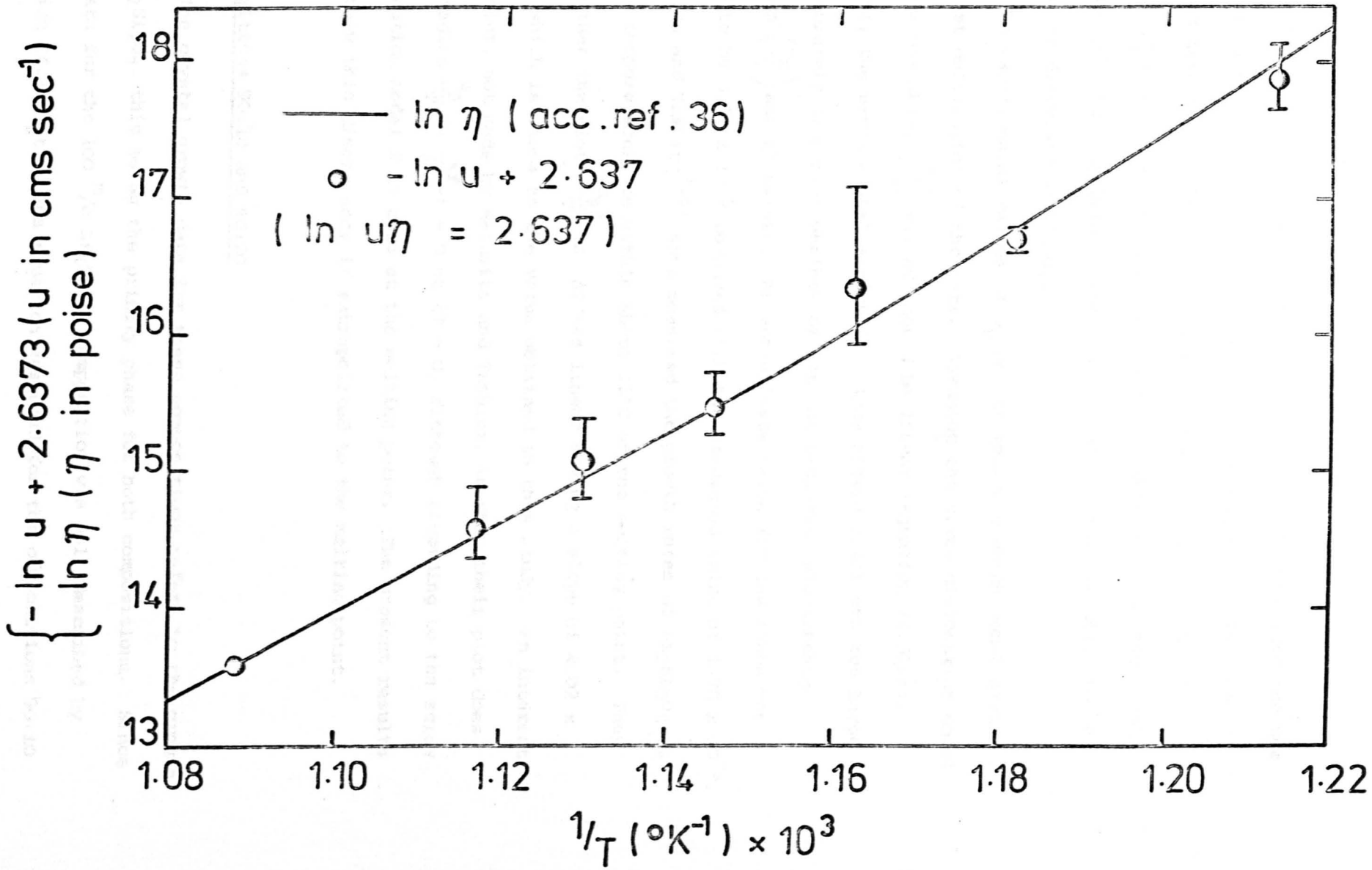

growth rates was 5-7 orders of magnitude. This may be because the use of viscosity data eliminates the unknown parameter $\Delta S_D'$, which was assumed zero in the theoretical calculations of intercept values. Also, $\Delta H_D'$ is not assumed to be constant. It should be stressed that the use of viscosity data assumes the Stokes-Einstein relation to be valid, as discussed previously.

The experimental values of u_R do not indicate which model gives the best description of the data. Assuming the screw dislocation model to be applicable, $\left(\frac{u_R}{T}\right)$ vs. ΔT should be linear (equation (4.31b)). However, the experimental errors in u (see Figure 3.41) are too large to accurately determine whether or not the proposed relationship between $\left(\frac{u_R}{T}\right)$ and ΔT exists. An approximate value for the slope was found to be 3.24×10^{-5} compared with the predicted value of 1.78×10^{-5}. Matusita and Tashiro[36] have measured the growth rates of $Li_2Si_2O_5$ at higher temperatures, to within about 12°C of the melting point. They found that the plot $\left(\frac{u_R}{T}\right)$ vs. ΔT was linear having a slope of 4.02×10^{-5}, which is close to the value obtained in this study. An interesting point, not made by Matusita and Tashior, is that their plot does not predict $\frac{u_R}{T} \left(= \frac{kf}{3\pi\lambda^2}\right) = 0$ at $\Delta T = 0$, although according to the screw dislocation model f is zero at the melting point. The present results also show this discrepancy if extrapolated to the melting point.

Compositions 90:10 and 80:20

The crystal growth data for these compositions refers to the growth of $Li_2Si_2O_5$, this being the primary phase for both compositions. Since the data for the 100 ^{m}/o $Li_2Si_2O_5$ composition was well described by equation (4.29), the same equation was used for the compositions 90:10

and 80:20. As shown in Figures 4.26 and 4.27 good fits were obtained, the values of $\Delta H_D'$ and $\ln A_D'$ being given in Table (4.5). These values are very similar to those estimated for the 100 $^m/_o$ $Li_2Si_2O_5$ composition using the same method of analysis.

Compositions 60:40, 50L:50, 25:75 and 10:90

In Chapter 3 it was suggested that these compositions exhibit eutectic growth. The data for the composition 50L:50 was therefore plotted according to equation (4.36) as shown in Figure 4.28. The fit is good and the values of $\Delta H_D'$ and $\ln A_E$ are given in Table (4.5). In view of the several assumptions required for equation (4.36) to be valid, the growth rate data for the composition 50L:50 was also plotted according to equation (4.29). A good fit was again obtained but in this case the values of both $\Delta H_D'$ and $\ln A_D'$ were close to those obtained for the three compositions 100 $^m/_o$ $Li_2Si_2O_5$, 90:10 and 80:20 (see Figure 4.29 and Table (4.5)). This might suggest that equation (4.29) is a better description of the eutectic growth rate data than equation (4.36), although the latter equation gives a slightly better straight line fit (compare Figures 4.28 and 4.29). The data for the remaining compositions exhibiting eutectic growth was therefore plotted according to equation (4.29), as shown in Figures 4.29, 4.30 and 4.31. The values of $\Delta H_D'$ and $\ln A_D'$ are given in Table (4.5), from which it is apparent that these parameters vary little between the compositions 100 $^m/_o$ $Li_2Si_2O_5$ and 10:90. Little variation was expected between the compositions 60:40 and 10:90 since they all have very similar growth rate curves.

FIG. 4.26. GROWTH RATE DATA FOR THE COMPOSITION 90 :10 AS A FUNCTION OF $^1/_T$. (EQUATION 4.29)

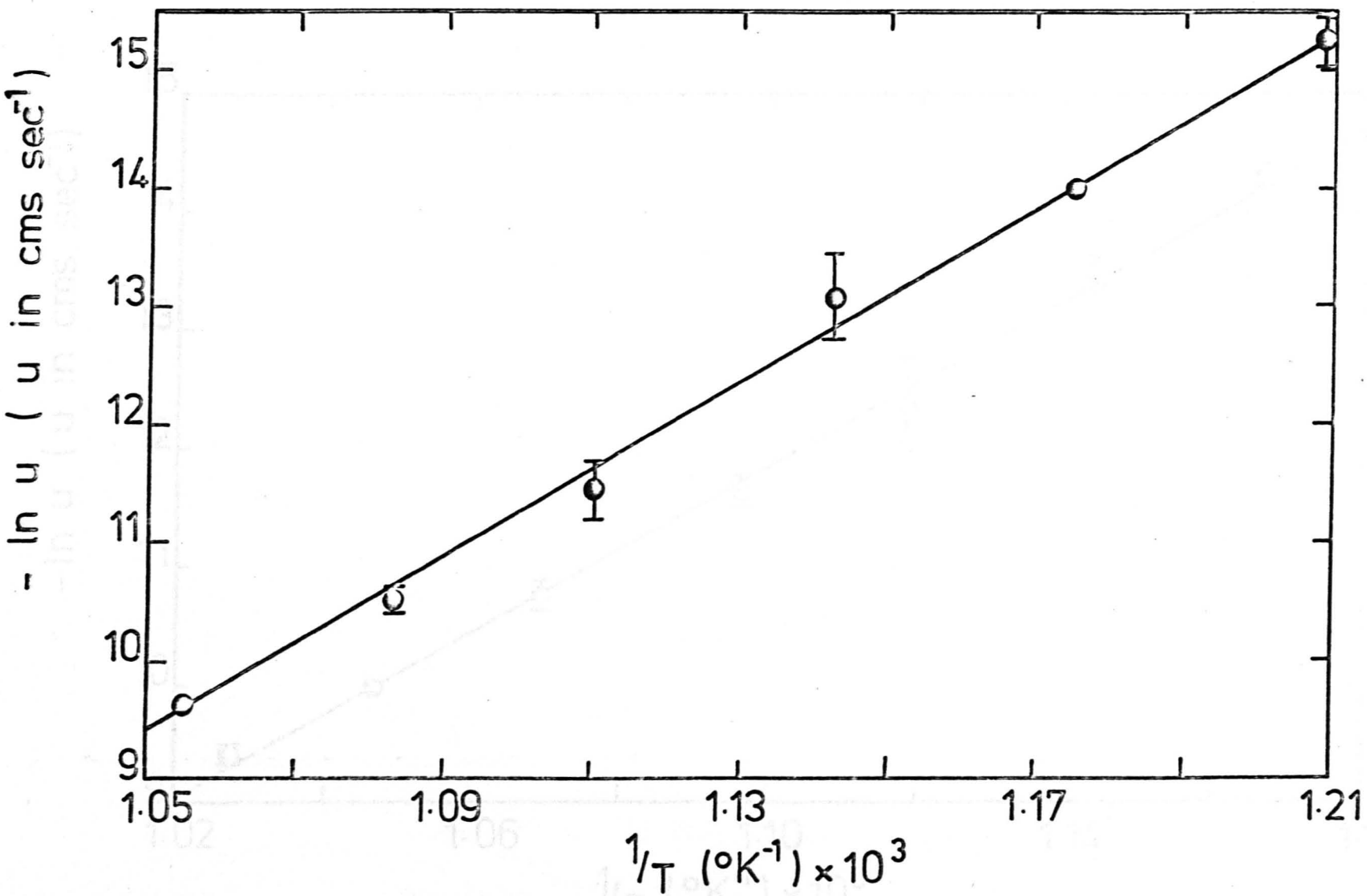

FIG. 4.27. GROWTH RATE DATA FOR THE COMPOSITION 80 : 20 AS A FUNCTION OF $^1/_T$ (EQUATION 4.29)

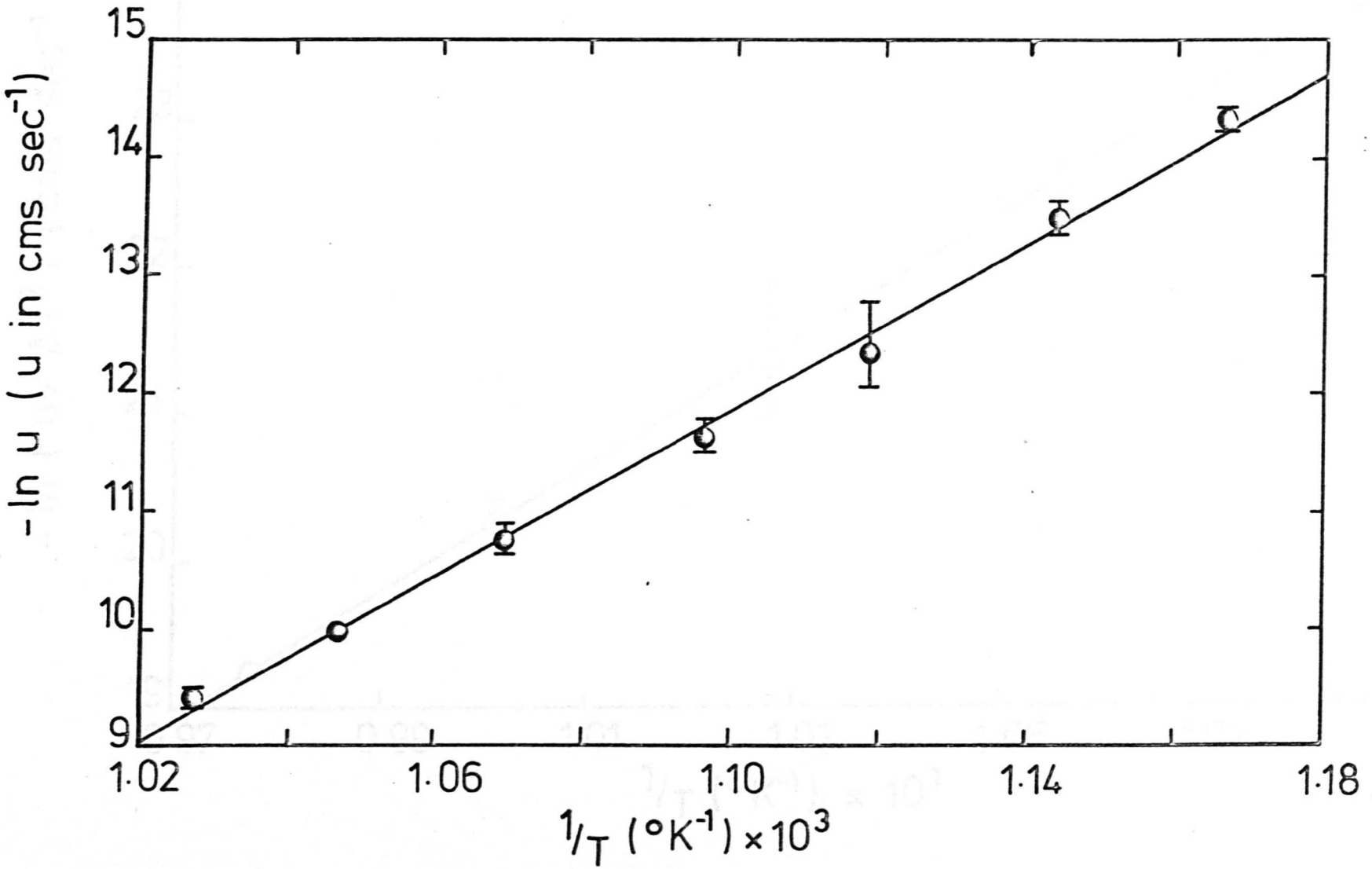

FIG. 4.28. GROWTH RATE DATA FOR THE COMPOSITION 50L : 50 ACCORDING TO THE EUTECTIC GROWTH MODEL. (EQUATION 4.36)

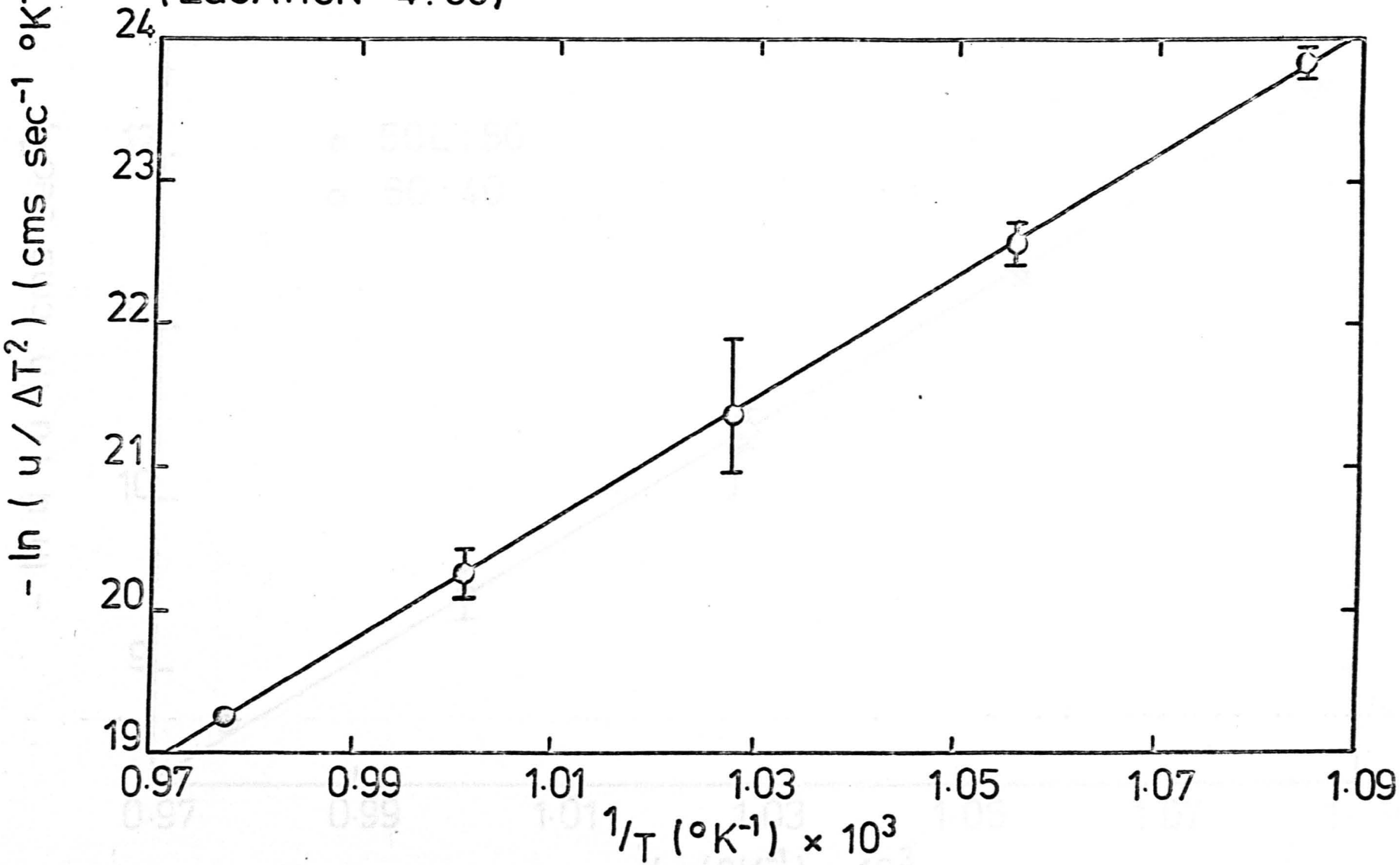

FIG. 4.29. GROWTH RATE DATA FOR THE COMPOSITIONS 50L:50 AND 60:40 AS A FUNCTION OF $^1/_T$ (EQUATION 4.29)

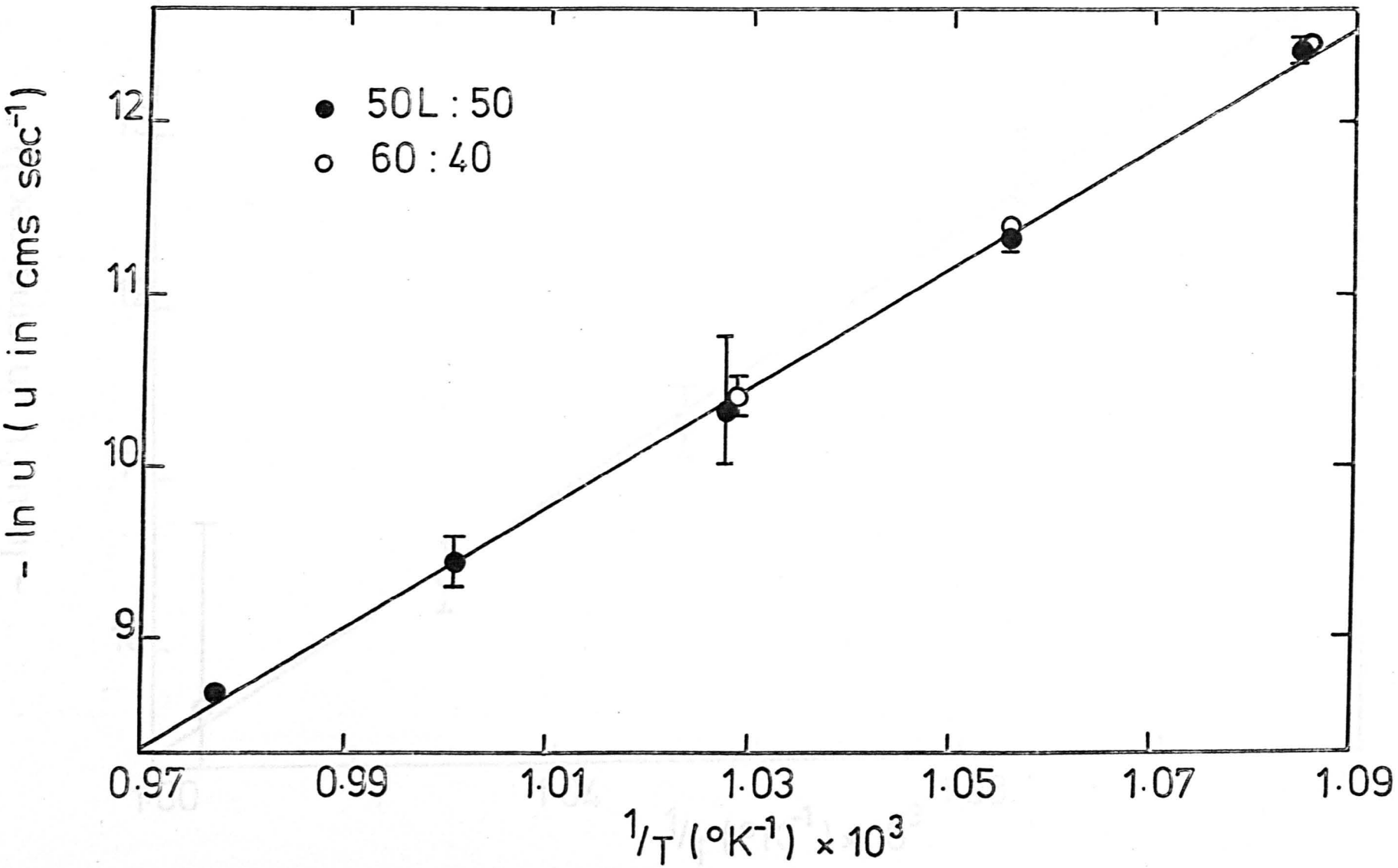

FIG. 4.30. GROWTH RATE DATA FOR THE COMPOSITION 25:75 AS A FUNCTION OF $^1/_T$ (EQUATION 4.29)

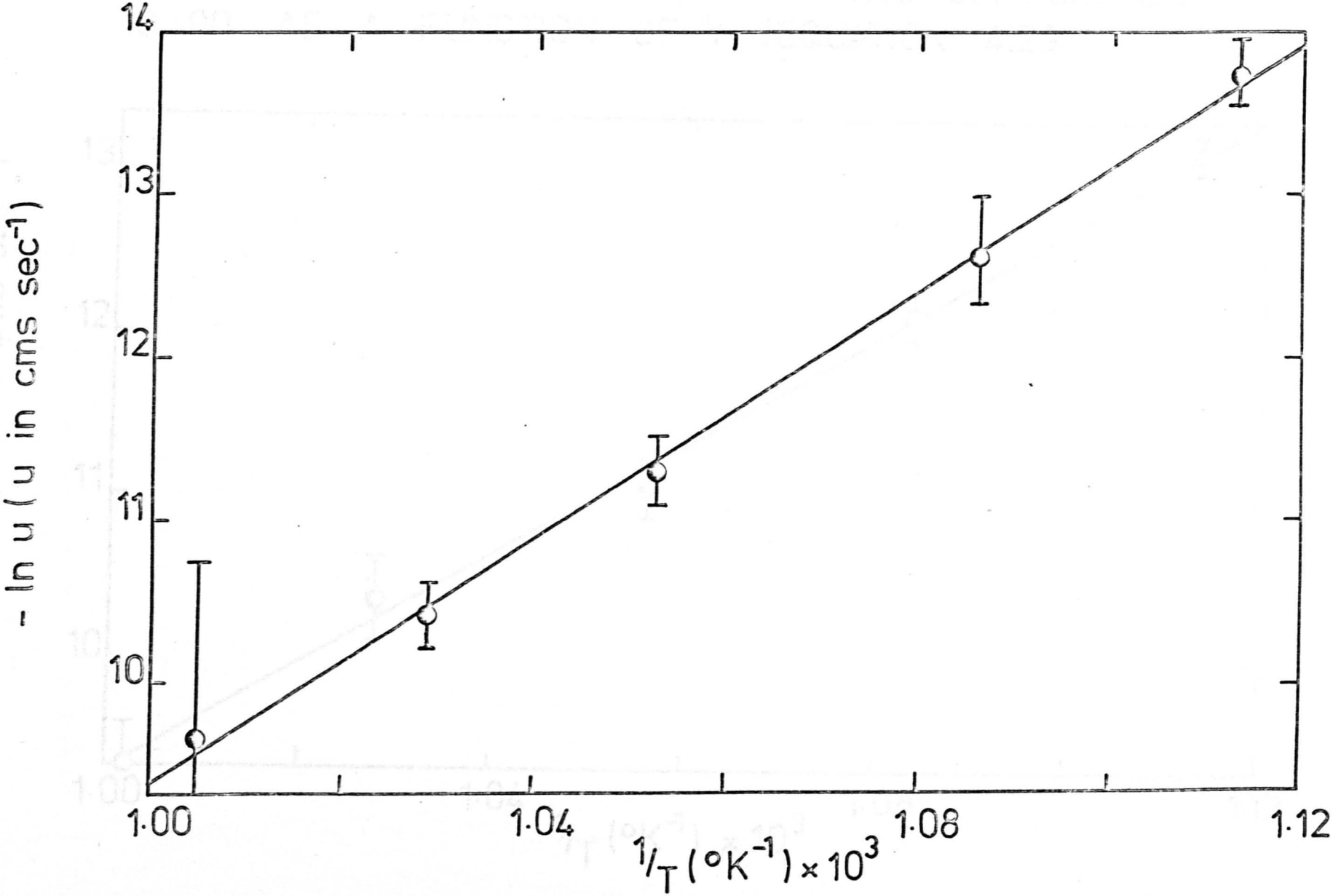

FIG. 4.31. GROWTH RATE DATA FOR THE COMPOSITION 10 : 90 AS A FUNCTION OF $1/T$ (EQUATION 4.29)

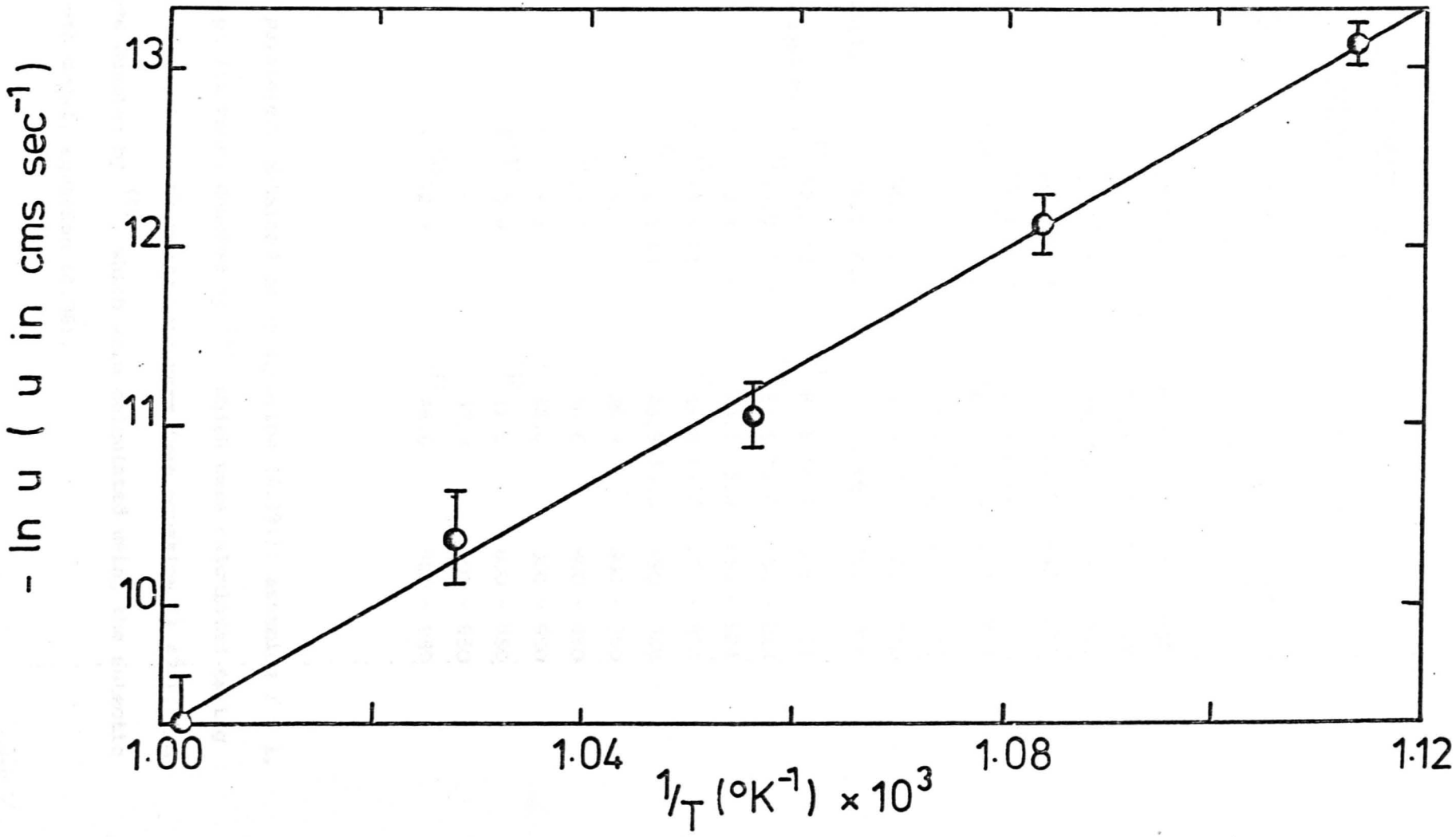

TABLE 4.5

GROWTH RATE PARAMETERS OBTAINED FOR COMPOSITIONS IN THE SYSTEMS $R_2Si_2O_5$-$BaSi_2O_5$ (R ≡ Li, Na)

Composition	$\ln A_D'$ (A_D' in cm sec^{-1})	$\Delta H_D'$ k cal $mole^{-1}$	$\Delta T^{\equiv}$ °C
100 m/o $Li_2Si_2O_5$	26.0 ±3.2	67.6 ±5.4	551 - 646
90:10	29.6 ±4.2	73.8 ±7.4	554 - 675
80:20	27.2 ±2.6	70.5 ±4.7	584 - 700
60:40	26.9 ±0.7	72.0 ±1.3	648 - 699
50L:50	25.4 ±2.3 (4) 22.2 ±1.1	69.2 ±4.4 (4) 84.3 ±2.1	649 - 750
25:75	28.3 ±3.2	74.9 ±6.1	625 - 722
10:90	24.1 ±4.1	66.5 ±7.7	625 - 725
100 m/o $BaSi_2O_5$	39.5 ±4.0	115 ±9	749 - 868
(2) 100 m/o $Na_2Si_2O_5$	(1) 22.0 ±3.6 (1) 16.7 ±1.7	(1) 62.5 ±6.3 (1) 52.4 ±3.4	575 - 654 654 - 813
50N:50	10.4 ±1.5 (1) 13.4 ±1.7 (1) 12.1 ±4.3	44.0 ±3.0 (1) 49.0 ±3.4 (1) 46.5 ±8.3	650 - 824 650 - 824 650 - 749
(3) 50N:50	6.2 (1) 13.2	36.9 (1) 50.6	800 - 950 800 - 950
(4) 40N:60	5.2 (1) 9.8	32.6 (1) 41.5	800 - 950 800 - 950
(3) 30N:70	8.3 (1) 12.7	37.7 (1) 46.6	900 - 950 900 - 950

Notes:-

(i) All parameters obtained using equation (4.29)), assuming f = 1, except for those denoted by (1), which were calculated taking into account the thermodynamic term (see equation (1.47)), and those denoted by (4), which were calculated using the eutectic growth model, equation (4.36).

contd /----

(ii) Growth rate data was obtained in the present study except for the compositions denoted [2] (see ref. 62) and [3] (see ref. 20).

(iii) 95% confidence limits quoted for $\ln A_D'$ and $\Delta H_D'$, except for the compositions denoted [3], for which only a small amount of data was available.

(iv) Parameters calculated for the temperature range ΔT

Composition 100 ^{m}/o $BaSi_2O_5$

Figure 4.32 shows the growth rate data for this composition according to equation (4.29). The fit is good, but the values of $\Delta H_D'$ and ln A_D' are considerably larger than those obtained for the previous compositions, as shown in Table (4.5). It should be noted that the growth rates for the composition 100 ^{m}/o $BaSi_2O_5$ were obtained at a substantially higher temperature range than for other compositions in the $Li_2Si_2O_5$-$BaSi_2O_5$ system. Since $\Delta H_D'$ generally increases with decreasing temperature, its value for the 100 ^{m}/o $BaSi_2O_5$ composition at the lower temperatures used for the remaining compositions would be larger than that given in Table (4.5).

According to the earlier analysis of liquidus data, ΔH_f for $BaSi_2O_5$ is 8.6 k cal mole^{-1}. Since T_m is 1693°K, ΔS_f is about 2.6R. Hence $BaSi_2O_5$ is predicted to lie somewhere between those materials of low ΔS_f (< 2R), which are predicted to have smooth crystal-liquid interfaces during growth, and those materials of high ΔS_f (> 4-6R) which should exhibit a faceted crystal-liquid interface during growth. By experiment, the interface was found to be faceted (see Figure 3.6(a)). This would suggest that the screw dislocation model should describe the growth rate data for $BaSi_2O_5$, particularly at small supercoolings. The present data is unable to distinguish between the normal and screw dislocation models.

Discussion

If it is assumed that the preceding analysis of growth rate data for the $Li_2Si_2O_5$-$BaSi_2O_5$ system is correct, the major effect of adding $Li_2Si_2O_5$ to $BaSi_2O_5$ is to cause a substantial lowering in the diffusion

FIG. 4.32. GROWTH RATE DATA FOR THE COMPOSITION 100 m/o $BaSi_2O_5$ AS A FUNCTION OF $1/T$ (EQUATION 4.29)

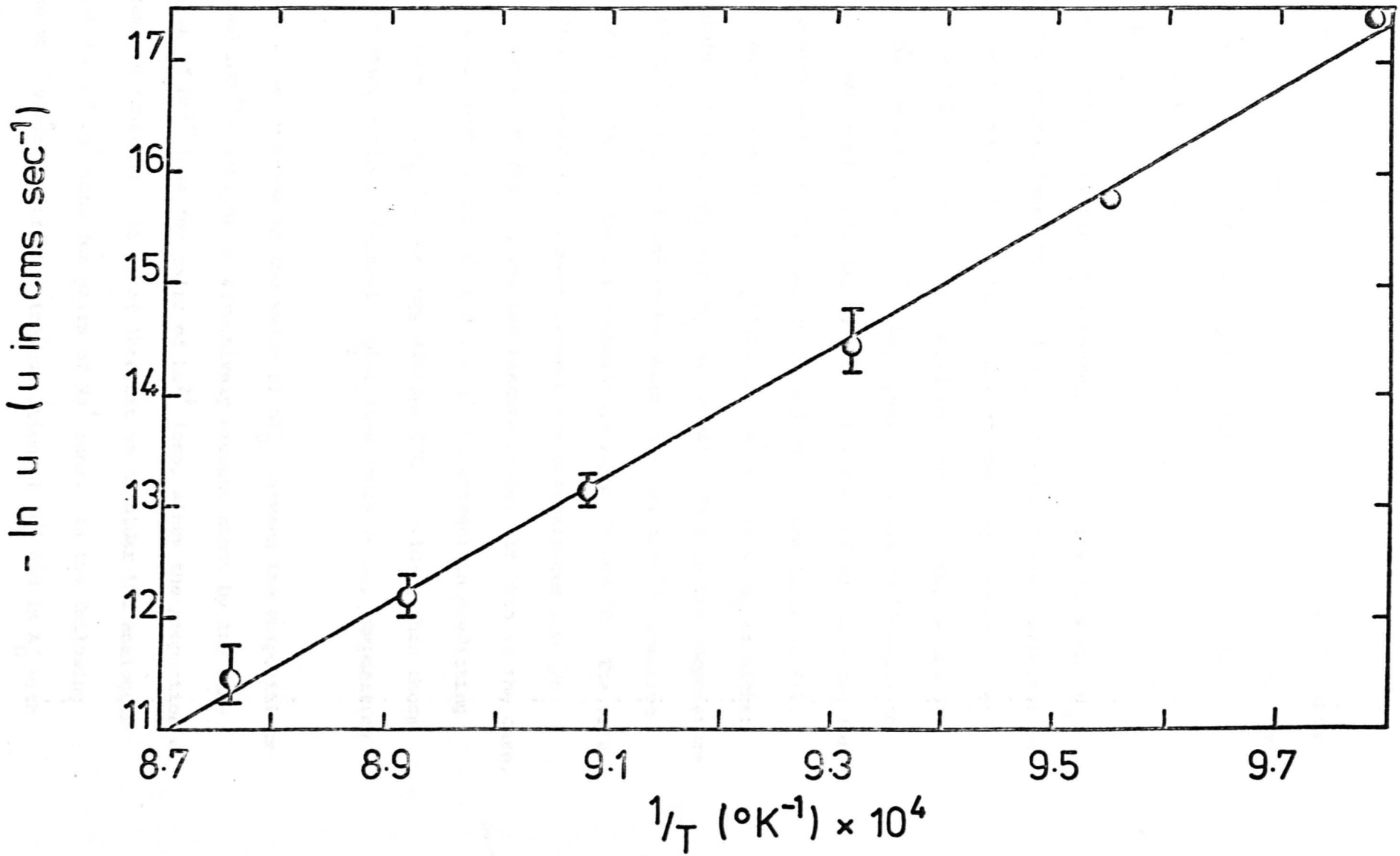

activation enthalpy for growth at the temperatures considered. This causes a large increase in the growth rates observed for compositions quite close to the 100 ^{m}/o $BaSi_2O_5$ composition in spite of the accompanying decrease in the value of A_D' by about 5 orders of magnitude.

The constancy, within experimental error, of the value of $\Delta H_D'$ between the compositions 100 ^{m}/o $Li_2Si_2O_5$ and 10:90 was unexpected in view of the increase in T_g which occurs between these compositions (see Figure 3.57). However, it should be noted that the values of $\Delta H_D'$ for the compositions 100 ^{m}/o $Li_2Si_2O_5$, 90:10 and 80:20 apply to somewhat lower temperature ranges than the values of $\Delta H_D'$ obtained for the compositions 60:40, 50L:50, 25:75 and 10:90 (see Table (4.5)). For the composition 100 ^{m}/o $Li_2Si_2O_5$ we can calculate $\Delta H_D'$ at higher temperatures assuming $\Delta H_D'$ and ΔH_η are equal. Thus in the temperature range 625-725°C $\Delta H_D'$ is found to be about 58 k cal mole^{-1}, compared with 67.6 k cal mole^{-1} for the temperature range 551-646°C. The value of $\Delta H_D'$ could therefore increase between the compositions 100 ^{m}/o $Li_2Si_2O_5$ and 60:40 for a given temperature range. If this is the case, the eutectic growth equation (4.36) might be correct in predicting larger values of ΔH_D for the compositions 50L:50 - 10:90 than those obtained using a simple Arrhenius plot (see Table (4.5), composition 50L:50).

The large increase in the value of $\Delta H_D'$ between the compositions 10:90 and 100 ^{m}/o $BaSi_2O_5$ is effectively brought about by the substitution of Ba^{2+} ions for pairs of Li^{2+} ions, since the proportion of SiO_2 remains constant. It is of interest to consider the analogous substitution of Ba^{+} ions for pairs of Na^{+} ions. In the following section we therefore determine the variation of $\Delta H_D'$ and ln A_D' with composition in the system $Na_2Si_2O_5$-$BaSi_2O_5$.

4.5.2 The system $Na_2Si_2O_5$-$BaSi_2O_5$

Composition 100 m/o $Na_2Si_2O_5$

The growth kinetics of this composition have been measured by several workers[60,61,62]. Meiling and Uhlmann[62] in addition to measuring growth kinetics also obtained viscosity data over a wide temperature range. This enabled them to determine the site factor, f, by utilizing the reduced growth concept discussed in Chapter 1. It was found that none of the simple growth models adequately described the reduced growth rate, although at supercoolings greater than 60°C (T_m = 874°C) a screw dislocation mechanism may be applicable. This is in agreement with the faceted morphology observed and the value of ΔS_f, which is about 3.7R. The growth rate of Scott and Pask[61] is in reasonable agreement with that of Meiling and Uhlmann. This would suggest that the work by Leontjewa[60] is unreliable since his data is considerably different from that of the previous workers mentioned. (This growth rate data given by Leontjewa for $Li_2Si_2O_5$ is also considerably different from that measured by later workers, including the present author).

The growth rate curve according to Meiling and Uhlmann is shown in Figure 4.33. The maximum growth rate occurs at about 810°C. In Figure 4.34, (curve A) the growth rates below 810°C have been plotted according to equation (4.29), assuming ln f to be relatively constant as compared with $\frac{1}{T}$. There is considerable curvature in the vicinity of T_{max}. This, however, is eliminated to a great extent by allowing for the thermodynamic term (see curve B, Figure 4.34). The thermodynamic term cannot be ignored as for $Li_2Si_2O_5$, since the measured rates are in this case for much smaller supercoolings. Thus at 650°C

FIG. 4.33. GROWTH RATE DATA FOR THE COMPOSITION 100 m/o $Na_2Si_2O_5$ ACC. REF. 62.

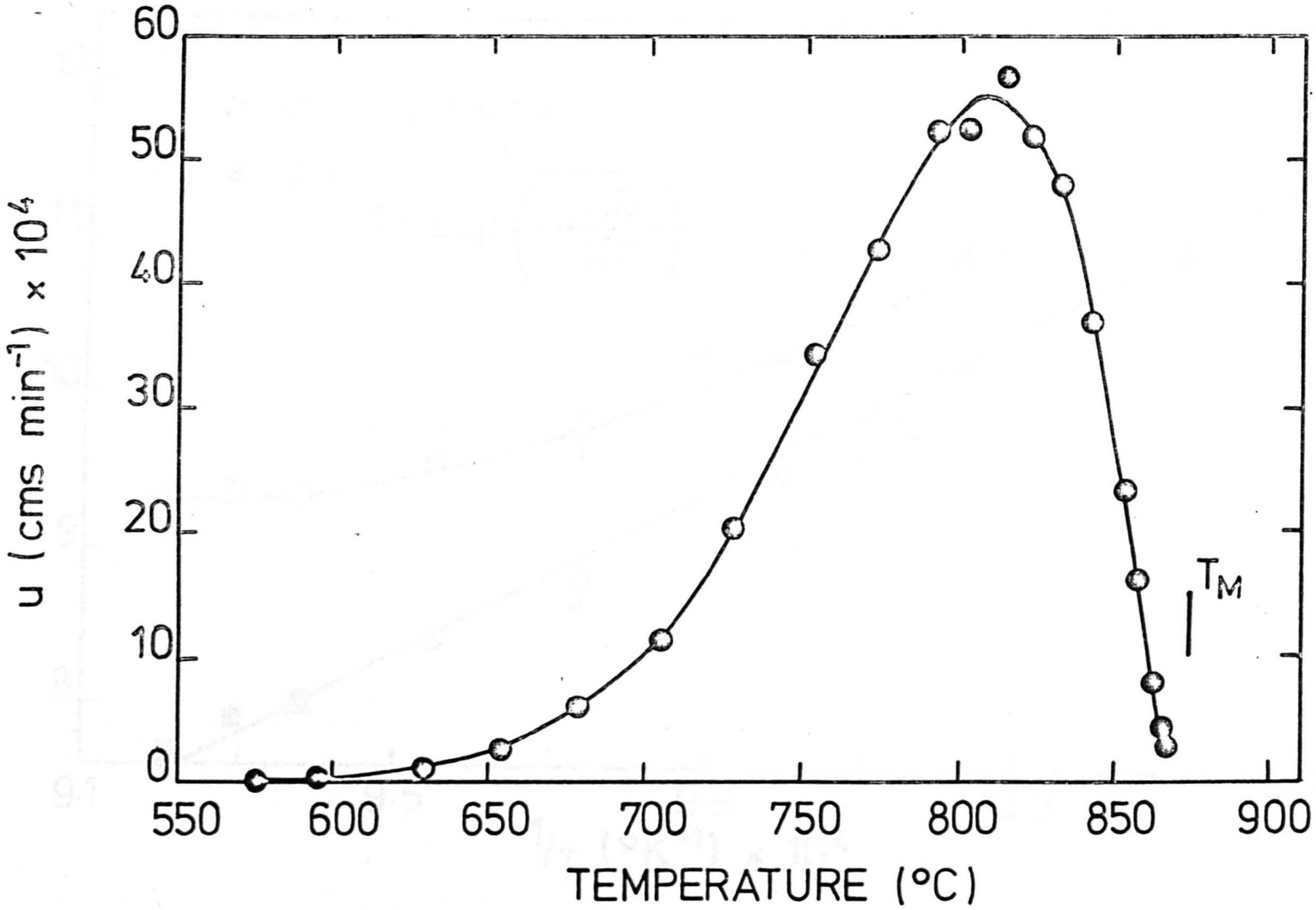

FIG. 4.34. GROWTH RATE DATA FOR THE COMPOSITION 100m/o $Na_2Si_2O_5$ AS A FUNCTION OF $1/T$. (DATA ACC. REF. 62)

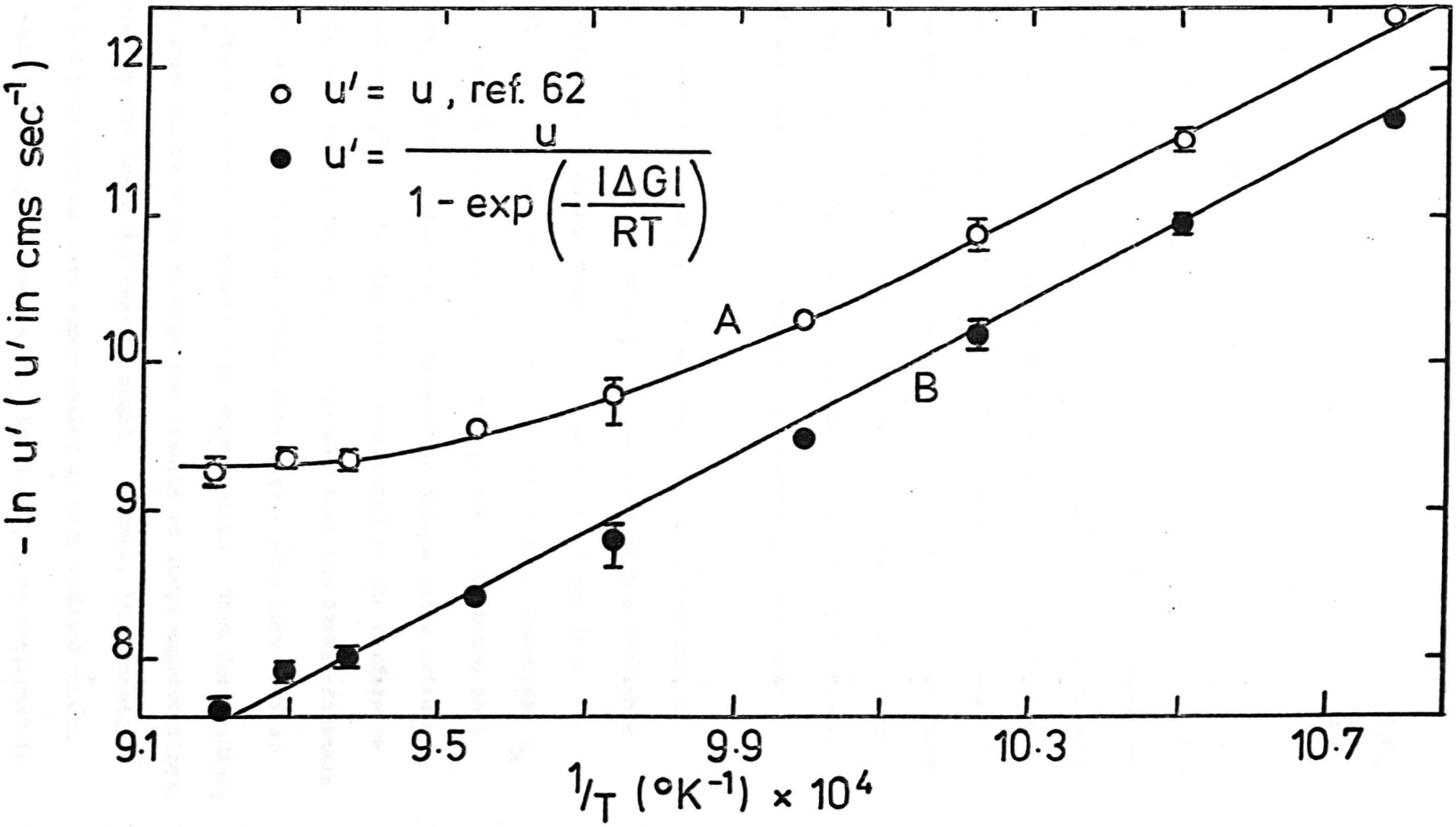

$[1 - \exp(-\frac{|\Delta G|}{RT})]$ equals about 0.88 and 0.63 for $Li_2Si_2O_5$ and $Na_2Si_2O_5$ respectively. In the simple Arrhenius plot, the thermodynamic term is assumed to be unity. From curve B, Figure 4.34, $\Delta H_D'$ and ln A_D' were calculated for the temperature ranges 575-645°C and 654-813°C respectively (see Table 4.5). A comparison with the values for $Li_2Si_2O_5$ calculated over a similar temperature range, shows that both parameters are probably lower in the case of $Na_2Si_2O_5$. It is interesting to note that although $Li_2Si_2O_5$ has a larger value of $\Delta H_D'$ than $Na_2Si_2O_5$, its growth rates are higher than those of $Na_2Si_2O_5$ by a factor of about 4. This is because A_D' is about 700 times larger for $Li_2Si_2O_5$. This shows that the equivalence of a low activation energy (enthalpy) with high growth rates, which is often assumed in the literature, is equivocal unless the magnitude of the pre-exponential factor is taken into account.

Whilst comparing $Na_2Si_2O_5$ with $Li_2Si_2O_5$, it is of interest to consider the growth rate data of $Na_2Si_2O_5$ in terms of the available viscosity data, as shown in Figure 4.35. As for $Li_2Si_2O_5$ (see Figure 4.25), $u\eta = u_R$ is almost constant and $AH_D' \simeq \Delta H_\eta$. Moreover, u_R is almost identical for $Na_2Si_2O_5$ and $Li_2Si_2O_5$, the values being 16.1 and 14.0 respectively. Thus the difference in growth rates between $Na_2Si_2O_5$ and $Li_2Si_2O_5$ can be completely attributed to the difference in viscosity between the two, if it is assumed that the Stokes-Einstein equation is valid. The reduced growth rate curves also show similar behaviour when plotted as a function of supercooling. Thus for $Na_2Si_2O_5$ a straight line can be drawn through the results at large supercoolings, as predicted by the screw dislocation model. However, this straight line does not pass through zero supercooling at zero reduced growth rate. A similar discrepancy is observed for $Li_2Si_2O_5$ as mentioned in section 4.51.

FIG. 4.35. A COMPARISON OF CRYSTAL GROWTH RATE DATA AND VISCOSCITY DATA AS A FUNCTION OF $^1/_T$ FOR THE COMPOSITION 100m/o $Na_2Si_2O_5$ (DATA ACC. REF. 62)

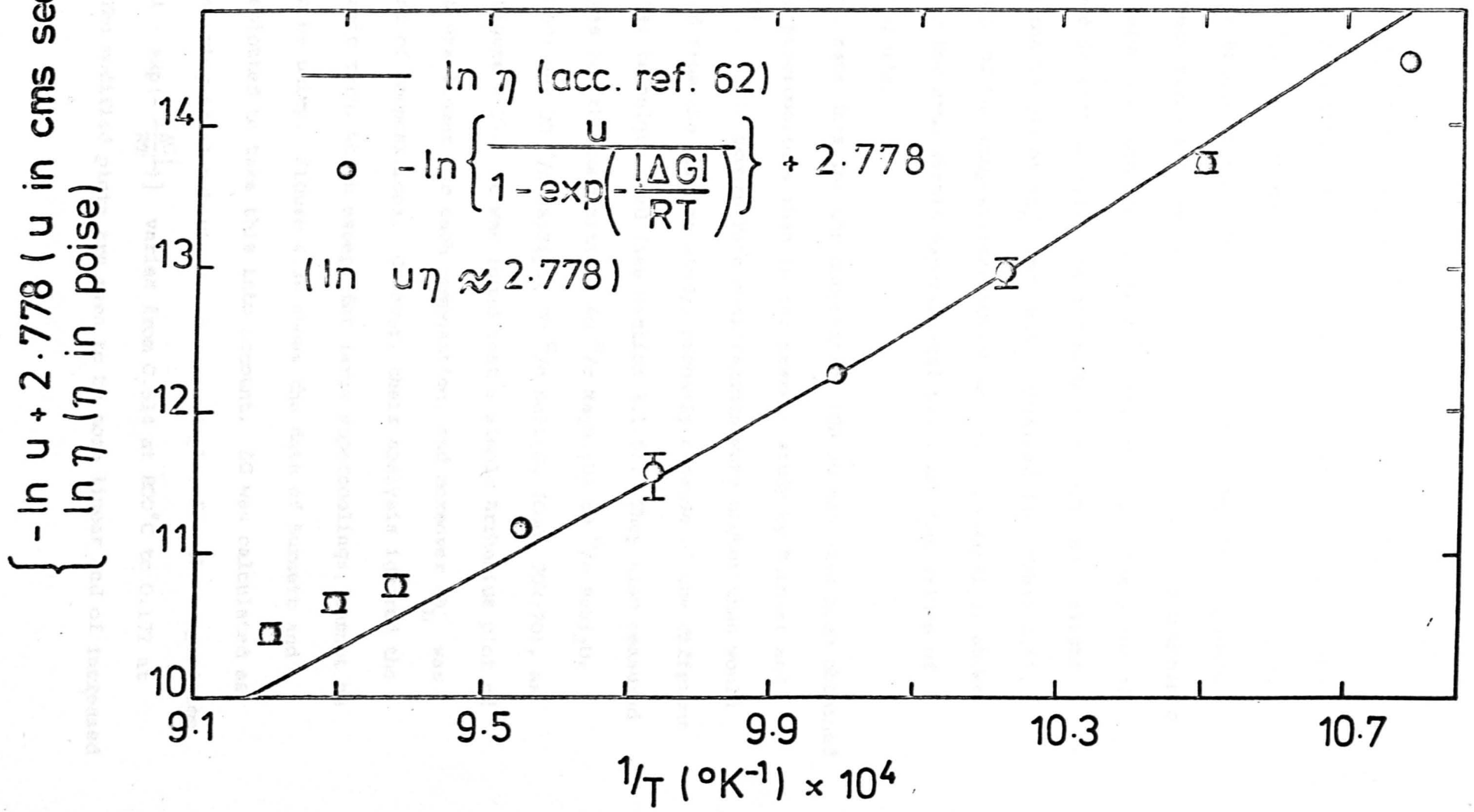

Composition 50 ^{m}/o $Na_2Si_2O_5$ 50 ^{m}/o $BaSi_2O_5$ (Code 50N-50)

Growth rate data for the composition 50N:50, obtained in the present study, is shown as a function of $\frac{1}{T}$ in Figure 4.36. Curve A is a simple Arrhenius plot, whereas for curve B the thermodynamic term has been taken into account (equation 1.47). The thermodynamic term was calculated assuming ΔG to be ideal and using the value of ΔH_f derived in section 4.1. The thermodynamic term has a slight effect on the values of $\Delta H_D'$ and ln A_D' obtained (see Table 4.5). A comparison of the compositions 50N:50 and 100 ^{m}/o $Na_2Si_2O_5$ shows that $\Delta H_D'$ is the same within experimental error and the values of ln A_D' are similar.

Growth rate data for the composition 50N:50 has also been obtained at smaller supercoolings than in the present study by Burnett and Douglas[20]. Their growth rate measurements were higher than would be expected from the present study, probably because of the different experimental technique used (see section 3.1.5). They also measured growth rates for the compositions 40 ^{m}/o $Na_2Si_2O_5$ 60 ^{m}/o $BaSi_2O_5$ (Code 40N:60) and 30 ^{m}/o $Na_2Si_2O_5$ 70 ^{m}/o $BaSi_2O_5$ (Code 30N:70), as shown in Figure 4.37. It was found that a simple Arrhenius plot of their data was linear for each composition, and moreover $\Delta H_D'$ was independent of compositions. However, their analysis ignored the thermodynamic term, which except for large supercoolings, cannot be assumed to be unity. Figure 4.38 shows the data of Burnett and Douglas replotted to take this into account. ΔG was calculated as before, assuming ideal behaviour. As an example, for the composition 40N:60, $[1 - \exp(-\frac{|\Delta G|}{RT})]$ varies from 0.614 at 800°C to 0.172 at 1050°C. The modified plots are seen to be more linear and of increased

FIG. 4.36. GROWTH RATE DATA FOR THE COMPOSITION 50N:50 AS A FUNCTION OF $^1/_T$.

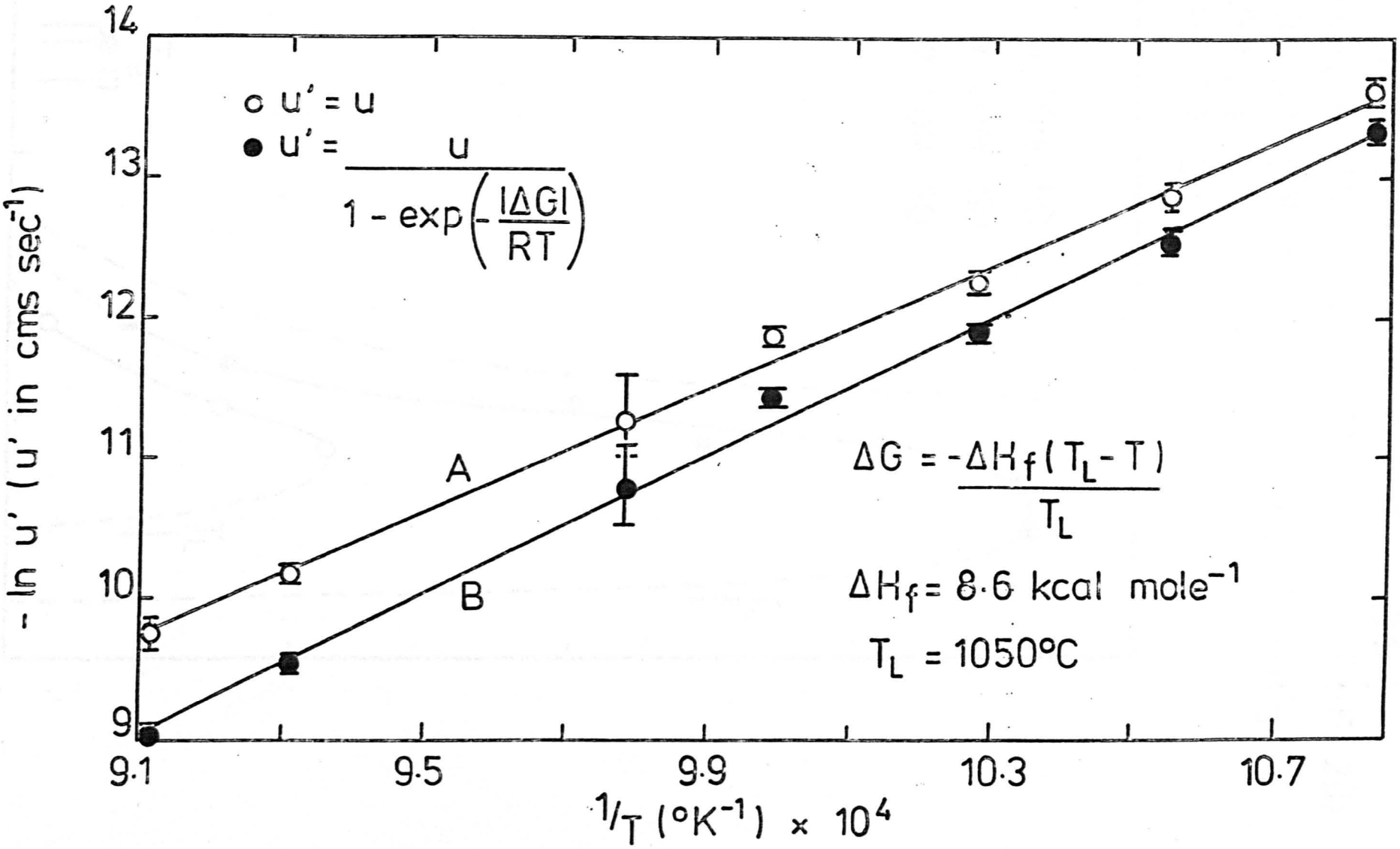

FIG. 4.37. CRYSTAL GROWTH RATE CURVES FOR COMPOSITIONS IN THE SYSTEM $Na_2Si_2O_5 - BaSi_2O_5$ (ALL DATA ACC. REF. 20)

CODE: 50N:50 50 m/o $Na_2Si_2O_5$ 50 m/o $BaSi_2O_5$
40N:60 40 " " 60 " "
30N:70 30 " " 70 " "

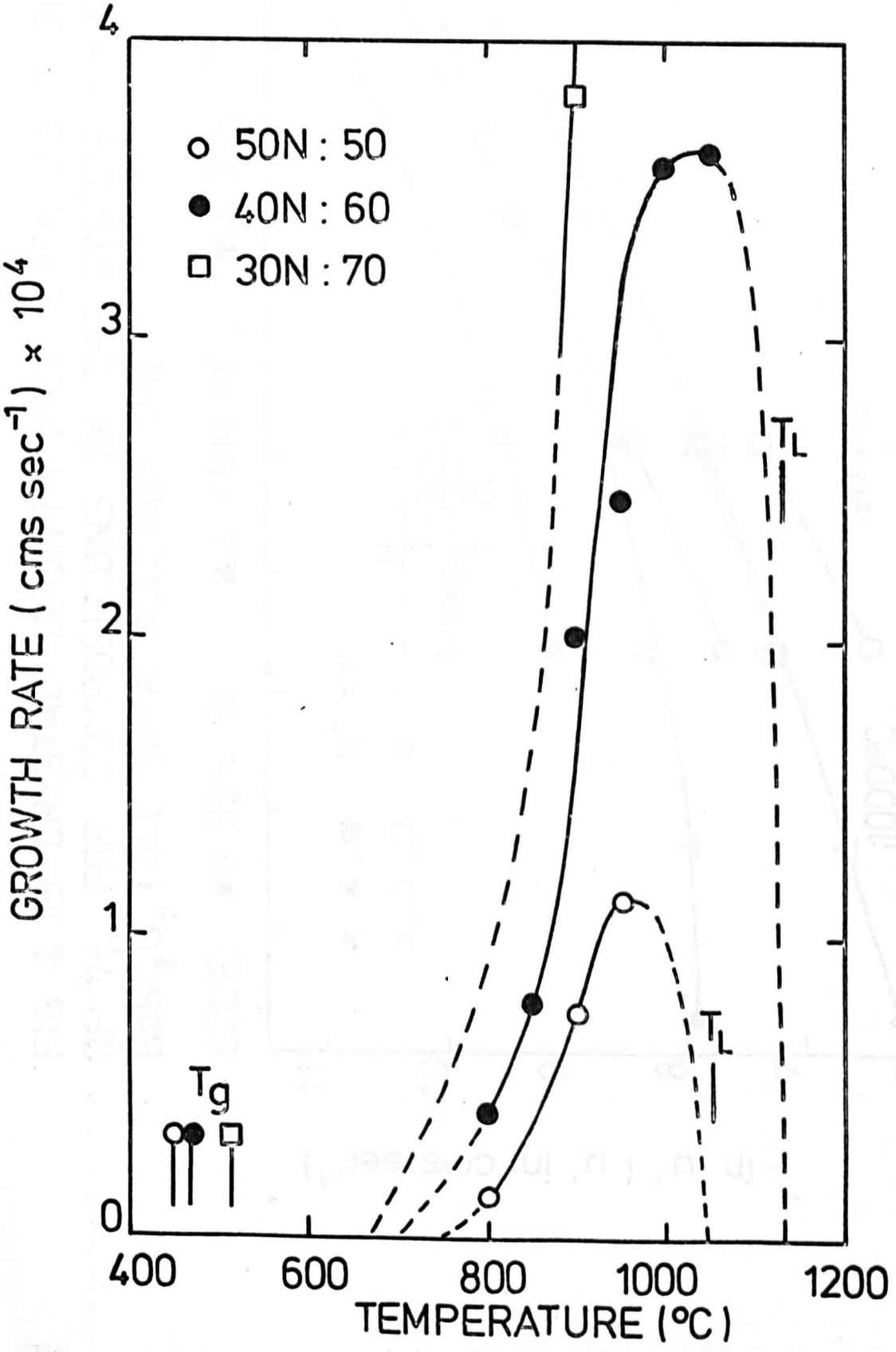

FIG. 4.38. CRYSTAL GROWTH RATE DATA AS A FUNCTION OF $^1/_T$ FOR COMPOSITIONS IN THE SYSTEM $Na_2Si_2O_5$ - $BaSi_2O_5$ (ALL DATA ACC. REF. 20)

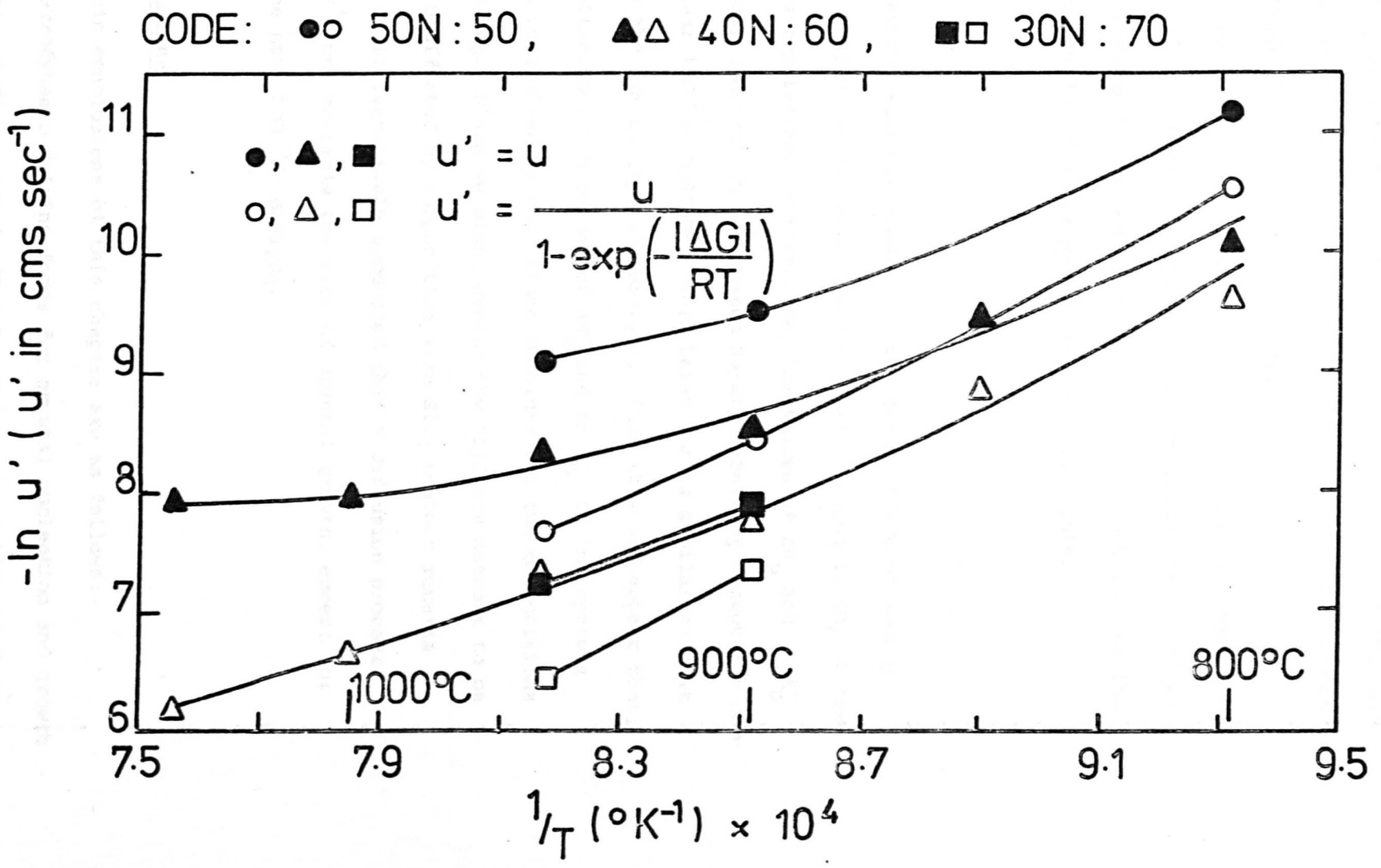

gradient. $\Delta H_D'$ has remained approximately independent of composition, but its value is in better agreement with that obtained in the present study (see Table (4.5)). It should be mentioned that T_g increases with $BaSi_2O_5$ content, as was found in the $Li_2Si_2O_5$-$BaSi_2O_5$ system (see Figure 4.37). Unfortunately, a direct comparison of T_g values for the two systems is not possible, as it is not known whether the DTA apparatus used by Burnett and Douglas was calibrated.

Discussion

The previous analysis shows that the major effect of adding $Na_2Si_2O_5$ to $BaSi_2O_5$ is to cause a substantial lowering in $\Delta H_D'$ at the temperatures considered. Furthermore, the values of $\Delta H_D'$ and $\ln A_D'$ are relatively constant in the system $Na_2Si_2O_5$-$BaSi_2O_5$ except for compositions near 100 $^m/_o$ $BaSi_2O_5$. This behaviour is similar to that observed in the system $Li_2Si_2O_5$-$BaSi_2O_5$. Thus it would appear that, as a generalisation, the values of $\Delta H_D'$ and $\ln A_D'$ in the systems $R_2Si_2O_5$ are determined by the values obtained for the compositions 100 $^m/_o$ $R_2Si_2O_5$. Since we might expect the silicate network to be relatively unaffected by composition (the SiO_2 content remains constant), it is tentatively suggested that a diffusion process involving R^+ ions controls the rate of crystal growth, except for compositions near 100 $^m/_o$ $BaSi_2O_5$.

4.6 Conclusions

The main conclusions of this chapter are as follows:-

1) The thermodynamic driving force for crystal nucleation and growth in the systems $R_2Si_2O_5$-$BaSi_2O_5$ (R ≡ Li, Na) can be estimated from liquidus data.

2) Nucleation kinetics can be analysed in three ways, the nucleation parameters obtained depending on the method chosen. In general, nucleation theory cannot be fitted to data below T_{max}. Also the experimental values of the pre-exponential factor are considerably larger than theory predicts.

3) The higher nucleation rates for 100 $^{m}/_{o}$ $BaSi_2O_5$, as compared with 100 $^{m}/_{o}$ $Li_2Si_2O_5$, are mainly due to the lower value of σ, the interfacial surface free energy, for the former composition. This assumes that k_5 equals $\frac{16\pi}{3}$ for both compositions.

4) The nucleation parameters are all dependent on composition. Thus nucleation behaviour cannot be simply related to liquidus data in the systems $R_2Si_2O_5$-$BaSi_2O_5$.

5) Growth kinetics can generally be analysed as simple Arrhenius plots at large supercoolings. However, the experimental values of the pre-exponential factor are larger than theory predicts, ignoring ΔS_D.

6) The addition of $R_2Si_2O_5$ to $BaSi_2O_5$ causes a large decrease in the growth rate parameters $\Delta H_D'$ and $\ln A_D'$. The values of $\Delta H_D'$ and $\ln A_D'$ are almost constant in the systems $R_2Si_2O_5$-$BaSi_2O_5$, except for compositions near 100 $^{m}/_{o}$ $BaSi_2O_5$, and are determined by the values obtained for the compositions 100 $^{m}/_{o}$ $R_2Si_2O_5$.

CHAPTER 5

FURTHER DISCUSSION AND SUGGESTIONS FOR FUTURE WORK

Chapter 5

Further discussion is restricted to nucleation kinetics, detailed consideration being given to the interfacial energy and free energy of formation of embryos.

The suggestions for future work are given as ideas for usefully extending the experimental results presented in this thesis.

5.1 Further discussion of classical nucleation theory

5.1.1. The microscopic interpretation of interfacial free energy and the capillary approximation

In Chapter 1 an embryo was treated as a microscopic quantity of bulk material having a definite geometrical surface. Furthermore, the interfacial energy of the embryo-parent phase boundary was assumed independent of embryo size. On a microscopic scale, however, an interface will not be uniquely located. Rather there will be gradients in both chemical composition and degree of ordering as one passes from the embryo into the parent phase. As far as the author is aware, no quantitative evaluation of this complex situation has been made in the case of a crystal-liquid interface. However, the interfacial energy between two liquids has been considered, assuming that compositional gradients are the major factor[63]. It is shown that the interface, although diffuse, can be considered as having a characteristic thickness which increases with increasing temperature until at the critical temperature, where the two liquids attain the same composition, the interface is infinite in extent. This diffuse interface theory is of particular importance in the theory of spinodal decomposition[10]. Spinodal decomposition in glass forming systems was briefly referred to in Chapter 1, while discussing liquid-liquid immiscibility.

It has been shown by several workers that if a spherical embryo is assumed to have a well defined geometrical surface, the interfacial energy defined with reference to this surface will decrease with decreasing embryo size[64,65]. Neglect of this effect is often referred to as the capillary approximation. Since direct measurements of interfacial energy refer to a relatively planar interface, they will give values larger than those obtained from nucleation kinetics. The discrepancy is perhaps about 15% for a critical nucleus containing 13 atoms[65]. Thus the use of experimentally measured (macroscopic) values of $\bar{\sigma}$ to predict nucleation rates could lead to considerable error if the critical nucleus contains only a small number of atoms.

5.1.2. Statistical mechanical contributions to the free energy of formation of embryos

Lothe and Pound[3,66] have reconsidered the several contributions to the free energy of formation of an embryo and conclude that several important contributions are neglected in the classical derivation of W, as given by equation (1.22). These are not concerned with the capillary approximation referred to above. They mainly arise from a consideration of the translational and rotational free energy of the embryo. Although r* and n* are only slightly changed by these additional free energy terms, the probability of finding a critical size nucleus per unit volume is considerably greater than that predicted by equation (1.25). This causes an effective increase in the value of the pre-exponential factor. In the case of homogeneous nucleation of crystalline embryos from a liquid the rotational contribution is suggested as being the most important. On the basis of results for

supercooled mercury[67] an approximate value of the pre-exponential factor is calculated to be 10^{47} cm^{-3} sec^{-1}, compared with the experimental value of 10^{42} cm^{-3} sec^{-1} and the theoretical value of 10^{35} cm^{-3} sec^{-1}. Thus the correction to classical theory is greater than would be required by experiment in the case of supercooled mercury. However, the discrepancy between classical theory and experiment found in the present study of supercooled silicates is far greater than the correction factor calculated by Lothe and Pound. Furthermore, Lothe and Pound suggest that the statistical mechanical contributions mentioned above may be smaller in the case of more complex liquids, leading to better agteement with classical theory.

5.1.3 The effect of a temperature dependent interfacial energy

Very recent results have been obtained for the homogeneous nucleation of supercooled gallium[68]. The pre-exponential factor was found to be almost 10^{40} cm^{-3} sec^{-1}, similar to the value of 10^{42} cm^{-3} sec^{-1} obtained for supercooled mercury, but a factor of 10^{6} greater than the value calculated from classical theory. This discrepancy was explained by assuming a linear temperature dependence for the interfacial free energy (see equation (4.3)), the interfacial entropy being negative. Thus the interfacial energy decreases with decreasing temperature. An analysis of the results for supercooled mercury gives similar results. It was concluded, therefore, that classical theory is able to explain nucleation data for metals, withour recourse to any statistical-mechanical corrections.

It is of interest to calculate the interfacial entropy required in order that the pre-exponential factor obtained for the nucleation of

$Li_2Si_2O_5$ is in agreement with classical theory. Combining the equations given in reference (68) with equation (4.22) (Method 4 for analysing nucleation rates) we find that the experimentally obtained value of $\ln A_\eta$ (112.9) is reduced to the theoretical value (82.1) if σ is expressed in ergs cm^{-2} as

$$\sigma = 120.7 + 0.054T \qquad (5.1)$$

Thus the interfacial entropy is negative as in the case of metals. It is interesting to note that a value of -0.055 was obtained for gallium. From equation (5.1), σ is 162 ergs cm^{-2} at 500°C compared with the constant value of 185 ergs cm^{-2}, obtained assuming σ to be independent of temperature. Thus we can account for the large values of A_η obtained by experiment if σ is assumed to decrease linearly as the temperature falls. It should be remembered, however, that the experimental values of A_η and the original temperature independent σ were determined from an analysis of nucleation data for temperatures above T_{max}. On the basis of these parameters the predicted nucleation rates below T_{max} were found to be greater than the nucleation rates observed by experiment (see Figure 4.14). This discrepancy in the overall magnitude of the nucleation rates below T_{max} will remain unaltered if σ is expressed as equation (5.1), since the equation is only valid above T_{max} and accounts solely for the magnitude of A_η. Indeed, if A_η is assumed to be constant at all temperatures, the discrepancy in the magnitude of the experimental nucletion rate below T_{max} can be explained in terms of a σ which increases with decreasing temperature below T_{max}. This is contrary to the temperature variation of σ predicted by

equation (5.1) for temperatures above T_{max}. Unfortunately the nucleation kinetics for gallium were not measured below T_{max} and therefore a comparison with the present results is not possible.

5.1.4 The free energy of formation of classical non-spherical clusters

In Chapter 1 we considered the free energy of formation of a spherical cluster (see equation (1.22)). However, consider the more general case of a cluster exhibiting 'i' facets. The free energy of formation in this case is given by

$$W = \frac{V\Delta G}{V_m} \sum_i A_i \sigma_i \qquad (5.2)$$

where V is the volume of the embryo,

A_i is the surface area of the 'i'th facet,

and σ_i is the interfacial surface energy of the 'i'th facet.

This neglects any contributions from the edges or corners of the cluster. The total area and volume of a given cluster can be expressed in terms of shape factors and a characteristic dimension, X (we will assume all clusters in a given system are of the same shape). Thus

$$\sum_{i=1} A_i = k_2 X^2 \qquad (5.3)$$

$$V = k_3 X^3 \qquad (5.4)$$

Also, we can define an average interfacial surface energy as follows

$$\bar{\sigma} = \frac{\sum_{i=1} A_i \sigma_i}{\sum_{i=1} A_i} \tag{5.5}$$

Substituting equations (5.3), (5.4) and (5.5) into equation (5.2) we obtain

$$W = \frac{k_3 \Delta G X^3}{V_m} + k_2 \bar{\sigma} X^2 \tag{5.6}$$

Differentiating W with respect to X and setting equal to zero we obtain

$$X^* = - \frac{k_4 \bar{\sigma} V_m}{\Delta G} \tag{5.7}$$

where $k_4 = \frac{2k_2}{3k_3}$

and the superscript * denotes a property of the critical nucleus, as in Chapter 1. Substituting equation (5.7) into equation (5.6), the free energy of formation of a critical nucleus is found to be

$$W^* = \frac{k_5 \bar{\sigma}^3 V_m^2}{\Delta G^2} \tag{5.8}$$

where $k_5 = \frac{1}{2} k_3 k_4^3$

It is of interest to consider certain simple shaped clusters in

more detail. In general nucleation kinetics only give information about the product $k_5\bar{\sigma}^3$. However, given the shape and dimensions of the critical nucleus it is possible to estimate $\bar{\sigma}$ and σ_i.

Spherical cluster

Since the total surface area and volume are simply given by

$$\sum A_i = 4\pi r^2$$

$$V = \frac{4}{3}\pi r^3$$

we find by comparison with equations (5.3) and (5.4)

$$X = r \ , \ k_2 = 4\pi \ , \ k_3 = \frac{4}{3}\pi$$

Hence from equations (5.7) and (5.8)

$$\left.\begin{aligned} r^* &= -\frac{2\sigma V_m}{\Delta G} \\ W^* &= \frac{16\pi\sigma^3 V_m^2}{3\Delta G^2} \end{aligned}\right\} \qquad (1.23)$$

as derived in Chapter 1. The interfacial surface energy is of course isotropic and $\bar{\sigma}$ has been replaced by σ.

Cylindrical cluster

The total surface area of a cylinder can be expressed as

$$\sum A_i = 2\pi (1 + \frac{\ell}{r}) r^2$$

where ℓ and r are the length and radius of the cylinder respectively. The volume is given by

$$V = (\frac{\pi \ell}{r}) r^3$$

By comparison with equations (5.3) and (5.4) we find

$$X = r \ , \ k_2 = 2\pi (1 + \frac{\ell}{r}) \ , \ k_3 = \pi \frac{\ell}{r}$$

Hence from equations (5.7) and (5.8)

$$r^* = - \frac{4}{3}(\frac{r}{\ell} + 1) \frac{\bar{\sigma} V_m}{\Delta G} \tag{5.9}$$

$$W^* = \frac{32\pi}{27} \frac{(r + \ell)^3}{r\ell^2} \frac{\bar{\sigma}^3 V_m^2}{\Delta G^2} \tag{5.10}$$

The shape factors k_2 and k_3 and hence the ratio $\frac{\ell}{r}$ are assumed to be independent of cluster size.

As shown in Appendix A5.1, $\bar{\sigma}$ for a cylindrical cluster can be expressed in terms of two interfacial surface energies, σ_1 and σ_2 (see Figure 5.1(b)). Thus

$$\bar{\sigma} = (\frac{3r}{r + \ell}) \sigma_1 \tag{5.11}$$

$$= \left\{ \frac{3\ell}{2(r + \ell)} \right\} \sigma_2 \tag{5.12}$$

FIG. 5.1. DEFINITION OF INTERFACIAL SURFACE ENERGIES FOR DIFFERENT SHAPED CLUSTERS.

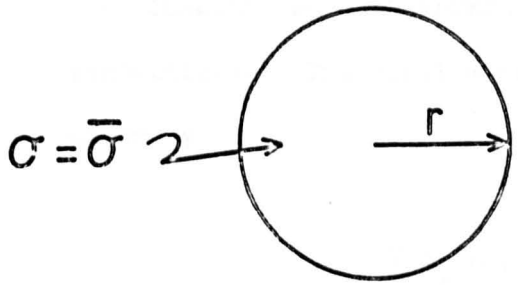

(a)
spherical cluster

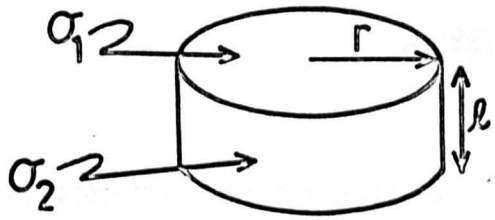

(b)
cylindrical cluster

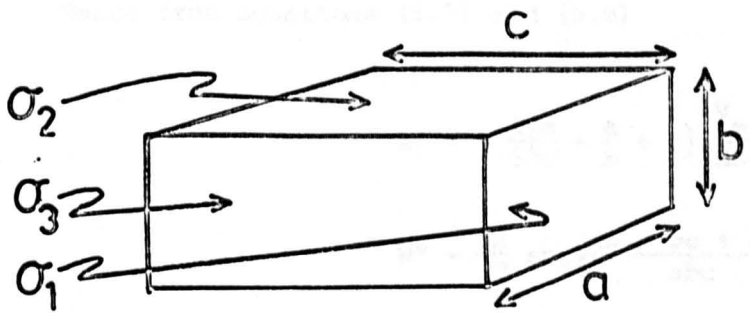

(c)
orthorhombic cluster

where σ_1 refers to the flat ends and σ_2 to the curved surface of the cylinder.

Orthorhombic cluster

Consider an orthorhombic cluster with sides of length a, b and c respectively. The total surface area and volume of the cluster are given by

$$\sum A_i = 2(ab + bc + ca)$$

$$= 2\left(\frac{b}{a} + \frac{bc}{a^2} + \frac{c}{a}\right)a^2$$

$$V = abc$$

$$= \left(\frac{bc}{a^2}\right)a^3$$

By comparison with equations (5.3) snd (5.4) we find

$$X = a \ , \ k_2 = 2\left(\frac{b}{a} + \frac{bc}{a^2} + \frac{c}{a}\right) \ , \ k_3 = \frac{bc}{a^2}$$

Hence from equations (5.7) and (5.8)

$$a^* = -\frac{4}{3}\left(\frac{a}{c} + \frac{a}{b} + 1\right)\frac{\bar{\sigma}V_m}{\Delta G} \qquad (5.13)$$

$$W^* = \frac{32}{27}\,abc\left(\frac{ab + bc + ac}{abc}\right)\frac{\bar{\sigma}^3 V_m^{\,2}}{\Delta G^2} \qquad (5.14)$$

The shape factor k_2 and k_3 and hence the ratios $\frac{a}{c}$ and $\frac{a}{b}$ are assumed to be independent of cluster size.

As shown in Appendix A.5.1, $\bar{\sigma}$ for an orthorhombic cluster can be expressed in terms of three interfacial energies, σ_1, σ_2 and σ_3 (see Figure 5.1(c)). Thus

$$\bar{\sigma} = \frac{3\sigma_1}{\left(1 + \frac{c}{a} + \frac{c}{b}\right)} \tag{5.15}$$

$$= \frac{3\sigma_2}{\left(1 + \frac{b}{a} + \frac{b}{c}\right)} \tag{5.16}$$

$$= \frac{3\sigma_3}{\left(1 + \frac{a}{b} + \frac{a}{c}\right)} \tag{5.17}$$

where σ_1, σ_2 and σ_3 refer to the sides of area ab, ac and bc respectively.

It is of interest to apply the above expressions to the nucleation results available for the composition 100 $^{m}/_{o}$ $Li_2Si_2O_5$ [23]. These were analysed in Chapter 4 assuming the critical nucleus to be spherical. However, high voltage transmission electron microscopy has shown that $Li_2Si_2O_5$ crystals are plate-like at a very early stage of crystallisation, as shown in Figure 5.2 [59]. The approximate shape is shown in Figure 5.3, the three crystallographic axes a, b and c being in the approximate ratio 2.7:1:4.5.

Let us first assume that this plate-like shape is approximately equivalent to a thin slice of a cylinder, radius $\sqrt{\frac{ac}{2}}$, length b. Hence $\frac{r}{\ell} = 1.743$ and k_5 is found to be 14π. Using Method 4 for analysing nucleation rates and assuming a cylindrical shaped critical nucleus we

Fig. 5.2 Thin-film electron micrographs taken at 1000 kV, showing lithium disilicate crystals in a glass of composition close to stoichiometric lithium disilicate. The bars denote 2 μm

Top: Glass heated at 490°C for 65 hours

Bottom: Glass heated at 490°C for 94 hours

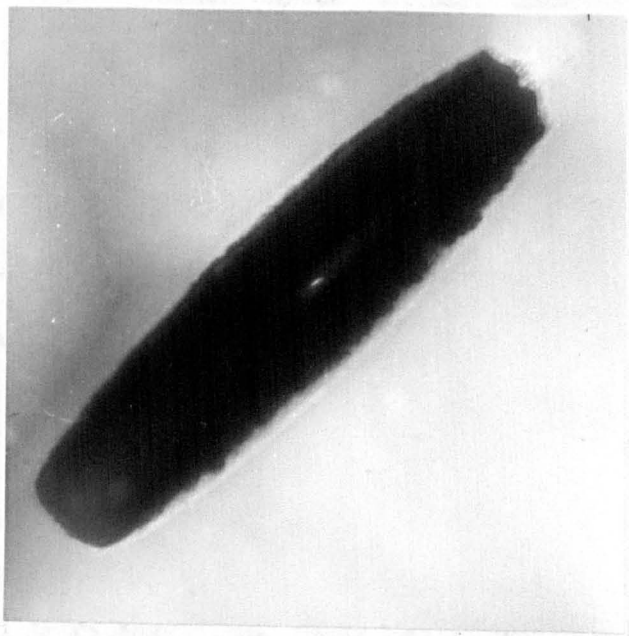

FIG. 5.3. APPROXIMATE SHAPE OF $Li_2Si_2O_5$ CRYSTALS DURING THE EARLY STAGES OF CRYSTALLISATION OF A 100 m/o $Li_2Si_2O_5$ GLASS, AS SEEN ALONG (i) [001]; (ii) [100], AND (iii) [010]. (ACC. REF. 59)

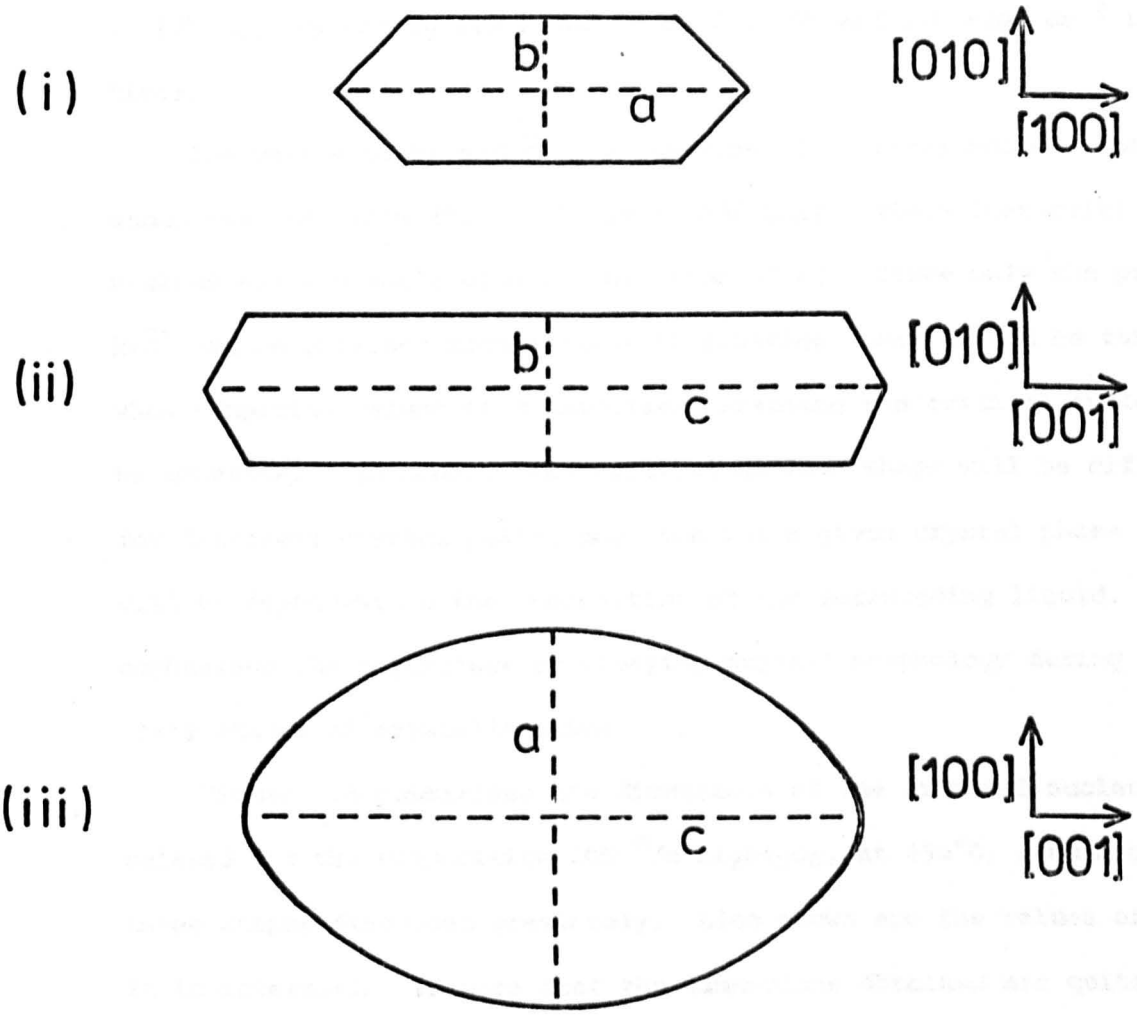

a : b : c = 2·7 : 1 : 4·5

therefore obtain $\bar{\sigma}$ = 135 ergs cm^{-2}, and from equations (5.11) and (5.12), σ_1 = 71 ergs cm^{-2} and σ_2 = 246 ergs cm^{-2}.

Secondly, we will assume that the plate-like shape is approximately orthorhombic, with sides of length a, b and c. Hence $\frac{a}{c} = 0.6$, $\frac{a}{b} = 2.7$ and k_5 is found to be 58.16 (= 18.5π). Using Method 4 for analysing nucleation rates and assuming an orthorhombic shaped critical nucleus we therefore obtain $\bar{\sigma}$ = 122.5 ergs cm^{-2}. From equations (5.15), (5.16) and (5.17), σ_1, σ_2 and σ_3 are found to be 293, 65 and 176 ergs cm^{-2} respectively.

The values of k_5 and $\bar{\sigma}$ as a function of critical nucleus shape are summarised in Table (5.1). It is immediately obvious that critical nucleus shape greatly affects the value of $\bar{\sigma}$. Since only the product $k_5\bar{\sigma}^3$ can be obtained from nucleation kinetics, care should be taken when comparing values of $\bar{\sigma}$ calculated assuming the critical nucleus to be spherical. In general the critical nucleus shape will be different for different crystal phases and even for a given crystal phase the shape will be dependent on the composition of the surrounding liquid. This emphasises the importance of studying crystal morphology during the very early stages of crystallisation.

Figure 5.4 summarises the dimensions of the critical nucleus calculated for the composition 100 $^{m}/_{o}$ $Li_2Si_2O_5$, at 450°C, assuming the three shapes discussed previously. Also shown are the values of σ_i. It is interesting to note that the dimensions obtained are quite reasonable. For example, assuming the critical nucleus to be orthorhombic, its volume is about 12 times that of the unit cell of $Li_2Si_2O_5$, calculated from X-ray diffraction[69]. Since the unit cell contains four formula units of $Li_2Si_2O_5$ i.e. eight SiO_2 tetrahedra, we expect the critical nucleus to contain approximately 96 SiO_2 tetrahedra. As discussed in

TABLE 5.1

k_5 AND $\bar{\sigma}$ AS A FUNCTION OF CRITICAL NUCLEUS SHAPE

Shape of critical nucleus	k_5	$\bar{\sigma}$ ergs cm^{-2}
spherical	5.3π	185.5
cylindrical	14.0π	134.5
orthorhombic	18.5π	122.5

NOTE: $\bar{\sigma}$ calculated using Method 4 of analysing nucleation kinetics

FIG. 5.4. PROPERTIES OF THE CRITICAL NUCLEUS FOR THE COMPOSITION 100 m/o $Li_2Si_2O_5$ AT 450°C, AS A FUNCTION OF NUCLEUS SHAPE.

a) spherical

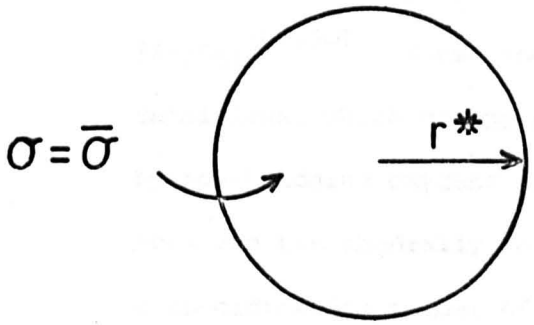

$r^* = 10.4$ Å
$\sigma = 186$ ergs cm^{-2}

b) cylindrical

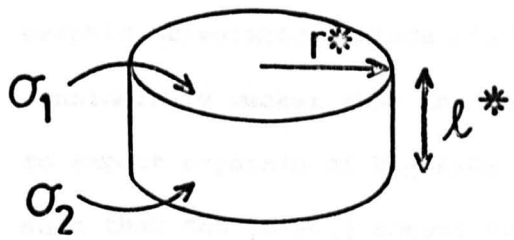

$r^* = 13.8$ Å
$\ell^* = 7.9$ Å
$\sigma_1 = 71$ ergs cm^{-2}
$\sigma_2 = 246$ ergs cm^{-2}

c) orthorhombic

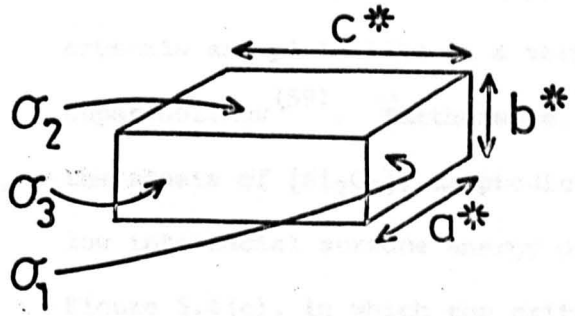

$a^* = 19.7$ Å
$b^* = 7.3$ Å
$c^* = 32.8$ Å
$\sigma_1 = 293$ ergs cm^{-2}
$\sigma_2 = 65$ ergs cm^{-2}
$\sigma_3 = 176$ ergs cm^{-2}

the next section, these tetrahedra will tend to form a sheet structure, parallel to (010).

5.1.5 The calculation of the interfacial energy

Both $Li_2Si_2O_5$ and $BaSi_2O_5$ are layer type silicates, the silica tetrahedra being joined together to form sheets of net composition $[Si_2O_5]$[69,70]. These sheets are effectively linked together by the metal ions, which occupy sites between the sheets and are co-ordinated by non-bridging oxygens and/or bridging oxygens. In $Li_2Si_2O_5$ the Li^+ ions are tetrahedrally co-ordinated and in $BaSi_2O_5$ the Ba^{2+} ions have a co-ordination number of ten. Projections of the structures of $Li_2Si_2O_5$ and $BaSi_2O_5$ are shown in Figures 5.5 and 5.6

The layered structure of the disilicates is expected to cause a marked anisotropy in their surface energy as a function of crystallographic orientation, since bonding between layers is expected to be considerably weaker than the bonding within layers. Thus it is reasonable to expect crystals of $Li_2Si_2O_5$ or $BaSi_2O_5$ to nucleate and grow as plates, such that the $[Si_2O_5]$ sheets are parallel to the plane of the crystal plate. In this way, the total crystal-liquid interfacial energy is kept to a minimum.

Recent electron microscopy work has indeed shown that $Li_2Si_2O_5$ crystals are plate-like at a very early stage of crystallisation at large supercoolings[59]. Furthermore, the plane of the plate is parallel to the sheets of $[Si_2O_5]$, as predicted (compare Figures 5.3 and 5.5). The low interfacial surface energy of this (010) plane is emphasised in Figure 5.4(c), in which the critical nucleus is assumed to be orthorhombic in shape. These observations are supported by earlier work in which crystals of $Li_2Si_2O_5$ were formed at temperatures near the melting

Left: Fig. 5.5 Crystal structure of $Li_2Si_2O_5$ showing projections along (a) [001], (b) [100] and (c) [010] acc. ref. 69. Chains of SiO_4 tetrahedra are linked together to form corrugated sheets. The lithium ions are represented by black triangles.

Right: Fig. 5.6 Crystal structure of high temperature $BaSi_2O_5$ showing (a) a projection along [010] and (b) a partial projection along [001] acc. ref. 70. Chains of SiO_4 tetrahedra are linked together to form corrugated sheets. The barium ions are represented by black dots.

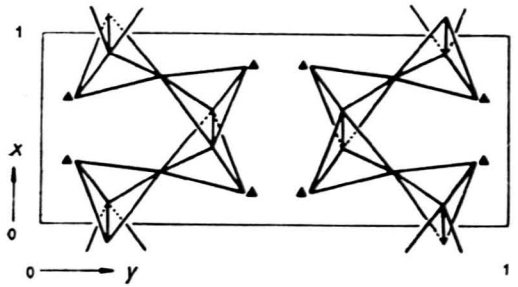
1
x
0
0
y
1

(a)

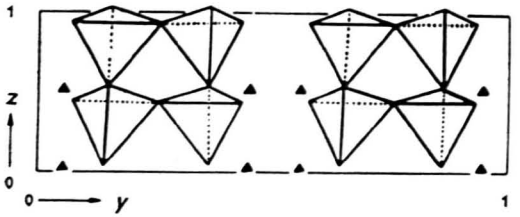
1
z
0
0
y
1

(b)

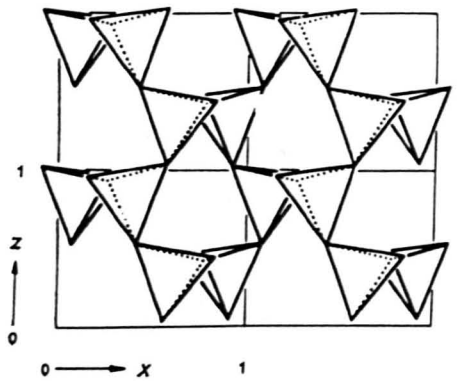
1
z
0
0
x
1

(c)

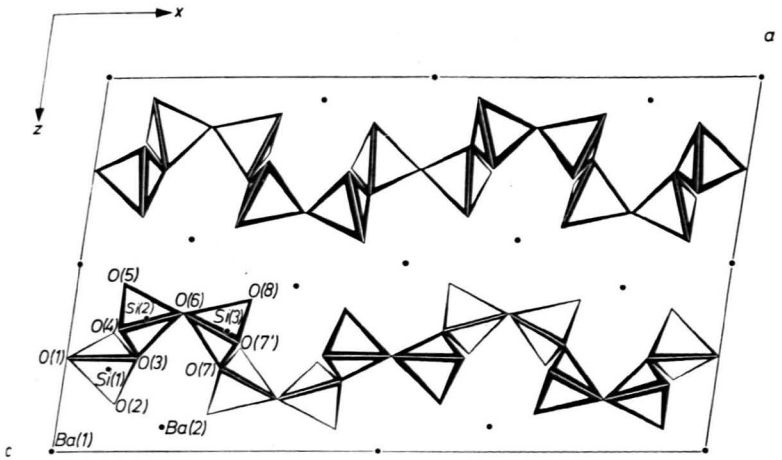
x
z
a
O(5)
O(6)
O(8)
Si(2)
Si(3)
O(4)
O(7')
O(1)
O(3)
O(7)
Si(1)
O(2)
Ba(2)
Ba(1)
c

a)

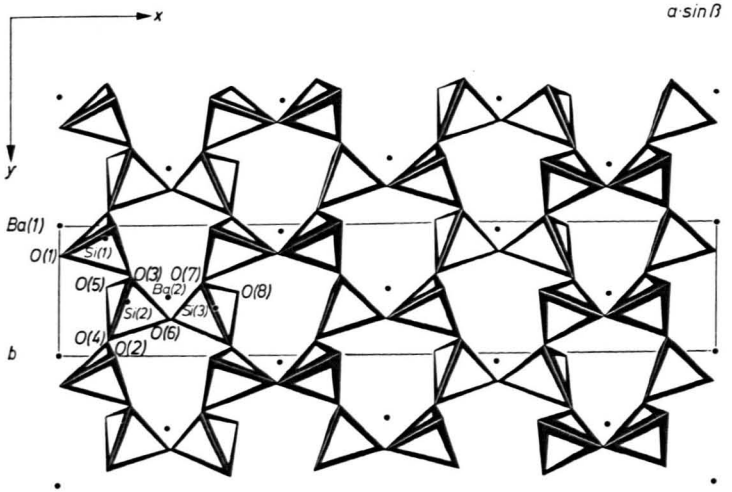
x
y
a·sin ß
Ba(1)
O(1)
Si(1)
O(3)
O(7)
Ba(2)
O(5)
O(8)
Si(2)
Si(3)
O(4)
O(6)
O(2)
b

b)

point[69,71]. Such crystals were also found to be (010) plates. A recent electron microscopy study of $BaSi_2O_5$[48] has not elucidated the crystallographic orientations of crystals formed during the crystallisation of 100 $^m/_o$ $BaSi_2O_5$ glass. This is probably because the crystals observed were not single crystals but probably small spherulites composed of many fine crystallites (see Figure 3.10).

In view of the above discussion we might reasonably expect $Li_2Si_2O_5$ liquid to possess a similar layered structure, the long range ordering of the $[Si_2O_5]$ sheets having been reduced relative to that of the $[Si_2O_5]$ sheets present in crystalline $Li_2Si_2O_5$. If this is the case we can propose a method of calculating the crystal-liquid interfacial surface energy, using a model basically similar to that developed by Skapski for metals[72].

Consider first a solid-air interface. Let ΔU_s be the change in internal energy per mole when a layer is transferred from the bulk of the solid to the surface. If we enlarge the surface by an amount equal to the molar area A_{ms}, the area occupied by N_A molecules forming a single layer, then

$$\sigma_s A_{ms} = \Delta U_s - T\Delta S_s \qquad (5.18)$$

where σ_s is the surface energy and ΔS_s is the change in entropy associated with such a transfer. If U_s is the bonding energy per mole between two layers then ΔU_s will be equal to U_s, since in the bulk a given layer has a layer either side of it, whereas at the surface it only has a layer on one side of it. This of course neglects any interaction between a chosen layer and layers not immediately adjacent, the assumption being that the chosen layer is effectively screened by the immediately neigh-

bouring layers. Hence equation (5.18) becomes

$$\sigma_s A_{ms} = U_s - T\Delta S_s \tag{5.19}$$

We can write a similar expression for the transfer of a layer from the bulk of the liquid to a liquid-air interface. Thus

$$\sigma_\ell A_{m\ell} = U_\ell - T\Delta S_\ell \tag{5.20}$$

where the subscript ℓ denotes the liquid phase. But $(U_s - U_\ell)$ is the change in bonding energy between two layers in going from liquid to solid. Thus

$$(U_s - U_\ell) = \frac{\Delta H}{2}$$

where ΔH is the difference in enthalpy of formation between solid and liquid at the temperature T. At the melting point, ΔH equals ΔH_f, the heat of fusion per mole. (In fact ΔH also includes some $p\Delta V$ work, since there is a change in volume in going from solid to liquid, but this is a very small correction). Thus combining equations (5.19) and (5.20) we obtain at the melting point, T_m

$$\sigma_s = \frac{\Delta H_f}{2A_{ms}} + \frac{A_{m\ell}}{A_{ms}}\sigma_\ell + \frac{T_m}{A_{ms}}(\Delta S_\ell - \Delta S_s) \tag{5.21}$$

At the melting point the liquid is assumed to completely wet the solid, the contact angle being 180°. Thus we can write

$$\sigma_s = \sigma_{s\ell} + \sigma_\ell \qquad (5.22)$$

where $\sigma_{s\ell}$ is the solid-liquid interfacial energy. Also the molar areas can be expressed as

$$A_m = N_A^{1/3} \left(\frac{M}{\rho}\right)^{2/3} \qquad (5.23)$$

where N_A is Avogadro's number, M is the molecular weight, and ρ is the density. Substituting for σ_s, A_{ms} and $A_{m\ell}$ in equation (5.21) we finally obtain

$$\sigma_{s\ell} = \frac{\Delta H_f}{2N_A^{1/3}} \left(\frac{\rho_s}{M}\right)^{2/3} + \left[\left(\frac{\rho_s}{\rho_\ell}\right)^{2/3} - 1\right] \sigma_\ell + \frac{T_m}{N_A^{1/3}} \left(\frac{\rho_s}{M}\right)^{2/3} (\Delta S_\ell - \Delta S_s) \qquad (5.24)$$

Although the value of $(\Delta S_\ell - \Delta S_s)$ is unknown we can make an approximate independent estimate of $\sigma_{s\ell}$, since the other parameters can be obtained by experiment.

For the composition 100 m/o $Li_2Si_2O_5$ these parameters are given in the literature and from equation (5.24) $\sigma_{s\ell}$ is found to be 220 ergs cm^{-2} at the melting point. This is considerably larger than the nucleation estimate of $\sigma_{s\ell}$ for the (010) plane, which is parallel to the $[Si_2O_5]$ sheets. Assuming an orthorhombic critical nucleus, $\sigma_{s\ell}$ for the (010) plane was earlier found to be 65 ergs cm^{-2}. Although the nucleation estimate of $\sigma_{s\ell}$ refers to a lower temperature range than the calculated value, such a large decrease in $\sigma_{s\ell}$ with temperature is not expected. It is interesting to note that the calculated value of $\sigma_{s\ell}$ does agree quite well with the average value of $\sigma_{s\ell}$ ($\bar{\sigma}_{s\ell}$) obtained from

nucleation kinetics, assuming a spherical critical nucleus (see Table 4.2, in particular Method 2(b)).

A similar calculation for the 100 ^{m}/o $BaSi_2O_5$ composition is not possible since σ_ℓ and ρ_ℓ have apparently not been determined. However, the second term in equation (5.24) is expected to be small since $\left(\frac{\rho_s}{\rho_\ell}\right)^{2/3}$ is not much greater than unity. For the composition 100 ^{m}/o $Li_2Si_2O_5$, $\left(\frac{\rho_s}{\rho_\ell}\right)^{2/3}$ is about 1.061, the second term being about 19 ergs cm^{-2}. Hence using only the first term in equation (5.24), $\sigma_{s\ell}$ for the composition 100 ^{m}/o $BaSi_2O_5$ was estimated to be 115 ergs cm^{-2} at the melting point. This compares reasonably well with the low temperature nucleation estimate of $\bar{\sigma}_{s\ell}$, which is 132 ergs cm^{-2} (see Table 4.3). It should be mentioned that the calculated value of $\sigma_{s\ell}$ is based on the value of ΔH_f derived from phase diagram data in Chapter 4.

From the above discussion it appears that the values of $\bar{\sigma}_{s\ell}$ for $Li_2Si_2O_5$ and $BaSi_2O_5$ can be calculated from equation (5.24), although the method must be considered approximate. Essentially, the value of $\bar{\sigma}_{s\ell}$ is determined by the magnitude of ΔH_f. This agrees with the results obtained by Matusita and Tashiro[25], which were reviewed in Chapter 1. They found that $\bar{\sigma}_{s\ell}$ could be expressed as

$$\bar{\sigma}_{s\ell} = \frac{0.45\ \Delta H_f}{N_A^{1/3}} \left(\frac{\rho_s}{M}\right)^{2/3}$$

for the compositions 100 ^{m}/o $Li_2Si_2O_5$, $Na_2Si_2O_5$ and $K_2Si_2O_5$ respectively, $\bar{\sigma}_{s\ell}$ being determined from nucleation kinetics using Method 4 and assuming a spherical critical nucleus. No physical significance was attached to this finding. However, crystalline $Na_2Si_2O_5$ is a layer type silicate[73]

similar to $Li_2Si_2O_5$ and $BaSi_2O_5$. The structure of crystalline $K_2Si_2O_5$ has apparently not been determined, but it is expected to be similar to that of the other alkali disilicates. Thus the constant 0.45 presumably arises as a result of this layered structure. According to equation (5.24) the constant should be 0.50, ignoring the σ_ℓ and $(\Delta S_\ell - \Delta S_s)$ terms. Table (5.2) summarises the measured and calculated values of $\sigma_{s\ell}$ for $Li_2Si_2O_5$, $Na_2Si_2O_5$, and $K_2Si_2O_5$. The measured values are those given by Matusita and Tashiro and the calculated values were obtained from equation (5.24). The agreement is quite good.

5.2 Suggestions for future work

5.2.1 Nucleation kinetics

Heterogeneous internal nucleation in eutectic glasses

In the present study of the Li_2O-BaO-SiO_2 system, internal nucleation could be observed without any intentional addition of a nucleation catalyst. However, internal nucleation did not occur in glasses of low liquidus temperature, i.e. those near eutectic compositions. Thus eutectic glasses could perhaps be used to elucidate the effects of metal nucleation catalysts such as Pt, Cu, Ag and Au. Small additions of these nucleation catalysts are not expected to affect the liquidus temperature. Hence for glasses near the eutectic composition in the $Li_2Si_2O_5$-$BaSi_2O_5$ system it would still be possible to calculate the thermodynamic driving force for nucleation of $BaSi_2O_5$ and $Li_2Si_2O_5$, and therefore analyse their heterogeneous nucleation rates, if observable.

TABLE 5.2

COMPARISON OF MEASURED AND CALCULATED VALUES OF $\sigma_{s\ell}$

Compound	Measured σ_{ℓ}, ergs cm^{-2}	Calculated σ_{ℓ}, ergs cm^{-2}
$Li_2Si_2O_5$	196	220
$Na_2Si_2O_5$	123 - 144	125
$K_2Si_2O_5$	88 - 104	106

NOTES:

Measured values of $\sigma_{s\ell}$ acc. ref. 25

Calculated values of $\sigma_{s\ell}$ acc. equation (5.24)

Analysis of nucleation kinetics using growth rate data

In Chapter 4, viscosity data was used in the analysis of both nucleation kinetics and growth kinetics of $Li_2Si_2O_5$ in the glass 100 $^m/_o$ $Li_2Si_2O_5$. This would suggest that the Stokes-Einstein relation (equation (1.56)) is valid for both nucleation and growth and that ΔG_D is equal to $\Delta G_D'$ i.e. the diffusion activation energy is the same for both processes. This might be expected when the nucleating phase is of the same composition as the glass. Combining the nucleation and growth equations we obtain

$$\ln\left(\frac{I}{u}\right) = \ln\left(\frac{A}{A'}\right) - \frac{k_5\bar{\sigma}^3}{kT\Delta T^2}\left(\frac{V_m T_m}{\Delta H_f}\right)^2 \qquad (5.25)$$

Hence from a plot of $\ln\left(\frac{I}{u}\right)$ vs. $\frac{1}{T\Delta T^2}$ we can obtain $\bar{\sigma}$ and compare the experimental value of $\frac{A}{A'}$ with that predicted by theory, without knowing the diffusion activation entropy, ΔS_D. This method provides an alternative means of analysing nucleation kinetics compared with Method 4, discussed in the previous chapter. However, the growth rate measurements would involve long periods of time, since the growth rate is often very low in the temperature range where nucleation occurs. In the case of the composition 100 $^m/_o$ $BaSi_2O_5$ such measurements would perhaps help to explain the apparent induction time effect described in Chapter 3.

Viscosity data for the analysis of nucleation and growth kinetics

In the present study viscosity data was only available for the composition 100 $^m/_o$ $Li_2Si_2O_5$. It would be of interest to measure the low temperature viscosities of compositions in the system $Li_2Si_2O_5$-

$BaSi_2O_5$ and use this data for analysing nucleation and growth kinetics. It would be of particular interest to compare the values of ΔH_η with the almost constant value of $\Delta H_D'$ obtained from growth measurements. Actual viscosity data would also enable an assessment to be made of the D.T.A. method for estimating T_g.

Viscosity measurements might be hindered by crystallisation. Least difficulty is expected for glasses near the eutectic composition since internal nucleation will not occur.

The compositions 90:10 and 80:20

The present study has shown that internal crystallisation of $Li_2Si_2O_5$ occurs in both these compositions. Furthermore it is possible to estimate the thermodynamic driving force for crystallisation, using liquidus data. Unfortunately, the low nucleation rates encountered prevented an accurate analysis of the nucleation kinetics being made because of the large errors in determining the nucleation densities. This could be overcome by making more extensive measurements than time allowed in the present study. Also, an advantage might be gained using transmission optical microscopy, rather than reflection optical microscopy for these two compositions. Transmission microscopy requires a parallel sided section of each specimen to be made. Since all the spherulites in the specimen can be counted, if the nucleation density is not too high, we are no longer dependent on sectioning a spherulite for it to be observed in the microscope. A further advantage of transmission microscopy is that the shape of the spherulite does not have to be determined. Thus we could avoid the problem of being unable to specify the shape of the spherulites for the 80:20 composition.

The system $K_2Si_2O_5$-$BaSi_2O_5$

A study of the system $K_2Si_2O_5$-$BaSi_2O_5$ would enable an interesting comparison to be made with the systems $Na_2Si_2O_5$-$BaSi_2O_5$ and $Li_2Si_2O_5$-$BaSi_2O_5$ already discussed. There are two points of particular interest. First, the effect of $K_2Si_2O_5$ on the nucleation kinetics of $BaSi_2O_5$ and secondly, the effect of composition on the diffusion activation energy for growth. The present study would suggest that the diffusion activation energy should be almost constant, close to the value obtained for the 100 ^{m}/o $K_2Si_2O_5$ composition, except for the 100 ^{m}/o $BaSi_2O_5$ composition. The growth kinetics of the composition 100 ^{m}/o $K_2Si_2O_5$ appear to have been measured only once previously[60] and, as mentioned in Chapter 4, these results are probably not accurate. Thus this work would have to be repeated. Also, the phase diagram of the $K_2Si_2O_5$-$BaSi_2O_5$ system is unavailable and this would have to be determined accurately prior to an analysis of the nucleation kinetics of $BaSi_2O_5$. It would be of interest to see if similar thermodynamic behaviour to the $Na_2Si_2O_5$-$BaSi_2O_5$ and $Li_2Si_2O_5$-$BaSi_2O_5$ systems is observed.

Practical application for the composition 10:90

Very high internal nucleation rates are observed for the composition 100 ^{m}/o $BaSi_2O_5$. However a homogeneous glass is difficult to obtain. The batch has to be sintered at about 1370°C for 24 hours followed by normal melting procedure at about 1550°C. The substitution of a small amount of Li_2O for BaO makes melting considerably easier. Thus the composition 10:90 which contains about 1.2 ^{w}/o Li_2O can be melted to a homogeneous glass at 1450°C without any previous sintering. Very high

nucleation rates are still observed, but there is an increase in the growth rate at large supercoolings. This causes very rapid internal crystallisation at temperatures above 700°C. Thus glass-ceramic articles might be formed from the composition 10:90 using very short, and therefore economical, heat treatment schedules. The thermal expansion of the low temperature modification of $BaSi_2O_5$ is relatively high, about $123 \times 10^{-7}\ °C^{-1}$[18]. Thus a specific application might involve the formation of glass-ceramic to metal seals as described by McMillan[15].

The determination of thermodynamic data

The present work has indicated the importance of thermodynamic data in interpreting measurements of nucleation and growth kinetics. Thus to calculate the thermodynamic driving force for nucleation and growth we require the heat of fusion of the crystallising phase and the activity of the crystallizing component in solution. In general such thermodynamic data is lacking, even in simple silicate systems.

One approach to this problem is to use liquidus data as described in Chapters 1 and 4 with reference to the systems $Na_2Si_2O_5$-$BaSi_2O_5$ and $Li_2Si_2O_5$-$BaSi_2O_5$. These systems are relatively simple in thermodynamic terms and exhibit near ideal behaviour. In general, however, silicate systems are non-ideal and the interpretation of liquidus data, if available, is not so straightforward. Other methods of obtaining thermodynamic data are therefore required if we are to interpret crystallisation kinetics in a much wider range of glass forming systems than possible at present. The use of D.T.A. to obtain an estimate of the heat of fusion of a crystallising phase has been referred to and is described in Appendix A4.1. Electromotive force measurements appear to be a promising

method of obtaining activity data in glass forming systems. Essentially this method consists of converting a free energy difference between say two glasses into an e.m.f., the magnitude of which is directly related to the activities of the current carrying components.

5.2.2 Growth kinetics

Eutectic growth

In Chapter 3 it was suggested that eutectic growth can be observed in the $Li_2Si_2O_5$-$BaSi_2O_5$ system, depending on composition and temperature. In order to verify this suggestion more accurately high temperature growth rates and further study of the crystal morphology are required. Hot-stage optical microscopy would obviously avoid the errors inherent in the quenching method when measuring growth rates above the maximum growth rate temperature. However, optical microscopy is unable to clearly resolve the crystal morphology. In particular, we are interested in the interlamellar spacing as a function of supercooling below the eutectic temperature. This would have to be determined using electron microscopy. However, for a given composition we can predict the ratio of the widths of two adjacent lamallae, this being independent of temperature. Consider the eutectic composition in the system $Li_2Si_2O_5$-$BaSi_2O_5$, which contains 64 $^{m}/_{o}$ $Li_2Si_2O_5$. The widths of the $Li_2Si_2O_5$ and $BaSi_2O_5$ lamellae are in a ratio given by

$$\frac{Y_L}{Y_B} = \frac{V_L}{V_B} = \frac{{}^{w}/_{o}\ Li_2Si_2O_5}{{}^{w}/_{o}\ BaSi_2O_5} \left(\frac{\rho_B}{\rho_L}\right)$$

where the subscripts L and B denote $Li_2Si_2O_5$ and $BaSi_2O_5$ respectively,

Y is the lamella width, V is the volume of phase present, and ρ its density. For the eutectic composition $\frac{Y_L}{Y_B}$ is found to be about 1.5.

It is possible that this eutectic composition could be used to produce crystalline silicate fibres of high mechanical strength, the lamella phases being aligned parallel to the fibre axis. A method of producing crystalline fibres starting from glass rod, has been recently described[74] and could perhaps be applied to the present eutectic glasses. Briefly the method consists of passing the glass rod through a heating coil which also acts as a support for the glass as it becomes molten. Since the coil temperature is above the liquidus temperature of the glass, any crystals formed in the rod as it enteres the coil will melt. However, as the glass is redrawn as a fibre from the far side of the coil it crystallises, the crystal front being perpendicular to the fibre axis. Since both $Li_2Si_2O_5$ and $BaSi_2O_5$ possess a sheet-like crystalline structure, the resulting crystalline fibres are expected to contain alternate sheets of these two phases, the sheets being aligned parallel to the fibre axis.

CONCLUSIONS

A study of nucleation and crystal growth in the lithia-baria-silica system has been made, with the purpose of examining nucleation and growth kinetics in terms of existing theories. The high viscosity of silicate melts results in crystallisation rates being relatively slow, the extent of crystallisation being 'frozen-in' on cooling to room temperature. Hence samples of glass were given accurately controlled heat treatments, quenched to room temperature, and observed using optical microscopy. Crystal growth rates were estimated directly from such observations, whereas crystal nucleation rates were generally estimated from a statistical analysis of optical micrographs. Further information regarding crystallisation kinetics was obtained from differential thermal analysis (D.T.A.) and the crystalline phases were identified by X-ray diffraction.

As a basis for discussing the results of this study, consideration has been given to the thermodynamic driving force for crystallisation together with a review of the theories of nucleation and crystal growth. This was followed by a summary of selected results obtained by other workers.

After a description of the various experimental techniques by which the present results were obtained, a general survey of the lithia-baria-silica system was presented. Only compositions containing between 50 and 70 $^{m}/_{o}$ silica formed transparent glasses on cooling from above the liquidus temperature down to room temperature. The lower limit was determined by the occurrence of rapid crystallisation and the upper limit by liquid-liquid immiscibility. Within this glass forming region it was noted that the most stable glasses were those with low liquidus temperatures. D.T.A. revealed two interesting features

for compositions lying on the constant silica sections containing $66\frac{2}{3}$ and 60 $^{m}/_{o}$ silica respectively. First, there was a large increase in the glass transformation temperature, the 'D.T.A. T_g', for baria rich compositions. Secondly, the crystallisation exotherm occurred at progressively higher temperatures as baria replaced lithia. In practice it was found that the 'D.T.A. T_g' and the temperature of the crystallisation exotherm defined the approximate temperature range over which crystal nucleation and growth kinetics could be conveniently determined. Internal nucleation of either lithium or barium silicates was observed on both constant silica sections, except for those compositions with low liquidus temperature. Since no nucleation catalysts were deliberately introduced it is likely that the nucleation observed was homogeneous.

A more detailed study of individual compositions on the $66\frac{2}{3}$ $^{m}/_{o}$ silica section was undertaken, since it is essentially a simple binary eutectic system, in which the primary phases are lithium disilicate and barium disilicate. Internal nucleation of either lithium disilicate or barium disilicate was observed, depending on which of these was the primary phase, except for compositions in the vicinity of the eutectic. Typical 'hump-shaped' nucleation curves were obtained. The addition of lithium disilicate to stoichiometric barium disilicate glass caused a decrease in the internal nucleation rates of barium disilicate. Similarly, the internal nucleation rates of lithium disilicate were decreased by additions of barium disilicate. Crystal growth rates at a given temperature, however, increased as the composition was varied from stoichiometric lithium disilicate to stoichiometric barium disilicate, although the largest part of that increase occurred for glasses close to the latter composition. Both crystalline disilicates

were detected by X-ray diffraction, in approximately the proportions expected from the composition of the crystallising glass. However, the crystal morphology altered in the vicinity of the eutectic composition below the eutectic temperature. Whereas lithia rich compositions exhibited dendritic growth, two phase eutectic growth was observed for baria rich compositions containing between $13\frac{1}{3}$ $^{m}/_{o}$ and 30 $^{m}/_{o}$ baria. High temperature growth rate measurements suggested that the primary phase grew as dendrites for both lithia and baria rich compositions, accompanied by two phase eutectic growth below the eutectic temperature. It was therefore concluded that at large supercoolings the primary phase lithium disilicate grows faster than the two phase eutectic for lithia rich compositions, whereas for baria rich compositions the two phase eutectic grows faster than the primary phase barium disilicate. An analogous baria rich composition in the soda-baria-silica system exhibited only dendritic growth of the primary phase barium disilicate. It is suggested that eutectic growth is not observed in this case because the eutectic temperature is 160°C lower. The driving force for eutectic growth is therefore considerably reduced.

An analysis of the detailed nucleation kinetics obtained for compositions in the lithium disilicate-barium disilicate system required the value of the heat of fusion of crystalline barium disilicate and also activity coefficients for both disilicates in solution. Such data were estimated from a thermodynamic analysis of the phase diagrams for the systems sodium disilicate-barium disilicate and lithium disilicate-barium disilicate. In both systems the activity coefficients of barium disilicate were found to be unity, the thermodynamic driving force for nucleation of barium disilicate being therefore directly

proportional to the supercooling. Detailed consideration was also given to the various methods of analysing nucleation and growth kinetics in terms of current theories. Nucleation kinetics could be analysed in three ways, the exact values of the nucleation parameters obtained depending on the method chosen. All the methods gave values of the pre-exponential factor which were far greater than predicted by homogeneous nucleation theory. From the present results and the results of other workers it was found that homogeneous nucleation theory could not be fitted to data below the temperature of maximum nucleation. Below that temperature the experimental nucleation rates were too low according to the nucleation parameters calculated from the experimental nucleation rates at higher temperatures. The nucleation parameters for barium disilicate in the systems lithium disilicate-barium disilicate and sodium disilicate-barium disilicate were all found to be dependent on glass composition. Thus the effect of glass composition on nucleation kinetics cannot be simply related to liquidus temperature. Crystal growth kinetics in the lithium disilicate-barium disilicate system were adequately described by simple Arrhenius plots, in spite of the change in crystal morphology in the vicinity of the eutectic composition. Similarly crystal growth rates in the sodium disilicate-barium disilicate system could be fitted to Arrhenius plots. In both systems the small addition of alkali disilicate to barium disilicate caused a large decrease in the growth parameters. For larger additions of alkali disilicate the parameters remained almost constant, similar in value to those obtained for the stoichiometric alkali disilicate glasses. It was therefore suggested that crystal growth in these systems may be controlled by a diffusion process in which the alkali ions play a predominant role.

A further discussion of nucleation theory was concerned with the interfacial free energy and the free energy of formation of non-spherical clusters. An interfacial energy which decreased with decreasing temperature could account for the very large apparent pre-exponential factors obtained from nucleation experiments assuming homogeneous nucleation theory. Equations have been derived for the free energies of formation of cylindrical and orthorhombic clusters. These shapes were used to approximately describe the plate-like morphology of lithium disilicate crystals, as observed at an early stage of growth. The critical nucleus sizes obtained assuming homogeneous nucleation theory were very reasonable. It was suggested that the plate-like morphology of lithium disilicate occurs as a result of the layered crystal structure common to several disilicate phases. A simple model predicted that the interfacial energy of this layer plane should be proportional to the heat of fusion of the crystalline phase. Experimental results for lithium, sodium, potassium and barium disilicates respectively indicated that there was a relation between interfacial free energy and the heat of fusion.

Several suggestions for future work on nucleation and crystal growth have been made. They include studies on metal nucleation catalysts, crystallisation in the system potassium disilicate-barium disilicate, and the occurrence of eutectic growth in the system lithium disilicate-barium disilicate.

APPENDIX

A1.1 Calculation of the thermodynamic driving force for crystallisation in multicomponent systems

The thermodynamic driving force, ΔG for crystallisation of pure crystalline A in a binary system A-B was calculated in Chapter 1. Consider now a modification of this system in which A and B form a compound D, composition x_D. The free energy diagram is shown in Figure A1.1. The sharp free energy curve at composition x_D represents the free energy of solid compound D. It follows from the discussion in Chapter 1 that ΔG for crystallisation of compound D from an initial composition x_A at the temperature of interest is estimated by drawing a tangent to the free solution free energy curve at composition x_A and measuring the length PR in Figure A1.1. PR can be expressed as (NR + MN - MP). NR is ΔG for the crystallisation of compound D from an initial composition x_D i.e.

$$NR = G_D^{os} - G_D^{o\ell} = - \frac{\Delta H_f (T_m - T)}{T_m}$$

where G_D^{os} and $G_D^{o\ell}$ are the molar free energies of pure solid and liquid D respectively, and ΔH_f and T_m refer to the compound D. MN is the free energy of mixing in forming liquid compound D from A and B at the temperature of interest and is given by

$$MN = RT[x_D \ln a_A^{\ell} + (1-x_D) \ln a_B^{\ell}]$$

where the activities a_A^{ℓ} and a_B^{ℓ} are evaluated at x_D. MP is given by the same expression as for MN but in this case the activities are evaluated at x_A, the composition of interest. In general activities

FIG. A1.1. FREE ENERGY DIAGRAM FOR A TWO COMPONENT SOLUTION, ILLUSTRATING THE CALCULATION OF ΔG FOR THE CRYSTALLISATION OF A COMPOUND D, COMPOSITION x_D.

$$\Delta G = PR = NR + MN - MP$$

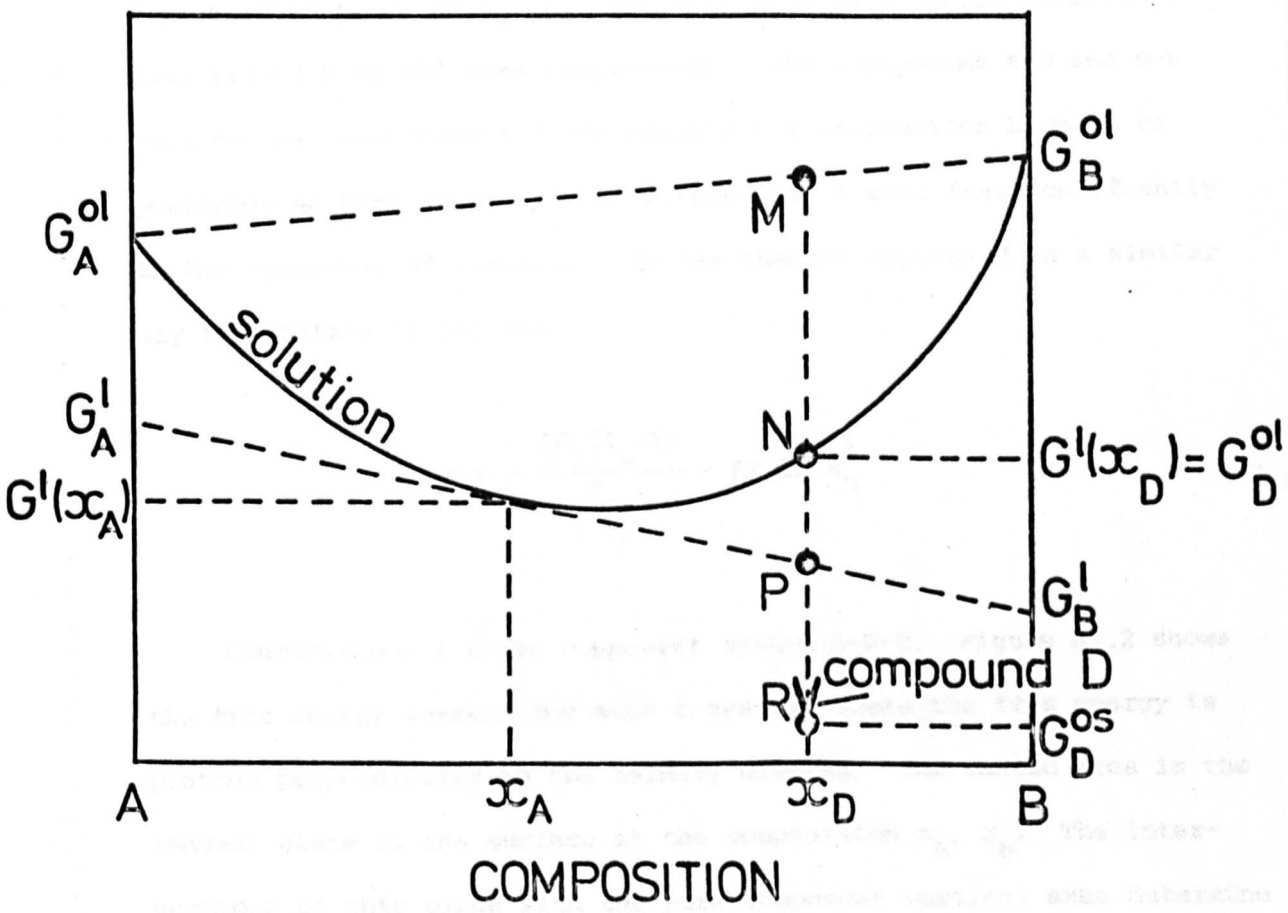

$$\left.\begin{aligned} G_A^l &= G_A^{ol} + RT\ln a_A^l \\ G_B^l &= G_B^{ol} + RT\ln a_B^l \end{aligned}\right\} \text{FOR COMPOSITION } x_A$$

are determined by drawing a tangent to the free energy curve at a given composition. This intersects the pure component ordinates and thereby defines the partial molar free energy and activity of each component for the chosen composition (see equation (1.16)). In Figure A1.1 a tangent has already been drawn at composition x_A to determine ΔG. The calculation of activity data for composition x_A is therefore illustrated in the figure.

Alternatively, ΔG for the crystallisation of compound D can be expressed in terms of a_D^{ℓ}, the activity of D in solution referred to pure liquid D at the same temperature. The subsystems A-D and D-B must now be considered and co-ordinate transformations have to be performed so that compound D corresponds to a mole fraction of unity in the subsystem of interest. ΔG can then be expressed in a similar way to equation (1.18) viz.

$$\Delta G = - \frac{\Delta H_f (T_m - T)}{T_m} - RT \ln a_D^{\ell}$$

Consider now a three component system A-B-C. Figure A1.2 shows the free energy surface for such a system, where the free energy is plotted perpendicular to the ternary diagram. The shaded area is the tangent plane to the surface at the composition x_A, x_B. The intersections of this plane with the pure component vertical axes determine ΔG for crystallisation of A, B and C, in a similar way to a two component system. Thus ΔG is equal to $- [G_C^{\ell} - G_C^{os}]$ for the crystallisation of pure component C in Figure A1.2, where G_C^{ℓ} is the partial molar free energy of component C in a solution of composition x_A, x_B and G_C^{os} is the molar free energy of pure solid C. G_C^{ℓ} can be

FIG. A1.2. FREE ENERGY DIAGRAM FOR A THREE COMPONENT SOLUTION ILLUSTRATING THE CALCULATION OF ΔG FOR THE CRYSTALLISATION OF PURE SOLID C.

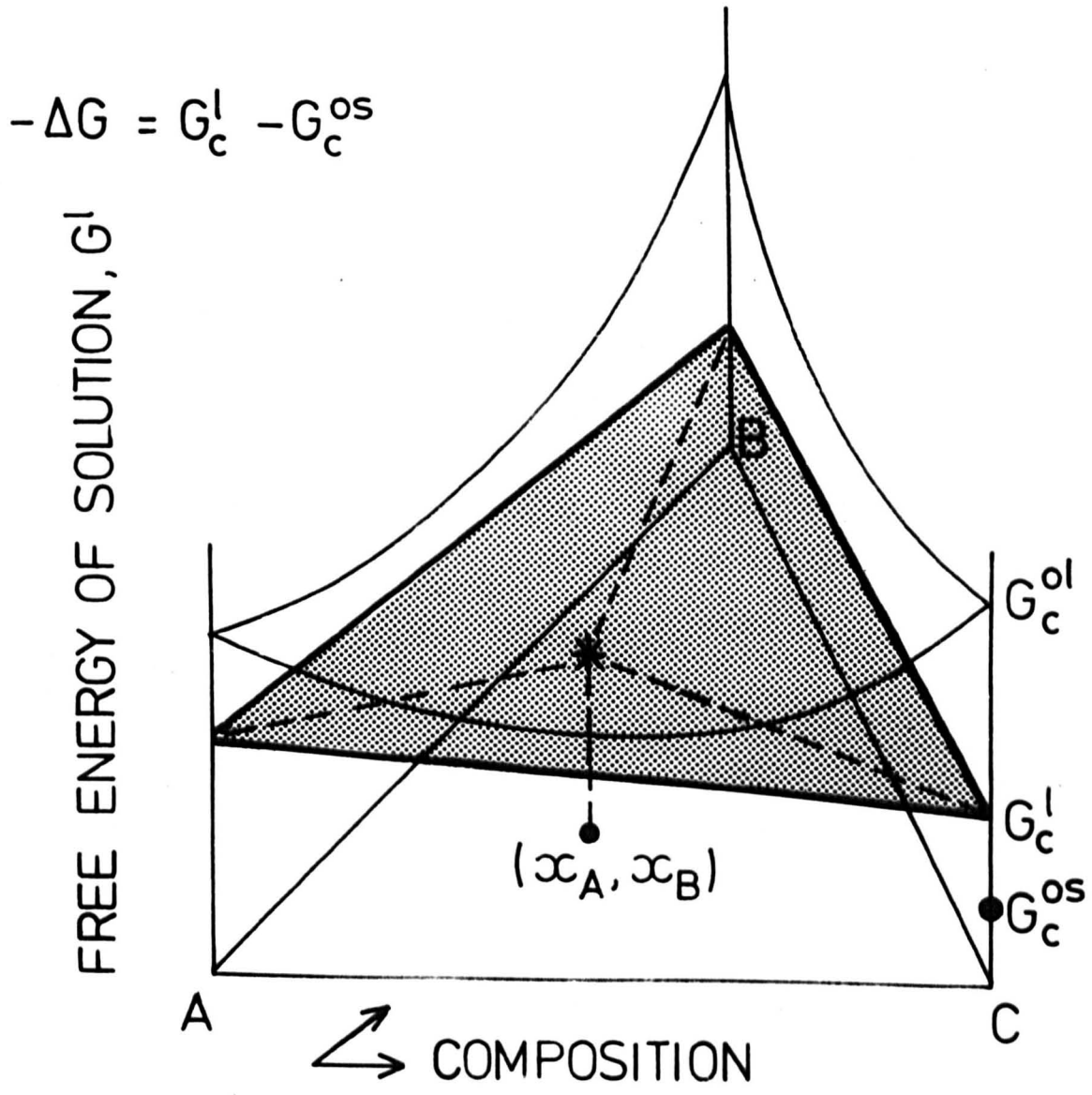

expressed in terms of the activity of component C, a_C^{ℓ} (equation (1.16)). ΔG for the crystallisation of pure component C is therefore given by equation (1.18) with a_A^{ℓ} replaced by a_C^{ℓ}

A1.2 The regular type solution model

In general terms, the free energy of mixing for a two component solution is given by

$$\Delta_m G = \Delta_m H - T\Delta_m S$$

$$= RT(x_A \ln a_A^{\ell} + x_B \ln a_B^{\ell})$$

where $\Delta_m H$ and $\Delta_m S$ are the enthalpy and entropy of mixing respectively, and x_i and a_i^{ℓ} are the compositions and activities of the components respectively. In regular type solution models the entropy of mixing is ideal and the enthalpy of mixing is a simple function of composition which does not vary with temperature[75,76]. Since

$$\Delta_m S \text{ (ideal)} = - R(x_A \ln x_A + x_B \ln x_B)$$

then $\Delta_m H$ is given by

$$\Delta_m H = RT(x_A \ln \gamma_A^{\ell} + x_B \ln \gamma_B^{\ell})$$

i.e. $\Delta_m H_A = RT \ln \gamma_A^{\ell}$ $\Delta_m H_B = Rt \ln \gamma_B^{\ell}$

where γ_i^{ℓ} is the activity coefficient given by $\frac{a_i^{\ell}}{x_i}$ and $\Delta_m H_i$ is the partial molar enthalpy of mixing. Thus ΔG for the crystallisation of say pure component A in a two component regular solution becomes (see equation (1.18))

$$\Delta G = - \frac{\Delta H_f (T_m - T)}{T_m} - RT \ln (x_A \gamma_A^{\ell})$$

$$= - \left\{ \frac{\Delta H_f (T_m - T)}{T_m} + \Delta_m H_A \right\} - RT \ln x_A$$

Since $\Delta_m H_A$ is not a function of temperature for the regular solution model, it can be calculated from the value of the activity at the liquidus (see equation (1.19)). Hence ΔG is altered by an amount equal to the partial molar enthalpy of mixing as compared with the ideal case.

From equation (1.19) the liquidus curve in a regular type system for component A is given by

$$\ln x_A = - \frac{1}{RT_L} (\Delta_m H_A + \Delta H_f) + \frac{\Delta H_f}{RT_m}$$

In the simplest one parameter regular solution model $\Delta_m H_A$ is given by

$$\Delta_m H_A = \alpha (1 - x_A)^2$$

where α is a constant which is simply related to bond energies between the A and B components in a two component system. Hence a plot of $\ln x_A$ versus $\frac{1}{T_L}$ will not be linear for a regular type model, in contrast to the ideal solution model (see equation (1.20)).

A2.1 Chemical analysis of Li_2O-BaO-SiO_2 glasses

The glass is decomposed in a mixture of hydrofluoric and sulphuric acids. The silica is evaporated off as silicon tetrafluoride and the barium oxide is precipitated as barium sulphate. The lithium ions remain in solution. Thus the barium oxide content can be determined gravimetrically from the weight of barium sulphate after filtration. The filtrate is then analysed for lithium ions using flame photometry. Standard solutions, made up from known weights of pure, dry lithium carbonate, are used to calibrate the photometer. Having estimated the lithium oxide and barium oxide contents, the silica content is obtained by difference.

A2.2 Typical calculations of nucleation densities

Composition 100 $^{m}/_{o}$ $BaSi_2O_5$, heat treated for 5 minutes at 868°C

d_i (cm x 10^3)	n_i
50	0
75	3
100	7
125	9
150	8
175	11
200	14
225	14
250	18
275	33
300	38
325	10
350	0
375	0

Shape of particles	Spherical (diameter d_i)
Total number of particles	165
Total area of prints	426.9 cm^2
Magnification on print	x 100

$$\bar{z} = \frac{\sum\left(\frac{n_i}{d_i}\right)}{\sum n_i} = 4.726, \quad k_2 = 2 \quad , \quad k_6 = \frac{\pi}{4}$$

From equation (2.9)

$$N_v = \frac{2}{\pi} \times \frac{165}{426,9} \times 4.726 \times 10^6 = 1.163 \times 10^5 \text{ cm}^{-3}$$

Composition 90:10, nucleated for 1 hr at 524°C,

then grown for 43 mins at 599°C

d_i (cm x 10^3)	n_i
50	0
75	8
100	9
125	13
150	21
175	23
200	28
225	25
250	38
275	47
300	27
325	6
350	2
375	0

Shape of particles	Prolate ellipsoid (minor axis d_i)
Total number of particles	247
Total area of prints	337.6 cm^2
Magnification on print	x 50

$$\bar{z} = \frac{\sum\left(\frac{n_i}{d_i}\right)}{\sum n_i} = 5.102 \quad , \quad k_6 = \frac{\pi}{2}$$

axial ratio = 0.64 , $k_1 = 1.21$ (ref. 39)

From equation (2.9)

$$N_v = \frac{2}{\pi} \times \frac{247}{337.6} \times \frac{0.25 \times 10^5}{1.21} \times 5.102 = 2.45 \times 10^5 \text{ cm}^{-3}$$

A2.3 Maximum growth rate temperature as a function of liquidus temperature

$$\text{At } T_{max}, \quad \frac{d\ln u}{dT} = 0$$

Hence from equation (1.47), assuming $\Delta G'_D$ is constant (but see later note), we find

$$-\frac{\Delta G'_D}{RT_{max}^2} = \frac{d}{dT}\{\ln[1 - \exp(\frac{-|\Delta G|}{RT})]\} \qquad \text{(A2.1)}$$

where, for an ideal solution

$$\frac{|\Delta G|}{RT} = \frac{\Delta H_f(T_L - T)}{RT_L T}$$

Let

$$f(T) = \exp\left(\frac{-|\Delta G|}{RT}\right) \qquad \text{(A2.2)}$$

Thus

$$f'(T) = \frac{df(T)}{dT} = \frac{\Delta H_f}{RT^2}\exp\left(\frac{-|\Delta G|}{RT}\right) \qquad \text{(A2.3)}$$

But

$$-\frac{\Delta G'_D}{RT^2_{max}} = \frac{d}{dT}\{\ln[1 - f(T)]\}$$

$$= -\frac{f'(T)}{1 - f(T)} \qquad \text{(A2.4)}$$

Therefore, substituting equations (A2.2) and (A2.3) into equation (A2.4) and evaluating at $T = T_{max}$ we obtain

$$\frac{\Delta H_f}{\Delta G'_D} = \frac{1 - \exp\left(\frac{-|\Delta G|}{RT_{max}}\right)}{\exp\left(\frac{-|\Delta G|}{RT_{max}}\right)} \qquad \text{(A2.5)}$$

from which it can be shown that

$$T_{max} = \frac{T_L}{1 + a} \qquad (2.12)$$

where
$$a = \frac{RT_L}{\Delta H_f} \ln\left(1 + \frac{\Delta H_f}{\Delta G'_D}\right)$$

$$\simeq \frac{RT_L}{\Delta G'_D} \qquad (2.13)$$

since $\frac{\Delta H_f}{\Delta G'_D}$ is small and less than unity.

As mentioned in Chapter 4, $\Delta G'_D$ is strictly a free energy term. However, the preceding equations are correct if we replace $\Delta G'_D$ by $\Delta H'_D$ (see euqation (4.28)).

A2.4 Internal crystal nucleation in BaO rich compositions on the 60 $^{m}/_{o}$ SiO_2 section

A limited nucleation study was made of the three glasses given in Table A2.1. As mentioned in Chapter 2, no internal nucleation was observed for the 20:20 composition, which has nearly the lowest liquidus temperature on the 60 $^{m}/_{o}$ SiO_2 section. The primary phase for this composition is $BaSi_2O_5$ (see Figure 2.5). The other two glasses do nucleate internally, the spherulite morphology being shown in Figure 2.7. For both glasses the spherulites were identified as a barium silicate, $Ba_5Si_8O_{21}$ (B_5S_8). This is in keeping with the recently determined phase diagram of the Li_2O-BaO-SiO_2 system[43], which shows the primary phase of the compositions 15:25 and 10:30 as B_5S_8 (see Figure 2.5).

Figures A2.1 and A2.2 show the approximate nucleation curves for these two compositions. The nucleation rates were simply determined by nucleating a specimen for up to 2 hours, followed if required by a short growth treatment at 640°C. The nucleation rate was then calculated from the number of spherulites after growth and the time spent at the nucleation stage. The nucleation rates for the composition 15:25 are very low and nearly unobservable (see Figure A2.1). For example, after 90 minutes at the maximum nucleation temperature followed by a growth treatment, only 9 spherulites were observed on a polished and etched section of the specimen. The nucleation rates for the composition 15:25 are therefore very approximate. The nucleation rates for the composition 10:30 are considerably larger, the maximum rate being about 1.3×10^3 cm^{-3} sec^{-1} (see Figure A2.2). This increase can be qualitatively understood in terms of the higher liquidus temperature

FIG. A2.1. APPROXIMATE NUCLEATION CURVE FOR THE COMPOSITION 15m/o Li_2O – 25m/o BaO – 60m/o SiO_2.

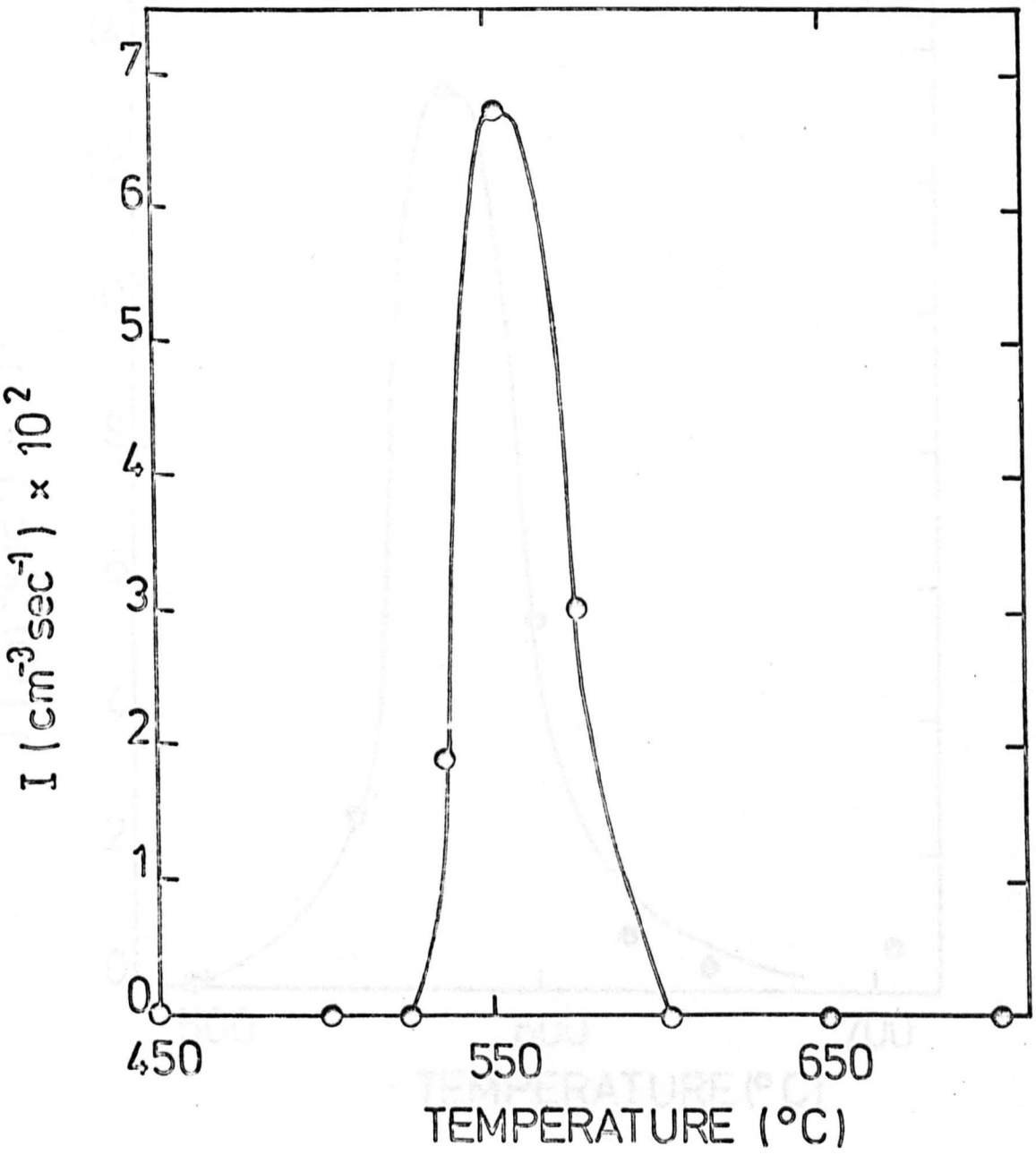

FIG. A2.2. APPROXIMATE NUCLEATION CURVE FOR THE COMPOSITION $10^{m}/_{o}\ Li_2O - 30^{m}/_{o}\ BaO - 60^{m}/_{o}\ SiO_2$.

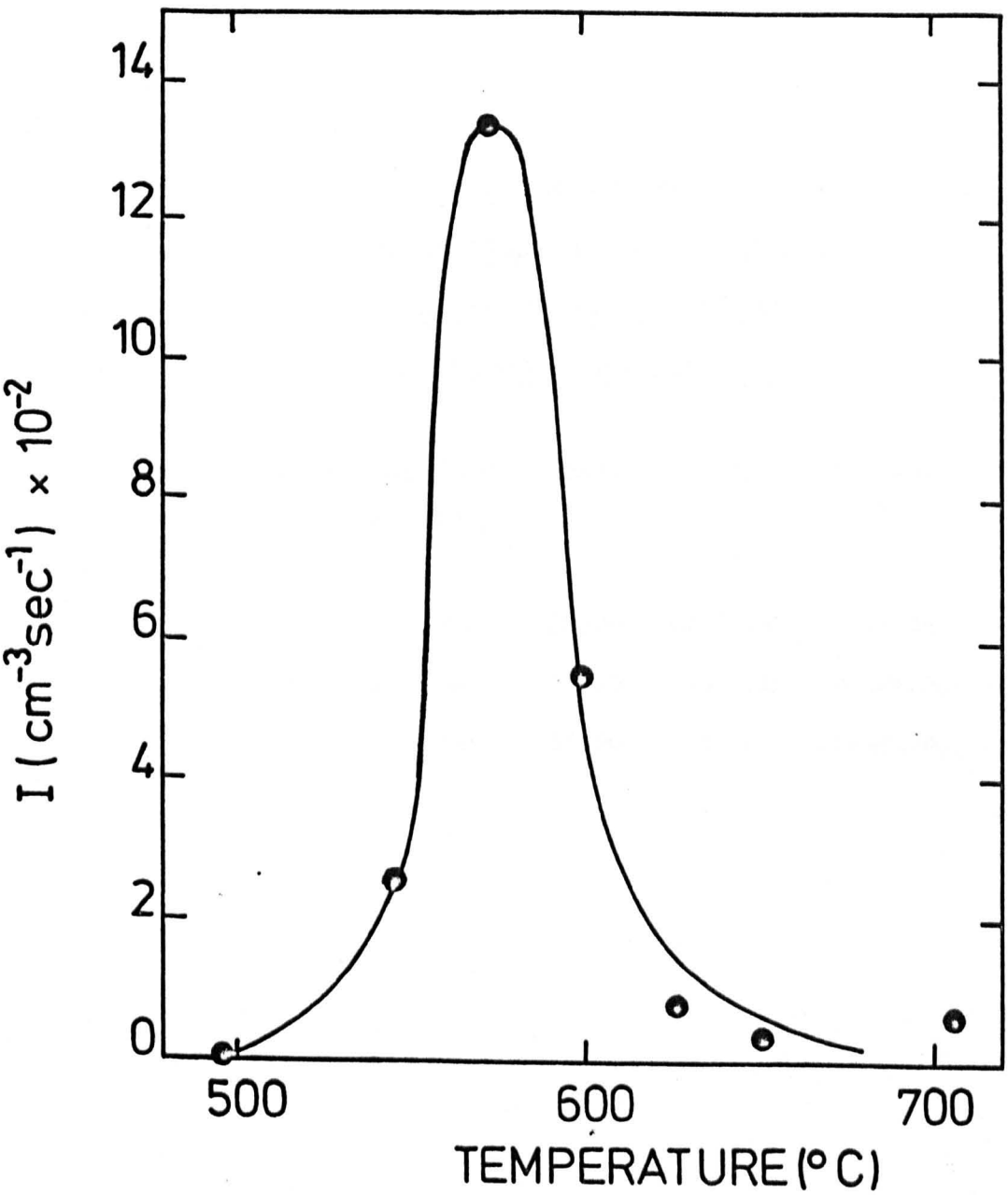

for the 10:30 composition compared with that of the 15:25 composition (see Table A2.1). Unfortunately a quantitative analysis of the nucleation kinetics for these compositions would require more detailed results. Also, thermodynamic data for the compound B_5S_8 would have to be obtained, since it is unavailable from the literature.

TABLE A2.1

PHASE DIAGRAM DATA FOR BaO RICH COMPOSITIONS ON THE 60 $^m/_o$ SiO_2 SECTION OF THE Li_2O-BaO-SiO_2 SYSTEM, AFTER REF. 43.

Composition ($^m/_o$)			Code	T_L (°C)	Primary Phase
Li_2O	BaO	SiO_2			
20	20	60	20:20	1017 ±9	$BaSi_2O_5$
15	25	60	15:25	1101 ±10	$Ba_5Si_8O_{21}$
10	30	60	10:30	~ 1226	$Ba_5Si_8O_{21}$

A4.1 Determination of ΔH_f for $BaSi_2O_5$ using D.T.A.

Differential thermal analysis of powdered glass samples results in a trace shown qualitatively in Figure 2.3. The exothermic peak with a maximum at T_x is due to crystallisation of the glass powder as the temperature increases at a constant rate. In general the area of a D.T.A. peak is related to the enthalpy of the process responsible for the observed peak[80]. Using materials which undergo a phase transformation of known enthalpy change, it is possible to calibrate the D.T.A. apparatus, provided that the sample and inert reference materials have similar thermal properties. This can be achieved by suitably diluting the sample material with the inert reference material.

The enthalpy of crystallisation at temperature T_x is related to the heat of fusion at the melting point as follows

$$\Delta H = - \Delta H_f - \int_{T_x}^{T_m} \Delta c_p dT$$

where Δc_p is the difference in specific heats between the crystalline and liquid phases. As a first approximation Δc_p can be assumed zero and therefore $|\Delta H_f|$ equals ΔH. Using sodium chloride as a standard material the melting point endotherm observed at 800°C can be related to the crystallisation exotherm observed for barium disilicate glass at 842°C as follows

$$\frac{\Delta H_f(BaSi_2O_5)}{\Delta H_f(NaCl)} = \frac{\text{Weight (NaCl)}}{\text{Weight } (BaSi_2O_5)} \times \frac{\text{Mol.Wt.}(BaSi_2O_5)}{\text{Mol.Wt.(NaCl)}} \times \frac{A(BaSi_2O_5)}{A(NaCL)}$$

where A denotes the area of the peak. Analogous equations can be written for determining the heat of fusion of sodium disilicate and lithium disilicate from their respective crystallisation exotherms.

Table A4.1 summarises the ΔH_f values obtained for $BaSi_2O_5$, $Na_2Si_2O_5$ and $Li_2Si_2O_5$ respectively, assuming that ΔH_f for NaCl is 6.73 k cal $mole^{-1}$[5]. The error in these values is about ±0.5 k cal $mole^{-1}$ due to uncertainties in determining the peak areas. If allowance is made for the neglected specific heat contribution to ΔH, the values of ΔH_f are expected to be increased. For $BaSi_2O_5$ the increase would probably be no greater than 1.5 k cal $mole^{-1}$ based on a comparison with specific heat data available for $Na_2Si_2O_5$ and $Li_2Si_2O_5$[5,81]. The D.T.A. estimates of ΔH_f for $Na_2Si_2O_5$ and $Li_2Si_2O_5$ are seen to be in close agreement with values given in the literature[5,81]. Therefore an upper limit on ΔH_f for $BaSi_2O_5$ would be 9.6 k cal $mole^{-1}$. This is in good agreement with the average phase diagram value of 8.6 ± 0.5 k cal $mole^{-1}$, obtained in Chapter 4. This phase diagram estimate of ΔH_f should also be corrected for specific heat contributions, although the correction is smaller than that required for the D.T.A. estimate, since the phase diagram value was determined at higher temperatures.

It should also be noted that the phase diagram estimate of ΔH_f for $Na_2Si_2O_5$ obtained in Chapter 4 was 8.8 ± 0.5 k cal $mole^{-1}$, again in good agreement with the published values given in Table A4.1.

Table A4.1

Summary of ΔH_f values for $BaSi_2O_5$, $Na_2Si_2O_5$ and $Li_2Si_2O_5$

Compound	Determined from phase diagram data in this study	Determined by D.T.A. assuming ΔH_f equals the enthalpy of crystallisation	Acc. ref. 5	Acc. ref. 81
$Ba_2Si_2O_5$	8.6 ± 0.5	7.6 ± 0.5	-	-
$Na_2Si_2O_5$	8.8 ± 0.5	8.6 ± 0.5	8.5	10.6
$Li_2Si_2O_5$	-	14.5 ± 0.5	12.9	14.6

A4.2 Entropy of mixing in the systems $Na_2Si_2O_5$-$BaSi_2O_5$ and $Li_2Si_2O_5$-$BaSi_2O_5$

Liquidus data for the system $Na_2Si_2O_5$-$BaSi_2O_5$ has indicated that the entropy of mixing is close to ideal for all compositions in the system. This can be understood in terms of the following atomistic model of the mixing process involved. Given that no interchange of metal cations with silicon 'ions' can occur and that the silicate network is the same for both stoichiometric $Na_2Si_2O_5$ and $BaSi_2O_5$ liquids, then the mixing process can be described in terms of the sites (i), (ii) and (iii) shown in Figure A4.1, assuming that sodium ions occur in pairs and that barium ions occur singly, both types of cation being in close proximity to non-bridging oxygens. The evidence for non-bridging oxygens occurring in pairs is discussed by Förland[77] and by Charles[78]. An estimate of the configurational entropy of mixing can be made using the relation

$$S = k \ln \Omega \qquad \text{(A4.1)}$$

where S is the entropy, Ω is the number of distinct combinations of the various sites, and k is Boltzmann's constant. This relation can only be used when the heat of mixing is small, otherwise the arrangements of the sites will be greatly altered. Consider a solution of composition x $Na_2Si_2O_5$ $(1-x)BaSi_2O_5$ containing a total of N formula units. The number of pairs of non-bridging oxygens associated with sodium and barium cations are xN and $(1-x)$N respectively. These are also the number of sites (i) and (ii). The number of bridging oxygens, i.e. the number of sites (iii), is 3N. Hence the total number of sites (i), (ii) and (iii) is 4N. The entropy after mixing, assuming the

FIG. A4.1. FOUR TYPES OF SITE CONTRIBUTING TO THE ENTROPY OF MIXING IN THE SYSTEMS $Na_2Si_2O_5$ - $BaSi_2O_5$ AND $Li_2Si_2O_5$ – $BaSi_2O_5$.

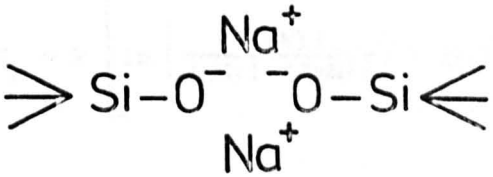

(i)

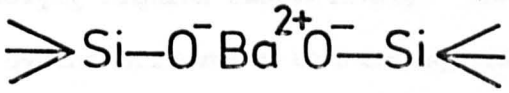

(ii)

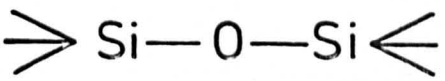

(iii)

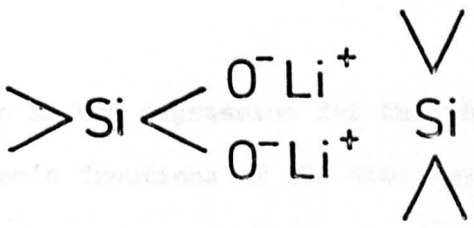

(iv)

size difference between the various sites is unimportant, is therefore given by

$$S = k \ln \left\{ \frac{4N!}{(xN)!\ [(1-x)N]!\ 3N!} \right\} \qquad \text{(A4.2)}$$

The entropy before mixing is given by

$$S_N + S_B = k \left[\ln \left\{ \frac{(4xN)!}{(xN)!\ (3xN)!} \right\} + \ln \left\{ \frac{[4(1-x)N]!}{[(1-x)N]![3(1-x)N]!} \right\} \right] \qquad \text{(A4.3)}$$

where S_N and S_B refer to the entropies of the stoichiometric $Na_2Si_2O_5$ and $BaSi_2O_5$ liquids respectively. Hence the entropy of mixing is given by the difference between equations (A4.2) and (A4.3). Using Stirling's approximation, $\ln x! = x\ln x - x$, to simplify these equations we obtain for the entropy of mixing per mole of solution

$$\Delta_m S = - R[x\ln x + (1-x)\ln(1-x)] \qquad \text{(A4.4)}$$

which is the expression for the ideal entropy of mixing in terms of the mole fractions of the disilicate components. This simple model therefore supports the result from liquidus data, which indicates that the entropy of mixing is ideal. Also, the model suggests that mixing of $Na_2Si_2O_5$ and $BaSi_2O_5$ can be considered as a process for which the silicate network remains constant for all compositions, the entropy of mixing being mainly due to the permutations of the different sites which may be occupied by oxygen ions.

The above model will be incorrect for the $Li_2Si_2O_5$-$BaSi_2O_5$ system since the $Li_2Si_2O_5$ liquidus was found to be non-ideal. In general to calculate the entropy of mixing we need to know the species participating in the mixing process. The simplest calculation assumes that the species are the components prior to mixing. Thus in the analysis of liquidus data for the system $Li_2Si_2O_5$-$BaSi_2O_5$ it was assumed that the species had the molecularity and stoichiometry of $Li_2Si_2O_5$ or $BaSi_2O_5$. In fact neither of these assumptions may be correct. Lithium disilicate might exist in solution as $(Li_2Si_2O_5)_n$ or as $(Li_2SiO_3 + SiO_2)$ to some unknown extent. Such association or dissociation of a component will have a marked effect on its liquidus temperatures. In addition, the other liquidus curves in the system will be affected, since they are also governed by the total number of species present in solution.

Quantitative assessment of these processes requires a knowledge as to the extent to which they occur and also the enthalpy changes accompanying them. The simplest case to study is that in which both the extent and the enthalpy of the processes are constant, independent of composition. Furthermore, it is assumed that all species mix ideally. Reisman[79] has analysed all the simpler types of eutectic systems in this way. He shows that in general a dissociating component has higher liquidus temperatures than would be expected for the non-dissociated case. Association, however, tends to cause a lowering of the liquidus temperature for that component. Considering the experimental $Li_2Si_2O_5$ liquidus in the $Li_2Si_2O_5$-$BaSi_2O_5$ system it would appear that $Li_2Si_2O_5$ dissociates in solution. The $BaSi_2O_5$ liquidus should also be raised, assuming that $BaSi_2O_5$ does not associate or dissociate. In fact it is raised by about 10°C at 50 $^m/_o$ $BaSi_2O_5$ when compared with the $BaSi_2O_5$ liquidus in

the system $Na_2Si_2O_5$-$BaSi_2O_5$. Thus qualitatively the positive deviation from ideality of the $Li_2Si_2O_5$ liquidus can be attributed to the dissociation of $Li_2Si_2O_5$, causing a non-ideal entropy of mixing.

To analyse the $Li_2Si_2O_5$ liquidus in more detail requires a model for the process of dissociation. Crystalline $Li_2Si_2O_5$ melts incongruently to give a slightly silica rich liquid plus a small amount of crystalline lithium metasilicate, Li_2SiO_3. Thus the dissociation of $Li_2Si_2O_5$ in solution might be represented by

$$Li_2Si_2O_5 \rightleftharpoons Li_2SiO_3 + SiO_2$$

One possible model, therefore, is to consider that the species $BaSi_2O_5$, $Li_2Si_2O_5$, Li_2SiO_3, and SiO_2 mix ideally in solution. Using this crude assumption and the approach of Reisman, an attempt has been made to estimate from the experimental liquidus data the two parameters which describe the dissociation process, i.e. the extent of dissociation, α and the enthalpy of dissociation, ΔH_D. Calculations showed that it was always possible to find for a given α a value of ΔH_D which could adequately explain the results and no unique solution for both parameters could be obtained. Furthermore, since no independent data for either α or ΔH_D was available, it is not possible to assess the model quantitatively.

The non-ideality of the $Li_2Si_2O_5$ liquidus may also be realted to the cation size. Table A4.1 gives the ionic radii of the cations of interest. Due to the smaller size of Li^+ it is possible that two Li^+ can form a site with two non-bridging oxygens on the same Si 'atom', as shown in Figure A4.1 (iv). Such a position would be unlikely for Ba^{2+} (and difficult for Na^+). Hence the Li^+ and Ba^{2+} sites would not

be equivalent, leading to non-ideal entropy of mixing. Larger additions of $BaSi_2O_5$ may be envisaged as forcing the Li^+ ions to occupy sites of type (i), Figure A4.1, leading to ideal mixing. It should be realised that the presence of this alternative Li^+ site implies a difference in the silicate network for $Li_2Si_2O_5$ as compared with that of $BaSi_2O_5$ and $Na_2Si_2O_5$. Thus for $Li_2Si_2O_5$ rich solutions there will be some Si^{4+} attached to four bridging oxygens and some to only two. Hence the structure is not sheet-like as sites of type (i) imply, but rather a mixture of chain-like and three dimensional-like structures. This is equivalent to the dissociation process above, since a melt of composition Li_2SiO_3 is probably chain-like in structure and SiO_2 will have a three dimensional structure.

Table A4.1 also gives the molar volumes of the glassy disilicates at room temperature. The equal values for $BaSi_2O_5$ and $Na_2Si_2O_5$ is in agreement with the previous discussion. The smaller value for $Li_2Si_2O_5$ suggests a more tight-knit structure in this case. Incorporation of large Ba^{2+} ions would thus be difficult and a deviation from ideality might be expected.

TABLE A4.2

CATION RADIUS AND MOLAR VOLUMES

FOR GLASSES $R_{(2)}Si_2O_5$

Glass $R_{(2)}Si_2O_5$	Ionic radius of $R^{(2)+}$ Å (Pauling)	Molar volume at 25°C, $cm^3\ mole^{-1}$
$Li_2Si_2O_5$	0.60	63.69
$Na_2Si_2O_5$	0.95	73.13
$BaSi_2O_5$	1.35	73.13

A5.1 Expressions for $\bar{\sigma}$ in terms of σ_i

Cylindrical cluster

With reference to Figure 5.1(b), the free energy of formation of a cylindrical cluster is given by

$$W = \frac{\pi r^2 \ell \Delta G}{V_m} + 2\pi r^2 \sigma_1 + 2\pi r \ell \sigma_2 \qquad \text{(A5.1)}$$

Differentiating W with respect to r and setting equal to zero we obtain for the critical nucleus

$$-\frac{\Delta G}{V_m} = \frac{2\sigma_1}{\ell^*} + \frac{\sigma_2}{r^*} \qquad \text{(A5.2)}$$

Also, differentiating W with respect to ℓ and setting equal to zero we obtain for the critical nucleus

$$-\frac{\Delta G}{V_m} = \frac{2\sigma_2}{r^*} \qquad \text{(A5.3)}$$

Thus combining equations (A5.2) and (A5.3)

$$\frac{\sigma_2}{r^*} = \frac{2\sigma_1}{\ell^*} \qquad \text{(A5.4)}$$

But σ_1 and σ_2 can be expressed in terms of $\bar{\sigma}$ as follows

$$\bar{\sigma}(2\pi r^{*2} + 2\pi r^* \ell^*) = \sigma_1 2\pi r^{*2} + \sigma_2 2\pi r^* \ell^* \qquad \text{(A5.5)}$$

Hence from equations (A5.4) and (A5.5) we find

$$\bar{\sigma} = \left(\frac{3r^*}{r^* + \ell^*}\right) \sigma_1 \qquad (5.11)$$

$$= \frac{3\ell^*}{2(r^* + \ell^*)} \sigma_2 \qquad (5.12)$$

More generally equations (5.11) and (5.12) can be expressed in terms of r and ℓ, since the ratio $\frac{\ell}{r}$ is assumed to be constant.

Orthorhombic cluster

With reference to Figure 5.1(c), the free energy of formation of an orthorhombic cluster is given by

$$W = \frac{abc\ \Delta G}{V_m} + 2ab\sigma_1 + 2bc\sigma_3 + 2ac\sigma_2 \qquad (A5.6)$$

Differentiating W with respect to c and setting equal to zero we obtain for the critical nucleus

$$\frac{\Delta G}{V_m} = -2\left(\frac{a^*\sigma_2 + b^*\sigma_3}{a^*b^*}\right) \qquad (A5.7)$$

Similarly differentiating W with respect to a and b and setting equal to zero respectively, we find

$$\frac{\Delta G}{V_m} = -2\left(\frac{a^*\sigma_1 + c^*\sigma_3}{a^*c^*}\right) \qquad (A5.8)$$

$$= -2\left(\frac{b^*\sigma_1 + c^*\sigma_2}{b^*c^*}\right) \qquad (A5.9)$$

Combining equations (A5.7), (A5.8) and (A5.9)

$$\frac{\sigma_1}{c^*} = \frac{\sigma_2}{b^*} = \frac{\sigma_3}{a^*} \qquad \text{(A5.10)}$$

But σ_1, σ_2 and σ_3 can be expressed in terms of σ as follows

$$\bar{\sigma}(ab + bc + ac) = \sigma_1 ab + \sigma_2 ac + \sigma_3 bc \qquad \text{(A5.11)}$$

Hence combining equations (A5.10) and (A5.11) we obtain

$$\bar{\sigma} = \frac{3\sigma_1}{(1 + \frac{c^*}{a^*} + \frac{c^*}{b^*})} \qquad (5.15)$$

$$= \frac{3\sigma_2}{(1 + \frac{b^*}{a^*} + \frac{b^*}{c^*})} \qquad (5.16)$$

$$= \frac{3\sigma_3}{(1 + \frac{a^*}{b^*} + \frac{a^*}{c^*})} \qquad (5.17)$$

More generally equations (5.15), (5.16), and (5.17) can be expressed in terms of a, b, and c, since the ratios $\frac{a}{b}$ and $\frac{a}{c}$ are assumed to be constant.

REFERENCES

1. Fine, M.E. (1964), 'Introduction to phase transformations in condensed systems', Macmillan, London.

2. Woodruff, D.P. (1973), 'The solid-liquid interface', Cambridge University Press, London.

3. Ed. Zettlemoyer, A.C. (1969), 'Nucleation', Marcel Dekker, New York.

4. Christian, J.W. (1965), 'The theory of transformations in metals and alloys', Pergamon Press, Oxford.

5. J.A.N.A.F. Thermochemical Tables, 2nd Edition, issued June 1971. U.S. Department of Commerce, National Bureau of Standards, Washington.

6. Rey. M. (1948), Discuss. Faraday Soc., 4, 259.

7. Uhlmann, D.R. (1971), 'Advances in nucleation and crystallisation of glasses', p.91, American Ceramic Society, Colombus.

8. Hillig, W.B. (1966), Acta Met. 14, 1868.

9. Hillig, W.B. & Turnbull, D. (1956), J.Chem.Phys., 24, 914.

10. James, P.F. (1975), J. mater. Sci., 10, 1802.

11. Cahn, J.W. (1969), J. Am. Ceram. Soc., 52(3), 118.

12. Seward III, T.P. (1970), 'Phase Diagrams', Vol.6I, p.295. Academic Press, London.

13. Anon (1957),Glass Ind., 38(6), 331.

14. Anon (1957),Bull. Am. Ceram. Soc., 36(7), 278.

15. McMillan, P.W. (1964), 'Glass-Ceramics', Academic Press, London.

16. Berezhnoi, A.I.(1970), 'Glass-Ceramics and photo-sitalls', Plenum Press, New York.

17. Hillig, W.B. (1962), 'Symposium on nucleation and crystallisation in glasses and melts', p.77, American Ceramic Society, Colombus.

18. MacDowell, J.F. (1965), Corning Research, p.101.

19. Burnett, D.G. & Douglas, R.W. (1970), Discuss. Faraday Soc., 50, 200.

20. Burnett, D.G. & Douglas, R.W., (1971), Physics Chem. Glasses, 12(7), 117.

21. British Patents 863,569 and 863,570 (1961).

22. Filipovitch, V.N. & Kalinina, A.M. (1968), Neorg. Mater. 4, 1532. Ibid., (1970), 6, 351. Ibid., (1971), 7, 1844.

23. James, P.F., (1974), Physics Chem. Glasses, 15(4), 95.

24. Ito, M. et al (1968), Bull. Tokyo Inst. Technol., 88, 127.

25. Matusita, K. & Tashiro, M. (1973), J. Non-Crystalline Solids, 11, 471.

26. Strnad, Z. & Douglas, R.W. (1973), Physics Chem. Glasses, 14(2), 33.

27. Hammel, J.J. (1967), J. chem. Phys., 46, 2234.

28. Burnett, D.G. & Douglas, R.W. (1970), Physics Chem. Glasses, 11(5), 125.

29. Heady, R.B. & Cahn, J.W., (1973), J. chem. Phys., 58(3), 896.

30. Turnbull, D. (1950), J. appl. Phys., 21, 1022.

31. Jones, D.R.H. (1974), J. mater. Sci., 9, 1.

32. Nagel, S.R. & Bergeron, C.G. (1974), J. Am. Ceram. Soc., 57(3), 129.

33. Nagel, S.R. & Bergeron, C.G. (1971), 'Advances in nucleation and crystallisation of glasses', p.183. American Ceramic Society, Colombus.

34. De Luca, J.P. et al (1969), J. Am. Ceram. Soc., 52(6), 322. Ibid., (1970), 53(4), 214.

35. Laird, J.A. & Bergeron, C.G. (1970), J. Am. Ceram. Soc., 53(9), 482.

36. Matusita, K. & Tashiro, M. (1973), J. Ceram. Soc. Japan, 81(11), 500.

37. Marshall, H.J. (1967), Ph.D. thesis, University of Sheffield.

38. De Hoff, R.T. & Rhines, F.N. (1968), 'Quantitative Microscopy', McGraw-Hill, New York.

39. De Hoff, R.T. & Rhines, F.N. (1961), Trans. Metall. Soc., A.I.M.E., 221, 975.

40. Charles, R.J. (1967), Physics Chem. Glasses, 8(5), 185.

41. West, A.R. & Glasser, F.P. (1971), 'Advances in nucleation and crystallisation of glasses', p.151. American Ceramic Society, Colombus.

42. Dietzel, Von A. et al (1954), Glastech. Ber., 27(5), 147.

43. Gunawardane, R.P. & Glasser, F.P. (1974), Trans. J. Br. Ceram. Soc., 73(6), 207.

44. Oehlschliegel, G. (1975), J. Am. Ceram. Soc., 58(3-4), 148.

45. Oehlschliegel, G. (1971), Glastech. Ber., 44(5), 194.

46. Tanigawa, H. & Tanaka, H. (1967), Osaka Kogyo Gijutsu Kiho, 18(3), 230.

47. Freiman, S.W. et al., (1972) J. Am.Ceram. Soc., 55(7), 354.

48. Ramsden, A., Ph.D. thesis. To be conferred.

49. Ogura, T. et al., (1968), J. Ceram. Assoc. Japan, 76(8), 277.

50. Amos, R.J. (1974), 3rd Year undergraduate project, Department of Ceramics, Glasses & Polymers, Sheffield University.

51. Greene, K.T. & Morgan, W.R. (1941), J. Am. Ceram. Soc., 24(4), 111.

52. Gunawardane, R.P. & Glasser, F.P. (1972), Physics Chem. Glasses, 13(5), 125.

53. Denbigh, K. (1971), 'The principles of chemical equilibrium', 3rd Ed. Cambridge University Press, London.

54. Seward III, T.P. et al., (1968), J. Am. Ceram. Soc., 51(5), 278.

55. Charles, R.J. (1967), J. Am. Ceram. Soc., 50(12), 631.

56. Rogers, P.S. & Williamson, J. (1969), Glas Technol., 10(5), 128.

57. Matusita, K. & Tashiro, M. (1973), Physics Chem. Glasses, 14(4), 77.

58. Macedo, P.C. & Litovitz, T.A. (1965), J. chem. Phys., 42(1), 245.

59. James, P.F. & Keown, S.R. (1974), Phil. Mag., 30(4), 789.

60. Leontjewa, A. (1942), Acta Physiocochim. U.R.S.S., 16(1-2), 97.

61. Scott, W.D. & Pask, J.A. (1961), J. Am. Ceram. Soc., 44(4), 181.

62. Meiling, G.S. & Uhlmann, D.R. (1967), Physics Chem. Glasses 8(2), 62.

63. Cahn, J.W. & Hilliard, J.E. (1958), J. chem. Phys., 28(2), 258.

64. Kirkwood, J.G. & Buff, F.P. (1949), J. chem. Phys., 36(8), 2080.

65. Benson, G.C. & Shuttleworth, R. (1951), J. chem. Phys., 19(1), 130.

66. Lothe, J. & Pound, G.M., (1962), J. chem. Phys., 36(8), 2080.

67. Turnbull, D., (1952), J. chem. Phys., 20(3), 411.

68. Miyazawa, Y. & Pound, G.M. (1974), J. Crystal Growth, 23, 45.

69. Liebau, Von F., (1961), Acta Crystallogr., 14, 389.

70. Katscher, H. et al., (1973), Zeit. fur Kristallographie, 137(2-3), 146.

71. Donnay, G. & Donnay, J.D.H., (1953), Am. Miner., 38, 163.

72. Skapski, A.S. (1956), Acta Met., 4, 576.

73. Liebau, Von F., (1961), Acta Crystallogr., 14, 395.

74. Maries, A. & Rogers, P.S. (1975), Nature, 256(5516), 401.

75. Hilderbrand, J.H. & Scott, R.L. (1962), 'Regular solutions', Prentice-Hill.

76. Hardy, H.K. (1953), Acta. Met., 1, 202.

77. Förland, T. (1955), ONR Technical Report No. 63, Contract N6ONR269 Task Order 8, NRO32-264, Pennsylvania State University.

78. Charles, R.J. (1969), Physics Chem. Glasses, 10(5), 169.

79. Reisman, A. (1970), 'Phase equilibria', Academic Press.

80. Mackenzie, R.C. (1970), 'Differential thermal analysis', Academic Press, London.

81. Takahashi, K. & Yoshio, T. (1973), Yogyo-Kyokai-Shi, 81(12), 18.